Preparation of Bio-waste derived Heterogeneous Catalysts for Methanolysis and Peroxidation Reactions

Thesis submitted in partial fulfilment of the requirements for the degree of

DOCTOR OF PHILOSOPHY

by

Himadri Sahu

Department of Chemical Engineering

Indian Institute of Technology Guwahati

Guwahati – 781039, India

April-2017

This Thesis is dedicated to my Grandfather who has inspired me and made me strong enough to achieve my goal.

Patience and Luck both reciprocate each other.

- Himadri Sahu

Department of Chemical Engineering

INDIAN INSTITUTE OF TECHNOLOGY GUWAHATI

CERTIFICATE

This is to certify that ***Himadri Sahu*** has been working under my supervision since July 2017. I hereby forward his thesis entitled **"*Preparation of Bio-waste derived Heterogeneous Catalysts for Methanolysis and Peroxidation Reactions*"** to be submitted for the award of the degree of Doctor of Philosophy to IIT Guwahati. I certify that he has fulfilled all the requirements according to the rules of this institute and the investigations embodied in his thesis have not been submitted elsewhere for a degree or diploma.

Dr. Kaustubha Mohanty

Professor

Department of Chemical Engineering

Indian Institute of Technology Guwahati

Date:

IIT Guwahati

ABSTRACT

Heterogeneous catalysts have the prospective to beat several of the barriers that impede the catalytic performance of homogeneous catalysts. The increasing interest in the use of heterogeneous catalysts is one of the important aspects of green chemistry. Such catalysts provide simpler, low-cost separation processes and reduced waste generation, and moreover can be recycled for several reaction cycles. In some instances, the materials can be directly used as catalysts themselves, whereas in other cases they are used as base from which materials of catalytic interest can be prepared. The application of catalysts is ubiquitous in the chemical industry in areas ranging from pharmaceuticals to polymers to petroleum processing. More than 90% of all industrial processes are based on catalysis. However, the cost of commercial catalysts is still an issue and there is a need to look for low-cost materials for the preparation of catalysts.

Heterogeneous catalysts are mostly solid and can be prepared from various materials such as industrial squanders (e.g. red mud, aluminum dross, fly slag, blast furnace and steel slag) and natural squanders (e.g. chicken egg shells, rice husks, fish skeletal substance, crab shell, oyster shell, snail shell, shrimp shell, biont Shell) etc. The use of such wastes to develop catalysts can be a win-win situation as this takes care of the disposal issues and the high volume waste can furnish an economical track to dynamic frameworks. As these squanders are to be used for catalyst preparation it is necessary to know the potential influence of its composition. Though industrial squanders are readily available, it may not contain the required precursors (such as MgO, Al_2O_3 etc.), whereas the natural squanders contain high amount of required precursors (such as CaO, $Ca_5(PO_4)_3(OH)$ etc.). Natural squanders are also low-cost alternatives, which is why many researchers focused their attention on these materials. Moreover, there are plenty of alternate natural squanders available which can be explored for preparing catalysts.

Apatite is a group of phosphate minerals which is available both in the form of synthetic as well as natural. Hydroxyapatite ($Ca_5(PO_4)_3(OH)$) is one of such apatite which is the mineral form of calcium apatite and is a potential candidate for catalyst preparation. There are few differences between synthetic and natural hydroxyapatite. Natural HAp has better dynamic response to the environment, high catalytic activity and good thermo-chemical stability than the synthetic HAp. As far as solubility and activity is concerned, crystallographic structure plays an important role. In line to synthetic HAp, the natural HAp has perturbed nanostructures and nonstoichiometric composition with low hydroxyl

content. As physical and chemical properties depend on structure, natural HAp will lead to good results. Because of these properties HAp can be used as a heterogeneous catalyst.

Groundnut shell, an agricultural waste produced in enormous amount is usually either discarded or often burnt. However, groundnut shell is considered as a potential adsorbent material, which is viable in terms of both economic and environmental prospective. Hence, it is considered as eco-rich agricultural by-product. There are many works reported on groundnut shell as very good adsorbents for water/wastewater treatment containing both heavy metals as well as organic pollutants such as phenol, dye etc.

To increase the surface properties and the activity during reactions, various metals and metalloids were doped on to these materials. Finally, five catalysts were prepared. These developed catalysts were characterized using various analytical techniques. Then the catalysts were used for methanolysis and peroxidation reactions of Neem oil and waste cooking oil. The reusability study of the catalysts was also carried out to observe the chemical stability of the catalyst.

ACKNOWLEDGEMENTS

I would like to take this opportunity to express my heart-felt gratitude to them, whose contribution has made this thesis possible.

In particular, the foremost appreciation goes to my supervisor Prof. Kaustubha Mohanty for his valuable guidance throughout the research work. I thank him for his encouragement, guidance and moral support throughout, which enabled to pursue my academic skills under his precious guidance and expertise. I would like to acknowledge my sincere gratitude to my doctoral committee members, Prof. Tamal Banerjee, Prof. Chandan Das and Prof. Pranab K. Ghosh, for their insightful advices and suggestions throughout the research. I also acknowledge the kind support of Prof. Pallab Ghosh during my research work.

My sincere thanks to Prof. Bishnupada Mandal, Head, Department of Chemical Engineering, for his moral support and inspiration. I would also like to convey my sincere thanks to the Head of Central Instruments Facility (CIF), IIT Guwahati, for providing me the analytical facilities of CIF.

I am indebted to the selfless help and co-operation of my Research group, Sanjukta Bhoi, Madhusmita Dash, Proloy Das, Kulbhushan Samal, Ranjeet Kumar Mishra, Sanjeev Mishra, Bikashbindu Das, Barasa Malakar, Sachankar Buragohain, Santosh Kumar Hotta, Sounak Bera, Pranab Jyoti Sarma, Madonna Roy and Munmi Bhattacharya in each and every stage of the work. I would also like to acknowledge the support and encouragement of Dr. S. Murugavelh, Dr. S. Sasmal and Dr. S. R. Pilli. I am also thankful to all my batch mates, Rashmi bhai, Sai bhai, Saptak, Sunny, Dr. Dharamshi Rabari for their constant help and motivation.

Last but not the least, I express my deepest sense of gratitude to my Parents, for their patience, endless support and inspiration towards the completion of my Ph.D thesis. My heartfelt love and appreciation to my brother Niladri will never end for bearing with me through the period. I extend my sincere thanks to all my dear friends and well-wishers who had consistently supported and encouraged me, without which this work would have never been completed. My sincere apology goes to them whom I forget to mention but helped me at any part of the research work.

Thank you all!!

Himadri Sahu

CONTENTS

LIST OF TABLES

LIST OF FIGURES

1 INTRODUCTION

"By seeking and blundering we learn"

Johann Wolfgang Von Goethe

(1749-1832, German Poet, Dramatist, Novelist)

For most of the 20th century, mankind and especially the industrialised nations have relied heavily on the cheap and abundant availability of fossil carbonaceous feedstock for transportation fuels, chemicals and energy production (in the form of heat and electricity). However, towards the end of the 20th century and the start of the 21st it has become increasingly evident that humanity faces a number of unprecedented challenges in terms of future energy resources and consumption [1], which may be sketched as:

The environmental challenge: The combustion of fossil oil, gas and coal releases the greenhouse gas CO_2 to the atmosphere from carbonaceous resources that have not been part of the global atmosphere or biosphere for millions of years. The effect of greenhouse gases on the atmosphere are well acknowledged both in terms of global and local climate changes and by a mean global temperature increase [2]. But also the combustion-related emissions of nitrogen oxides, sulphur oxides and aromatic particulates from the consumption of fossil fuels have negative environmental effects as well as being harmful to the health of human beings. The massive human use of consumable goods of all kinds also leads to build up of solid or liquid waste, which must be treated or disposed of in an ecologically safe and sustainable manner. This recognition is not always fulfilled.

The social challenge: The global population is increasing, and the increasing populations especially in the developing countries require a higher standard of living, thereby increasing the demand for electricity, housing, fuel, sanitation, consumables, clean water, and food.

The resource challenge: The projected gradual depletion of easily accessible fossil resources of oil, gas, and coal, especially mineral oil deposits, is leading to the search for and extraction of less accessible carbonaceous resources like tar sands, deep-water oil deposits or deposits in ecologically sensitive areas. These extraction methods will become more costly in terms of both energy, processing and labour, and will take place in increasingly inhabitable areas of the world like the Arctic, Canada, Siberia, or the like [1]. This happens while the global energy demand is increasing.

The ostensibly ever-increasing demand for fertiliser, plastics, consumables, electrical devices, chemicals, fuels and energy put pressure on the existing energy supply and infrastructure, but also spark search for sustainable alternatives and furthers the focus on energy and resource efficiency. This is especially the case for fuel-consuming vehicles.

The most critical feedstock in the chemical industry and refineries is oil, and transportation fuels constitute the largest part of the oil consumption. This means that a global shift towards renewable feed stocks is necessary [3], and biomass is the only renewable carbonaceous material available apart from CO_2. Its use as a base for sustainable fuels and chemicals in the future is therefore indispensable. With respect to the environmental issues, waste disposal problems as well as depletion of non-biodegradable oleochemical-based resources in late [4], plenty of bio-based natural polymer products such as polyhydroxy alkonate, polylactic acid, cellulose plastics, thermoplastic starch and vegetable oils have been widely developed and commercialized [5, 6]. Among them, there has been a growing trend in utilizing the vegetable oils extensively as raw material in various applications due to their inherent biodegradability, low cost, societal favourably advantages and availability [7-10]. Due to curiosity as to the versatility of vegetable oil constituents that are made up of complex multi-component mixtures of fatty acids and glycerol ester, various researches have been conducted to make full use of linseed, castor, soya, safflower or tall oils in oleoresinous production [11-13]. In general, advances in oleochemistry technology today make possible for researchers to chemically modify and transform the triglycerides into polymerizable monomer via epoxidation, metathesis of double bonds, acrylation of epoxies, reaction with maleic anhydride or transesterification [7, 13]. Among those reactions, epoxidation

is a commercially important reaction in organic synthesis since the high reactivity of oxirane rings makes them to be readily transformed into desired functionality [14-16].

For 80% of all compounds produced in chemical and pharmaceutical industries at least one catalytic step is essential during their synthesis [17]. Catalysis has been commonly divided in three main groups, based on the nature of the catalyst-substrate interactions. Hence, in homogeneous catalysis the catalyst is in the same phase as the reactants, whereas in heterogeneous catalysis they are in a different phase.

1.1 Catalysis - Setting the scene

Efficient, economical, and environmentally sound chemical production usually require the aid of catalysis to run at acceptable rates. Most of the western standard of living may be said to be based on the ability of the chemical industry to turn available raw materials efficiently into fuels, chemicals and applicable energy.

It is useful to notice the definition of catalysis: A catalyst is a substance that takes part in and enhances the rate of a chemical reaction without being consumed by the reaction. The science concerned with the rate of reactions is chemical kinetics, which also embodies catalysis.

However, reactions have to be thermodynamically favourable to occur, i.e. the reaction must be spontaneous i.e. it must have a negative Gibbs-free energy. A catalyst does not change the position of chemical equilibrium, but it accelerates the tendency of the reaction towards equilibrium. Popularly coined thermodynamics defines what is possible, and catalysis and kinetics how and how fast it is possible.

Industrial catalysis as a discipline, especially heterogeneous catalysis, has developed largely concurrently with the modern methods of industrial petroleum refining and has steadily allowed more sophisticated use of feed stocks for a growing range of and demand for petroleum products [3, 18]. Catalysis will likely gain an even higher importance as a discipline, and a profound knowledge of the science behind it, as well as harnessing it on a technical scale will be of utmost importance for the future chemical industry.

1.2 Importance of Methanolysis of oil

1.2.1 Diesel as a biofuel

The production of biomass diesel is growing. The different possibilities for producing diesel oils from biomass resources have undergone substantial research in the latter years, and a number of catalytic methods have now been established: Fats and oils can either be transesterified with alcohol to form fatty acid alkyl esters [19-24], deoxygenated with hydrogen to form n-alkanes [25-33], or cracked at elevated temperatures to form a hydrocarbon mixture [27, 34-36]. Carbohydrates may be converted by aqueous-phase-reforming to form unfunctionalised or monofunctional hydrocarbons [37-40]. Biomass in general may be gasified to syn-gas and undergo Fischer-Tropsch-synthesis [41-44], or bio-oils can be produced by flash pyrolysis and upgraded by cracking or hydrogenation [45-50]. The term "biodiesel" usually refers solely to as fatty acid alkyl esters, and again mostly the methyl esters (FAME) are considered [51]. However others have suggested wider definitions and raised points about too narrow focus regarding naming the fuels [52, 53]. For the sake of clarity, the term "biodiesel" will be avoided in the present thesis and the technical-chemical terms for each fuel will be used instead. The market share of FAME is the largest of the diesel oils from biomass, but it is nonetheless the only one.

Pure vegetable oils or fats are not biodiesel fuels and cannot be used as such. Engine and fuel system require modifications to be able to run on these fuels, and these changes are often illegal for road vehicles and lead to annulment of engine warranties and specifications for emissions. The combustion in the engine has a tendency to become incomplete, and both particle and NOx emissions are reported to rise. Plant oils are also too viscous to be pumped in the fuel and injector systems [22, 54].

1.2.2 Fatty acid alkyl esters from fats and oils

The most applied method for producing diesel from biomass as well as the one which has received most attention the latter years is the alcoholysis or transesterification of fats and oils to yield fatty acid alkyl esters (FAAE). Usually the alcohol is methanol due to lowest cost, easiest separation and highest reaction rates obtained, whereby methyl esters of the fatty acids (FAME) result [55, 56]. FAME can be used directly in the engine without modification and can be mixed in all ratios with traditional diesel fuel.

1.2.2.1 Transesterification

Fats and oils consist primarily of triglycerides (TG). These, as well as mono- and di-glycerides, can be transesterified into FAMEs by methanol, see Figure 1-1. The sources of the TGs can be all types of vegetable oils, animal fats, or waste greases [56, 57]. A successful transesterification leads to two phases: a bottom phase containing the glycerol and an upper phase containing the FAME.

In industrial practise, the reaction is performed at 60-70 °C and is catalysed by a few wt% of a strong base - the hydroxides or methoxides of sodium or potassium are used as homogeneous catalyst, KOH being the norm due to its low price [56, 58, 59]. One molecule of glycerol is obtained as a by-product for every three FAME molecules produced.

The transesterification is equilibrium-driven and in fact reversible. However, due to use of 2-3 times molar excess of methanol and the immiscibility of FAME and alcohols, above 99% yield of FAME can usually be obtained within a few hours of reaction [55, 56]. The oil- and FAME-phase (non-polar) and the alcohol phase (polar) are not directly miscible with each other. This means that, initially, the reaction is slow and dependent on vigorous mixing of the two phases (e.g. by stirring) to get a large contact area between the two phases. During reaction, di- and mono-glycerides are formed, and these compounds act as emulsifiers for the reaction mixture. Once the transesterification is nearing completion, the two phases start to separate again (settling) [22]. Industrially the transesterification is normally performed in a stirred batch-reactor, and as sufficient settling often requires longer time than the transesterification reaction itself, the settling is often performed in a separate settling-tank [60].

1.2.2.2 Esterification

The homogeneous, base-catalysed transesterification is working efficiently, but it gives rise to a number of challenges. First and foremost, oils and fats may contain free fatty acids (FFA). Most fresh vegetable oils usually do not contain problematic amounts of free fatty acids, but especially waste fats are challenging: 2 to 7 wt% FFA for used cooking oils, 5 to 30 wt% for waste animal fats and abattoir waste, and some trap greases can contain over 50 wt% FFA [21, 22]. The FFAs will react with the basic catalyst and form soap, and when the feedstock contains more than about 0.5-1 wt% the reaction

becomes unacceptably slow due to consumption of base otherwise intended for transesterification, and the formed soap emulsifies the phases and hinders the settling and separation after reaction [56].

For this reason, the FFAs must first be reacted with methanol to form FAME. Esterifications are acid-catalysed, and in the industry a few wt% sulphuric acid, H_2SO_4 is often used for this purpose. An acidic esterification step is therefore performed prior to the basic transesterification. Sulphuric acid is the cheapest acid and has the advantage of being both strong and very hygroscopic. The mixture of methanol and fat is esterified for a few hours at 60-70 °C , around the boiling point of methanol, with stirring so as to bring the content of free fatty acids below 0.5 wt% (as is shown in Figure 1-2) prior to the transesterification [56].

Thus, two consecutive reaction steps are needed. The esterification by homogeneous acid leads to a number of other challenges: First of all the acid solution from esterification must be neutralised and made alkaline with the addition of the base for the transesterification, and even by the end of transesterification acid must again be added to neutralise the alkaline alcohol-phase. This naturally yields large amounts of salts as by-products (usually K_2SO_4 and $KHSO_4$). This has no immediate use. Furthermore, it is necessary to use new homogeneous catalysts for each FAME batch. Another issue with this is the purification of glycerol and excess methanol afterwards, which is often contaminated with water and salt [60]. An immediate decantation removing most of the salt can however be made after settling.

In principle, the transesterification can be catalysed by both bases and acids leaving room for a one-step acid-catalysed process, but the base-catalysed reaction is 3-4 orders of magnitude faster than the acid-catalysed reaction [19, 55, 56, 61]. Heating the batch to at least 150-200 °C must be performed for completion of the transesterification with acid catalyst within an acceptable time-scale. This requires working with pressurised equipment (due to the vapour pressure of methanol, which has a normal boiling-point of 64.6 °C (STP)), and is therefore usually disregarded and considered uneconomical at least with sulphuric acid.

It is of major interest to substitute the homogeneous catalysts with heterogeneous catalysts. This would avoid the formation of inapplicable salt by-products, lower the

expenses for buying catalysts for each batch of FAME, and prevent the equipment corrosion by dissolved H_2SO_4 in the methanol. Water formed by the neutralisation of H_2SO_4 with KOH will contribute to soap formation of FFAs formed via basic hydrolysis of glycerides. Also, a solid catalyst would allow easier operation in a liquid-liquid-solid plug-flow-reactor with static mixers, which may be much more desirable with regards to labour demand, process control, -layout and -supervision, and optimisation of product quality [56, 62].

1.3 Importance of Peroxidation

Peroxidation or Epoxidation occurs when a cyclic ether is formed at sites of ethylenic unsaturation (C=C) located along the fatty acid (FA) chains by the addition of an oxygen atom. This epoxy group has the general structure shown in Figure 1-3. Peroxidation means the reaction of fatty acids with peracid. The bond angles are about 60°, making the ring highly strained and highly reactive [63].

The presences of these 'high strain energy' rings on the fatty acid chains promote cross linking when the epoxy resin is cured. The higher the amount of epoxy rings that are opened by the process, the more cross linking can occur, and the higher the quality of the resulting plastic [64]. The method of epoxidising vegetable oil that has received the most attention in the literature is by reacting vegetable oil with peroxy carboxylic acid. The peroxy carboxylic acid donates the oxygen atom required to form the epoxy group and returns carboxylic acid to the bulk mixture. Peroxy carboxylic acid is formed *in-situ* by the reaction of carboxylic acid and hydrogen peroxide in the presence of an acidic ion exchange resin (AIER) as a heterogeneous catalyst [63-67]. The *in-situ* method is used because high concentrations of peroxy carboxylic acids can be unstable and explosive. By forming the peroxy carboxylic acid in the presence of a well dispersed oil phase, its consumption in the epoxidation reaction prevents regions of high concentration from occurring. Epoxidation of fatty acids is a reaction of a carbon – carbon double bond with active oxygen, which results in the addition of an oxygen atom, converting the original double bond into a three membered epoxides (oxirane) ring. In general, olefins can be epoxidized with various per-acids is a chemical reaction in which an oxygen atom is joined to an olefinically unsaturated molecule to form cyclic, three membered ether. The products of epoxidation are known as oxirane compounds or epoxide. Epoxidation of

vegetable oils is a commercially important reaction because the epoxides obtained from these renewable raw materials and from their alkyl esters, their trans-esterification products, have applications in such materials as plasticizers and polymer stabilizers. Furthermore, these epoxides can be used as intermediates in the production of a variety of derivatives, because of the high reactivity of the strained epoxide ring.

1.3.1 Industrial Significance

The bond angles are about 60°, making the ring highly strained and highly reactive [63]. Today, one of the most important epoxidized oil is soybean oil (ESO), and its worldwide production is about 20,00,000 t/year, but will further increase is approximately 7% for next year. Fatty Epoxides are used directly as plasticizers which are compatible with polyvinylchloride (PVC), and as stabilizers (HCl scavenger) for PVC resins to improve flexibility, elasticity and to impart the stability of polymers towards heat and UV radiation. The efficiency of these epoxides is directly related to the amount of epoxy group present in the molecule oil, expressed with Oxirane Number. Epoxidized oils are natural, non-toxic, non-corrosive and biodegradable and for this can be good substitutes of phthalates, other plasticizers derived by petroleum, banned by EU in many countries due to their toxicity [68]. Due to high reactivity of the oxirane ring epoxides also act as raw materials for a variety of chemicals, such as alcohols, glycols, alkanolamines, carbonyl compounds, olefinic compounds, and polymers like polyesters, polyurethane (PU), and epoxy resins. The modified soy-based vegetable oil polyoils could be incorporated as a replacement for conventional polyoils to produce flexible PU foams, elastomers and coating [69].

1.3.2 Epoxidation methods

There are basically four known technologies to produce epoxides from olefins:

a) Epoxidation with percaboxylic acids [70] (Prileschajew), the most widely used in industry. The percaboxylic acid is formed *in-situ* by the reaction of carboxylic acid and hydrogen peroxide, catalyzed by acids or by enzymes [71].
b) Epoxidation with organic and inorganic hydroperoxides, which includes hydrogen peroxide epoxidation as well transition metal-catalyzed epoxidation [72].
c) Epoxidation with haloydrines, using hypohalous acids (HOX) and their salts as

reagents for the epoxidation of olefin with electron-deficient double bonds [73];

d) Epoxidation with molecular oxygen [73].

Among the ways of the epoxidation methods, the available technologies that needs to be explored are only the a) and b) as described above, which are clean and efficient. These technologies can be rendered cleaner by using heterogeneous catalysts replacing traditional homogenous ones.

1.4 Selectivity and Types of catalysis

The main advantages of catalysis is that you get the desired product faster, using fewer resources and generating less waste. The catalyst opens a selective route to the desired product. There are various kinds of product selectivity. Chemical selectivity, or chemoselectivity, denotes a situation where two different chemical reactions can occur, giving two different products. Similarly, regioselectivity occurs when the same chemical reaction in different regions of the molecule leads to different products. When a reaction gives two (or more) diastereomers, the selectivity to each of these is called diastereoselectivity. In the special case when two products are mirror-image diastereomers, or enantiomers, we talk about enantioselectivity. Figure 1-4 shows examples of the various product selectivity types.

Basically there are three types of catalysis *viz.* Homogeneous Catalysis, Heterogeneous catalysis, and Biocatalysis.

1.4.1 Homogeneous catalysis

In homogeneous catalysis, the catalyst is in the same phase as the reactants and products. Here we will concentrate on homogeneous catalysis in the liquid phase. In the classic case, the reactant (also called the substrate) molecules and the catalyst are reacted in a solvent. For example, the transesterification of fatty acid triglycerides with methanol (Figure 1-1) is catalyzed by hydroxide (OH^-) ions. This is an important process for making fatty acid methyl esters which are then used as biodiesel. It can be noticed that in Figure 1-1 that the "OH^-" is written above the reaction arrow, rather than on the same line as the reactants and products. This notation reminds us that the catalyst, although it participates in the reaction, remains unchanged when the reaction is completed. This does not mean that the catalyst does not change during the reaction. A catalytic reaction is made up of

several steps. These form a cyclic process, called a catalytic cycle. Although the catalyst can (and often does) change during the catalytic cycle, it returns to its original form at the "end" of the cycle.

The easiest way to illustrate this is using an example. Figure 1-5a shows the classic catalytic cycle for the Pd-catalyzed cross-coupling between an alkene and an aryl halide. This reaction, discovered independently by Heck and Mizoroki in 1968, is known as the Heck reaction [74]. Since its discovery it has become ubiquitous in organic chemistry, and is used today in several fine-chemical processes [75]. We see that the catalyst goes through at least six different structures (these are called the catalytic intermediates). Each of these is "the catalyst" as much as any other. The point is, however, that at the end of the cycle the original catalyst is regenerated and is ready to catalyze the coupling reaction of two new substrate molecules.

Figure 1-5b shows a "black box" version of the same catalytic cycle. This is what we actually observe: the substrates (aryl halide and alkene) enter the reactor and the products and by-products leave it. The catalyst remains in the reactor and, for all practical purposes, remains unchanged.

Many homogeneous catalysts are based on a (transition) metal atom that is stabilized by a ligand. The ligand is usually an organic molecule that attaches to the metal atom. By changing this ligand, one can change the catalyst's properties. Selecting the right metal and the right ligand can improve the catalyst's activity, selectivity, and stability. In some cases, it also allows the use of renewable feedstock and reagents, an important aspect of green chemistry.

1.4.2 Heterogeneous catalysis

Heterogeneous catalysis covers all the cases where the catalyst and the substrate are in different phases. However, when chemists speak about heterogeneous catalysis, they usually refer to a system where the catalyst is a solid and the reactants are (most often) gases or liquids. In fact, the solid/gas combination is so common that some books and journals refer to it as 'classic' heterogeneous catalysis or even simply as 'catalysis'. This has historical origins: most 'classic' heterogeneous catalysis was developed in the petrochemicals and bulk-chemicals industry. Due to reactivity and process size

considerations, these industries favour continuous processes at high temperatures. This meant that working with solid catalysts and gaseous reactants was often the best, and often the only, option. One important advantage of heterogeneous catalysis is the ease of catalyst separation. In gas/solid systems the catalyst is easily separated and cleaned, and in liquid/solid systems it can be simply filtered.

Once again, reactants enter the catalytic cycle and products leave, while the catalyst changes during the cycle but regains its original form at the end of the cycle. A simple example of gas/solid heterogeneous catalysis is the hydrogenation of propene to propane. In this reaction, a hydrogen molecule is added to the propene double bond in the presence of a group VIII metal catalyst (Ni, Pd, or Pt). The catalytic cycle (Figure 1-6) involves several steps. First, a propene molecule is adsorbed on the catalyst surface. The carbon–carbon p-bond breaks and bonds with the surface are created. Meanwhile, H_2 molecules are also adsorbed on the catalyst. The H-H bond then breaks, and the H atoms move across the metal surface. Eventually, an H atom diffuses close to one of the bonded C atoms. The C–metal bond is then replaced by a C-H bond. When this happens at the other C atom also, the connection with the surface breaks and the new propane molecule diffuses back into the gas phase.

Note that each of these simple elementary reactions is reversible, and so the entire catalytic cycle is also reversible. This is known as the principle of microscopic reversibility. Consequently, if platinum is a good hydrogenation catalyst, then it must also be a good dehydrogenation catalyst. In fact, as we will see later, catalysts change only the reaction rate, not the equilibrium. Every catalyst catalyses both the “forward” and the “reverse” reactions in the same proportions. In the above example, the reverse reaction is actually more interesting for industry, because propene is a valuable monomer for making poly(propylene) and other polymers. Not all heterogeneous catalysis occurs on metal surfaces. Zeolites, for example, are excellent solid acid catalysts. These are porous crystalline structures of metal oxides, often made from silicon, titanium, aluminium, and oxygen. By substituting cations in the zeolite framework, one can create Brønsted and/or Lewis acid sites.

1.4.3 Biocatalysis

Biocatalysis is a rather special case, somewhere between homogeneous and heterogeneous catalysis. In most cases, the biocatalyst is an enzyme – a complex protein that catalyses the reactions in living cells. Enzymes are extremely efficient catalysts. An enzyme typically completes 1000 catalytic cycles in one second. Compared to this, conventional homogeneous and heterogeneous catalysts are slow and inefficient (100–10,000 cycles per hour). Speed, however, is not the only advantage: enzymes specialize in converting one specific reactant into another specific product. This specificity even includes chiral centres, so an enzyme will catalyse the reaction of one substrate enantiomer, but not of the other. Such enantiospecific reactions are extremely important in the pharmaceutical and food industries, because often only one enantiomer has the desired activity. This is the case for many drugs, food additives, flavourings, and fragrances.

Further advantages of biocatalysis over "chemical catalysis" include shorter synthesis routes and milder reaction conditions. Enzymatic reactions are not confined to *in vivo* systems – many enzymes are also available as isolated compounds which catalyze reactions in water and even in organic solvents [76]. Despite these advantages, the activity and stability of most wild-type enzymes do not meet the demands of industrial processes. Fortunately, modern protein engineering methods can be used to change enzyme properties and optimize desired characteristics.

Although biocatalysis is the "new kid on the block," more and more companies are using enzymes for chemical manufacture. One reason for this is that biocatalysts give sustainable alternatives to chemical manufacture, and not just for making chiral products. The synthesis of acrylamide via an enzyme-catalyzed water addition to acrylonitrile (2-propenenitrile) is a classic example (Figure 1-7). It uses the Rhodococcus enzyme nitrile hydratase. Commercialized in 1985 by Nitto Chemicals in Japan, this process replaced an acid-catalyzed process, and also avoided the acrylic acid by-product [77]. Biocatalytic acrylamide processes are now running at 50,000 tpa worldwide.

Bio-catalytic processes really can replace the traditional chemical manufacturing routes however; it will take time. Although petroleum prices are increasing, there is still no shortage of benzene for chemical production (>90% of the worldwide petroleum

demand ends up as transportation fuel; chemicals production accounts only for ~7%). The bulk-chemical industry is very conservative, and enzymes are expensive compared to conventional catalysts.

1.5 Waste materials: catalytic opportunity

In general, catalysts used for above mentioned reaction processes are mineral acids such as sulfuric acid, Nitric acid. Hence, environmental problems related to salt disposal after neutralization and technical problems such as corrosion and separation remains the primary concerns. This is the sole reason for which the use of heterogeneous catalysts has become important in chemical industries. These catalysts are easy to separate as well as generate minimum waste. Another important characteristic is regeneration of the catalyst [78]. Catalysts based on various standard metal oxides such as manganese, rhenium, titanium and tungsten have already been explored. However, the high cost of these catalysts restricts their use. Consequently, since more than a decade research on catalysis is focused on the development of catalysts either from low-cost substrates or from waste materials.

Large-scale waste products afford opportunities in terms of catalysis. Whilst the use of such wastes in this context, by definition, does not alleviate disposal problems, which are significant and also costly in some cases, high volume waste can provide an inexpensive route to active systems. A survey of the literature demonstrates that this area is starting to attract more attention. This interest is primarily driven by a combination of economic and environmental considerations. A number of different approaches to the utilization of waste materials in this context has been reported: (i) their direct application as active materials, (ii) their direct use as pre-catalysts (i.e. materials which undergo transformation to active phases under reaction conditions), (iii) their modification to yield catalytically active phases and (iv) their use as precursors for the synthesis of active catalysts. In the sections which follow, we will present selected examples of large scale waste materials being used in these ways to provide an overview of some of the current activity in this area. The waste materials we describe can be broadly divided into those generated by large scale industrial processes (e.g. red mud, aluminium dross) and those which originate from biological sources (e.g. chicken egg shells and rice husks) and so we have sub-divided them in this manner. In terms of the latter class of materials, we have

concentrated specifically on wastes rather than the development of renewable resources for catalytic applications. The reported production rates for a number of the industrial and biological wastes described are reproduced in Table 1-1.

1.5.1 Large scale industrial wastes

1.5.1.1 Red mud

Red mud is the large scale waste product of the Bayer process for alumina production. In this process, bauxite ore is digested in hot caustic soda to extract most of the aluminium content which is subsequently processed. The insoluble residues of the digestion procedure, which are filtered off, constitute red mud, which is a finely divided highly alkaline heterogeneous mixture of different oxidic phases. The exact composition of red mud reflects that of the bauxite ore from which it is generated and there can be significant geographical and temporal variations. The current global production of red mud is around 70 million tonnes per annum and it is mostly disposed of by land dumping [79]. Since it is such an abundant resource, there has been much interest in its valorization [80-82]. In terms of catalysis, the primary interest has centred upon the relatively large iron content of red muds, which is expected to impart a wide range of interesting catalytic behaviour, including oxidation and hydrocarbon activation activity. Whilst red mud has been applied directly as received to catalytic reactions both as an active component and a catalyst support phase, activation procedures which are designed to increase its activity by enhancement of surface area and/or minimization of the effects of the variability of its composition, are possible. One of the most commonly applied activation procedures is that reported by Pratt and Christo version in which initial acid dissolution is followed by base precipitation, filtering and calcination yielding a material with significantly enhanced surface area. Red mud has been applied to a very wide range of catalytic reactions including hydrogenation [83, 84], coal liquefaction [85], hydrodechlorination [86], exhaust gas treatment [87] and the conversion of polymers into fuel oil [88] as has been recently reviewed elsewhere [82].

1.5.1.2 Aluminium dross

Aluminium dross is a by-product of aluminium manufacture and recycling. It is generated by the reaction of molten aluminium with air where surface phases of

aluminium oxide and nitride form. The dross is classified into "white" and "black" grades depending upon its metallic aluminium content, with the latter comprising a lower aluminium and higher salt content [89]. Salt cake is also produced in secondary aluminium processes and contains a still lower aluminium content (typically 5–10% Al) White dross, which typically comprises around 80 wt% metallic aluminium, is formed in the Hall–Heroult process of aluminium manufacture in which alumina obtained from the Bayer process is dissolved in molten cryolite and electrochemically processed to yield metallic aluminium [89]. Black dross, which typically contains 5–20% Al, is a by-product of aluminium recycling and secondary processing of white dross. Annually, around 5 million tonnes of dross are produced globally of which about four million tonnes are white dross [90]. Whilst some dross is recycled for use as a deoxidizer in steel manufacture, much of the rest is disposed of by landfill where, for some waste products of the aluminium industry, there can be concerns over leaching of components and concomitant contamination of groundwater, as well as hydrolysis yielding noxious gases such as NH_3. Therefore, there is great incentive to develop uses of dross and associated by-products. In terms of catalytic application, there have been a number of reports of dross being applied as an alternative source of aluminium for the preparation of catalytically active materials.

Aluminium dross can be used as an alternative source of aluminium for the preparation of materials of catalytic interest. However, when used directly, the presence of impurity phases or their effects on, for example, the crystallite size of the target material are considerations. Extraction of the aluminium component can be undertaken at the expense of increasing the number of stages in the process.

1.5.1.3 Fly ash

Fly ash is a residue generated by combustion that consists of fine particles with a composition which reflects that of the inorganic components of the particular fuel being burned and the combustion technology applied. It is therefore a heterogeneous material with a variable composition, dependent upon source and process operation, which predominantly comprises Al_2O_3 and SiO_2 along with additional components such as Fe_2O_3, MgO, CaO, K_2O and Na_2O. The lighter particles produced consist of censospheres (hollow ceramic microspheres). As would be expected, fly ash is a significant by-product of thermal power generation and its predominant disposal route is by means of landfill or

dumping at sea. This results in obvious concerns which are particularly apparent when the scale of ash generation is considered. Utilisation of this residue is possible and various routes, including the manufacture of cement, concrete, ceramics, zeolites and adsorbents, have been documented [91]. Among the high value applications of fly ash, its use as a catalyst and catalyst support is an active area of investigation which has been reviewed recently [91]. Due to its silica and alumina content, several studies have examined the use of coal fly ash as a support [92-95]. To enhance the surface area of the fly ash, in many cases thermal or chemical treatment has been undertaken prior to the loading of active phases. An example of this procedure involves the application of steam treated and nitric acid activated fly ash, which was used as a support for copper, nickel and iron catalysts, which were subsequently applied to the environmentally important selective catalytic reduction of NOx using NH_3 [92]. As would be anticipated, the nature of the pre-treatment of fly ash will influence its acid–base properties. The composition of coal fly ash makes as a catalyst support phase and also a feedstock for the preparation of zeolites. In instances where the iron oxide content is high, it can be extracted or the fly ash by itself can be used for applications where iron/iron oxide is active. Also, in addition to coal fly ash, wood fly ash and municipal incinerator fly ash have been used as catalysts, mainly for oxidation applications [96-99].

1.5.1.4 Others

In addition to the materials discussed above, there are other wastes that have been investigated as catalysts in a number of studies. Waste sludge's from sewage treatment and industrial sources (tannery, electroplating, textile dyeing, steel electro polishing, using different mechanical and thermal pre-treatment) have been [100] applied to propane oxidation in which the iron, copper and chromium contents impart activity [101]. The waste generated from the processing of the negative electrode for Ni metal hydride batteries was subjected to a series of chemical treatments to isolate NiO, CeO_2 and $LaCoO_3$. Blast furnace and steel slags are major waste products originating from iron manufacture and processing [102, 103]. It has been reported that the global production of slag during 2008 was in the range of 240–290 million tons [103]. The SiO_2 and Al_2O_3 content appears to be of interest for the preparation of aluminium rich zeolites, the presence of such large amounts of CaO is reported to be problematic. It has been reported

that materials containing in excess of 15 wt% CaO are unsuitable for zeolite synthesis because of the formation of calcium silicate, which leads to inhibition of zeolite nucleation [102].

1.5.2 Wastes originating from biological sources

1.5.2.1 Shells

Recently, there have been a number of reports detailing the application of waste shells to the preparation of catalysts. It has been reported that the shell constitutes about 10% by mass of a hen egg and that around 4 million tonnes per annum of egg shell waste is produced in China alone [104]. Disposal of these shells is mainly by landfill dumping. There is interest in their use as they can be thermally decomposed at high temperatures to generate CaO from the decomposition of $CaCO_3$ which is their major constituent. CaO based catalysts are currently of interest as solid bases for transesterification to produce biodiesel [105]. Within the literature, it has been reported that the catalyst generated by high temperature decomposition of chicken egg shells is active for biodiesel production from methanol and soybean oil. Despite having a similar elemental composition, catalysts derived by calcination of egg shells were found to be more active for production of biodiesel from palm oleic oil and methanol than those derived from golden snail shells which were in turn more active than those derived from Venus meretrix. In all cases, highly crystalline CaO was reported to be the predominant phase and the order of activity was explained on the basis of surface area and particle size, with the egg shell derived catalyst having the highest area (1.1 m^2 g^{-1}).

Crab shells are a source of chitin, poly-β(1→4)-N-acetyl-D-glucosamine. Chitin is also found in the shells of other crustaceans, as well as in the exoskeletons of insects and as a component of fungal cell walls. It is, after cellulose, the second most abundant biopolymer with an estimated annual production rate of 10^{11} tonnes per year [106]. It is therefore a highly abundant natural resource. For example, the estimated annual production of waste from the Malaysian fishery industry alone is of the order of 70,000 tonnes [88]. There are a number of large scale applications of chitin, or its derivatives, which include those in the pharmaceutical industry, agriculture and the food industry. A number of applications of chitin or chitosan based materials as supports for catalytic

applications are detailed in the literature [107-109]. Applications of shells as sources of chitin have also been reported.

1.5.2.2 Fish bone

Globally in excess of ninety one million tons of fish are caught and around 55% of this are used for human consumption, while rest are discarded [110]. The discard materials generate undesirable impact on environment. To reduce any adverse environmental effects, it is advisable to use these discard materials for high value added products. Few fish species are export after extracting the bones. These discarded bones are the cheap source of calcium phosphate. So this is also termed as hydroxyapatite, with stoichiometric formula $Ca_{10}(PO_4)6(OH_2)$.

However, there are few differences between synthetic and raw hydroxyapatite. Natural hydroxyapatite has and better dynamic response to the environment, high catalytic activity and good thermo-chemical stability than the synthetic hydroxyapatite [111, 112]. As far as solubility and activity is concerned, crystallographic structure plays an important role. In line to synthetic hydroxyapatite, the natural hydroxyapatite has perturbed nanostructures and nonstoichiometric composition with low hydroxyl content. As physical and chemical properties depends on structure, natural hydroxyapatite will lead to good results [100]. Because of these properties hydroxyapatite can be used as a heterogeneous catalyst. Although natural hydroxyapatite has favourable structure but the surface area is bit low, which can be increased by doping metal ions on to it.

1.5.2.3 Rice husk

Rice husk is the indigestible hard protective coating of rice grains which is removed during processing. It is a major agricultural waste product. Various estimates of annual global production of rice husks and rice husk ash can be found in the literature. For example, annual rice husk production of more than 40 million tonnes was reported in 1992 and it has recently been reported that about 70 million tonnes of rice husk ash is produced yearly worldwide. Rice husks are composed of cellulose, lignin and silica and it is the latter component that has generated most interest. Low levels of additional inorganic components can also be found in rice husk and, whilst the concentration of these may vary with location, these influences appear to be relatively small [113]. Rice husks

and their ash have attracted interest in terms of the extraction of the SiO_2 component and this can act as a source for the synthesis of catalytically important materials such as zeolites and mesoporous silicates. The forms of silica which can be produced and their particle size control have attracted attention with chemical pre-treatment and/or controlled atmosphere calcination being employed as the methods of extraction in some studies. Rice husk has also been used as a precursor for preparing carbon honeycomb monoliths which have potential as catalyst supports. The monoliths prepared by extrusion of carbonized rice husk along with clay binder had a high surface area after alkali activation (more than 300 m^2 g^{-1}) and good mechanical strength [114]. Since rice husks also contain an organic component, routes to reacting the organic and silica components can be envisaged.

1.5.2.4 Peanut husk

India is the second largest producer of groundnut shell throughout the world, which has 8-million hectares' area of cultivation producing 800400 metric tons/y. The shell of groundnut is a carbonaceous, fibrous solid waste which is often burned or discarded directly into the farm lands, which would produce waste gas and dust or unpleasant smell. Fortunately, a possible solution was found and that is to utilize peanut husk as an adsorbent material to remove contaminants from waste water. It will solve both of the problems we concern about above and bring economic and environmental benefits to the industrial wastewater treatment. Therefore, researchers have studied about the removal of heavy metal onto peanut husk from aqueous solutions or how to modify peanut hulls [115].

Table 1-1 Reported production rates of various large scale wastes which can be used for catalytic purposes

Waste material	Reported production rate
Red mud	>70 million tonnes globally per annum
Aluminium dross	5 million tonnes globally per annum
Fly ash	430 million tonnes globally in 2003
Slag from iron manufacture	240-290 million tons globally in 2008
Chicken egg shells	4 million tonnes annually in China alone
Rice husk ash	About 70 million tonnes globally per annum

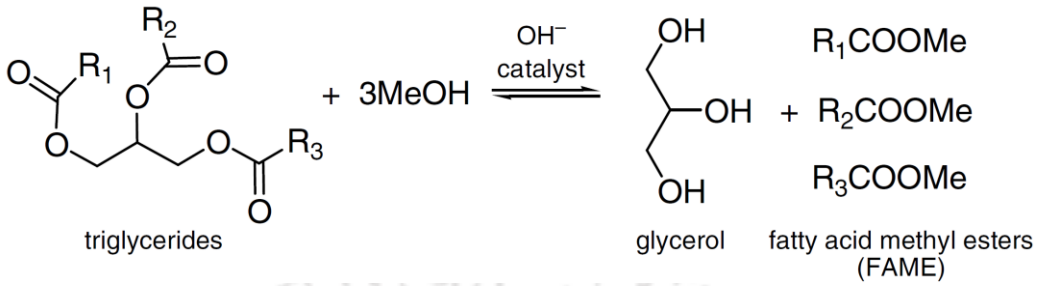

Figure 1-1 Transesterification of a triglyceride with methanol, yielding glycerol and fatty acid methyl esters

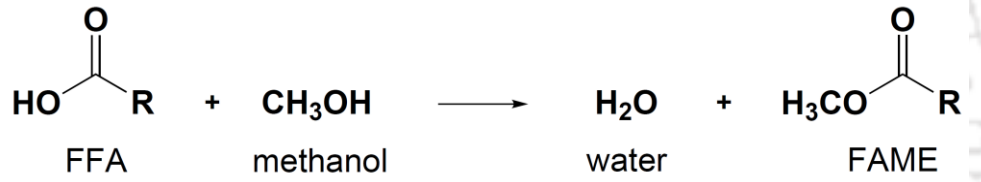

Figure 1-2 Esterification of a Free Fatty acid (FFA) with methanol to yield FAME and water

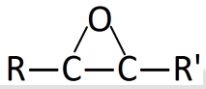

Figure 1-3 Epoxy group structure, where R and R' represent the continuation of fatty acid chain either side of the epoxy group

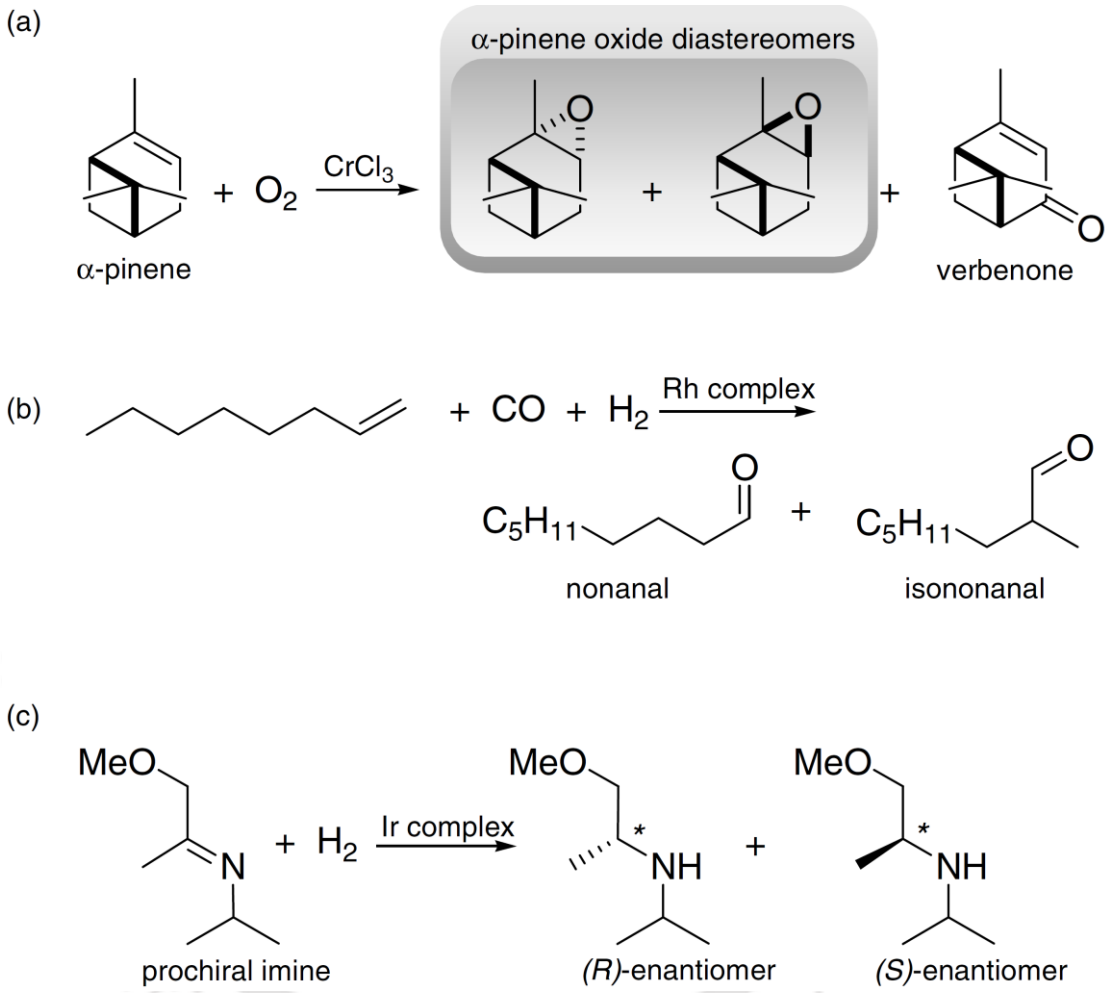

Figure 1-4 Examples of (a) chemoselectivity and diastereoselectivity in the oxidation of a-pinene, (b) regioselectivity in the hydroformylation of 1-octene, and (c) enantioselectivity in the hydrogenation of the prochiral isopropyl (2-methoxyisopropyl) imine (* indicates the asymmetric carbon atoms)

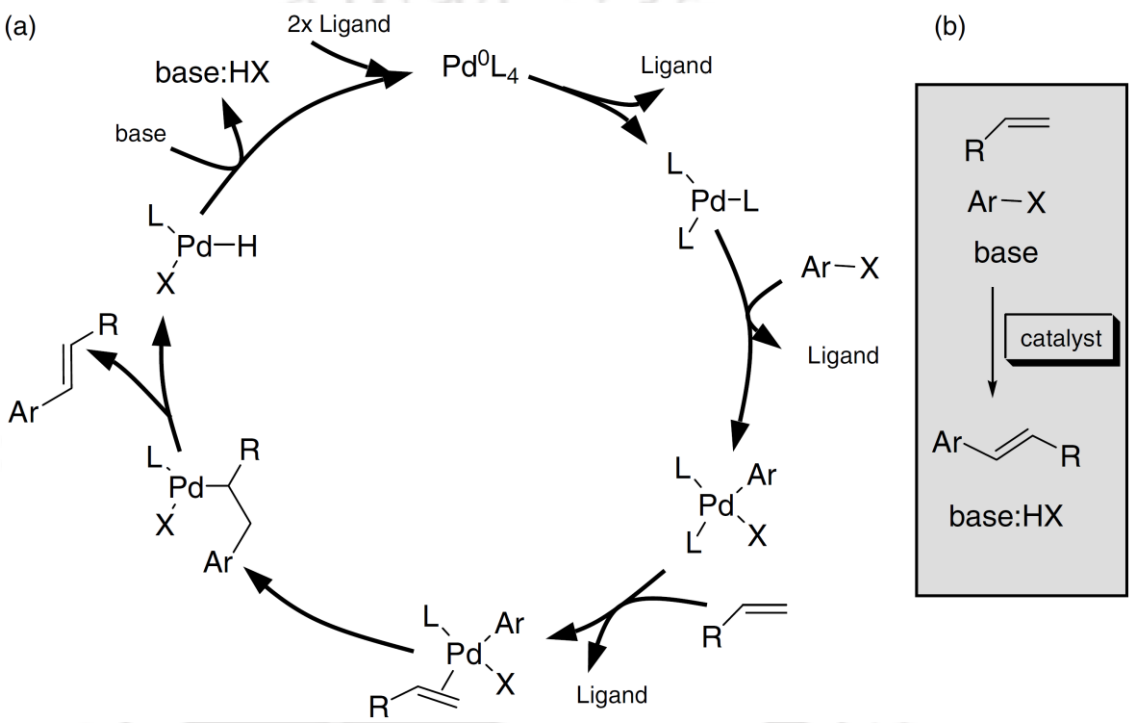

Figure 1-5 Proposed catalytic cycle for the Heck reaction, showing a) the various catalytic intermediates and b) the "black box" version

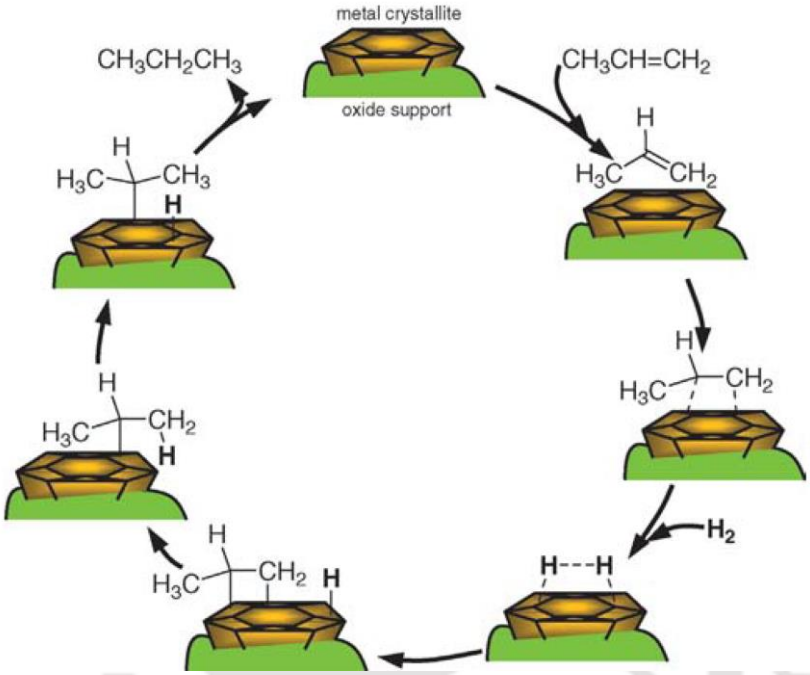

Figure 1-6 Hydrogenation of propene to propane in the presence of a supported metal catalyst (the reverse arrows are omitted for clarity)

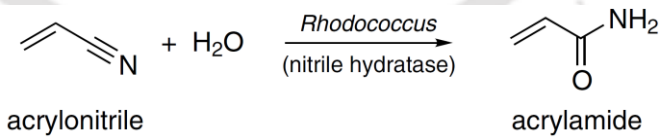

Figure 1-7 Biocatalytic synthesis of acrylamide from acrylonitrile

2 LITERATURE REVIEW AND OBJECTIVES

"The first step to knowledge is to know that we are ignorant"

Socrates

(470 – 399 B.C., Philosopher)

The catalysts which were used for methanolysis and epoxidation by researchers are discussed thoroughly. It includes the process parameters affecting the methanolysis and peroxidation processes. The advantages and disadvantages of using homogeneous, heterogeneous and enzymatic catalysts are also discussed subsequently. The literature study will ultimately lead to the knowledge gaps present in the earlier studies.

2.1 Methanolysis

2.1.1 Basic catalysts for transesterification

2.1.1.1 Inorganic metal-oxide bases

A wide range of basic oxides were investigated as catalysts for transesterification of oils and fats with methanol. Alkali or earth-alkali metal oxides or hydroxides are generally very basic and thus active, but usually the monometallic metal oxides tend to dissolve in the methanol over time. Calcining MgO with ZrO_2, however, yielded a bimetallic oxide with high basicity almost unaffected by dissolution [116, 117]. CuO, CoO, and MnO supported on Al_2O_3 was studied and yielded up to 97% FAME at room temperature, dependent on the calcination temperature [118]. ZnO and Al_2O_3–ZnO mixed oxide [119, 120] were investigated as well as rare-earth oxides [121], but both required high temperatures (at least 200 °C) for conversion of vegetable oils and methanol to FAME. However, bimetallic oxides of calcium ($Ca_2Fe_2O_5$, $CaMnO_3$, $CaCeO_3$, $CaTiO_3$ and $CaZrO_3$) were also investigated and catalysed transesterification with methanol at 60 °C, usually with good reusability of the oxide [122].

Porous materials like zeolites BEA, USY, and FAU and mesoporous silicalites like KIT-6, ITQ-6, SBA-15, and MCM-41 were ion-exchanged with La^{3+}, Mg^{2+}, or K^{+} and tested [123-125], however, high activities for transesterification to FAME are usually only obtained at higher temperatures (>150 °C) with some ion-exchanged porous silicalites, and it is a question if too small pores in the material is not a hindrance for reaction.

Basic hydrotalcites was extensively tested. These are comprised of layered units of mixed Al_2O_3−MgO, and due to their basicity and special porosity they are potential catalysts for transesterification to form FAME. Compared to other inorganic porous bases hydrotalcites often have superior activities for transesterification [126, 127]. Several researchers have characterised their properties and catalytic activity in relation to composition and calcination conditions [128-132]. Activity enhancements of the hydrotalcites was studied as well, for instance by doping with Cs, Ba, Sr, or La [133], by substitution of Al with Fe [134], or substitution of part of the Mg with Co [135]. Embedding hydrotalcite on a polymer-support was as well successful [136].

2.1.1.2 Organic amine bases

A number of different organic amines and derivatives functionalities were applicable for the transesterification of oils and fats: Earlier a number of alkylguanidines or cyclic guanidines were suggested as very active catalysts for transesterification, and substituted tetramethyl guanidine (R-TMG) or substituted 1,5,7-triazabicyclo(4,4,0)dec-5-ene (R-TBD) nested on PS/PVB polymer supports were suggested as heterogenised analogoues - due to very strong Lewis-basic sites [137, 138]. Up to 90% yield after 1 h methanlysis over 1 wt% of the homogeneous guanidines was obtained, and almost the same could be achieved over the heterogenised analogues [137, 138]. Carbon nanotubes doped with amines or gem-diamines have recently shown activity in the transesterification of triglycerides, however, reaction times were longer even at slightly elevated temperatures (up to 115 °C) [139, 140].

Methyl-substituted phosphazenium catalysts (based on units of $P{-}(N{-}(CH_3)X)_4$) could be applied as a strongly basic catalyst, either unsupported or linked to silica support [141, 142]. The unsupported catalysts yielded over 90% FAME in 15 min [142] at 60 °C,

while the supported phosphazeium had much lower activity, dependent on the loading of active compound on SiO_2 [142].

Transesterification reactions to achieve various alkyl mono- and diesters were performed with moderate success with amino-functionalised SBA-15, which however required 110 °C and 24 h reaction time [143]. Base-functionalisedmetal-organic frameworks (MOF) and supported quarternary substituted ammonium groups for methanolysis of various esters were investigated [144, 145], but the highest ester formation activity reported was 60% after 4 h at 60 °C, over 1 wt% of quarternary substituted ammonium functionalities [145].

2.1.2 Acidic catalysts for esterification

2.1.2.1 Acidic inorganic oxides and derivatives

Metal-oxide supported and zirconiumphosphate-supported tungstated catalysts (WO3/M(P)Ox) were investigated for the esterification of FFA, which readily takes place between 60 and 200 °C - at the highest temperatures the transesterification reaction of the glycerides is also pronounced [146-150]. Related to the solid tungstated oxides are the so-called heteropolyacids, based most regularly on tungsten or molybdenum phosphate. They are strong acids in their protonated form, and may be supported on metal oxide or even carbon [151]. By substituting some protons with a cation, for instance $Zr_{0.7}H_{0.2}PW_{12}O_{40}$, the acids became even more acidic and catalysed both esterification and transesterification at 65 °C within 4 to 8 h [152]. Completely protonated forms of tungstated and molybdated phosphate and silicates ($H_3PW_{12}O_{40}$, $H_4SiW_{12}O_{40}$, $H_3PMo_{12}O_{40}$, and $H_4SiMo_{12}O_{40}$) had different acidity, which however did correlate with transesterification activity: Molybdated samples where more active than tungstated ones [153]. This trend changed when supporting the catalysts on silica support [154]. A range of experiments were conducted with 12-tungstophosphoric acid ($H_3PW_{12}O_{40}$) supported on various materials, which easily catalysed the esterification of FFA in waste oils between 25 °C and 60 °C [155-157]. Also, a multifunctionalised mixture of $H_3PW_{12}O_{40}$ supported on Nb_2O_5 or Ta_2O_5 (and optionally SiO_2) was active for esterification at benign conditions [158, 159], and tuning this by adding non-polar alkyl groups to the structure enhanced reaction rates [160]. Some heteropolyacids may, however, suffer from leaching of the acidic species to methanol [161].

Related again to the tungstated oxides are sulphatedmetal oxides. For instance, the sulphated oxides of TiO_2, SnO_2 and ZrO_2 were suggested as novel acidic catalysts for the esterification of FFA with methanol to form FAME, as well as for the simultaneous transesterification of the triglycerides [162-167]. The same oxides were as well evaluated supported on or mixed with high-surface-area supports of Al_2O_3 or SiO_2 [162, 168-171]. It should be noted that some authors have reported leaching of sulphate species to the methanol solution from SO_{2-4}/MOx by hydrolysis due to formation of water by esterification. This is likely dependent on calcination conditions [167].

2.1.2.2 Acidic micro- and mesoporous silicalites

Various Brøndsted-acidic zeolites were shown to remove FFA via esterification at 60°C [172]. Higher temperatures were, however, required for Brøndsted-acidic Al-MCM-41 to esterify FFA [173]. By functionalisation of MCM-41 and SBA-15 through impregnation and grafting with respectively acidic WO3, Keggin- & Preyssler-type heteropolyacids and sulphonic acid functionalities, esterification of FFA with methanol could be achieved [174, 175]. However, the grafted sulphonic acid had far more superior activity to the other grafted acids on mesoporous supports, providing 55% ester yield at 60 °C after 6 h over 0.4 wt% catalyst. MCM-41 functionalised with organic linkers and tin-triflate functionalities were tested for FAME synthesis from methanol and soybean oil at 65-70°C with ultrasonic or microwave activation and up to 74% yield at 70 °C after 2 h were achieved [61] due to the use of microwaves.

2.1.2.3 Organic sulphonic acids

Amongst the acidic catalysts for esterification of FFA one type of organic acid was studied most extensively, namely sulphonic acids ($R{-}SO_3H$). Simple sulphonic acids soluble in methanol include methanesulphonic acid ($MeSO_3H$) and p-toluenesulphonic acid, however solid sulphonic acids can be prepared by sulphonation in sulphuric acid and thus grafting the functionality onto polymeric supports; the resulting acid is often as strong as or stronger than sulphuric acid. Commercial resin-type sulphonic acids can be purchased even in amounts applicable on a technical scale, for instance ion-exchange resins [176], and some are specifically marketed as catalysts for esterification of FFA. Esterification was performed over various Amberlyst-resins and Dowex HCR-W2-resins between 30 °C and 65 °C [177, 178], and satisfactory lowering of the FFA amount was

achieved within these conditions. Amberlyst BD20-resin was found superior to Amberlyst 15-resin, both with respect to recycling of the catalyst and tolerance to water [179]. A study between the commercial cation exchange resins NKC-9, 001x7, and D61 proved the former to be superior with FFA and methanol, yielding about 90% conversion of FFA at 62 °C after 2 h [180].

A number of polymer-based sulphonic-acids have been prepared for the esterification reaction and studied in the literature, for instance starting from PVA-PS/PVB [181], PS [182, 183], sulphonated PV and PS [184], or mesoporous silica with grafted functional groups [185], or polyanilines deposited on carbon [186]. The yields of sulphonic acid groups are usually between 0.6 and 6.0 mmol/g of the total supported catalyst mass. In all cases, esterification of FFA may be performed under normal operating conditions of 60 °C with 1-2 times molar excess of methanol.

Another approach for obtaining a sulphonic acid-containing polymer was first proposed by Toda et al. [187]. Initially a carbohydrate source, eg. sucrose, glucose, starch, or cellulose is carbonised (or pyrolysed) under inert atmosphere at around 400 °C for 4-24 h, then the resulting carbonated carbohydrate (now consisting of small graphene layers [188]) is sulphonated with concentrated or fuming sulphuric acid at elevated temperatures (around 150 °C) for 4-24 h. Low surface areas are obtained of the carbon material itself and its sulphonated derivative, which however increase upon swelling in hydrophilic solvent. Nonetheless the catalyst is very active in the esterification of FFA at 60 °C [189, 190]. The sulphonic acid obtained by this scheme had comparable strength to that of H_2SO_4 [191]. By following this procedure, a carbohydrate-based sulphonic acid was obtained which was investigated for both esterification and transesterification in methanol at 150 °C and 17 bar. While FAME did result from both reactions, leaching of sulphonic acid functionalities occurred at these conditions [192]. If the carbohydrate source is first impregnated on mesoporous silica, porosity and hydrophobicity can be tailored to the reaction desired [193], and esterification can take place at a faster rate due to an increased surface area induced by the support [194].

2.2 Peroxidation

2.2.1 Acid catalysts

The epoxidation of mahua oil (*Madhumica indica*) by hydrogen peroxide was studied by Goud et al. [64]. Mahua oil (*Madhumica indica*) was epoxidized *in-situ* with hydrogen peroxide as oxygen donor and glacial acetic acid as active oxygen carrier in presence of catalytic amount of an in organic acid. Catalytic loading of two different acids, i.e., H_2SO_4 and HNO_3 were studied and H_2SO_4 was found to be more effective in terms of conversion to oxirane. The effects of these parameters on the conversion to the epoxidized oil were studied and the optimum conditions were established. Relative conversion data showed that it was possible to develop epoxides from locally available natural renewable resources such as mahua oil. The epoxidation of mahua oil using *in-situ* generated peracetic acid could be carried out at moderate temperature range of 55-65 °C. Higher temperatures and higher sulphuric acid concentrations reduced reaction time and resulted in higher oxirane content with lesser cleavage to glycol. H_2SO_4 was found to be more effective in terms of oxirane conversion. The epoxidation reaction of mahua oil fell into kinetically controlled regime at stirring speeds >1500 rev/min. From the relative conversion data obtained for various reaction parameters, it could be concluded that it was possible to develop value added products such as epoxides from Mohua oil.

The kinetics of epoxidation of cottonseed oil by peroxyacetic acid generated *in-situ* from hydrogen peroxide and glacial acetic acid in the presence of liquid in organic acid catalysts were studied by Dinda et al [14]. It was possible to obtain up to 78% relative conversion to oxirane with very less oxirane cleavage by *in-situ* technique. The order of effectiveness of catalysts was found to be sulphuric acid > phosphoric acid > nitric acid > hydrochloric acid. Acetic acid was found to be superior to formic acid for the *in-situ* cottonseed oil epoxidation. The epoxidation of cottonseed oil using *in-situ* generated peroxyacids could be carried out at moderate temperature of about 60 °C. CH_3COOH was found to be more effective oxygen carrier than HCOOH. Out of all the liquid inorganic acid catalysts studied, H_2SO_4 was found to be the most efficient and effective. Higher temperature and higher acid concentrations reduced the reaction time needed to reach the maximum conversion to oxirane value; however, it simultaneously increased the extent of oxirane ring cleavage to glycols. The reaction was kinetically controlled beyond a

stirring speed of about 1800 rev/min. Maximum yield of oxirane with negligible amount of oxirane cleavage could be obtained if the epoxidation of cottonseed oil, using *in-situ* generated peroxyacetic acid, is carried out at optimum conditions. These optimum conditions include a temperature range of 50-60 °C, H_2O_2-to unsaturation mole ratio range 1.5-2.0, CH_3COOH-to unsaturation mole ratio of about 0.5 and H_2SO_4 loading of about 2% (by weight) of the aqueous phase.

Improved low temperature properties of 2-ethylhexyl 9(10)-Hydroxy-10(9)-Acyloxystearate Derivatives was done by Salimon and Salih. The epoxidation of oleic acid and other unsaturated hydrocarbon chains using H_2SO_4 as catalyst constitutes one of the most useful reactions in organic synthesis [195]. As the epoxide group is an active intermediate, it can be readily transformed to the required functionality. Here, they have report the synthesis of seven useful branched 2-ethylhexyl α-hydroxy stearate esters from commercially available oleic acid and common organic acids. The common organic acids used herein were octanoic, nananoic, lauric, myristic, palmitic, stearic and behenic acids. One of the products, the behenic ester of 2-ethylhexyl hydroxy stearate showed to have pour point, flash point and viscosity indices of -53, 161 °C and 215 cp, respectively, which are favorable properties in the synthesis of a bio-based lubrication base fluid. Overall, the epoxidation of oleic acid using H_2SO_4 as catalyst was successfully proceed and the data indicated that most of these synthesized derivative compounds have significant potential as lubricant base oil.

The impact of the relevant process variables on the reaction of soybean oil fatty acid methyl esters with per-formic acid (PFA) was studied. It was generated *in-situ* using concentrated hydrogen peroxide (up to 60 wt.%), to produce an epoxidized product in high yield, were studied in detail by Campanella et al [196]. The various parameters such as degree of mixing, temperature, concentration and molar ratios of reactants and/or use of diluents were considered. Temperature increases are significantly detrimental for achieving high oxirane numbers, as the selectivity to ring-opening reactions increases. Higher concentrations of either formic acid or H_2O_2 are also harmful (particularly, the carboxylic acid) but much less than temperature. a proposed alternative process, employing moderate temperature (up to 40 °C) and concentrated H_2O_2, compares favorably with the conventional one; higher conversion combined with high epoxide

productivity and selectivity are attainable. Using economically sound reactants molar ratios, under well-mixed regimes, in which the immiscible polar and organic phases are well dispersed, the epoxidation process can be adequately described using an (equilibrated) two-phase reaction model. The model accounts for both the reversible per acid formation (in the aqueous phase) and the epoxidation reaction proper, together with the attacks on the epoxide ring by formic acid and per formic (in the organic phase). In the epoxidation of soybean fatty acid methyl esters with PFA generated *in-situ* from FA using highly concentrated hydrogen peroxide (up to 60 wt.%) and moderate temperature (preferably 40 °C), the impact of temperature increases is significantly detrimental for achieving high yields and/or high oxirane-number. Higher concentrations of either formic acid or hydrogen peroxide are also harmful (particularly, the carboxylic acid) but much less than temperature. Nevertheless, this process alternative compares favourably to the conventional one, which is conducted at 60 °C using 30 wt.% H_2O_2; higher double bond conversion combined with high epoxide productivity and excellent selectivity are attainable. FA-to-double bonds and H_2O_2-todouble bonds molar ratios were used under well-mixed regimes. It was immiscible polar and organic phases which were well dispersed. Hence, the epoxidation process can be adequately described using an (equilibrated) two-phase reaction model accounting for just the reversible per acid formation (in the aqueous phase). As well as epoxidation reaction occured together with the attacks on the epoxide ring by FA and PFA (in the organic phase). The rate constants of epoxidation were determined by reacting formic acid with a number of oils, pure triglycerides (TAG) and pure fatty acid methyl ester (FAME) [197].

These results showed that FA composition had a significant effect on the value of the rate constant. In TAG, the double bonds of oleic acid and linoleic acid were equally reactive and the double bonds of linolenic acid were approximately three times more reactive than oleic and linoleic acids. For FAME, the rate constants of epoxidation increased as the level of unsaturation increased. Furthermore, the rate constants of epoxidation for the fatty acid methyl ester were higher than their respective TAG. It can be concluded that steric and electronic effects caused fatty acid with different levels of unsaturation to have different reactivities. These results were used to derive a model that predicts the epoxidation kinetics of oils from their FA composition. The predictions of the model closely match the experimentally determined rate constants.

The kinetics epoxidation of Rubber Seed Oil (RSO) by peroxyacetic acid generated *in-situ* were studied at various temperatures [198]. It was found that epoxidation with almost complete conversion of unsaturated carbon and negligible oxirane cleavage can be attained by the *in-situ* technique. The rate constant for epoxidation of RSO was found to be of the order of 10-6 L/mol/sec and activation energy of epoxidation of 15.7 kcal mol^{-1} was determined. Some thermodynamic parameters: enthalpy, entropy and free energy activation of 15.2, -31.94 and 25.44 kcal mol^{-1}, respectively were obtained for the epoxidation of RSO. The results from this study show that the epoxidation of RSO by peroxyacetic acid generated *in-situ* can be carried out at moderate temperatures with minimum epoxide degradation. The kinetic and thermodynamic parameters of epoxidation obtained from this study indicate that an increase in the process temperature would increase the rate of epoxide formation.

2.2.2 Enzymes

Epoxy alkyl stearates were synthesized by lipase catalysed esterification and per hydrolysis followed by epoxidation of oleic acid in a one-pot process [199]. Immobilized Candida Antarctica lipase (Novozym® 435) was used as the catalyst. The esterification reaction occurred relatively quickly and was followed by epoxidation of the alkyl ester and the remaining fatty acid. Higher degree of esterification was achieved with n-octanol, n-hexanol and n-butanol as compared to that with ethanol and iso-propanol. The rate and yield of epoxidation was enhanced with isopropanol but was lowered with the other alcohols. The lipase suffered significant loss in activity during the reaction primarily due to hydrogen peroxide. The presence of alcohols, in particular ethanol, further contributed to the enzyme inactivation. The epoxidation reaction could be improved by step-wise addition of the lipase. The enzymatic approach for the synthesis of alkyl epoxy stearates is a simpler and energy efficient alternative to the chemical process and the solvent-free conditions and good product yields further result in energy savings during product separation processes. The main limitation, however, is the low stability of the lipase under the reaction conditions employed. Possibility to use anhydrous reaction conditions and to minimize the exposure of the enzyme to the peroxide would be beneficial for improving product yields and performance of the biocatalyst. Unsaturated carboxylic acids are converted to percarboxylic acids catalyzed by an immobilized lipase from Cundid~z

Antarctica (Novozym® 435) [71]. These unsaturated percarboxylic acids are only intermediates and epoxidized themselves in good yields and almost without consecutive reactions. The mechanism of the oxygen-transfer is found to be predominantly intermolecular and the formation of the percarboxylic acids proceeds via two different catalytic reactions. The lipase is surprisingly stable under the reaction conditions; it is recovered and reused fifteen times to produce epoxy-steak acid on a multi-gram scale. The effect of reaction parameters on lipase-mediated chemo-enzymatic epoxidation of linoleic acid was investigated by Orellana-Coca et al [200]. Hydrogen peroxide was found to have the most significant effect on the reaction rate and degree of epoxidation. Excess of hydrogen peroxide with respect to the amount of double bonds was necessary in order to yield total conversion within a short time period, as well as at temperatures above 50 °C to compensate for hydrogen peroxide decomposition. However, prolonged incubation with high excess of hydrogen peroxide leads to the accumulation of peracids in the final product. The reaction rate increased also with increasing hydrogen peroxide concentration (between 10 and 50 wt. %); however, at the expense of enzyme inactivation. Linoleic acid was completely epoxidized when used at a concentration of 0.5-2 M in toluene at 30 °C, while in a solvent-free medium, the reaction was not complete due to the formation of a solid or a highly viscous oily phase, creating mass transfer limitations. Increasing the temperature up to 60 °C also improved the rate of epoxide formation. The parameters affecting the lipase activity and operational lifetime during chemo-enzymatic epoxidation of fatty acids were investigated [201]. Immobilized Candida Antarctica lipase B (Novozym® 435) was incubated in the presence of various reaction components (i.e., toluene, water, H_2O_2, oleic acid, perpalmitic acid and epoxystearic acid, respectively) at temperatures between 20 and 60°C followed by measurement of residual enzyme activity. Epoxy stearic acid was shown to slightly inactivate the enzyme at 50 °C, while oleic acid and perpalmitic acid did not. No deactivation of the enzyme was observed in presence of toluene/water mixture within 48 h at 20-60 °C. In the presence of 6-12 M hydrogen peroxide, the enzyme was rather stable at 20 °C, while at 60 °C the enzyme lost activity rapidly, with the rate of deactivation increasing with increasing hydrogen peroxide concentration. The authors reported that the parameters found to be most crucial for the activity. Hence operational stability of Novozym®435 in chemo-enzymatic epoxidation of fatty acids using hydrogen peroxide

at high concentrations with elevated temperatures was conducted. For epoxidation processes run at elevated temperatures, controlled addition of H_2O_2 is hence important for enzyme stability, especially in the beginning before the formation of water is sufficient to dilute the added H_2O_2. Since, the reaction is exothermic; a large-scale process would probably be most efficient if a temperature program is used. Concurrently with improving the process design, development of a more stable biocatalyst preparation would be an alternative strategy. Enzymes were found to have significant effect on the reaction rate and degree of epoxidation with good yields.

2.2.3 Heterogeneous catalyst

2.2.3.1 Ti (IV)-grafted Silica catalysts

The liquid-phase epoxidation of mixtures of Fatty Acid Methyl Esters (FAMEs) over titanium-containing silica materials, using tertbutylhydroperoxide (TBHP) as oxidant, was reported [78]. The mixtures were obtained from vegetable renewable source, i.e., from high oleic sunflower oil, coriander oil, castor oil and soya-bean oil. The influence of the nature and the position of functional groups on the C-18 chain of the FAMEs were studied. Very high activity and selectivity were obtained in the epoxidation of castor and soya-bean oil methyl esters in a reaction medium free from organic acids. Ti-MCM-41 ordered mesoporous titanium-grafted silica) displayed in this case, for the first time, superior performances, from a synthetic point of view, with respect to non-ordered mesoporous titan silicates. Titanium-grafted mesoporous silica materials showed to be suitable catalysts for the epoxidation of unsaturated FAME mixtures in a reaction medium that is completely free from organic acids. They are also versatile, as they were used over a series of four FAME mixtures obtained from different vegetable sources exhibiting interesting performances. In particular, very high conversion and selectivity values were obtained with Ti-MCM-41 in the epoxidation of castor oil or soya-bean oil FAME mixtures. In such cases, the superior catalytic performances displayed by this ordered mesoporous titan silicate with respect to the other non-ordered materials can be explained by the concurrence of various favorable factors. The presence of large amounts of highly accessible and well defined Ti(IV) tetrahedral active sites and the peculiar environment around the Ti(IV) sites (i.e., the high density of silanols surrounding the Ti(IV) sites), which accounts for the enhanced formation of epoxidized species when

highly polar moieties (for instance, hydroxy-group in methyl ricinoleate or an epoxy-ring in methyl mono epoxyoctadecenoate) are already present on the substrate molecules. However, interesting performances were also recorded over grafted non-ordered silicas and, over these materials, the titanium sites (considered singularly) showed remarkable turnover frequency values, even higher than those obtained over Ti-MCM-41.

2.2.3.2 Tungsten-based catalyst

A solvent-free, rather complete and selective cis epoxidation of Methyl Oleate (MO) using a tungsten containing catalyst is called Tetrakis [202, 203]. High epoxide yields were obtained by adjusting the reaction parameters (reaction time, temperature, gas phase, oxidant molar ratio and concentration). The highest selectivities are the result of a synergetic effect of hydrogen peroxide and air (or oxygen) used as oxidizing agents that decreases the MO dimerization and then favourable the complete conversion of MO into its epoxide. The use of the Tetrakis phosphotungstate catalyst leads to a rather complete and selective transformation of cis MO into cis epoxide under greener conditions than what was obtained in previous studies because it is performed with a stoichiometric amount of hydrogen peroxide, without solvent and at a lower temperature leading to a maximal H_2O_2 efficiency. Such a high yield is the result of a synergetic effect of hydrogen peroxide and air (or oxygen) used as oxidizing agents at a rather low temperature (313 K). This really high yield is also probably due to the low MO dimerization under these conditions because of the catalyst saturation by oxygen and also because of the modification of the H_2O_2 decomposition equilibrium. Finally, this epoxidation method can be extended to other unsaturated fatty compounds and crude vegetable oils.

2.2.3.3 Transition metal complexes

The epoxidation of methyl linoleate was examined using transition metal complexes as catalysts [204]. With a catalytic amount of methyltrioxorhenium (4 mol%) and pyridine, methyl linoleate was completely epoxidized by aqueous H_2O_2 within 4 h. Longer reaction times (6 h) were needed with 1 mol% catalyst loading. Manganese tetraphenylporphyrin chloride was found to catalyse the partial epoxidation of methyl linoleate. A mono epoxidized species was obtained as the major product (63%) after 20 h.

2.2.3.4 Ion exchange resin

Wild safflower oil (WSO) with an iodine value of 155 (g I_2/100g), and containing 13% oleic acid (C 18:1) and 72% linoleic acid (C 18:2), was epoxidised using a peroxy acid generated *in-situ* by the reaction of aqueous hydrogen peroxide and carboxylic acid in presence of strongly acidic Cation exchange resin, Amberlite® IR-122 [205]. Acetic acid was found to be a better oxygen carrier than formic acid and the use of catalyst improved the epoxide yield. A high temperature of above 60 °C is detrimental since at continued reaction it accelerated the rapid destruction of oxirane rings. Higher concentrations of acetic acid and hydrogen peroxide (above 0.5 & 1.5 mol/mol of ethylenic unsaturation respectively) are also unfavourable as they lead to epoxy ring opening. The study shows that a relative conversion to epoxide ring moiety of 85% can be achieved by using the optimum molar ratio 1:0.5:1.5 (ethylenic unsaturation: acetic acid: hydrogen peroxide) at temperature 60 °C and 2000 rpm. The results of the present investigation shows that WSO can be successfully utilized for epoxidation using peroxy acid generated *in-situ*. Acetic acid–IR- 122 combination was found to be most effective for higher epoxide yield at shorter reaction time. The optimized parameters to get higher degree of epoxidation with minimum epoxy ring breaking were noted as temperature of 60 °C, stirring speed 2000 rpm ensuring kinetically control of reaction, an acetic acid to ethylenic unsaturation molar ratio of 0.5:1, a hydrogen peroxide to ethylenic unsaturation molar ratio of 1.5:1, and a catalyst (IR-122) loading of 20 wt% of WSO. Under these optimum conditions, 7.87% oxirane oxygen content in synthesized ESWO was obtained. Canola oil with an iodine value of 112/100 g and containing 60% oleic acid and 20% linoleic acid, was epoxidised using a peroxyacid generated *in-situ* from hydrogen peroxide and a carboxylic acid (acetic or formic acid) in the presence of an Acidic Ion Exchange Resin (AIER), Amberlite IR 120H. Acetic acid was found to be a better oxygen carrier than formic acid, as it produced about 10% more conversion of ethylenic unsaturation to oxirane than that produced by formic acid under otherwise identical conditions. A detailed process developmental study was then performed with the acetic acid/AIER combination. The parameters optimized were temperature (65 °C), acetic acid to ethylenic unsaturation molar ratio (0.5), hydrogen peroxide to ethylenic unsaturation molar ratio (1.5) and AIER loading (22%). An iodine conversion of 88.4% and a relative conversion to oxirane of 90% were obtained at the optimum reaction conditions. The

heterogeneous catalyst, AIER, was found to be reusable and exhibited a negligible loss in activity. The epoxidation of canola oil using peroxy carboxylic acid generated *in-situ* was carried out most effectively using the acetic acid-acidic ion exchange resin combination. The epoxidation process with minimum oxirane cleavage was, therefore, optimized using acetic acid and the Amberlite IR- 120H (AIER) catalyst system. It was found that the epoxidation reaction occurred optimally at a temperature of 65°C, an acetic acid to ethylenic unsaturation molar ratio of 0.5:1, a hydrogen peroxide to ethylenic unsaturation molar ratio of 1.5:1 and a catalyst (AIER) loading of 22 wt.% of total canola oil used. Under these optimum conditions, 90% conversion of ethylenic unsaturation to oxirane was obtained, with a similar conversion of iodine. The AIER catalyst was found to be reusable. The formation of the epoxide adduct of canola oil was confirmed by FTIR and ^{1}HNMR spectral analysis. From the relative conversion data obtained, it can be concluded that it is possible to develop value-added products, such as epoxide, from canola oil. The kinetics of the epoxidation of soybean oil in bulk by peracetic acid formed *in-situ*, in the presence of an ion exchange resin as the catalyst, was studied by Sinadinović-Fišer et al. [65]. The proposed kinetic model takes into consideration two side reactions of the epoxy ring opening in vegetable oil living the formation of hydroxy acetate and hydroxyl groups as well as the reactions of the formation of the peracid and epoxy groups. The catalytic reaction of the peracetic acid formation was characterized by adsorption of only acetic acid and peracetic acid on the active catalyst sites and irreversible surface reaction was the overall rate determining step. Kinetic parameters were estimated by fitting experimental data using the Marquardt method. Good agreement between the calculated and experimental data indicated that the proposed kinetic model was correct. The effect of different reaction variables on epoxidation was also discussed. The conditions for obtaining optimal epoxide yield (91% conversion, 5.99% epoxide content in product) were found to be: 0.5 mole of glacial acetic acid and 1.1 mole of hydrogen peroxide (30% aqueous solution) per mole of ethylenic unsaturation, in the presence of 5 wt.% of the ion exchange resin at 75 °C, over the reaction period of 8 h.

2.2.3.5 Methyltrioxorhenium (VII)

Soybean oils (oleic, linoleic and linolenic acids and their methyl esters) were epoxidised readily with Urea-Hydrogen Peroxide (UHP) when Methyltrioxorhenium

(VII) supported on nobia was used as the catalyst in chloroform. Simple alkenes are epoxidised by the same method. The epoxide and not a diol is produced And also has been used the methyltrioxorhenium (MTO)-CH_2Cl_2/H_2O_2 biphasic system for epoxidizing soybean oil [206]. The reactions were optimized (reactant ratio, time and temperature), which resulted in a better performance (higher conversion and selectivity) than those described in the literature. Total double bond conversion and 95% selectivity were obtained in 2 h at room temperature. Furthermore, it was possible to reach desired epoxidation degrees by changing the oxidant and MTO amounts. The rhenium-epoxidised soybean oil remained stable in the absence of stabilizers for up to 30 day when stored at mild conditions. Methyltrioxorhenium (MTO) catalysed direct epoxidation by hydrogen peroxide. The reaction was carried out in pyridine, avoiding acidic conditions detrimental to high epoxide yield and uses less concentrated hydrogen peroxide (30%) than other methods. This method epoxidised soybean and metathesized soybean oil in high yield. The epoxidised metathesized oil was more stable to polymerization than that produced using m-chloroperbenzoic acid, presumably because it was free of acidic impurities. These and other novel approaches to epoxidation have recently been reviewed. None has yet found industrial application.

2.2.3.6 Amorphous $Ti.SiO_2$

A study of the epoxidation of soybean oil and soybean methyl esters with hydrogen peroxide in dilute solution (6 wt.%) using an amorphous heterogeneous Ti/SiO_2 catalyst in the presence of tert-butyl alcohol was studied by Campanella et. al. [207]. The influence of some relevant process variables such as temperature and the hydrogen peroxide-to-double bond molar ratio on performance is examined. The highest yields of epoxidized olefins were obtained upon using a H_2O_2: substrate molar ratio of 1.1:1. Higher ratios than this were not effective for speeding up the reaction. Under the experimental conditions employed in this work, no degradation of the oxirane ring was observed.

2.2.3.7 Alumina

Two commercial aluminas and one produced by the sol-gel process were compared for the epoxidation of unsaturated fatty esters using anhydrous or aqueous hydrogen peroxide as oxidant and ethyl acetate as solvent [208]. The aluminas showed a

good catalytic activity and excellent selectivity towards the epoxides. The sol-gel alumina was more efficient and when using aqueous hydrogen peroxide could be recycled several times. Alumina synthesized by the sol-gel method was shown to be an inexpensive and efficient catalyst in the epoxidation of methyl oleate and soybean oil methyl esters with aqueous hydrogen peroxide as oxidant. A conversion of 95% and selectivity >97% for the epoxide were obtained after 24 h without the use of any kind of homogeneous acid. After 4 cycles, a conversion of 87% was obtained. These results showed that sol-gel alumina is an alternative catalyst for the epoxidation of vegetable oils.

2.2.3.8 Chlorinated KU-2× 8 cation exchanger

A study of the epoxidation of soybean oil in the Course of Co-oxidation with Hydrogen Peroxide in the presence of propanoic Acid and Chlorinated KU-2×8 Cation Exchanger was studied by Gurbanov et al. [209]. The influence of some relevant process variables such as acetic acid and the hydrogen peroxide-to-double bond molar ratio on performance was examined. The catalyst. Some kinetic and activation parameters of soybean oil epoxidation were determined. The catalysts, chlorinated KU-28 Cation exchanger with a 9.5 wt % chlorine content and a Chlorinated KU-2×8 Cation exchanger was highly active and stable catalyst for Soybean oil epoxidation in the presence of acetic acid and hydrogen peroxide Chlorinated KU-2×8 Cation exchanger catalyzes only the formation of peroxy propionic acid and has no effect on the rates of oxidation of the double bond of soybean oil and of the opening of the epoxy ring of the target product, which increases the selectivity and efficiency of epoxidation and improves the quality of the target product.

2.3 Waste materials used for Methanolysis

2.3.1 Shells

2.3.1.1 Mollusc shells

Calcium oxide derived from mollusc shells was proven to be a potential heterogeneous catalyst for biodiesel production. Boey et al. investigated the use of waste mud crab shells (*Scylla serrata*) as a catalyst for the transesterification of palm olein and the report revealed that the calcined shell contains mainly CaO [210, 211]. Under the optimal conditions of 0.5:1 (mass ratio of MeOH:oil); catalyst amount, 4–5 wt.% and

reaction temperature 65 °C, the calcined catalyst could be reused several times without much reduction in its effectiveness. The performance of waste crab shells was comparable to the laboratory grade CaO. A similar observation was noticed for the catalyst from waste cockle shells (*Anadora granosa*), in which the calcined shell (900 °C, 2 h) could transesterify chicken fat [212]. Both of the waste catalysts recorded 98.2–99.0% methyl ester conversion in 3 h reaction time.

Xie et al. investigated the carbonization of biont shell (from turtle shells) [213]. The catalyst was prepared via a series of treatments; incomplete carbonization at 500 °C, followed by impregnation in KF, for 6 h at 25 wt.%, and, finally, thermal activation at 300 °C. The authors reported by observation at CO_2-TDP spectra that strong basicity sites were formed on the catalyst after the impregnation of KF. Chitin, the major constituent of the biont shell formed the active sites after reaction with KF. The report concluded that the heterogeneous catalyst from biont shell exhibited an excellent activity as well as stability under mild reaction conditions. Similar work was reported using shrimp shells [213]. The catalyst was prepared in a similar manner as the biont shell, except for the carbonation temperature (450 °C) and activation temperature (250 °C). While using biont shell recorded a yield of 97.5% in 3 h (3% catalyst), this waste reported a conversion of 89.1% in 3 h (2.5% catalyst).

Nakatani et al. [214] investigated the use of waste oyster shells as a catalyst in the transesterification of soybean oil. In a 5 h reaction, a methyl ester content of 98.4% was achieved. Similar to mud crab and cockle shells, the main constituent of the calcined oyster shell is CaO. Sea snail shells (*Turbonilla striatula*) were also found to be a source of CaO in the investigation by Boro et al. [215]. The calcined (800 °C, 4 h) shell was able to transesterify mustard oil with a yield of 93.3 wt.%, in a 6 h reaction. In term of reusability, the catalyst was stable until the second cycle and exhibited a sharp reduction for the third and fourth cycles. However, the authors found that the used catalyst can be reactivated upon calcination at 900 °C for 3 h.

Another CaO source was derived from calcined waste freshwater mussel shells, from the work of Hu et al. [216]. The catalyst was prepared by calcination (900 °C, 4 h) then impregnation in deionized water before being thermally activated again (600 °C, 3 h). In this way, a ‘honey-comb’ catalyst structure was obtained, which recorded the

highest surface area at 23.2 m^2 g^{-1}. The resultant catalyst was able to yield 90% methyl ester in 1.5 h of reaction time. Interestingly, the catalyst can be reused seven times before the yield dropped below 90%, maintaining 80% yield up to the twelfth cycle and 60% yield at the seventeenth reuse.

Calcium oxide can also be derived from waste egg shells, snails (golden apple), and clams (Meretrix venus) [217]. The calcined (800 °C, 2–4 h) shells were able to produce methyl ester content over 90%, in 2 h reaction time; egg shells and snail shells have higher initial activities.

2.3.1.2 Egg shell

Chicken and quail egg shells were found to be a reliable source of CaO, consisting of 85–95% of calcium carbonate and 15–5% other components ($MgCO_3$, phosphate, organic matter and a small amount of metal) in dry egg shells [218]. The catalytic performance was comparable to laboratory grade CaO in transesterification. In a 3 h reaction time, Wei et al. [104] achieved 95% biodiesel yield and reported that the catalyst can be reused 13 times without any significant loss of activity. Viriya-empikul et al. [217] also reported the good performance of egg shells in transesterification. Chicken egg shell contains the highest calcium and has larger surface area as compared to golden apple snail and Meretrix venus shell. Recently Semwal et al. [219] prepared the metal oxide $CaTiO_3$ using egg shell by calcination at 1050 °C for 3.5 h; yielding over 95% methyl ester content. The metal oxide catalyst was stable for four reuse without any major structural changes as confirmed through XRD. It proves that regardless of the origin, CaO could catalyze the reaction with success. Calcium oxide from these waste sources compliments where they could be co-used with laboratory grade CaO.

2.3.2 Ashes

2.3.2.1 Empty palm fruit bunch-based boiler ash

Empty palm fruit bunch (EPFB) fibre (dry basis) consists mainly of glucan (42.85%), xylan (24.01%), lignin (11.70%) and other components. As for oxides, EPFB contains potassium oxide as the major constituent, followed by silica, calcium oxide and others [220]. The ash was successfully utilized by Boey et al. [221] as a catalyst in the transesterification of palm olein. With oven drying (105 °C, 2 h), 3 wt.% ash was capable

of transesterifying palm olein at 90% conversion in a 0.5 h reaction time. However, since the ash acts as pseudo-homogeneous, it is intolerant to the presence of moisture and FFA at 1 wt.% in the feedstock.

The transesterification reaction of palm oil with methanol using a methanolic extract of empty fruit bunch ash (EFBA) as a homogeneous catalyst was reported by Imaduddin et al. [222]. In contrast, Yaakob et al. [223] used EFBA as a heterogeneous catalyst. They made a comparison between EFBA and the EFBA doped with 20 wt.% KOH and used Jatropha curcas oil for the transesterification. Optimum conditions for the EFBA-catalyzed reaction were 20 wt.% EFBA; MeOH/oil molar ratio 15:1 at 65 °C, for 90 min; a maximum oil conversion of 98.54% was achieved and the report showed that the KOH/EFBA catalyst reaction has better activity than the EFBA alone; 99.45% conversion in the much shorter reaction time of 45 min at 15 wt.%. The reusability study of the catalyst indicated that KOH/EFBA is a better catalyst for repeated use. After five cycles, the conversion of both catalysts was more than 85%. The decreased activity of the catalyst after the fifth run was confirmed by XRF analysis due to the absence of metals like K and Ca, which indicates leaching of the active ingredients.

2.3.2.2 Fly ash

Fly ash as an inorganic waste generated from coal combustion processes has a typical chemical composition (on dry basis), of around 55% SiO_2, 30% Al_2O_3 and other oxides [224]. It is obvious that the oxides of both silica and alumina could work excellently as a catalyst support. Consequently, researchers have used thermally activated fly ash as a support for loading CaO for chemical production. This supported catalyst gave higher conversions of up to three cycles and the catalyst was able to be reused without much loss in the activity. The presence of the high amount of SiO_2 and Al_2O_3 prompts its potential applicability as a low-cost catalyst support. In a recent work, fly ash supported CaO has been employed as a recyclable solid base catalyst [225]. Fly ash supported heterogeneous CaO catalyst from egg shells have been investigated to transesterify soybean oil [226]. Fly ash supported a CaO catalyst prepared by wet impregnation method, with 30 wt.% CaO loading and followed by calcination at 1000 °C for 2 h. A maximum FAME yield of 96.97% was achieved with 6.9:1 methanol/oil molar ratio. The study of the reusability of catalyst showed higher catalytic activity in which the

catalyst showed remarkable repeated usability of 16 times without major loss in activity; indicating a high degree of catalyst stability. However, the catalyst became completely deactivated after being used more than 18 times. Fly ash-based base catalyst was investigated by Kotwal et al. [227], in the transesterification reaction of sunflower oil. The catalyst was prepared by the conventional wet impregnation method using KNO_3. In the work, fly ash loaded with 5 wt.% KNO_3, followed by calcination at 500 °C was able to convert the oil at 87.5% in 8 h reaction time. However, the catalyst suffered from being reused, probably due to the leaching of active species. Similarly, Babajide et al. [228], reported that fly ash loaded with 5 wt.% KNO_3 could transesterify sunflower oil to about 86% but at an elevated reaction temperature of 160 °C. Similar to the previous study, the catalyst also suffers with respect to its reusability.

2.3.3 Rocks

Alum ($KAl(SO_4)_2$) has a traditional role in water treatment and potential as a catalyst in the transesterification of palm oil. Aderemi and Hameed reported the preparation of alum as a catalyst in the transesterification of palm oil [229]. The alum successfully transesterified the oil to 92.5%, with 7.09 wt.% catalyst and MeOH/oil molar ratio of 18:1 in 12 h reaction time at an elevated temperature of 170 °C. Another potential catalyst with high carbonate content originating naturally are dolomite ($CaMg(CO_3)_2$) and calcite ($CaCO_3$). At present, the low cost of dolomite is the main reason of major domestic usage in cement manufacturing and landfill. While dolomite consists of 23.5% Ca, 12.1% Mg, 63% CO_3 and 1.4% other components (Fe, SiO_2, PO_2, SO_4) [230], calcite contains high purity of $CaCO_3$ (over 91 wt.%) [231]. Both dolomite and calcite could be easily transformed to CaO and MgO by thermal activation. Comparison of dolomite and calcite was reported by Ngamcharussrivichai et al [231], in the transesterification reaction of palm kernel oil (PKO). In their study, the dolomite successfully transesterified the PKO, over 98% methyl ester, under the reaction conditions of: 6 wt.% catalyst, MeOH/oil molar ratio 30:1 in 3 h reaction at 60 °C. Meanwhile, calcite performed at 46.8% methyl ester under the same reaction conditions. The calcined dolomite at 800 °C for 2 h could be reused up to seven cycles without much loss in the activity.

2.3.4 Bones

Bone from waste Rohu fish (*Labeo rohita*) was reported as another low-cost heterogeneous catalyst for the synthesis of biodiesel from soybean oil [232]. The analysis of TGA and XRD revealed that a significant portion of the main component of fish scale, hydroxyapatite, could be transformed into b-tri-calcium phosphate when calcined above 900 °C for 2 h, with optimal conditions of MeOH/oil molar ratio, 6.27:1, catalyst at 1.01 wt.% for 5 h. This compound was able to yield 97.73% of methyl ester. The reusability of the catalyst shows that it could be reemployed up to six times. Similar work was reported using sheep bone [111]; the calcined bone at 800 °C, transformed calcium phosphate of the bone into hydroxyapatite with an increase in surface area. In a 4 h reaction, methyl ester content of 96.78% was obtained under the reaction conditions of: methanol to oil 18:1 (molar ratio) and 20% catalyst at 65 °C. The catalyst was stable for five cycles at 83.7% conversion. On the other hand, cuttle bone (calcined at 800 °C for 2 h) could also catalyze transesterification of PKO but with much lower conversion (24%) although the bone contains over 91 wt.% $CaCO_3$ [231]. Increasing the calcination temperature of the bone to above 800 °C may increase the methyl ester conversion.

2.4 Waste materials used for Peroxidation

To the best of our knowledge no work has been reported on peroxidation of vegetable oil using waste materials as catalyst.

2.5 Knowledge gaps and objectives

The literature survey motivated to grab the particular node which was a major lacuna in the earlier work published. Based on the knowledge gaps the major 3 objectives to the current research was decided and planned accordingly.

2.5.1 Knowledge gaps

Cost-effectiveness plays a major role when a lab grade experiment is escalated to the industrial grade application. In the literature survey section, it was clearly observed that most of the works were based on costly homogeneous catalyst. The homogeneous catalysts such as HNO_3, H_2SO_4, HCl, KOH which are difficult to separate from the mixture were used extensively. The enzymatic catalysts are more effective; however, the

cost is high. Though some of the heterogeneous catalysts used were synthetic which are less costly than homogeneous and enzymatic; however, low cost catalysts from natural sources with scantly reported.

The moment natural sources or the waste product is considered, there were a number of materials were listed and thoroughly discussed. Still there are enough materials being available and are having catalytic potential were not explored.

The potential of waste material for catalytic purpose was verified by various physical and chemical characterization. However, the major issue lies in the application part. It was observed that very scant information was available on the application of the materials for peroxidation and methanolysis.

The above knowledge gaps helped identifying three objectives which are listed as follows.

2.5.2 Objectives

1. Preparation of heterogeneous catalysts by deposition of metal and metalloid on bio-wastes

2. Study of catalytic activity of the developed catalysts during methanolysis and peroxidation reactions

3. Comparative study of these catalysts used for methanolysis and peroxidation reactions along with the reusability study

3 MATERIALS AND EXPERIMENTAL METHODS

"Research is to see what everybody else see and to think what nobody else has thought"

A. Szent-Gorgyi

(Hungarian Biochemist, 1937 Nobel Prize for Medicine)

3.1 Materials required for preparation of catalyst

The catalyst was developed from 3 waste materials i.e. waste fish bone, groundnut shell and red crab shell. The cooked waste fish bone (CWFB) was collected from Indian Institute of Technology (IIT) Guwahati hostel messes. Waste groundnut shell (WGS) was obtained from a dumping yard of nearby market located in Amingaon, Guwahati, Assam. The neem oil was collected from Rourkela, Odisha. The waste cooking oil was collected from Brahmaputra hostel mess, IIT Guwahati. The chemicals viz. 25% aqueous ammonia solution, KOH, methanol, Aluminum nitrate ($Al(NO_3)_3.9H_2O$), Magnesium Sulfate ($MgSO_4.7H_2O$), Sodium Silicate ($Na_2O_3Si.9H_2O$), sulfuric acid, NaOH, formic acid, hydrogen peroxide and zinc sulfate ($ZnSO_4$), Titanium tetraisopropoxide ($Ti(OCH(CH_3)_2)_4$) were procured from Sigma Aldrich, India and Merck, India. Except waste raw materials the purchased consumables were used as it is without any further treatment.

3.2 Pre-treatment of Raw materials

The CWFB was washed under the tap water for the removal of flesh and adhered proteinaceous part and dried under sun for 2 days. After that it was plunged in acetone for 24 h and dried at 60 °C for complete evacuation of oily matters. The CWFB was consequently crushed and biological hydroxyapatite (CWFB-HAp) was obtained. The WRCS was also pre-treated as per CWFB pre-treatment because both the waste materials are from biological sources. WGS was first jet washed to remove impurities and dirt

present in it. Then it was sun dried for 2-3 days and then kept in hot air oven for 6 h. Finally, all the materials viz. CWFB, WRCS and WGS were crushed to fine powder and stored in an air tight container till further use.

The neem oil and waste cooking oil was passed through a sieve to remove solid floating materials. Then the oil was characterized to observe the basic properties which are listed in Table 3-1.

3.3 Wet impregnation of metal oxides

The wet impregnation method is followed to prepare heterogeneous catalysts. A typical wet impregnation is followed by dissolving the active metal precursor in an aqueous or organic solution. Then the metal-containing solution is added to a catalyst support. The capillary action plays a major role and draws the solution into the pores of support material. Solution added in excess of the support pore volume causes the solution transport to change from a capillary action process to a diffusion process, which is much slower. The catalyst can then be dried and calcined to drive off the volatile components within the solution, depositing the metal on the catalyst surface. The maximum loading is limited by the solubility of the precursor in the solution. In this section various metal precursors were used to prepare metal supported catalyst.

3.3.1 Waste fish bone/HAp (HAp-Al, HAp-Zn, HAp-Mg, HAp-Na-Si)

Aluminium was doped on HAp to prepare the doped catalyst (HAp-Al) using the wet impregnation method. For this, 0.5:1, 1:1 and 1:0.5 wt. proportions of HAp and the concerned oxide, Aluminium nitrate were mixed followed by calcination at 650 °C temperature. For preparation of 1:1 HAp-Al catalyst, 30 g of $Al(NO_3)_3.9H_2O$ was added to 100 mL of water (Millipore) to get a ready solution of Aluminium nitrate. To this solution, 30 g of fine powder of HAp was added gradually according to the wet chemical precipitation technique and blended rigorously using a mechanical agitator under aggregate reflux time of 30 mins. The pH was maintained at 11.0 by using 25% aqueous ammonia solution. The entire solution was again mechanically mixed at 700 rpm at 60 °C for 2 h. The resultant solution was kept for 24 h at room temperature so as to allow the deposition of Aluminium ions on HAp. Then the mother liquor was removed by vacuum filtration and a sticky precipitate was obtained which was then subjected to

drying using a hot air oven. The dried mass was then subjected to calcination at 650 °C for 3 h [4]. Similar procedure was applied for making catalysts with different HAp to Aluminium nitrate loading in order to analyse the effects of Aluminium nitrate loading on the properties of catalyst. Thus, as per the three weight proportions *i.e.* 0.5:1, 1:1 and 1:0.5 of HAp to Aluminium nitrate, the catalyst were herein after designated as $0.5H_A$, $1H_A$ and $2H_A$ respectively.

For ZnO deposition on HAp, $ZnSO_4$ was used as metal precursor and the pH was maintained at 6.0 by 25% aqueous sulfuric acid solution. The final sticky matter was oven dried (110 °C) followed by calcination for 3 h at 650 °C. The final product was crushed to fine powder and then characterized. Another set of samples were also prepared to study the catalytic effect of metal oxide. For this set, HAp was calcined at 650 °C for 3 h and kept in an airtight container in the form of powder. For the present work, three heterogeneous materials i.e. HAp, calcined HAp (CHAp: 650 °C calcination temperature) and HAp-Zn were readied for the comparison purpose during peroxidation.

For the preparation of HAp-Mg, Magnesium sulfate was used as the precursor for metal ions during wet impregnation. Following the method, 1:1 wt. proportions of HAp and MgO were prepared. 30 g of $MgSO_4.7H_2O$ was added to 100 mL of water (Millipore) to get a solution of Magnesium sulfate. To this solution, 30 g of fine powder of HAp was added gradually and blended rigorously using a mechanical agitator under aggregate reflux time of 30 min. 25% aqueous ammonia solution was used to maintain pH at 11. The entire solution was mechanically stirred for 2 h at 700 rpm at 60 °C. The final solution was kept for 24 h at room temperature so as to allow the deposition of Magnesium ions on HAp. After that mother liquor was vacuum filtered and the sticky precipitate obtained was dried in hot air oven. The dried mass was then calcined at 650 °C for 3 h and final Mg grafted HAp (HAp-Mg) was sent for characterization.

Similar method was followed to prepare HAp-Na-Si, however the precursor used was Sodium Silicate.

3.3.2 Waste groundnut shell (WGS-Mg)

For Mg ion deposition, $MgSO_4.7H_2O$ was used as a precursor. To prepare a typical 1:1 weight proportions of WGS and Mg (WGS), initially a salt solution of

Magnesium sulfate was prepared by mixing 50 g of $MgSO_4.7H_2O$ and 100 mL of water (Millipore). Subsequently, 50 g of crushed WGS was mixed steadily in the salt solution followed by uniform blending using a mechanical stirrer. Finally, the pH of the mixture was maintained by the gradual addition of 1 N ammonia salt solution. After maintaining 12 pH, the whole mixture was rigorously agitated under mild heating condition. For aging purpose, agitation was stopped after 2 h and the uniform mixture was kept untouched overnight under ambient condition. After that the unit mother liquor was separated using vacuum filtration. The remaining precipitated matter was oven dried for 2 h. The dehydrated and agglomerated mass was thus obtained was put in a closed furnace. The calcination was continued for 3 h at 700 °C. Following the same method 1:2 and 2:1 weight proportions of WGS to Mg was prepared and the Mg grafted WGS was kept in an air tight container. The final product then sent for characterization.

3.4 Characterization methods of materials

3.4.1 X-ray diffraction

The structural analysis was done using X-ray diffractometer (Bruker D8 advance, Massachusetts, United States). Cu anode was used as X-ray radiation source. Kα radiation wavelength (λ) was 0.154 nm and subsequent operating voltage and current was 45 kV and 40 mA respectively. The scanning was done within the 2θ range of 10° and 90°. For all the prepared samples the scanning increment was fixed to 0.05 with the rate at 0.5 s/step.

3.4.2 FTIR (Fourier transform infrared spectroscopy) analysis

Fourier transform infrared spectroscopy (FTIR) provides information with respect to various functional groups present in the sample. DRS connected with Excalibur Bio-Rad spectrophotometer (Model FTS 3500 GX) FTIR analyser was utilized for the same. The IR range was between 400 and 4000 cm^{-1} at a scan rate of 40 and at a step size of 4 cm^{-1}.

3.4.3 Surface area analysis

The surface area analysis was studied using Beckman-Coulter; Model: SA3100 (California, United States) surface analyser. The porous properties, for example BET

surface area, average pore measurement and pore volume (t-plot strategy) were calculated by physical adsorption-desorption of N_2 at the boiling point (77 K). Preceding the examination, the reactant was subjected to a preheating at 423 K under vacuum for 90 min.

3.4.4 Micro structure analysis

The powder morphology studied under the specified conditions was contemplated by a field emission scanning electron microscope (JEOL-JSM-6390LV, Japan) furnished with an EDAX PV 9760 detector for Energy Dispersive X-ray spectroscopy (EDX) to investigate nearby chemical arrangement. When mounting on a sample holder for FE-SEM investigation, the samples were dispersed in methanol and deposited on an aluminium foil and then coated with Gold-Palladium to make the specimen fit for microstructures investigations.

3.4.5 TEM analysis

The microcrystalline nature of the developed catalyst was observed from transmission electron micrographs (TEM) and selected area electron diffraction (SAED) pattern. It was acquired from JEM 2100 (USA) electron microscope operated at 200 kV.

3.4.6 Thermogravimetric analysis

The weight loss with reference to temperature was observed in NETZSCH (STA 449F3 Jupiter, Selb, Germany) thermal analyser. The degradation profile of the catalyst was studied in a noble gas (Argon) environment. For all the prepared samples the rate of heating was pre-set to 10 K min^{-1}. The maximum temperature was set at 1000 °C.

3.4.7 Particle size analysis

Particle size distribution of the developed catalyst was carried out using a particle size analyzer (Make: Beckman Coulter, Model: Delsa^{TM} Nano C, California, United States). The sample was prepared by dispersion of catalyst in deionized water (Millipore) followed by sonication for 20 minutes.

3.5 Methanolysis of Neem oil and waste cooking oil

Methanolysis (Figure 3-3) was performed by means of a batch reactor system consisted of three mouth vessel (max. capacity 500 mL) and a Microprocessor based PID controlled heating system. In a typical reaction 50 g of oil and measured volume of methanol were taken. To prevent methanol evaporation 2 condensers were attached to the reactor. The whole mixture was constantly stirred using a mechanical agitator. To study the effect of stirring the rpm value was varied during the course of reaction. With continued stirring, slowly the catalyst (measured wt.%) was added to the reactor for uniform mixing. For every batch the reaction temperature was varied. After completion of reaction, the mixture was immediately centrifuged to remove the catalyst and then transferred to a separating funnel. The reacted mixture was kept overnight to allow gravity separation of esterified product. Then the rest of the liquid transferred to a rotary evaporator to remove excess methanol. Subsequently, to ensure complete removal of catalyst, water and glycerol, the solution was centrifuged at 2000 rpm. After catalyst removal the remaining reaction mixture was sent to characterization lab for the methyl ester yield analysis. Following the conventional method, effect of catalyst loading was studied with varying temperature between 60 °C to 90 °C. A controlled run was also carried out without presence of the catalyst to observe the usefulness of the developed catalyst. An extensive catalytic effect was studied by observing the reaction kinetics during the progress of reaction. For the kinetic study, a specific volume of sample was taken out from the reaction chamber which was considered negligible compared to the total reaction mixture. The collected samples were finally analysed to observe the methyl ester yield. The yield was calculated using the method reported elsewhere [5]. The samples were then sent for qualitative and quantitative characterization.

3.6 Peroxidation of neem oil

Peroxidation (Figure 3-4) of pure neem oil was carried out in a batch reactor using the conventional heating system. The batch reactor consisted of a three-mouth flask, mechanical stirrer, and a reflux condenser. 20 g of oil and specified amount of catalyst was weighed and transferred to the reactor. Formic acid was then added with constant stirring speed (800 rpm) followed by dropwise addition of Hydrogen peroxide. After a specified reaction time, the reaction mixture was taken out of the reactor, and catalyst was

vacuum filtered out of the mixture. Then the solution was put in a centrifuge to separate the upper layer i.e. epoxide oil product. Carboxylic acid was completely removed from the product using water washing followed by centrifugation. The final product was analysed by measuring Iodine value and Oxirane Oxygen content (OOC).

3.7 Characterization of oil and final products

3.7.1 FTIR (Fourier transform infrared spectroscopy) analysis

Fourier transform infrared spectroscopy (FTIR) provides information with respect to various functional groups present in the sample. For liquid samples KBr pellet method was used. This method exploits the property that alkali halides become plastic when subjected to pressure and form a sheet that is transparent in the infrared region. Potassium bromide (KBr) is the commonest alkali halide used in the pellets. Approximately 200 to 250 mg fine KBr powder is to be put into a pellet-forming die. A force of approximately 8 tons is applied under a vacuum of several mm Hg for several minutes to form transparent pellets. Degassing is performed to eliminate air and moisture from the KBr powder. Inadequate vacuum may result in easily broken pellets that scatter light. Before forming the KBr powder into pellets, pulverize it to 200 mesh max. and then dry at approximately 110 °C for two to three hours. After drying the powder, it was stored in a desiccator. When performing measurements, the background can be measured with an empty pellet holder inserted into the sample chamber. However, background measurements on a pellet holder with a pellet of KBr only, that contains no sample, can correct for infrared light scattering losses in the pellet and for moisture adsorbed on the KBr. The sample holder is connected with Excalibur Bio-Rad spectrophotometer (Model FTS 3500 GX) FTIR analyzer was utilized for the same. For sample analysis, 10 mg of sample was put on KBr pellet. The IR range was between 400 and 4000 cm^{-1} at a scan rate of 40 and at a step size of 4 cm^{-1}.

3.7.2 ^{1}HNMR

The sample was first dissolved in Chloroform-d, 99.8 atom% D and was placed in NMR tube. The analysis was conducted using 600 MHz Nuclear Magnetic Resonance (NMR) Spectrometer (Made: Bruker, Massachusetts, United States).

3.7.3 Physico-chemical property analysis

The Acid Number of oil *(Azadirachta indica)* and transesterified product was determined by colorimetric titration as per ASTM D974 and saponification number of raw oil was calculated as per ASTM D5558 [233].

Qualitative studies were done by analyzing its Iodine value conversion (IV_C), Oxirane Oxygen content (OOC %) and Turnover number (TON). Wijs method was applied to find out the Iodine value.[234] To determine iodine value and a conversion following equations were used.

For Iodine value: $$\frac{(B-S)\times N\times 12.69}{W} \quad \textbf{3-1}$$

For Iodine value Conversion: $$\frac{IV_{PNO}-IV_{ENO}}{IV_{PNO}} \quad \textbf{3-2}$$

Where, B=Volume of $Na_2S_2O_3$ solution required for titration of the blank (mL), S=Volume of $Na_2S_2O_3$ solution required for titration of the sample (mL), W=Weight of sample used (g), N= Normality of the $Na_2S_2O_3$ (0.1N), IV_{PNO}= Iodine value of pure neem oil, IV_{ENO}= Iodine value of epoxidized Neem oil.

The Oxirane Oxygen content and simultaneously OOC % conversion was determined by an adapted method [235]. The following equations were used to obtain Oxirane oxygen content.

For experimental Oxirane Oxygen content: $$\frac{(V_b-V_s)\times N\times 16\times 100}{W\times 1000} \quad \textbf{3-3}$$

For theoretical Oxirane Oxygen content:

$$\left(\frac{IV_{PNO}\Big/2A_{Iodine}}{100+\left(IV_{PNO}\Big/2A_{iodine}\right)A_{Oxygen}}\right)A_{Oxygen}\times 100 \quad \textbf{3-4}$$

Relative OOC % Conversion: $$\frac{OOC_{\exp}}{OOC_{the}}\times 100 \quad \textbf{3-5}$$

Where, V_b, V_s are Volume NaOH used for blank (mL) and sample (mL) respectively, N = Normality of the NaOH (0.1N), W =Weight of sample used (g), I_{PNO}= Iodine value of PNO, A_{Iodine}= Atomic weight of Iodine, A_{Oxygen}=Atomic weight of Oxygen, OOC_{exp}= Experimental Oxirane Oxygen content, OOC_{the}= Theoretical Oxirane Oxygen content.

Table 3-1 Physico-chemical properties of oils

Properties	Neem oil	WCO
Colour	Pale yellow	Brown
Physical state (25 °C)	Liquid	Liquid
Density (g cc^{-1})	0.91	0.921
Acid Value (mg KOH g^{-1})	41.62	2.8
Saponification value (mg g^{-1})	227.24	191.3
Iodine Value (g 100 g^{-1})	80.75	92.7
Oleic acid (wt. %)	67.3	42.5
Steric acid (wt. %)	16.3	3.8
Palmitic acid (wt. %)	15.1	32.4
Linoleic acid (wt. %)	0.15	15.3
Myristic acid (wt. %)	0.11	-
Vaccenic acid (wt. %)	-	-

Figure 3-1 Waste materials for catalyst support (a) waste fish bone, (b) waste ground-nut shell

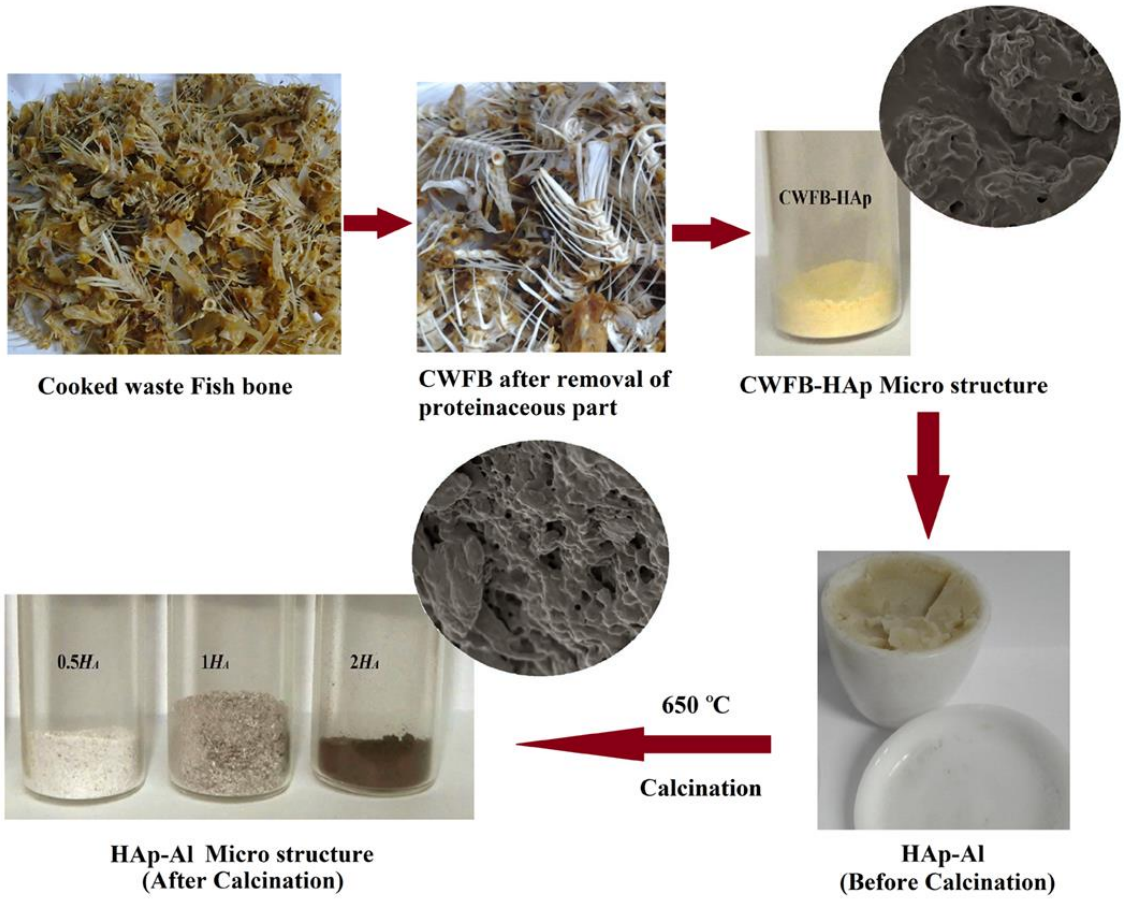

Figure 3-2 Flow chart of Al metal oxide wet impregnation on HAp to prepare HAp-Al

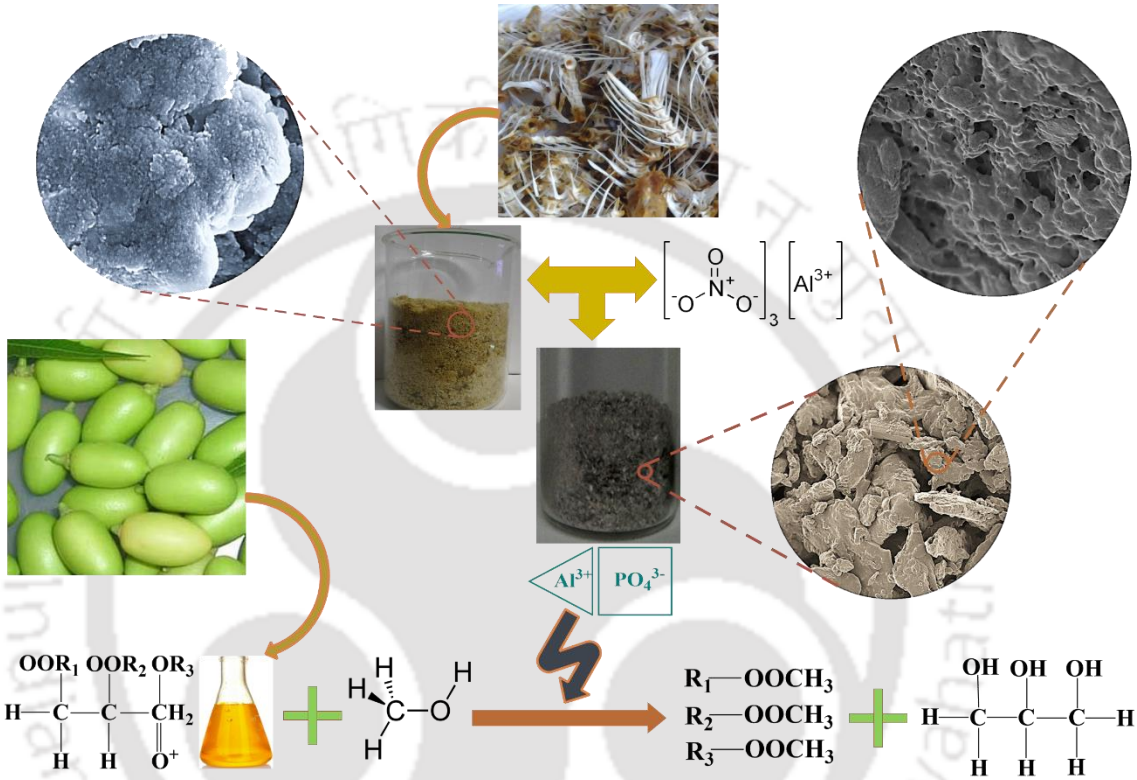

Figure 3-3 Schematic presentation of standard methanolysis showing reaction of methanol and neem oil in the presence of HAp-Al catalyst

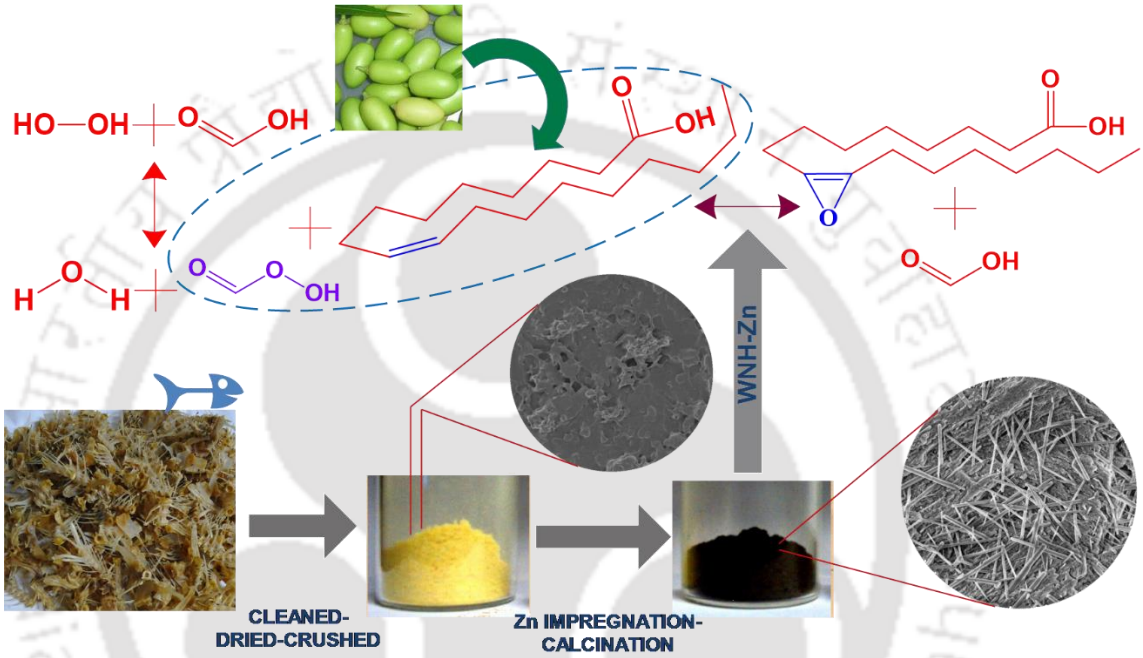

Figure 3-4 Schematic presentation of standard peroxidation showing reaction of peracid and neem oil in the presence of HAp-Zn catalyst

4 RESULTS AND DISCUSSIONS

"Real is what can be measured"

Max Planck

(1858-1947, German Physicist)

4.1 Characterization of raw materials and catalysts

4.1.1 Hydroxyapatite based catalyst

Four different metal and metalloid supported HAp catalyst were prepared and characterized which are discussed in the following subsections.

4.1.1.1 Al-HAp

XRD patterns of HAp and HAp-Al are delineated in Figure 4-1. Well resolved characteristic peak for HAp was observed at 2θ value of 31.77° corresponding to 211 planes. Apart from it, peak for Fluorapatite was also observed at 21.8° and 22.8°. The phase formed was clear and matches well with standard pattern reported in literature [236]. The standard corresponding plane for HAp (viz. 100,101, 200, 002, 211, 202, 301, 130, 131, 113, 203, 222, 132, 321, 004, 240, 241, 502, 323, and 511) were well observed in case of the synthesized catalyst. The diffraction peaks at 2θ = 37.0°, 46.0° and 66.7° corresponds to the crystalline Al_2O_3 support as registered on the XRD patterns (Figure 4-1). Al_2O_3 and CaO in HAp agglomerated to give another species Vastmanlandite at 39.64° was observed which is responsible for having Al (2 2 2) planar structure.

Figure 4-2 shows the FTIR spectrum of HAp, HAp-Al and used HAp-Al. The representative FTIR spectrum shows all characteristic absorption peaks of HAp. The principal evidence for framing of HAp was in the form of a strong complex broad FTIR band focused at about 1000-1120 cm^{-1} because of asymmetric stretching mode of vibration for PO_4 group [237]. The band at 570 cm^{-1} corresponds to P-O stretching vibration of the PO_4 group. As a major peak of phosphate group, the vibration peak could be distinguished in the region between 1120-960 cm^{-1} for both CWFB-HAp and CWFB-

HAp-Al which were due to P-O asymmetric stretching of PO_4^{3-}. Many of the compounds can be acknowledged to be analogues of ethers, especially when an alkoxy group was available, featuring the P-O-C linkage at 1240cm^{-1}. The IR absorption spectra show only some change in the shape of the absorption band within wave numbers 400-800 cm^{-1}, probably indicating a variety of M-O-M bonds [238]. At 871 cm^{-1} an intense peak was observed affirming M-O-M bond [239]. The samples showed a very intense broad band at approximately 3569 cm^{-1} that could be ascribed to the νOH stretching vibration of the hydroxyl groups attached to Al_2O_3.

Apart from these, a clear comparison can be made on the basis of organic functional groups. A peak at 1746 cm^{-1} for HAp responsible for saturated aliphatic is absent in HAp-Al. But again same peak appeared for HAp-Al (used) at 1748 cm^{-1}. Similar type of disappearance of peak (medium intensity) was observed at 2922 cm^{-1} and 2852 cm^{-1} which are responsible for alkanes (C-H) and again same peak appeared in the used HAp-Al (used).

Figure 4-3 shows a typical Nitrogen adsorption-desorption isotherm of HAp, CHAp and HAp-Al. The isotherms display a type IV curve with a hysteresis loop which corresponds to mesoporous materials. As can be seen from the figure, the process is not completely reversible which expedites the presence of a hysteresis between the curves of adsorption and desorption. HAp, CHAp and HAp-Al have BET surface areas of 10.865 $m^2 g^{-1}$, 167.86 $m^2 g^{-1}$ and 168.96 $m^2 g^{-1}$ respectively. Different types of surface area analysis are classified in Table 4-1. It can be seen from the Table 4-1 that, the BJH pore volumes were close to the BET pore volumes for all. Further, it was confirmed that the doping of Al on HAp and further calcination has significantly increased the BET surface area as well as pore volume. Also a comparison was made between other researchers work in the Table 4-1 which shows the superiority of the HAp-Al.

The morphologies of HAp and HAp-Al are presented in Figure 4-4. These FE-SEM micrographs gave understanding into the structure with respect to pore sizes and distribution. As can be seen from the micrographs, the HAp (Figure 4-4 (a), (b)) surface has very less number of pores and the distribution of pores were not uniform. Figure 4-4 (c) and (d) are FE-SEM micrographs showing the surface morphologies of the HAp-Al and it appears as a polycrystalline material. For HAp-Al, the pores seem to be uniformly

distributed on the surface. The calcination at 650 °C resulted in decomposition of carbonate which helped in forming uniform pores. Hence, the surface area as well as the pore volume was higher in case of HAp-Al than HAp which was evident from the BET results. The EDX analysis of HAp-Al showed the presence of C (13.46%), O (44.53%), Mg (0.39%), Al (15.79%), P (7.6%), and Ca (18.24%). The wt. % analysis confirmed the oxide formation of Ca, Al and Mg. Also the EDX analysis of HAp confirms the presence of C (2.21%), O (39.05%), P (16.12%), Ca (34.36%), and Mg (8.26%).

Microcrystalline structure of HAp-Al is obtained from TEM analysis and is presented in Figure 4-5 (a), which shows the self-assembled structure of the hydroxyapatite and Aluminum oxide. Al grafted on HAp was examined from SAED patterns (Figure 4-5 (b)). The ring pattern proves the polycrystalline nature of the material. The *d* spacing for some of the rings were calculated using the formula $d=L*\lambda/r$, where r is the radius of the ring in SAED pattern (mm), L is the distance between the sample and the photographic plate (450 mm), λ is the wavelength of electron beam (0.0251 Å at 200 keV) and d is the inter planar spacing of the ring (Å). The *d*-spacing obtained are 2.38 Å, 2.25 Å, 1.94 Å, 1.41 Å are consistent with the (1 1 1), (1 0 1), (2 0 0) and (2 1 1) lattice planes Aluminum.

Figure 4-6 demonstrates the TGA analysis of HAp, CHAp and HAp-Al. In case of HAp, initial weight loss of 6.84% occurred in between the temperature regime of 90 °C to 180 °C because of the evaporation of water molecules. After that the weight loss was found to be about 35% which was due to the decomposition of carbonate as mentioned below.

$$CaCO_3 \xrightarrow{\Delta} CaO + CO_2 \qquad \textbf{(4-1)}$$

However, in case of HAp-Al, the initial weight loss was only about 4.46% (within 180 °C). Moreover, no crest was found within a temperature region of 180 °C to 1000 ºC and the reported weight loss was only 7%. The TGA curve within this specified temperature range was thought to be the aftereffect of continuous de-hydroxylation of -HAp-Al powder. It is clear from the TGA that the total weight loss at 1000 °C was 11.46% for HAp-Al compared to 41.7% for HAp. Thus, it was confirmed that Al doping resulted in a more stable HAp-Al. Also CHAp has shown stability up to 1000 °C, with total weight

loss of 12.3%. Thus, the prepared catalysts were more stable at higher temperature compared to other catalysts as reported in literature [240]. The catalyst prepared by Chakraborty and RoyChowdhury [240] has lower stability at higher temperatures which was clearly noticeable in their TGA graph. According to their TGA analysis, Copper doped hydroxyapatite degrades to the same extent as natural hydroxyapatite.

4.1.1.2 Hap-Zn

Figure 4-7 shows the various relevant HAp functional groups at different wavenumbers, among which an asymmetric stretching vibration for the PO_4 group was observed at 1120-1000 cm^{-1}. Another P-O stretching vibration was noted at 570 cm^{-1} responsible for the PO_4 group. Apart from above-mentioned wavenumbers, few major peaks of phosphate group were spotted between 1120-960 cm^{-1} is liable to PO_4^{3-} asymmetric stretching. For HAp and CHAp, the stronger absorption between 2950 cm^{-1} and 2850 cm^{-1} represents the -CH_2 stretching vibration. However, this was more prominent in HAp comparison to CHAp and finally disappeared in HAp-Zn. Also, the band at 3317 cm^{-1} of HAp-Zn is assigned to O-H stretching. Another interesting peak of carbonate stretching band was observed in the region between 1600 cm^{-1} to 1400 cm^{-1}. The carbonate peak at 1454 cm^{-1} is neither type A or type B carbonated apatite. These may have resulted by absorption of carbonate upon apatite crystals or another carbonate phase with apatite. Apart from carbonate and phosphate bands, HAp-Zn showed another characteristic band between 500 cm^{-1} and 400 cm^{-1}. It was responsible for the distinct stretching mode of ZnO nanocomposite [241].

XRD patterns (Figure 4-8) of HAp and HAp-Zn showed the HAp characteristic peak at a 2θ value of 31.77°. The well-resolved peak Corresponds to 211 plane. The clear phase obtained from XRD patterns matches to the standard pattern [242]. ZnO nanocomposite has a crystalline nature which was clearly observed from the peak at 2θ= 34.8° corresponds to 002 plane. After deposition of Zn metal ions, few changes were noticeable such as the lattice parameters concerning intensity that was changed due to the wet impregnation method. The use of metal precursor played an important role to produce a crystalline structure [243].

Figure 4-9 shows N_2 adsorption-desorption isotherm of HAp and HAp-Zn and pore volume distribution. The isotherm shows the existence of hysteresis because the

process is not completely reversible. Also, the isotherm is a type IV curve which inferred that the material is mesoporous. The surface area of the materials is listed in Table 4-2. The surface area of HAp was10.865 $m^2 g^{-1}$. However, for CHAp and HAp-Zn the surface area was 167.86 $m^2 g^{-1}$ and 217.29 $m^2 g^{-1}$ respectively which is much higher than HAp. The insight of the Figure 4-9 shows a plot of the pore diameter and pore volume. Similarly, a pore volume of HAp was found to be lower than CHAp and HAp-Zn. The total pore volume of HAp was 0.08 $cm^3 g^{-1}$, whereas for CHAp and HAp-Zn pore volume were 0.49 $cm^3 g^{-1}$ and 0.42 $cm^3 g^{-1}$ respectively. Further, it was confirmed that the deposition of Zn on HAp followed by calcination was responsible for the significant increase in surface properties.

TGA analysis (Figure 4-10) of HAp showed an initial weight loss of 6.84% due to exterior water molecules evaporation. After water loss with an increase in temperature, the weight loss of 35% corresponds to carbonate decomposition. Similarly, initial weight loss of 6.14% was observed in HAp-Zn within a temperature range of 30-180 °C. Afterward, the weight loss occurred due to continuous de-hydroxylation. It can be clearly inferred from TGA graph that all three materials are significantly comparable. The total weight loss of HAp was 42.7% whereas in the case of CHAp and HAp-Zn was 12.3% and 22.15% respectively. The calcination of the material plays a very important role in the formation of hydroxyapatite. The formation of hydroxylapatite formed in the temperature region of 600 ºC to 900 ºC. However, HAp-Zn was prepared at 650 °C which leads to the further degradation in TGA profile. The additional mass loss was due to the removal of all the organic compounds present in the core of the sample. The similar profile was observed in Singh and Jonnalagadda work [244]. But the hydroxyapatite prepared was synthetic i.e. prepared in the laboratory.

The surface structure and elemental composition of HAp is described in the subsection 4.1.1.1. The FE-SEM micrographs, (Figure 4-11) of CHAp and HAp-Zn, gave insight into the structure of pores formed after calcination, ZnO deposition as well as elemental study. After calcination at 650 °C, the carbonates are decomposed, and the surface structure becomes irregular i.e. number of pores were formed (Figure 4-11 a and b). However, the pores of CHAp are slit-like structure. The porous structure led to the increased surface area as well as the volume which was evident from the Table 4-2. Figure

4-11 c, d, e and f represent the surface structure of HAp-Zn which clearly shows the non-uniform slit structured pores over the sample material surface. Apart from the pores, the deposition of the various sized nanocomposite was found at various positions. The nanocomposites were aggregated and were compact as well as well structured. These aggregations were in the form of Nanorods having an average size of 200 nm.

The typical Nano-rod formation was due to the wet impregnation method at a lower concentration. The presence of Zn nanocomposites makes the amphoteric surface which provides an active surface area during reaction. The elemental composition of CHAp (C 15.3%, O 33.24%, P 10.29%, Ca 29.82%) and HAp-Zn (C 14%, O 35.36%, 11.23%, Ca 27.46%, Zn 11.94%) was observed during EDX analysis.

4.1.1.3 HAp-Mg

XRD patterns of HAp and HAp-Mg are delineated in Figure 4-12. Well-resolved characteristic peak of most elevated intensity for HAp was acquired at 2θ value of 31.77° corresponding to 211 planes. The phase formed was clear and matches well with standard pattern reported in literature [236]. The standard corresponding plane for HAp (*viz.* 100,101, 200, 002, 211, 202, 301, 130, 131, 113, 203, 222, 132, 321, 004, 240, 241, 502, 323, and 511) were well observed in case of the synthesized catalyst. The diffraction peak at 2θ = 62.97° with plane 502 corresponds to the Mg support as registered on the XRD patterns (Figure 4-12).

The principal evidence for framing of HAp was in the form of a strong complex broad FTIR band (Figure 4-13) focused at about 1000-1120 cm^{-1} because of asymmetric stretching mode of vibration for PO_4 group [237]. The band at 570 cm^{-1} corresponds to P-O stretching vibration of the PO_4 group. As a major peak of phosphate group, the vibration peak could be distinguished in the region between 1120-960 cm^{-1} for both HAp and Hap-Mg, which were due to P-O asymmetric stretching of PO_4^{3-}. Many of the compounds can be acknowledged to be analogs of ethers, especially when an alkoxy group was available, featuring the P-O-C linkage at 1240 cm^{-1}. In case of HAp-Mg the bands at 780-980 cm^{-1} and the peak in the range of 900-1200 cm^{-1} were resulted due to the peroxide formation (M-O-O-M) and the M-O-M bonding respectively [243].

Figure 4-14 shows a typical Nitrogen adsorption-desorption isotherm of HAp and HAp-Mg. The isotherms display a type IV curve with a hysteresis loop which corresponds to mesoporous materials. HAp and HAp-Mg have BET surface areas of 10.865 $m^2 g^{-1}$ and 134.1 $m^2 g^{-1}$ respectively. Different types of surface area analysis are classified in Table 4-3. Figure 4-14 (in side) shows a plot of varying pore volume distribution with reference to pore diameter (nm). The total pore volumes were found to be 0.0894 cc g^{-1} and 0.45 cc g^{-1} for HAp and HAp-Mg respectively. It can be seen from the Table 4-3 that, the BJH pore volumes were close to the BET pore volumes for both the samples. Further, it was confirmed that the doping of Mg on HAp has significantly increased the BET surface area as well as pore volume.

The morphologies of HAp and HAp-Mg are presented in Figure 4-15 (a), (b) and Figure 4-15 (c), (d) respectively. These SEM micrographs gave understanding into the structure with respect to pore sizes and distribution. The surface of HAp is almost plane and less porous. But after doping of Mg followed by calcination at 650 °C leads to surface roughness and porous formation. As can be seen from the micrographs, surface morphologies of the HAp-Mg appear as a polycrystalline material. Figure 4-15 (d) shows the porous structure is uniform but the slit like porous structure was observed. The calcination at 650 °C resulted in decomposition of carbonate which helped in forming uniform pores. Hence, the surface area as well as the pore volume was higher in case of HAp-Mg than HAp which was evident from the BET results. The EDX analysis of HAp-Mg showed the presence of C (7.89%), O (43.83%), Mg (19.77%), P (14.13%), Ca (17.37%). The wt. % analysis confirmed the oxide formation of Ca and Mg.

Figure 4-16 demonstrates the TGA analysis of HAp and HAp-Mg. In case of HAp, initial weight loss of 6.84% occurred in between the temperature regime of 90 °C to 150 °C because of the evaporation of water molecules. After that the weight loss was found to be about 35% which was due to the decomposition of carbonate.

However, in case of HAp-Mg, the initial weight loss was only about 3.48% (within 150 °C). Moreover, no crest was found within a temperature region of 150 °C to 1000 ºC and the reported weight loss was only 7.5 %. The TGA curve within this specified temperature range was thought to be the aftereffect of continuous de-hydroxylation of HAp-Mg powder. It is clear from the TGA that the total weight loss at 1000 °C was 10.98

% for HAp-Mg compared to 41.7% for HAp. Thus, it was confirmed that Mg doping resulted in a more stable HAp-Mg.

4.1.1.4 HAp-Na-Si

XRD patterns of raw hydroxyapatite and Na/Si doped hydroxyapatite are delineated in Figure 4-17. Well-resolved characteristic peak of most elevated intensity for hydroxyapatite was acquired at 2θ value of 31.77° corresponding to 211 planes. The phase formed was clear and matches well with standard pattern reported in literature [236]. The standard corresponding plane for hydroxyapatite (viz. 100,101, 200, 002, 211, 202, 301, 130, 131, 113, 203, 222, 132, 321, 004, 240, 241, 502, 323, and 511) were well observed in case of the synthesized catalyst. The diffraction peak at 2θ = 21.8° with plane 2, 0, 0 corresponds to the Si support [245] as registered on the XRD patterns (Figure 4-17).

The principal evidence for framing of raw hydroxyapatite was in the form of a strong complex broad FTIR band (Figure 4-18) focused at about 1000-1120 cm^{-1} because of asymmetric stretching mode of vibration for PO_4 group [237]. The band at 570 cm^{-1} corresponds to P-O stretching vibration of the PO_4 group. As a major peak of phosphate group, the vibration peak could be distinguished in the region between 1120-960 cm^{-1} for both raw hydroxyapatite and Na/Si doped hydroxyapatite, which were due to P-O asymmetric stretching of PO_4^{3-}. Many of the compounds can be acknowledged to be analogs of ethers, especially when an alkoxy group was available, featuring the P-O-C linkage at 1240 cm^{-1}. In case of Na/Si doped hydroxyapatite the bands at 780-980 cm^{-1} and peak in the range of 900-1200 cm^{-1} are resulting to the peroxide formation (M-O-O-M) and the M-O-M bonding respectively [243].

Figure 4-19 shows a typical Nitrogen adsorption-desorption isotherm of raw, calcined and Na/Si doped hydroxyapatite. The isotherms display a type IV curve with a hysteresis loop which corresponds to mesoporous materials. Raw, calcined and Na/Si doped hydroxyapatite have BET surface areas of 10.865 $m^2\ g^{-1}$, 167.86 $m^2\ g^{-1}$ and 57.124 $m^2\ g^{-1}$ respectively. The total pore volumes were found to be 0.0894 cc g^{-1}, 0.4926 cc g^{-1} and 0.4943 cc g^{-1} for raw, calcined and Na/Si doped hydroxyapatite respectively. It can be seen from the Table 4-4 that, the BJH pore volumes were close to the BET pore volumes for the samples.

Figure 4-20 demonstrates the TGA analysis of raw, calcined and Na/Si doped hydroxyapatite. In case of raw hydroxyapatite, initial weight loss of 6.84% occurred in between the temperature regime of 90 °C to 150 °C because of the evaporation of water molecules. After that the weight loss was found to be about 35% which was due to the decomposition of carbonate. For calcined hydroxyapatite the total weight loss at 1000 °C was 12.3% and after 450 °C the degradation was thought to be the aftereffect of continuous de-hydroxylation. However, in case of Na/Si doped hydroxyapatite, no crest was found within a temperature region of 30 °C to 1000 ºC and the reported weight loss was only 4.18 %. It confirms the stability of Na/Si doped hydroxyapatite.

The morphologies of raw and Na/Si doped hydroxyapatite is presented in Figure 4-21. These FESEM micrographs gave understanding into the structure with respect to pore sizes and distribution. As can be seen from the micrographs, surface morphologies of the Na/Si doped hydroxyapatite appears as a polycrystalline material. For Na/Si doped hydroxyapatite, the pores are uniformly distributed on the surface. The calcination at 650 °C resulted in decomposition of carbonate which helped in forming uniform pores. Hence, the surface area as well as the pore volume was higher in case of Na/Si doped hydroxyapatite than raw hydroxyapatite that was evident from the BET results.

The EDX analysis (Figure 4-22) of raw hydroxyapatite and Na/Si doped hydroxyapatite showed the presence of C, O, Mg, P, Ca, Na, Si and the corresponding weight percentages are tabulated in sight. The wt. % analysis confirmed the oxide formation of Si.

4.1.2 WGS-Mg

N_2 adsorption and desorption isotherm of WGS-Mg 11 is presented in Figure 4-23 which shows a hysteresis loop corresponding to a type IV curve. The isotherm is bit peculiar i.e. it is opened towards the end of desorption, which is supposed to be closed. The probable reason behind this type of isotherm is low-pressure hysteresis i.e. presence of very narrow slit pores or bottle shaped pores. The wider portion of ink bottle fills up at high relative pressures but difficult to empty during desorption. This is because of swelling non-rigid pores. Hence the size of narrow neck becomes the limiting factor for the relative pressure at which the pore becomes empty [246, 247]. The BET surface area

was 47 m^2 g^{-1}. The pore volume distribution with reference to various pore sizes is presented inside the Figure 4-23. The average pore size was 0.28 Å. Also the graph clearly shows the pore volume during adsorption was 0.051 cc g^{-1}, whereas during desorption it was bit lower i.e. 0.047 cc g^{-1}. The total pore volume was found to be 0.072 cc g^{-1}. The surface area of WGS-Mg 12 and WGS-Mg 21 are mentioned in the Table 4-5. A comparison was also made with earlier published works presented in Table 4-5 and was found that few researchers [248-250] used peanut shell as catalyst. The surface area was found to be high and the average pore size is low compared to the present work. The reason for higher surface area is may be due to the content of the material or the activation temperature. In addition to that the deposition of Mg and formation of new composite also lead to the higher surface area. The higher surface area will lead to the exposure of major active sites to the reactants thus, resulting in higher conversion.

Particle size analysis of WGS-Mg (Figure 4-24) shows the distribution of particle diameter with reference to differential intensity at 25 °C. The cumulant mean diameter of 8.1 µm, 7.7 µm and 11.2 µm was exhibited for WGS-Mg 11 (Figure 4-24a), WGS-Mg 12 (Figure 4-24b) and WGS-Mg 21 (Figure 4-24c) respectively. The polydispersive index for WGS-Mg 11, WGS-Mg 12 and WGS-Mg 21 were found to be 0.061, 0.18, 0.086 which inferred the absence of agglomeration in material. Further the micro range of synthesized material will lead to the easy separation by filtration technique after completion of reaction.

The development of porous structure was studied for WGS (Figure 4-25 a, b and c) and WGS-Mg 11 (Figure 4-25 d, e and f). The structure of WGS is non-homogeneous polyhedral agglomerates. However, the primitive pores were formed in WGS-Mg11 after chemical activation with Ammonia solution followed by calcination. As the groundnut shell is mainly comprised of cellulose and hemi-cellulose, they start to swell under electrolytic activity of Ammonia [251]. Hence the order of molecules changes due to breaking of lateral bonds resulting in inter- and intra-micelle voids. Also, addition of metal precursor and subsequent calcination helps forming porous structure and extending the surface area. Also it can easily be observed the formation of Mg composites on WGS-Mg 11. The spherical balls are measured to be the size of 2 microns (Figure 4-25 d, e) and 0.8 microns (Figure 4-25 f).

The Mg metal ion dispersion on the catalyst support was extensively studied using SEM-EDX surface mapping technique (Figure 4-26). The simultaneous topological and elemental imaging is a valuable means to illustrate the metal ion dispersion. The electron scanning was done on selected area of interest. The bright spots show that the distribution of Mg is quite non-homogeneous. Basically the higher the concentration of element, the brighter will be the color that appears in the image. The surface mapping also giving a clear information about two important active sites. First one is Si (metalloid) present in WGS and second one is Mg (metal) composite deposited on WGS will play a vital role during methanolysis reactions.

The HR-TEM images (Figure 4-27) are in good compliance with surface morphology as shown in FE-SEM and EDX mapping. The TEM images (Figure 4-27) inferred well dispersed nano range MgO throughout the WGS char. However, in some places prominent aggregation of MgO (Figure 4-27b, d) was also observed. The selected area electron diffraction (SAED) patterns (Figure 4-27f) of dispersed MgO on the WGS, shows the polycrystalline nature of the specimen. The *d*-spacing was calculated and matched with the XRD data file to confirm the peak. The relevant *d*-spacing obtained were 2.92 Å, 4.38 Å, 4.01 Å which are consistent with (220), (200), (111) lattice planes of Mg. In addition, the Figure 4-27e inferred the nano range Mg (2-5 nm) grains having polycrystalline structure [252]. This type of aggregated morphology would provide more surface area than the base material and hence the area of contact during reaction process.

Figure 4-28 shows XRD patterns of raw WGS and all WGS-Mg as well. The WGS shows amorphous morphology and a broaden peak at 2θ value of 21.8 presents the lignin rich portion [253]. Whereas WGS-Mg catalysts shows well defined Mg metal based composite. Three notable peaks were observed at 2θ value of 20.2 (*d*-spacing 4.38 Å), 22.1 (d-spacing 4.01 Å) and 30.59 (d-spacing 2.92 Å). The notable peaks are attributed to Epsomite ($H_{14}Mg_1O_{11}S_1$, Reference code: 98-000-5657) and Monticellite ($CaMgO_4Si$, Reference code: 00-011-0353). The presence of Magnesium silicate composite also will play an important role in the adsorption of any soap formed during the reaction [254].

4.2 Methanolysis of Neem oil using HAp-Al

4.2.1 Parametric effects and regression model

Transesterification of RNO utilizing CWFB-HAp-Al ($0.5H_A$, $1H_A$, $2H_A$) was carried out using the response surface methodology (RSM) furnished by Design-Expert programming 6.0.6 (Stat-Ease Inc., Minneapolis, USA). A five factorial Face Central Composite Design (FCCD) was fit to the model and the response *i.e.* Acid value conversion (AVC) was optimized. Similarly, the impact of other independent variables on AVC was figured out. The five variables explored were reaction temperature (T_R), CWFB-HAp to Aluminium nitrate weight proportion (H_A), time of response (t), stirring speed (S_{rpm}) and oil/methanol ratio ($R_{O/M}$). Before exploratory plan, achievability analyses were performed to verify the T_R, H_A, t, S_{rpm}, $R_{O/M}$. The ranges of variables were decided based on the feasibility tests and from previous works reported in literature [255, 256]. The errors were minimized from the methodical patterns in the variables by taking irregular runs.

Individual parametric effects on actual acid value conversion can be clearly studied from the perturbation curve as shown in Figure 4-30. It can be depicted from the figure that the AVC_{act} gradually increased with increase in reaction temperature, time of reaction and oil to methanol ratio. However, AVC_{act} showed a negative declination with increase in CWFB-HAp to Aluminium nitrate weight proportion, whereas stirring had very less effect on the overall conversion. The response surface plots are shown in Figure 4-31.

In Figure 4-31 the effect of H_A with respect to other factors were highlighted and most of the individual terms had a positive effect on the response. Keeping H_A constant and increasing the T_R value from 70 °C to 90 °C, the response showed a positive effect (Figure 4-31 a). However, keeping T_R constant and increasing H_A from 0.5 to 2 resulted in a negative response. Similarly, with increase in t and $R_{O/M}$ at constant H_A showed positive effect on the response (Figure 4-31 b and c). It was found that the S_{rpm} factor had very less effect on response.

A peculiar variation in response was found out when H_A, S_{rpm} were taken in to consideration. At lowest value of H_A the response showed slightly negative effect with increase in S_{rpm} and at highest value of H_A the response showed slightly positive effect

with increase in S_{rpm} (Figure 4-31 d). However, at lowest value of both the factors the response was high which clearly inferred that the Al metal ions had more impact on the reaction. The lowest stirring speed allowed most of the reactant to adhere to the metal ion surface.

When T_R and S_{rpm} were taken in to consideration it was found that at constant S_{rpm} along with increase in T_R there was a gradual increase in response up to 85 °C and after that it decreased to some extent (Figure 4-31 e). At constant lowest S_{rpm} *i.e.* 400 and increase in *t* resulted in a positive response but at constant highest S_{rpm} *i.e.* 800 and increase in *t* showed a slight negative response (Figure 4-31 f). Though S_{rpm} has little negative effect on response when H_A was considered (Figure 4-31 d), but at lowest *t i.e.* 2 h and keeping all other parameters constant and by increasing S_{rpm} (Figure 4-31 f) a positive effect was observed in response and vice versa. However, at 3 h there was no significant changes were observed in response (Figure 4-31 f). Effect of $R_{O/M}$ with respect to *t* (Figure 4-31 g) and S_{rpm} (Figure 4-31h) was also studied. It was observed that with increasing $R_{O/M}$ at constant lowest value of *t* and S_{rpm}, the response gradually increased. But at highest value of both the parameter no significant changes in response were noticed. This trend line clearly indicated that the rate of mass transfer decreased with increasing the stirring speed after optimal point.

With a specific end goal to optimize the independent reaction parameters in transesterification of RNO, the FCCD was chosen with five factors with three levels. 32 outlined runs were led arbitrarily, and the outcomes were examined by means of multiple regression. At last, the quadratic regression model (QRM) was found to be the best fitting model by means of regression. The quadratic regression model in terms of coded factors (based on the FCCD) is given in following equation.

$$AVC_{pre}=+90.96+2.62\times T_R-5.95\times H_A+2.85\times R_{O/M}+2.28\times T_R\times H_A2.10\times T_R\times S_{rpm}+3.45\times H_A \times t+3.49\times H_A\times S_{rpm}+2.84\times H_A\times R_{O/M}-2.94\times t\times S_{rpm}-3.11\times t\times R_{O/M}-2.35\times S_{rpm}\times R_{O/M} \quad \textbf{4-2}$$

After fitting the data, degree of freedom was 31 out of 32 and R^2 value was 0.99. Also the standard error was found to be very small *i.e.* 0.00481. Keeping AVC to be maximum the optimization of the model was done and the optimized parametric values

for T_R, H_A, t, S_{rpm}, $R_{O/M}$ were found to be 78.16 °C, 1.20, 2.06 h, 710.7, 19.48 which showed maximum desirability.

4.2.2 Reaction kinetics

The transesterification reaction is simply presented by,

$$T + 3M \Leftrightarrow FE + G \quad \textbf{4-3}$$

Where *T*, *M*, *FE*, *G*, presents triglyceride, methanol, FAME and glycerol respectively.

The general rate equation can be written as,

$$-dC_T/dt = kC_T^y C_M^z \quad \textbf{4-4}$$

where, C_T and C_M are concentration of reactant after time t; *y* and *z* are the order of reactant *T* and *M* respectively and *k* is the reaction rate constant.

C_T and C_M can be written as,

$$C_T = C_{T0}(1 - X) \quad \textbf{4-5}$$

$$C_M = C_{M0}(\delta - 3X) \quad \textbf{4-6}$$

$$\delta = C_{M0}/C_{T0} \quad \textbf{4-7}$$

where, C_{T0} and C_{M0} are the initial concentration of reactants, X is the conversion, and δ is the ratio of C_{M0} to C_{T0}. Eq. 4.4 can be written as:

$$\frac{dX}{dt} = kC_{T0}^{(y+z-1)}(1 - X)^y(\delta - 3X)^z \quad \textbf{4-8}$$

To obtain order of transesterification reaction, 8 cases i.e. (*y*= 0, *z*= 0), (*y*= 1 , *z*= 0), (*y*= 0 , *z*= 1), (*y*=1 , *z*= 1), (*y*=2 , *z*= 0), (*y*= 0 , *z*= 2), (*y*=2 , *z*= 1), (*y*=1 , *z*= 2) were considered. For every case, the integral form of Eq. 4.8 was calculated and the final equations were obtained is tabulated (Table 4-6). The LHS of every equation presented in the Table 4-6 is an ordinate and $C_{T0}t$, C_{T0}^2t on RHS are abscissas. Hence, by plotting those linear graphs *k* values can be calculated for each case and the one which has higher correlation coefficient was used for determining the reaction order.

Reaction kinetics was studied at optimal conditions obtained. For each case discussed the R^2 and standard error was calculated (Table 4-7). Considering highest correlation co-efficient, overall transesterification reaction order was found to be 2 along with the reaction rate constant of $3.46 \times 10^{-5} mol^{-1} l^{-1} \text{ min}^{-1}$. Few runs were carried out using HAp, CHAp, $0.5H_A$, $1H_A$, $1.2H_A$, $2H_A$ for 135 minutes keeping other parameters at optimal level. The conversion obtained was plotted (Figure 4-32) against time interval of 15 minutes which shows gradual increment.

4.2.3 Characterization of Transesterified neem oil at optimal conditions

FTIR spectrum of the Transesterified neem oil (TNO) sample is demonstrated in Figure 4-33 and various absorption peaks are presented in Table 4-8. From the Table, it can be found that the RNO was already transesterified [257]. The frequency 1728 proved that the TNO sample was the kind of structures having long-chain fatty acid esters.

Few physical properties such as final acid value, density and viscosity were measured as per the ASTM standards and were found to be 0.714 mg KOH g^{-1} TNO, 840 g cm^{-3} at 15 °C, 4.5 mm^2 sec^{-1} at 40 °C. The pour point and flash point of the TNO were found to be 5.8 °C and 154 °C respectively. The values of physical properties gave a clear confirmation that the TNO properties were very close to the biodiesel properties.

4.2.4 Possible reactant interaction with the catalyst surface

Al metal ions that were doped on to hydroxyapatite surface have both acidic and basic sites. Hence, the reaction mechanism involved three basic steps, i.e. adsorption of reactants on to the active sites, reaction on the catalytic surface and desorption of final product (Figure 4-34) [258]. At first (Step-1) a carbonyl group from a fatty acid and one methanol molecule get attached to the active sites because of van der Waals force. Then in the next phase (Step-2), one oxygen anion nucleophilically attacked the Carbon atom and the oxygen anion from methanol molecule at basic site attacked the carbonyl group in triglyceride molecule for esterification and transesterification reactions, respectively. Later on this nucleophilic attack creates a tetrahedral on both the sites. In step 3, desorption of water and methyl ester molecule occur on acidic site. From basic site desorption of one methyl ester and one di-glyceride molecule occur and which again go through the catalytic cyclic process to produce two more methyl ester and glycerol.

4.2.5 Comparison of HAp-Al with the earlier reported Work

Table 5 compared different heterogeneous catalysts and their methyl ester yield at different operating parameters reported earlier [123, 125, 259-267]. It shows the efficacy of presently developed HAp-Al. The catalyst without alumina support could not yield methyl oleate or glycerol within 1 h span of time, and only 7% methyl oleate yield was obtained over 12 h at 150 °C. But on the other hand, K_2CO_3, KNO_3 and NaOH loaded with Alumina, resulted in higher yield of methyl oleate over 1 h at 60 °C. Thus, it provides the evidence that alkaline metal salt loaded porous supports is more efficient during transesterification.

Consider few established works [123, 259, 262, 267], in which the methyl ester yield was above 90%. However, the presently developed HAp-Al shows excellent catalytic activity in various aspects. For example, the catalyst wt. %, reaction time and reaction temperature is very high [259, 262]. Although Xie et al. [123] have used only 1 wt. % of catalyst, very low methanol to oil ratio, but the time taken to yield 90% is huge i.e. 600 minutes.

Although Liu et al. [267] observed above 90% methyl ester yield at comparatively less span of time i.e. 65 minutes and low methyl to oil ratio i.e. 12:1, but the reaction temperature was very high. Apart from these if Al based catalyst is considered, a very less methyl ester yield was also reported [261] where the reaction time span was 600 minutes. Al based catalysts such as Mg-Al-CO_3 (Hydrotalcite) [260], MgO, ZnO, Al_2O_3 [263], Mg-Al-CO_3 HT [264], Al-Mg hydrotalcite [265], KNO_3/Al_2O_3 [266] had shown yield in between 80%-90% but the reaction temperature and methanol to oil ratio was very high. So, considering all the pros and cons of the reported works, the present work was optimized and the comparative catalytic effect has notified.

4.2.6 Reusability of HAp-Al

Reusability of the developed catalyst was studied by repeating the transesterification experiments at optimal conditions for at least 7 times. After centrifugation, the catalysts are taken out and washed with Methanol and then dried completely for further use. It was found that the AVC didn't vary much which confirmed

the stability of the catalyst. Regeneration of the catalyst was done before each run. The variation of AVC was within ±0.5.

4.3 Methanolysis of Neem oil using HAp-Mg

4.3.1 Parametric effects

4.3.1.1 Effect of oil to methanol ratio on methyl ester yield

The usual esterification reaction is conducted in excess of methanol, which leads to forward reaction because of reversibility. In order to analyze the outcomes of oil to methanol ratio on the reaction, few experiments were conducted with molar ratio of 1:5, 1:10, 1:15, 1:20, and 1:25 at constant weight of catalyst as shown in Figure 4-35. It shows the effect of neem oil to methanol molar ratio on methyl ester yield with reference to reaction time. Significant effect was clearly observed affecting the methyl ester yield. The time required to reach highest yield at lower concentration of HAp-Mg (2 Wt.% of oil) and lower oil to methanol ratio (1:5), was approximately 250 minutes. But with increase in oil to methanol ratio the time required to reach highest conversion gradually decreased to 135 minutes.

The concentration of methanol has dominant role during esterification reaction. The methyl ester yield was increased significantly with the addition of methanol. Nevertheless, higher concentration of methanol may adsorb on the catalyst active sites because of which the esterification process inhibited. As shown in the Figure 4-35 the oil to methanol molar ratio was increased by keeping catalyst loading constant in the reaction system. It can be seen that after 1:15 oil to methanol ratio the reduction in conversion was clearly observed.

4.3.1.2 Effect of varying weight loading of catalyst on methyl ester

The methyl ester yield vs. reaction time data were obtained at varying HAp-Mg weight % but at constant oil to methanol ratio (1:15) and reaction temperature (70 °C) are presented in Figure 4-36. It shows the percentage increase in methyl ester yield with and without catalyst. In the figure, the 0% HAp-Mg shows that the whole reaction was conducted without catalyst. Further the catalyst loading was gradually increased by 1% to see the catalytic effect on the yield obtained.

The interaction between catalyst and reactant was more obvious at early stage of the reaction. It was evident from the analysis that without using catalyst the equilibrium conversion was achieved after three and half hour. Also it can be clearly noted that the time required to reach equilibrium conversion has gradually been decreased with increase in HAp-Mg Wt.%. There is increase in reaction rate perhaps due to the increase in number of active sites inside the reaction chamber. Highest yield of 96.7% was observed when the HAp-Mg loading increased to 6%. Methyl ester yield was increased from 48.7% (0% HAp-Mg) to 95% (6% HAp-Mg) in 135 minutes. The gradual increase in yield can be attributed to the increase in number of active catalytic sites available in the reaction chamber.

4.3.1.3 Effect of reaction temperature on the methyl ester yield

Reaction temperature plays an important role during esterification reaction. The effect of varying reaction temperature on methyl ester yield was shown in Figure 4-37. The rate of reaction increased with temperature, although at equilibrium state the concentrations remain same for all the temperature [151].

The reactions were conducted at 60 °C, 70 °C, 80 °C and 90 °C in presence and absence of catalyst at fixed 1:15 oil to methanol ratio. A significant and rapid rise in methyl ester yield was clearly observed with increase in reaction temperature. This is due to the higher molecular activity and mass transfer which eventually lead to faster reaction rate.

4.3.2 Reaction kinetics study of the process

The esterification reaction is reversible and the stoichiometric relation between reactant and product is presented below.

$$fa + me \Leftrightarrow fame + w \qquad \textbf{4-9}$$

where *fa*, *me*, *fame* and *w* are presenting fatty acid present in oil, methanol, fatty acid methyl ester and water.

To fit the data in the kinetic model few assumptions were made, as given below.

- In the whole reactant mixture, fatty acid content was limiting and methanol content was in excess.

- The esterification reaction is a heterogeneous process, however the stirring rate is adequate to overcome the diffusion limitation in between reactive species and catalyst [268].

Considering the above, the generalized rate equation can be written as,

$$-r_f = -dC_{fa}/dt = k_f C_{fa} C_{me} - k_b C_{fame} C_w \quad \textbf{4-10}$$

where C_{fa}, C_{me}, C_{fame}, C_w are the concentration of fatty acid in neem oil, methanol, fatty acid methyl ester and water. k_f is forward rate constant and k_b is backward rate constant.

So, according to 1st assumption, $C_{me} \approx C_{me_0}$

Thus, Eq. 4-10 can be written as,

$$-dC_{fa}/dt = k_f' C_{fa} - k_b C_{fame} C_w \quad \textbf{4-11}$$

If χ_{fa} is the fatty acid conversion, C_{fa_0}, C_{fame_0}, C_{w_0} are initial concentrations of respective reactants then C_{fa}, C_{fame}, C_w can be expressed as,

$$C_{fa} = C_{fa_0}(1-\chi_{fa}) \quad \textbf{4-12}$$

$$C_{fame} = C_{fame_0} + C_{fa_0}\chi_{fa} \quad \textbf{4-13}$$

$$C_w = C_{w_0} + C_{fa_0}\chi_{fa} \quad \textbf{4-14}$$

As initially $C_{fame_0} = C_{w_0} = 0$, C_{fame} and C_w can be written as $C_{fame} = C_{fa_0}\chi_{fa}$ and $C_w = C_{fa_0}\chi_{fa}$.

Now Eq. 4-11 can be expressed as,

$$C_{fa_0} d\chi_{fa}/dt = k_f' C_{fa_0}(1-\chi_{fa}) - k_b C_{fa_0}^2 \chi_{fa}^2 \quad \textbf{4-15}$$

$$\Rightarrow d\chi_{fa}/dt = k_f' - k_f' \chi_{fa} - k_b C_{fa_0} \chi_{fa}^2 \quad \textbf{4-16}$$

When equilibrium state is reached, then $d\chi_{fa}/dt = 0$.

Eq. 4-16 thus becomes,

$$k_f'(1-\chi_{fa_e}) = k_b C_{fa_0} \chi_{fa_e}^{\ 2} \qquad \textbf{4-17}$$

$$\Rightarrow K_e = \frac{k_f'}{k_b} = \frac{\chi_{fa_e}^{\ 2}}{1-\chi_{fa_e}} C_{fa_0} \qquad \textbf{4-18}$$

Where K_e is the equilibrium constant and χ_{fa_e} is the fatty acid conversion at equilibrium state.

Now, Eq. 4.16 is rearranged as

$$\frac{d\chi_{fa}}{k_f'(1-\chi_{fa}) - \frac{k_f'}{K_e}\chi_{fa}^{\ 2} C_{fa_0}} = dt \qquad \textbf{4-19}$$

$$\Rightarrow \frac{d\chi_{fa}}{k_f'\left(1-\chi_{fa} - \frac{C_{fa_0}}{K_e}\chi_{fa}^{\ 2}\right)} = dt \qquad \textbf{4-20}$$

$$\Rightarrow \int_0^{\chi_{fa}} \frac{d\chi_{fa}}{1-\chi_{fa} - p\chi_{fa}^{\ 2}} = k_f' dt \qquad \textbf{4-21}$$

where $p = \frac{C_{fa_0}}{K_e}$

$\int_0^{\chi_{fa}} \frac{d\chi_{fa}}{1-\chi_{fa} - p\chi_{fa}^{\ 2}}$ vs t is plotted and by linear fit the k_f' can be calculated.

The rate of esterification reaction is higher at lower activation energy. Hence the reaction temperature effect on kinetic model was studied by using Arrhenius equation which is listed as:

$$k_f' = Ae^{-\left(E_a/RT\right)} \qquad \textbf{4-22}$$

where E_a is activation energy (kJ mol^{-1}), *A* is Arrhenius constant, *R* is universal gas constant (8.314 J K^{-1} mol^{-1}) and T (K) is reaction temperature. So to study the effect at varying temperature, Eq. 4-22 can be rewritten as:

$$\ln k_f' = -E_a/RT + \ln A \qquad \textbf{4-23}$$

Eq. 4-21 shows the reaction kinetic model for the pseudo-first-order reaction. This equation was used for regression analysis of the obtained experimental data at varying catalyst loading and reaction temperature so as to calculate the reaction rate constant. After linearly fitted, the slope i.e. k_f' is listed in the Table 4-10. It's clearly showing the significant rise in rate with increase in reaction temperature.

The catalyst loading has also significant effect on the forward rate constant, which is explained by the following equation.

$$k_f' = k_{HAp-Mg} W_{HAp-Mg} \qquad \textbf{4-24}$$

Where, k_{HAp-Mg} is the HAp-Mg loading coefficient and W_{HAp-Mg} is the weight ratio of catalyst to oil. Following Eq. 4-24, a graph (Figure 4-38) was plotted between forward rate constant vs weight ratio of catalyst to oil. The slope of the plot presents the k_{HAp-Mg} i.e. 0.575 min^{-1}.

The kinetics parameter of esterification *viz.* rate constant, activation energy (E_a) and pre-exponential factor (A) were calculated from Arrhenius equation. E_a was calculated for two set of reactions separately, first is at 0% HAp-Mg loading and second at 6% HAp-Mg. Figure 4-39 illustrates a linear correlation between $\ln k_f'$ and 1/T. The slope of the line gives E_a. The final value of E_a and A is enlisted in Table 4-11. It's clearly showing that the activation energy decreases from 47.86 kJ mol^{-1} to 32.35 kJ mol^{-1} after addition of HAp-Mg.

4.3.3 FTIR results of purified and esterified neem oil

Figure 4-40 presents the graph in between wave number (cm^{-1}) and Transmittance (%) for esterified neem oil produced at constant reaction temperature (70

°C), oil to methanol ratio (1:30) and HAp-Mg weight % (2%). At first it is clear from the figure that alkane is present without phosphorous and sulfur. This confirms that leaching of catalyst didn't occur and it was separated clearly. Also a C=O group is identified at 1742 cm^{-1} which refers to ester. Other wavenumbers and corresponding functional groups are marked in the figure.

4.3.4 Comparison of HAp-Mg with earlier reported work

Table 4-12 compared different natural and synthetic hydroxyapatite based heterogeneous catalysts and their methyl ester yield at different operating parameters reported in literature [111, 240, 269-271]. It can be observed from the data that all the catalyst developed possess very less BET surface area in comparison to present developed catalyst. But Al_2O_3/H_3PO_4 (synthetic hydroxyapatite) has very good surface area i.e. 120 m^2 g^{-1}. Jazie et al. [269] tried to produce methyl ester from peanut oil using animal bone powder and observed more than 80 % of yield with gradual increase in reaction time period. However, reaction time was bit higher than present study. They also have studied methyl ester yield of rapeseed oil using the same catalyst and found above 85% yield. In this case also reaction time period as well as methanol to oil ratio was extensively high [269]. Chakraborty and RoyChowdhury [240] tried to produce oleic acid ethyl ester using Cu grafted fishbone derived hydroxyapatite. The catalyst has very low surface area. In spite of having lower surface area the yield obtained was commendable. But effect of yield with and without metal doping was not discussed [240]. Xie et al. [272] also produces methyl ester from rapeseed oil using biont shell without metal support. The results were much promising considering all the parameters except catalyst loading [271]. Obadiah et al. used palm oil to produce methyl ester, for which the yield was above 80% at 15 wt. % catalyst loading and 4h reaction time period. They observed above 95% conversion when catalyst wt. % loading was 20%, which is very high if the same process is considered in a large scale [111]. Araujo et al. [271] used synthetic hydroxyapatite with Al metal support for esterification of Oleic acid. They observed highest conversion of 95% within 1h, but only demerit in the work was reaction temperature i.e. 350 °C [271]. Thus, observing all the positive and negative aspects of the proclaimed works, the present experiments were conducted. It is noticeable from the comparison that such types of reactions can give promising results using the developed catalyst.

4.3.5 Reusability study of HAp-Mg during esterification

Reusability of HAp-Mg was studied by multiple repetition (5 times) of esterification experiments at constant oil to methanol ratio (1:15), reaction temperature (70 °C) and catalyst loading (6 wt. %). After each reaction, the final mixture was centrifuged to remove the catalyst. Then it was regenerated by washing with methanol several times and then dried for 2 h at 110 °C. The regeneration process was continued for 5 times after each run. Figure 4-41 inferring that the yield after regeneration doesn't vary significantly up to 5^{th} regeneration. After 5^{th} regeneration the yield was decreased to 91.5% from 96.7% after 160 min. The low variation in yield after regeneration affirming the stability of HAp-Mg.

4.4 Methanolysis of Neem oil using HAp-Na-Si

4.4.1 Parametric effects on acid value conversion

Figure 4-42 (a) shows the effect of neem oil to methanol molar ratio on acid value conversion (%) with respect to reaction time. It can be clearly observed that the time required to reach highest conversion (%) at lower concentration of Na/Si doped hydroxyapatite 1:2 and lower oil to methanol ratio (1:10), was approximately 195 minutes. But with increase in oil to methanol ration the time required to reach highest conversion gradually decreased to 135 minutes.

Further, the reduction in acid value (%) vs. reaction time data were obtained at various Na/Si doped hydroxyapatite, constant oil to methanol ratio (1:20) and reaction temperature (70 °C) are presented in Figure 4-42 (b). It was evident from the analysis that the equilibrium conversion was achieved after three and half hour.

For Na/Si doped hydroxyapatite 2:1 the stability over certain reaction time (160 min.) was studied at constant oil to methanol ratio (1:20) and reaction temperature (70 °C) and 2 wt. % catalyst. The catalyst was regenerated after complete separation from the reacting mixture. It was first washed with methanol several times and then dried for 2h at 110 °C. Then the dried sample was again calcined at 650 °C for 1h and finally the regenerated catalyst was further used. Figure 4-43 depicting the acid value conversion of purified neem oil with respect to time (min.). It is clear that the conversion after

regeneration doesn't vary significantly up to 4th regeneration. But after 5th regeneration the conversion was decreased to 90.3 % from 96.7% after 160 min.

The physical properties of the transesterified product obtained at constant oil to methanol ratio (1:20) and reaction temperature (70 °C) and 2 wt. % Na/Si doped hydroxyapatite 2:1 catalyst was analyzed by following ASTM standards. The physiochemical properties of both neem oil and transesterified product is presented in Table 4-13.

4.4.2 FTIR results of purified and trans-esterified neem oil

Figure 4-44 presents the graph in between wave number (cm^{-1}) and Transmittance (%) for trans-esterified neem oil produced at constant reaction temperature (70 °C), oil to methanol ratio (1:30) and Na/Si doped hydroxyapatite 2:1. At first it is clear from the figure that alkane is present without phosphorous and sulfur. Which confirms that leaching of catalyst didn't occur and it was separated clearly. Also a C=O group is identified at 1742 cm^{-1} which refers to ester. Along with other wavenumbers and functional groups are also presented in the Table 4-14.

4.5 Methanolysis of Waste cooking oil using WGS-Mg

4.5.1 Catalytic effects on yield and kinetic study

Figure 4-45 presents the percentage change in methyl ester yield at different reaction time period (max. 180 minutes), however keeping ratio of oil to methanol as well as quantity of catalyst as constant. The entire experiments were conducted at 1:15 oil to methanol proportion and 2 weight % of catalyst. From the kinetic perspective, variation in temperature has a crucial effect during the reaction. The figures clearly inferring the positive variation in yield with escalation of reaction temperature by 10 °C. The variation in reaction temperature was in the range of 60-90 °C. The gradual rise in methyl ester yield in the batch reactor was proportionate to the rise in temperature. The obvious reason behind this phenomenon is that intensification of temperature consequently resulting in more reactant molecules activity. Hence, the molecular activity escalates the mass transfer rate which leads to higher reaction rate.

To justify the use of any catalyst for the methanolysis of WCO, a set of experiments conducted without using any catalyst. It was observed that only 20% yield

was achieved at 60 °C reaction temperature after 180 minutes. Also a highest conversion of 32% yield was observed at 90 °C. Again, to justify the use of activated WGS, an experiment was conducted using raw WGS at 60 °C. The final conversion was 22.3% after 180 minutes. Then effect of varying Mg support upon WGS was also studied by carrying out methanolysis reactions at different temperatures using WGS-Mg 11, WGS-Mg 12, WGS-Mg 21. Considering the reaction temperature at 70 °C, it can be observed from the figure that the final yield was high in case of WGS-Mg 12 i.e. 74.2%. Similarly, the highest conversion of 95% was obtained at 90 °C reaction temperature and also the equilibrium condition was reached earlier i.e. 150 minutes. From Figure 4-45, it is also observed that after 180 minutes the corresponding highest conversion for WGS-Mg 11 and WGS-Mg 21 were 65.1% and 55.8% at 70 °C of reaction temperature. This variation in total yield was attributed to the active catalytic sites created by Mg and Si composites on WGS.

4.5.2 Kinetics study of WCO methanolysis

The methanolysis reaction is reversible. The following equation shows the stoichiometric relation.

$$ffa + CH_4O \Leftrightarrow fame + H_2O \qquad \textbf{4-25}$$

Where *ffa* (free fatty acid) reacts with *CH_4O* (methanol) to produce *fame* (fatty acid methyl ester) and *H_2O* (water). Few assumptions were considered for the development of the kinetic model which are listed below.

1. The reaction sites on catalyst surface are almost same.

2. The rate controlling step is surface reaction.

3. Adsorption of reactants and desorption of products are fast at equilibrium.

4. During heterogeneous methanolysis process the rate of mechanical agitation is acceptable to beat the reactant and catalyst diffusion constraints [21].

The simplified rate equation for the Eq. 4-25 is presented below (Eq. 4-26).

$$-r_{ffa} = -dC_{ffa}/dt = k_f C_{ffa} C_{CH_4O} - k_b C_{fame} C_{H_2O} \qquad \textbf{4-26}$$

Where C_{ffa}, C_{CH_4O}, C_{fame}, C_{H_2O} represents concentration of *ffa*, *CH4O*, *fame*, and *H2O* respectively. k_f and k_b are forward and backward rate constants.

If χ_{ffa} is the fatty acid conversion, $C_{ffa_0}, C_{CH_4O_0}, C_{fame_0}, C_{H_2O_0}$ are initial concentrations of *ffa*, *CH4O*, *fame*, and *H2O* respectively then C_{ffa}, C_{CH_4O}, C_{fame}, C_{H_2O} are represented as,

$$C_{ffa} = C_{ffa_0}(1-\chi_{ffa}) \quad \textbf{4-27}$$

$$C_{CH_4O} = C_{ffa_0}(\alpha-\chi_{ffa}),\ \alpha = \frac{C_{CH_4O_0}}{C_{ffa_0}} \quad \textbf{4-28}$$

$$C_{fame} = C_{ffa_0}\chi_{ffa} + C_{fame_0} \quad \textbf{4-29}$$

$$C_{H_2O} = C_{ffa_0}\chi_{ffa} + C_{H_2O_0} \quad \textbf{4-30}$$

As initial concentration of *fame* and *H2O* are zero, C_{H_2O} and C_{fame} are re-written as $C_{H_2O} = C_{ffa_0}\chi_{ffa}, C_{fame} = C_{ffa_0}\chi_{ffa}$.

Now Eq. 4.26 can be written as,

$$C_{ffa_0}\frac{d\chi_{ffa}}{dt} = k_f C_{ffa_0}(1-\chi_{ffa}).C_{ffa_0}(\alpha-\chi_{ffa}) - k_b {C_{ffa_0}}^2 {\chi_{ffa}}^2 \quad \textbf{4-31}$$

$$\Rightarrow \frac{d\chi_{ffa}}{dt} = C_{ffa_0}\{k_f(1-\chi_{ffa})(\alpha-\chi_{ffa}) - k_b {\chi_{ffa}}^2\} \quad \textbf{4-32}$$

However, $\frac{d\chi_{ffa}}{dt}$ becomes zero when the reaction reaches its equilibrium state.

Now, Eq. 4-32 becomes,

$$k_f(1-\chi_{ffa_e})(\alpha-\chi_{ffa_e}) = k_b {\chi_{ffa}}^2 \quad \textbf{4-33}$$

$$\Rightarrow k_f/k_b = \frac{{\chi_{ffa_e}}^2}{(1-\chi_{ffa_e})(\alpha-\chi_{ffa_e})} = K_e \quad \textbf{4-34}$$

Where K_e and χ_{ffa_e} are the equilibrium constant and χ_{ffa} at equilibrium condition respectively. Right now Eq. 4-32 can be modified and re-written as,

$$\frac{d\chi_{ffa}}{dt} = k_f C_{ffa_0}\left\{(1-\chi_{ffa})(\alpha-\chi_{ffa}) - {k_b}/{k_f}\cdot\chi_{ffa}^{\,2}\right\} \quad \textbf{4-35}$$

$$\Rightarrow \frac{d\chi_{ffa}}{dt} = k_f C_{ffa_0}\left\{(1-\chi_{ffa})(\alpha-\chi_{ffa}) - {\chi_{ffa}^{\,2}}/{K_e}\right\} \quad \textbf{4-36}$$

$$\Rightarrow \frac{d\chi_{ffa}}{dt} = k_f C_{ffa_0}\left\{\alpha-\chi_{ffa}-\alpha.\chi_{ffa}+\chi_{ffa}^{\,2} - {\chi_{ffa}^{\,2}}/{K_e}\right\} \quad \textbf{4-37}$$

$$\Rightarrow \frac{d\chi_{ffa}}{dt} = k_f C_{ffa_0}\left\{\alpha-\chi_{ffa}(1+\alpha)+\chi_{ffa}^{\,2}\left(1-{1}/{K_e}\right)\right\} \quad \textbf{4-38}$$

$$\Rightarrow \int_0^{\chi_{ffa}} \frac{d\chi_{ffa}}{\alpha-\xi\chi_{ffa}+\psi\chi_{ffa}^{\,2}} = \int_0^t C_{ffa_0} k_f\, dt \quad \textbf{4-39}$$

Where, $\xi = 1+\alpha$ and $\psi = 1-{1}/{K_e}$.

By plotting $\int_0^{\chi_{ffa}} \frac{d\chi_{ffa}}{\alpha-\xi\chi_{ffa}+\psi\chi_{ffa}^{\,2}}$ vs $C_{ffa_0}t$, the value of k_f can be calculated.

As higher rate depends on lowering the activation energy, it is necessary to find out the activation energy (E_a in kJ mol^{-1}) of WGS-Mg 12, WGS-Mg 11 and WGS-Mg 21 to show the effectiveness of the developed catalyst. Consequently, the Arrhenius equation implies relation between k_f and T, which is presented in Eq. 4-40.

$$k_f = Ae^{-\left({E_a}/{RT}\right)} \quad \textbf{4-40}$$

Where, the reaction temperature (T in K) varies with the rate constant (k_f). *R* stands for universal gas constant, whereas *A* is the Arrhenius constant varies for all the samples. For graphical interpretation it is convenient to take logarithm of both sides, Eq. 4-40 becomes:

$$\ln k_f = {E_a}/{RT} + \ln A \quad \textbf{4-41}$$

By plotting a graph between lnk_f and 1/T the E_a of the catalysts during the reaction can be found out.

The kinetic parameters of the present reaction process using three different catalysts loading were calculated from the Arrhenius equation. Figure 4-46 a, b and c illustrated the linear correlation between $\int_0^{\chi_{ffa}} \frac{d\chi_{ffa}}{\alpha - \xi\chi_{ffa} + \psi\chi_{ffa}^2}$ and $C_{ffa_0}t$, from which the k_f value was calculated and presented in Table 4-15. Another graph was plotted between $\ln k_f$ and $1/T$ is reported in Figure 4-46 d, e, f and the variation in values of activation energy and the Arrhenius constant are presented in Table 4-16. From the E_a values it can be clearly inferred that the activation energy of WGS-Mg 12 is lower.

4.5.3 ^{1}HNMR spectrum study of WCO and esterified product

Figure 4-47 shows the typical ^{1}HNMR spectra of WCO and its esterified product. The esterified product was obtained at 80 °C reaction temperature keeping other parameters constant i.e. ratio of oil to methanol and catalyst weight percentage. After separation final products were analyzed and compared with WCO. The relevant corresponding ^{1}H resonance is attributed in Table 4. The validation of fatty acid conversion and methyl ester formation was observed through disappearance and appearance of distinctive peaks [30]. Spectra of ^{1}HNMR of WCO shows a signal at 4.15 and 4.29 ppm which is attributed to glycerol -CH_2 groups. If the spectrum of esterified products at 80 °C reaction temperature will be considered, then a clear shift at 3.67 ppm (strong signal) can be observed which is attributed to methoxy protons of methyl ester. Most importantly, the spectrum shows absence of double duplets.

4.5.4 Comparison of WGS-Mg with earlier reported work

Various attributes viz. precursor, strength, different operating parameters and reusable capacity were considered to compare the present work with the earlier reported work [248, 249, 273]. Table 5 lists information about the various precursors used. Zeng et al. [248] and Shang et al. [273] reported sulfonation using H_2SO_4 whereas Dai et al. [249] used Li_2CO_3. Although the surface area reported was less compared to the present work, the catalysts have shown excellent results during methanolysis of various oil/fatty

acids. They have used cottonseed oil, soybean oil and oleic acid out of which two are edible. So, a comparable study was done using a sample of waste cooking oil. It was observed that the yield above 85% was obtained at reaction temperature above 80 °C though Dai et al. obtained the same yield at 65 °C reaction temperature. However, for the same yield the ratio of oil to methanol (molar) lies in between 1:9 to 1:15. Apart from these, another important factor is catalyst weight percentage used during the reaction because it creates a huge difference when the lab scale experiment is translated in to a large scale industry. From the comparison it was found that maximum yield can be obtained using only 2% of WGS-Mg catalyst and the same was also obtained by Zeng et al. Whereas Dai et al. and Shang et al. have used around 7% of the catalyst to get the higher yield i.e. above 85%. Similarly, time of reaction also plays an important role and the comparison shows that Shang et al. took 6 h to obtain a highest yield whereas rest of the work reported 2-3 h reaction time to obtain the same.

4.5.5 Reusability of WGS-Mg

Apart from these factors responsible for the reaction enhancement, another factor i.e. reusability of the developed catalyst has a role in chemical industry. So, an extensive reusability study was conducted by regenerating the WGS-Mg 11 catalyst and conducting the same methanolysis experiment repeatedly for 7 times after every regeneration. The experimental protocol remains the same as mentioned under section 2, however the parameters were fixed i.e. reaction temperature was set to 80 °C, the oil to methanol ratio was 1:15, catalyst wt.% was 2% and reaction time period was 180 minutes.

After every experiment the catalyst was separated from the mixture and was rinsed in methanol followed by calcination at 350 °C. The catalyst was calcined to ensure removal of liquid mixtures i.e. methanol and ester as well as for the catalyst activation. The yield obtained after every reaction is shown in Figure 4-48a. It was observed that the overall decrease in yield after 7 reaction cycle was only 2.9% and similar result was also obtained by Shang et al. However, rest of the work reported the overall decrease to be above 30%. The decrease in yield occurs due to the leaching of active sites in to methanol. This confirms the higher stability of the WGS-Mg based catalyst. The FESEM image of recovered catalyst after 7^{th} cycle is presented in Figure 4-48b and c. The microscopic view clearly showing that the metal composites are still intact on the surface.

4.6 Peroxidation of Neem oil using HAp-Zn

4.6.1 Parametric effects on IV_C and OOC_C

Experiments for Peroxidation of PNO were done by Response Surface Methodology using Design-Expert version 6.0.6. A Face Central Composite Design (FCCD) was constructed with five input variables and two response variables. The input variables with 5 different levels ensued from the design are presented in Reaction time (h) Table 4-19. With certain combinations of input variables i.e. Temperature (T), Time (t), HAP-Zn (H_{Zn}), H_2O_2:PNO ($\gamma_{H:FA}$), HCOOH:PNO ($\gamma_{F:FA}$) experiments were conducted, and the results i.e. Iodine value conversion (IV_C) and Oxirane Oxygen Conversion (OOC_C) were recorded in Table 4-20.

The response surface plots are shown in Figure 4-49. At constant H_{Zn} value (Figure 4-49a) and increasing in T value, there is a gradual increase in IV_C and vice versa. But at 70 °C with an increase in H_{Zn}, slight decrement in IV_C was noticed after 20:1 of H_{Zn}. At constant $\gamma_{H:FA}$ (Figure 4-49b) and increase in T resulted in a gradual increment of IV_C. But at constant T value there is an increase in IV_C up to 20:1 of $\gamma_{H:FA}$ but after it, IV_C gradually decreased to some extent. Though H_2O_2 concentration increases the reaction rate, at higher concentration stability of Oxirane ring becomes poor. So, at the same temperature and higher concentration the conversion decreased relatively.

Apart from the catalyst loading another two factors which plays a major role in the reaction are the amount of formic acid and hydrogen peroxide. The individual along with group effect of these two parameters are illustrated in Figure 4-49 c and d. Figure 4-49c shows the interaction of $\gamma_{H:FA}$, $\gamma_{F:FA}$ with IV_C, where it can be easily observed that at the lowest value of $\gamma_{F:FA}$ there is an increase in IV_C up to $\gamma_{H:FA}$ of 20:1 and then IV_C decreased to some extent because of poor stability. But at higher concentration of $\gamma_{F:FA}$ a gradual increase in IV_C was observed with increase in $\gamma_{H:FA}$ because of sufficient peroxy carboxylic acid formation. The Same trend line in IV_C was observed with constant lowest and highest $\gamma_{H:FA}$ with increasing in $\gamma_{F:FA}$. Also, this IV_C trend line has complete resemblance with the OOC_C (Figure 4-49d).

The FCCD model with 5 factors with 3 levels each was chosen. These factors are individual dependable reaction parameters which will be locally optimized with the

precise end goal. Table 4-20 records the variable trial settings based on the FCCD model. The model gave 32 contoured experiments set which was led randomly. Multiple regression fitted the final results. The parametric coefficients of the model were assessed using regression analysis and significance of each term were tested. From the "Analysis of Variance" (ANNOVA) given in Table 4-21, it is clear that most of the terms are significant *i.e. p*-values (Probability Value) are less than 0.05. But few terms are insignificant such as $\gamma_{H:FA}$, T^2, Tt, $T\gamma_{F:FA}$, TH_{Zn}, $t\gamma_{H:FA}$, $t\gamma_{F:FA}$, $t\ H_{Zn}$, $\gamma_{F:FA}\ H_{Zn}$ for IV_C and $\gamma_{H:FA}$, T^2, t^2, Tt, $T\gamma_{F:FA}$, TH_{Zn}, $t\gamma_{H:FA}$, $t\gamma_{F:FA}$, $t\ H_{Zn}$, $\gamma_{F:FA}\ H_{Zn}$ for OOC_C. The R^2 value was found to be 0.9516 and 0.9387 for IV_C and OOC_C respectively.

The "Analysis of Variance" (ANNOVA) given in Table 4-21 (Supporting information), it is clear that most of the terms are significant *i.e. p*-values (Probability Value) are less than 0.05. After doing "Sequential Model Sum of Squares" and "lack of fit tests", it was observed that the quadratic regression model was best fitted. The mathematical model with significant factorial values is presented in the following equation.

$$IV_C = 39.19 + 3.93\times T + 2.69\times t + 3.25\times \gamma_{\text{F:FA}} + 3.014\times H_{Zn} - 2.345\times {\gamma_{H:FA}}^2 - 3.94\times {\gamma_{F:FA}}^2 - 2.23\times {H_{Zn}}^2 + 1.88\times T\times \gamma_{H:FA} + 4.6\times \gamma_{H:FA}\times \gamma_{F:FA} + 2.023\times \gamma_{H:FA}\times H_{Zn} \quad \textbf{4-42}$$

$$OOC_C = 34.3 + 3.804\times T + 2.69\times t + 2.64\times \gamma_{\text{F:FA}} + 2.64\times H_{Zn} - 1.92\times {\gamma_{H:FA}}^2 - 4.01\times {\gamma_{F:FA}}^2 - 2.18\times {H_{Zn}}^2 + 4.44\times \gamma_{H:FA}\times \gamma_{F:FA} \quad \textbf{4-43}$$

A graph between actual, predicted values of IV_C and OOC_C are shown in Figure 4a and 4b. All the data was fitted, and the degree of freedom was 31. For both the responses, the R^2 value was 0.99. The Model F-value for IV_C and OOC_C was 10.82 and 8.23 respectively. The corresponding IV_C and OOC_C "Model F-value" could be this largely due to noise, and the chances are 0.01% and 0.05% respectively. The standard error was 0.01059 and 0.01288 for IV_C and OOC_C respectively. The whole analysis inferred that Figure 4a and 4b were the best fitted. Local model optimization was done by keeping IV_C and OOC_C to be maximum and the parameters within the range. The optimized parametric values for T, t, H_{Zn}, $\gamma_{H:FA}$, $\gamma_{F:FA}$ were found to be 60 °C, 3.88 h, 20 wt%, 19.05:1, 19.85:1 which showed maximum desirability i.e. 0.971.

4.6.2 Analysis of ENO obtained at optimal condition

To evident oxirane ring in ENO, the final product was screened through FTIR. The comparison between FTIR spectra of PNO and ENO is illustrated in Figure 4-51. Wave number ranging between 815 cm^{-1} - 950 cm^{-1} is the boundary to detect Oxirane ring, while HC=CH (cis) bonding peak and C=O stretching peaks were detected at wave numbers 1650 cm^{-1} - 1600 cm^{-1} and 1720 cm^{-1}. Most importantly, in ENO the Oxirane ring peak was detected at 844 cm^{-1} for ENO [274]. Apart from it few more important regions are also detected, which are -C-O stretching (1000-1100 cm^{-1}), C-H bending (1400-1500 cm^{-1}), -CH stretching (2850-3000 cm^{-1}). The presence of O-H stretching vibration in ENO was detected at 3458 cm^{-1} indicates. During peroxidation, the simultaneous reverse reaction of the acid and hydrogen peroxide follows the production of another molecule of peracid again and a free hydroxyl group (O-H).

After getting a clarification from FTIR images, concordant spectrum for O-ring was observed in Figure 4-52. The figure is depicting the ^{1}HNMR spectrum of PNO, in which the very first peak 1 (δ= 0.87 ppm) represents methyl protons. The protons of fatty acid i.e. $(CH)_2$-CO- were at peak 6 (δ= 2.3 ppm) while -CH_2- near the C=C was referred to peak 5 (δ= 2.17 ppm). Apart from it rest of the -CH_2- were assigned to peak 2 (δ= 1.24 ppm). The methyl protons of glycerol were observed in the range of δ= 4.0-4.5 ppm. Hence the peak 8 (δ= 4.12 ppm) and peak 9 (δ= 4.27 ppm) were the methyl protons; these peaks were considered as a basic reference as the intensity should not alter throughout the reaction process. Another methyl proton was observed at peak 7 (δ= 3.6 ppm) which is attached to the hydroxyl group (OH-CH-). The most important characteristic peak was marked at peak 10 (δ= 5.32 ppm), responsible for fatty acid double bond (-CH=CH-) where the peroxidation ring was supposed to form. Figure 4-52 illustrating the ^{1}HNMR of ENO and the peak 10 (δ= 3.3 ppm) was marked for protons of epoxide ring. It clearly inferred the peroxidation reaction had occurred successfully. As it was observed that the reaction was not 100% completed, a small peak of double bond protons (-CH=CH-) popped up at δ= 5.3 ppm and was marked as unreacted fatty acid.

4.6.3 Probable reaction mechanism during peroxidation

A single molecular reaction occurs in nano-fraction of a second. Therefore, the reaction mechanism is based on the final product and there is basic chemistry involved to

propose a best probable reaction intermediates. Figure 4-53 shows the mechanism of probable reaction intermediates formation in 4 stages. In stage 1, the formation of performic acid (HCOOOH) is shown. Among two reactants peroxide has nucleophilic sites (hydrogen and oxygen) whereas, formic acid has electrophilic sites (carbonyl carbon). The *p* orbital in oxygen and π^* orbital in carbonyl carbon interact to produce tetrahedral transitional state with the loss of H_2O molecule. Stage 2 shows the fatty acid adsorb to the active site by means of van der Waals force of attraction [275]. The bond exchange in peroxidation occurs in stage 3 in between performic acid and the fatty acid adsorbed to the catalyst active site. Here, C=C of fatty acid is the nucleophile and oxygen of performic acid is somewhat electrophile. The π electron of carbonyl attack and break the outer weak O-O bond of performic acid leads to formation of C=O. The subsequent breaking of earliest C=O forms O-H. Again breaking of original O-H lead to the formation of C-O bond. Stage 4 is the desorption phase, where the final peroxidation process completed giving rise to the fatty acid with O ring and regenerated formic acid molecule.

4.6.4 Comparison of HAp-Zn with earlier reported works

Table 5 gives the comparison of IV_C of various oils for different types of catalysts including homogeneous, heterogeneous (polymeric and metallic) catalysts that are reported in the literature [276-287]. In the present work, all the experiments were conducted for a limited period to show the dependent variables effect on the IV_C. For the comparison purpose, another experiment was conducted at the local optimal values with an extended reaction period of 10 h and the IV_C was 84.3%. Few works reported IV_C above 80%, but the reaction temperature was above 70 °C and the reaction time was 24 h.[276, 278, 280, 284, 285] In contrast to the present work, the IV_C was above 80% for a reaction time of 10 h but the catalyst used was 20%. Goud et al. [277] have used homogeneous catalysts such as H_2SO_4, HNO_3 for peroxidation of Mahua oil, and the IV_C was 60% and 36% respectively at the same reaction time of 10 h. Also, few works reported earlier, in which the IV_C of vegetable oil peroxidation was reported to be below 35%. Cai et al. [281], Sharma et al. [282] have used 12 and 20 weight % catalyst for vegetable oil peroxidation. Although the reaction time was less than 10 h however, the reaction temperature was above 75 °C. Farias et al. [285] observed a very high conversion after 24 h of reaction period and higher reaction temperature of 110 °C which is

comparable to our present work. However, the use of homogeneous Molybdenum catalyst per reaction was only 1%. Another work, by Benaniba et al. [286] is comparable because they also used Tungsten based catalyst for sunflower oil epoxidation and reported a promising result after 8h. Recent development of organometallic oxidant by Yao et al. [287] showed the performance in peroxidation of Olive oil and Linseed oil. They reported a high conversion i.e. 87.9% for olive oil in 12h and 92.4% for linseed oil in 9 h at ambient temperature. However, for each experiment they used 3.55 g of oxidant per 0.5 g of oil i.e. the catalyst wt.% was 710% in excess. Although the conversion was so high, the catalyst wt.% used in the experiment was the major disadvantage. After studying the various catalyst performances during peroxidation reaction, Amberlite based catalyst shows the promising result however, it is very costly. Hence, considering results of all the reported work on peroxidation of vegetable oils and FAME using heterogeneous catalyst it is thus confirmed that HAp-Zn is a more efficient and less costly catalyst.

4.6.5 Reusability of HAp, CHAp, HAp-Zn

Regeneration of the catalyst was carried out to make it reusable during the repetition of peroxidation at its optimal points. The recovered catalysts were washed with Methanol to dissolve traces of oil followed by oven drying at 150 °C. Except HAp, rest two materials were again calcined up to 500 °C to reactivate it for further use. To verify the stability of the original and regenerated catalysts, they were used for peroxidation of neem oil at 60 °C (T), 300 minutes (t), 20 (H_{Zn}), 20:1 ($\gamma_{H:FA}$), 20:1 ($\gamma_{F:FA}$). Figure 4-54 shows the IV_C w.r.t reaction time for HAp, CHAp, HAp-Zn and ZnO before and after four consecutive regenerations.

To justify the use of catalyst during peroxidation reaction, a primary run was conducted in absence of catalyst. The maximum IV_C achieved in absence of any catalyst was 17%. Afterwards it was observed for the first use of HAp (before washing), the IV_C value was limited to 20% after 300 minutes. However, CHAp and HAp-Zn showed a gradual increase in IV_C i.e. up to 41% and 58% respectively. After each regeneration, it was found that IV_C value doesn't vary significantly for HAP-Zn. However, for HAp, CHAp a significant change in IV_C was noticed, which confirmed that ZnO deposition increased the stability of the base material. The catalytic effect of Zn metal was studied by another set of experiments which were conducted using commercialized ZnO.

Although the conversion was bit less than HAp-Zn, the stability of the catalyst remains same throughout the peroxidation reaction. The difference between the % conversion was insignificant which is clearly inferred from the figure. It was observed that the catalyst (HAp-Zn) activity stayed the same even if after four cycles. FTIR analysis was conducted for every regenerated catalyst to study the qualitative analysis. Figure 4-55 shows the comparison between fresh HAp-Zn and regenerated catalyst samples. A very precise difference was noticed at 3317 cm^{-1} which were responsible for O-H stretching caused by absorbed water molecules. This peak disappeared after the first wash. However, the stretching mode of ZnO nanocomposite remains unchanged. The regenerated catalysts maintained similar trend which confirming a stable catalyst during peroxidation.

Table 4-1 Different surface area (m^2 g^{-1}) measurements and pore volume (cc g^{-1})

Surface area and Pore volume	HAp	CHAp	HAP-Al	Cu-NHAp [240]	Animal bone [269]	Waste animal bone [111]	H_3PO_4 /Al_2O_3 [271]
Langmuir Surface area (m^2 g^{-1}) at P_s/P_0=0.9814	5.708	164.77	157.96	-	-	-	-
One point BET Surface area (m^2 g^{-1}) at P_s/P_0=0.3	8.879	165.1	164.68	-	-	-	-
Adsorbed BET Surface area (m^2 g^{-1})	10.86	167.86	168.96	16.78	4.01	110.96	120
Adsorbed t-plot Surface area (m^2 g^{-1})	27.26	161.23	181.62	-	-	-	-
Total pore volume (cc g^{-1}) at P_s/P_0=0.9814	0.089	0.49	0.81	0.031	0.016	-	0.3
Total BJH pore volume (cc g^{-1})	0.108	0.49	0.88	-	-	-	-

Table 4-2 Significant comparison of surface area (m^2 g^{-1}) and pore volume (cc g^{-1}) of HAp, CHAp and HAp-Zn

Parameter	Materials			
	HAp	CHAp	HAP-Zn	Hap-Al
BET Surface area (m^2 g^{-1})	10.86	167.86	217.29	168.96
Total pore volume at Ps/P0=0.981 (cc g^{-1})	0.0894	0.4926	0. 4232	0.8062

Table 4-3 Different surface area (m^2 g^{-1}) measurements and pore volume (cc g^{-1})

Parameter	HAp-Mg
Langmuir Surface area (m^2 g^{-1}) at P_S/P_0=0.9814	128.45
One Point BET Surface Area (m^2 g^{-1}) at Ps/Po=0.3	131.24
Adsorbed BET Surface area (m^2 g^{-1})	134.1
Adsorbed t-plot Surface area (m^2 g^{-1})	136.3
Total pore volume (cc g^{-1}) at P_S/P_0=0.9814	0.45
Total BJH pore volume (cc g^{-1})	0.46

Table 4-4 Different surface area ($m^2\ g^{-1}$) measurements and pore volume (cc g^{-1})

Parameter	HAp-Na-Si
Langmuir Surface area ($m^2\ g^{-1}$) at P_S/P_0=0.9814	55.9
One Point BET Surface Area ($m^2\ g^{-1}$) at Ps/Po=0.3	56.1
Adsorbed BET Surface area ($m^2\ g^{-1}$)	57.1
Adsorbed t-plot Surface area ($m^2\ g^{-1}$)	57.3
Total pore volume (cc g^{-1}) at P_S/P_0=0.9814	0.49
Total BJH pore volume (cc g^{-1})	0.54

Table 4-5 Surface area analysis of WGS-Mg and comparison with other research works

Parameter	WSG-Mg			Peanut shell [248]	Peanut husk [249]	Sulfonated peanut shell [250]
	12	11	21			
Surface area ($m^2\ g^{-1}$)	49.4	47.8	46.2	12.35	1.21	10.45
Total Pore volume (cc g^{-1}) $\times 10^{-2}$	7.6	7.2	7.4	34	0.35	-
Average pore size (D in nm)	0.062	0.056	0.058	39.25	-	41.95

Table 4-6 Final Integral form of Eq. 4-8 for 8 cases

	y=0	**y=1**	**y=2**
z= 0	$C_{T0}X = kt$	$\ln(\frac{1}{1-X}) = kt$	$\frac{X}{(1-X)} = kC_{T0}t$
z= 1	$-\frac{1}{3}[\ln\frac{(\delta-3X)}{\delta}] = kt$	$\frac{1}{(\delta-3)}\ln[\frac{(\delta-3X)}{(1-X)\delta}] = kC_{T0}t$	$\frac{1}{(\delta-3)}\{\frac{X}{(1-X)} - \frac{3}{(\delta-3)}\ln[\psi]\} = kC_{T0}^2t$
z= 2	$\frac{X}{(\delta-3X)\delta} = kC_{T0}t$	$\frac{1}{(3-\delta)}\{\frac{3X}{(\delta-3X)\delta} - \frac{1}{(3-\delta)}\ln[\frac{1}{\psi}]\} = kC_{T0}^2t$	------

Where $\psi = \frac{(\delta-3X)}{\delta(1-X)}$

Table 4-7 The value of standard error and R^2 value for all 8 cases

Cases	R^2	Standard error
y=0, z=0	0.9796	2.64E-04
y=1, z=0	0.9815	8.86E-04
y= 0, z= 1	0.98207	1.96E-05
y= 1, z= 1	0.9787	5.46E-05
y= 2, z= 0	0.8288	0.01698
y= 0, z= 2	0.9842	1.46E-06
y= 2, z=1	0.8199	0.00146
y= 1, z=2	0.9729	7.11E-06

Table 4-8 FTIR frequencies of TNO obtained at optimal condition

Frequency (cm^{-1})	Absorption intensity	Functional group	Vibration
691	Weak	$-CH_2$	Plane vibration
1023	Weak	-C-O-C-	Asymmetric stretching vibration
1126	Moderate	-C-O-C-	Symmetric stretching vibration
1311	Moderate	$-CH_3$	Bending vibration
1410	Moderate	$-CH_2$	Shear-type vibration
1728	Strong	-C=O	Stretching
2766	Strong	$-CH_2$	Symmetric stretching vibration
2912	Strong	$-CH_2$	Asymmetric stretching vibration
3018	Strong	=C-H	Stretching
3422	Weak	-O-H	Stretching

Table 4-9 FAME yields using various catalysts in the transesterification of vegetable oil and comparison with present work

Vegetable oil	Catalyst Types	Reaction Condition				Methyl ester yield (%)
		CA[a]	RT[b]	Rt[c]	MO[d]	
Soybean oil [259]	WO_3/ZrO_2	>10	1200	200-300	40	90
Soybean oil [125]	La/Zeolite beta	2	240	160	14.5	48.9
Palm oil [260]	Mg-Al-CO_3 (Hydrotalcite)	7.5	360	100	30	86.6
Rapeseed oil [123]	$CaTiO_3$	1	600	60	6	90
Soybean oil [261]	$MgO.MgAl_2O_4$	3	600	65	3	57
Sunflower oil [262]	CaO/SBA-14	-	300	160	12	95
Soybean oil [263]	MgO, ZnO, Al_2O_3	5	420	70-130	55	82
Cotton seed oil [264]	Mg-Al-CO_3 HT	1.5	720	180-210	6	87
soybean oil [265]	MgO	10	100	120	60	< 40
soybean oil [265]	Al-Mg hydrotalcite	10	100	180	60	< 80
Jatropha oil [266]	KNO_3/Al_2O_3	6	70	420	12:01	87
soybean oil [267]	CaO	8	65	180	12:01	> 95
Neem oil	CWFB-HAp-Al	3	120	70	30	95

[a]CA: Catalyst amount (wt.%), [b]RT: Reaction time (minutes), [c]Rt: Reaction temperature (°C), [d]MO: Methanol to oil ratio

Table 4-10 k_f' (min^{-1}) for 0% and 6% HAp-Mg loading with respective reaction temperature (K) and 1:15 oil to methanol ratio

Rt	MO	k_f'	
		HAp-Mg=0%	HAp-Mg=6%
333	1:15	0.0135	0.0137
343	1:15	0.0265	0.0179
353	1:15	0.037	0.0244
363	1:15	0.0591	0.0364

Table 4-11 Activation energy and Arrhenius constant with and without catalyst*

HAp-Mg loading	E_a (kJ mol^{-1})	A
HAp-Mg=0%	47.86	464167.1
HAp-Mg=6%	32.35	1575.9

* All the reaction was carried out with 1:15 oil to methanol ratio

Table 4-12 Methyl ester yields using various natural and synthetic hydroxyapatite based catalysts in vegetable oil/fatty acid esterification and comparison with the present work

Fatty acid / Vegetable oil	Catalyst	BET surface area (m^2 g^{-1})	Parameters	Methyl ester yield (%)
Peanut [269]	Animal bone powder	4.01	4 h, 60 °C, 600 rpm	<80%
Oleic acid [240]	Cu/ Hydroxyapatite (Fishbone)	16.78	1h, 70 °C, 800 rpm, 0.4 mL min^{-1} ethanol flow rate	<83.57%
Rapeseed [270]	Biont shell	88.53	3h, 70 °C, 600 °C (calcination), 9:1 methanol to oil	<80%
Palm [111]	Waste animal bone	88.53	4h, 65 °C, 800 °C (catalyst calcination), 200 rpm, 15 wt. % catalyst loading	80%
Rapeseed [269]	Animal bone powder	4.01	4h, 60 °C, 24:1 methanol to oil, 600 rpm	85%
Oleic acid [271]	Al_2O_3/H_3PO_4 (Synthetic)	120	1h, 350 °C, 0.15 (mmol acid/g product)	95.5%
Neem oil (Present work)	HAp-Mg	131.24	2.25h, 70 °C, 1:15 (oil to methanol), 6 wt.% catalyst loading, 650 °C (calcination)	95%

Table 4-13 Physiochemical properties of Neem oil and transesterified product

Properties	Unit	ASTM method	PNO	TNO
Acid value	mg KOH/ g oil	D974	23.8	0.78
Density	g cm^{-3}	D4052	910	872
Viscosity	mm^2 sec^{-1}	D445	52.1	4.82
Flash point	°C	D93	---	165
Pour point	°C	D4419-90	3	-4

Table 4-14 FTIR frequencies of purified and trans-esterified neem oil

Frequency (cm^{-1})	Functional group	Frequency (cm^{-1})	Functional group
722	$-CH_2$	1742	-C=O
1163	C-O-C	2766	$-CH_2$
1375	$O-CH_2$	2912	$-CH_2$
1379	$O-CH_2$	3018	=C-H
1436	$(CO)-O-CH_3$	3422	-OH

Table 4-15 Rate constant for various WGS-Mg with respective reaction temperature

T (°C)	k (L mol^{-1} min^{-1})		
	WGS-Mg 12	WGS-Mg 11	WGS-Mg 21
60	8.3×10^{-04}	6.36×10^{-04}	5.55×10^{-04}
70	1.02×10^{-03}	8.98×10^{-04}	8.57×10^{-04}
80	1.39×10^{-03}	1.24×10^{-03}	1.19×10^{-03}
90	1.89×10^{-03}	1.55×10^{-03}	1.67×10^{-03}

Table 4-16 Activation energy and Arrhenius constant for various WGS-Mg

Catalyst	Ea (J mol^{-1})	A
WGS-Mg 12	28.04×10^{03}	20.0001
WGS-Mg 11	30.15×10^{03}	34.707
WGS-Mg 21	36.59×10^{03}	311.31

Table 4-17 Attribution of various ^{1}HNMR resonance

δ_H (ppm)	Attributes (proton)	Functional group type
0.87, 0.88, 0.89	C-CH_3	Terminal methyl group
1.25, 1.27, 1.3	-(CH_2)n-	-CH_2 Backbone
1.53, 1.56, 1.6, 1.62	-CH_2-CH_2-$COOCH_3$-	β-methylene proton
2.0, 2.01	=CH-CH_2-	α-methylene attached to one double bond
2.3, 2.31, 2.32	-CH_2COOR	α-methylene group to ester
3.67	-CO(CH_3)O	Methyl group to ester
4.15, 4.29	-CH_2-, -CH-	Glycerol -CH_2 group
5.34, 5.35	-CH=CH-	Olefinic proton

Table 4-18 Comparison of present work with earlier presented works

Attributes	WGS-Mg (Present work)	Peanut shell [248]	Peanut husk [249]	Peanut shell [273]
Precursor used	$MgSO_4.7H_2O$	Sulfonation using H_2SO_4	Li_2CO_3	Sulfonation using H_2SO_4
Oil/Fatty acids for methanolysis	WCO	Cottonseed oil	Soybean oil	Oleic acid
Conditions for Conversion above 85%	RT[a]= 90 O:M[b]= 1:15 CW[c]= 2 Rt[d]= 3	RT= 85 O:M= 1:9 CW= 2 Rt= 2	RT= 65 O:M= 1:12 CW= 6 Rt= 3	RT= 85 O:M= 1:12 CW= 7 Rt= 6
Extensive reusability study	Yield decreased by 2.9% after Seven cycles	Yield decreased by 39.9% after Five cycles	Yield decreased by 33.84% after Six cycles	More than 95% retained after Six cycles

a Reaction temperature (C), *b* Oil:methanol (molar ratio), *c* Catalyst weight (wt.%), *d* Reaction time (h)

Table 4-19 Input variables and ranges of their levels

Level	Temperature (°C)	Time (minutes)	HAp-Zn (wt.%)	H_2O_2:PNO (molar ratio)	HCOOH:PNO (molar ratio)
---	30	60	5	5:1	5:1
--	40	120	10	10:1	10:1
*	50	180	15	15:1	15:1
++	60	240	20	20:1	20:1
+++	70	300	25	25:1	25:1

Table 4-20 Experimental matrix for Neem oil peroxidation

Run	Factors					Responses		[c]TON
	T	t	H_{Zn}	$\gamma_{H:FA}$	$\gamma_{F:FA}$	[a]IV_C	[b]OOC_C	
1	40	120	10	10:01	20:01	23.71	19.68	433
2	40	240	10	10:01	10:01	29.3	24.87	536
3	40	240	20	10:01	20:01	28.3	22.94	270
4	50	180	5	15:01	15:01	21.34	16.93	774
5	50	180	15	25:01	15:01	25.8	22.06	328
6	30	180	15	15:01	15:01	26.22	24.69	335
7	40	120	20	20:01	20:01	34.52	29.48	320
8	50	180	25	15:01	15:01	38.55	33.67	279
9	50	180	15	15:01	15:01	39.5	34.62	502
10	50	180	15	15:01	15:01	39.2	33.57	482
11	60	120	20	20:01	10:01	22.6	19.56	204
12	50	180	15	15:01	15:01	38.86	33.81	489
13	50	300	15	15:01	15:01	37.86	33.28	476
14	60	240	10	20:01	10:01	27.07	24.6	495
15	40	120	10	20:01	10:01	21.78	16.34	418
16	50	180	15	5:01	15:01	33.22	30.67	408
17	60	240	10	10:01	20:01	32.56	28.31	595
18	60	120	20	10:01	20:01	29.84	24.65	285
19	50	180	15	15:01	15:01	39.1	35.82	494
20	50	180	15	15:01	25:01	24.6	18.47	316
21	60	240	20	10:01	10:01	32.7	28.74	297

22	50	180	15	15:01	15:01	40.3	34.82	508
23	50	60	15	15:01	15:01	29.6	24.74	358
24	70	180	15	15:01	15:01	42.1	38.4	533
25	50	180	15	15:01	15:01	38.8	33.71	488
26	50	180	15	15:01	5:01	21.6	17.52	262
27	40	120	20	10:01	10:01	25.3	21.64	232
28	60	120	10	20:01	20:01	37.14	32.84	708
29	60	120	10	10:01	10:01	27.8	25.15	493
30	40	240	10	20:01	20:01	28.4	24.75	517
31	40	240	20	20:01	10:01	24.06	19.89	217
32	60	240	20	20:01	20:01	48.36	45.63	443

a Iodine value conversion

b Relative OOC % Conversion

c Turn over number (TON) defined as moles of unsaturated double bonds converted per moles of metal ion

Table 4-21 Analysis of Variance

Source	Sum of Squares		DF	Mean Square		F Value		Prob > F	
	IV_C	OOC_C	IV_C & OOC_C	IV_C	OOC_C	IV_C	OOC_C	IV_C	OOC_C
Model	2264.5	1988.01	20	113.22	99.4	10.81	8.41	0.0001	0.0004
T	371.77	347.39	1	371.77	347.39	35.51	29.41	< 0.0001	0.0002
t	173.77	157.44	1	173.77	157.44	16.60	13.32	0.0018	0.0038
$\gamma_{H:FA}$	17.374	13.66	1	17.37	13.66	1.65	1.156	0.2241	0.3051
$\gamma_{F:FA}$	254.93	167.42	1	254.93	167.42	24.35	14.17	0.0004	0.0031
H_{Zn}	218.04	167.85	1	218.04	167.85	20.82	14.21	0.0008	0.0031
T^2	41.04	11.39	1	41.04	11.39	3.92	0.96	0.0732	0.347
t^2	48.84	46.35	1	48.84	46.35	4.66	3.92	0.0537	0.0732
$\gamma_{H:FA}^2$	161.36	107.94	1	161.36	107.94	15.41	9.13	0.0024	0.0116
$\gamma_{F:FA}^2$	457.19	471.87	1	457.19	471.87	43.67	39.94	< 0.0001	< 0.0001
H_{Zn}^2	146.75	139.98	1	146.75	139.98	14.01	11.85	0.0032	0.0055
T t	0.12	0.19	1	0.12	0.19	0.012	0.016	0.9134	0.8999
T $\gamma_{H:FA}$	56.7	50.58	1	56.7	50.58	5.41	4.28	0.0401	0.0628
T $\gamma_{F:FA}$	0.65	0.1	1	0.65	0.1	0.062	0.0085	0.8069	0.9281
T H_{Zn}	25.15	21.6	1	25.15	21.6	2.402	1.83	0.1494	0.2025
t $\gamma_{H:FA}$	15.28	17.87	1	15.28	17.87	1.46	1.51	0.2522	0.2443
t $\gamma_{F:FA}$	33.75	21.22	1	33.75	21.22	3.22	1.79	0.1	0.2071
t H_{Zn}	2.05	1.35	1	2.059	1.35	0.19	0.11	0.666	0.7415
$\gamma_{H:FA}$ $\gamma_{F:FA}$	338.56	316.21	1	338.56	316.21	32.34	26.77	0.0001	0.0003

$\gamma_{H:FA}$ H_{Zn}	65.52	56.51	1	65.52	56.51	6.26	4.78	0.0294	0.0512
$\gamma_{F:FA}$ H_{Zn}	0.015	0.004	1	0.015	0.004	0.001	0.0003	0.9699	0.9858
Residual	115.14	129.93	11	10.46	11.81				
Lack of Fit	113.61	126.17	6	18.93	21.03	61.74	28.01	0.0002	0.0011
Pure Error	1.53	3.75	5	0.307	0.75				
Cor Total	2379.6	2117.95	31						

Table 4-22 Comparison of neem oil IV_C using bio-waste materials with various vegetable oil IV_C using commercial catalysts (earlier reported work)

Oil and pure fatty acids	Catalyst	WC[a]	RT[b]	Rt[c]	IV_C (%)
Soybean oil [278]	Al_2O_3	5	80	24	97
Oleic acid methyl ester [279]	Ti-silicas	20	70	24	20
Vegetable oil mixture [276]	Ti(IV)-grafted silica	8	-	24	85
Oleic acid [280]	Silica-sulphuric acid	5	70	24	88
FAME [281]	$(C_3SO_3HMIM)(HSO_4)$	12	85	2	30
Canola oil [282]	Amberlite IR-120	20	100	5	35
Mahua oil [277]	H_2SO_4	3.12	30	10	60
Mahua oil [277]	HNO_3	3.12	30	10	36
Soybean oil [283]	Ti/SiO_2	2.5	80	26.7	34.78
Soybean oil [284]	Amberlite IR-120	15	75	7	96.9
Soybean oil [285]	$(MoO_2(acac)_2)$/ TBHP	1	110	24	83.2
Sunflower oil [286]	$WO_5O=P(NMe_2)_3$	25	55	8	75.5
Olive oil [287]	Oxidant SiO_2@ $(CH_2)_2COOOH$	710	Ambient	12	87.9
Linseed oil [287]	Oxidant SiO_2@ $(CH_2)_2COOOH$	710	Ambient	9	92.4
Present Work	HAp-Zn	20	60	10	84.3

a WC: Wt.% catalyst, b RT: Reaction Temperature (°C), c Rt: Reaction time (minutes)

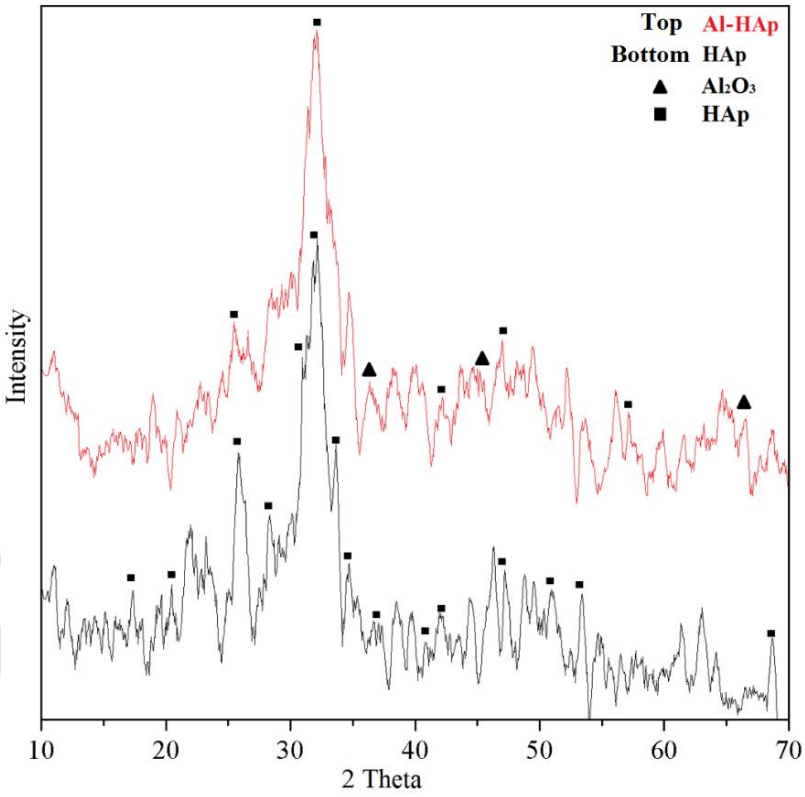

Figure 4-1 X-ray diffraction patterns of HAp and Al-HAp showing characteristic peaks

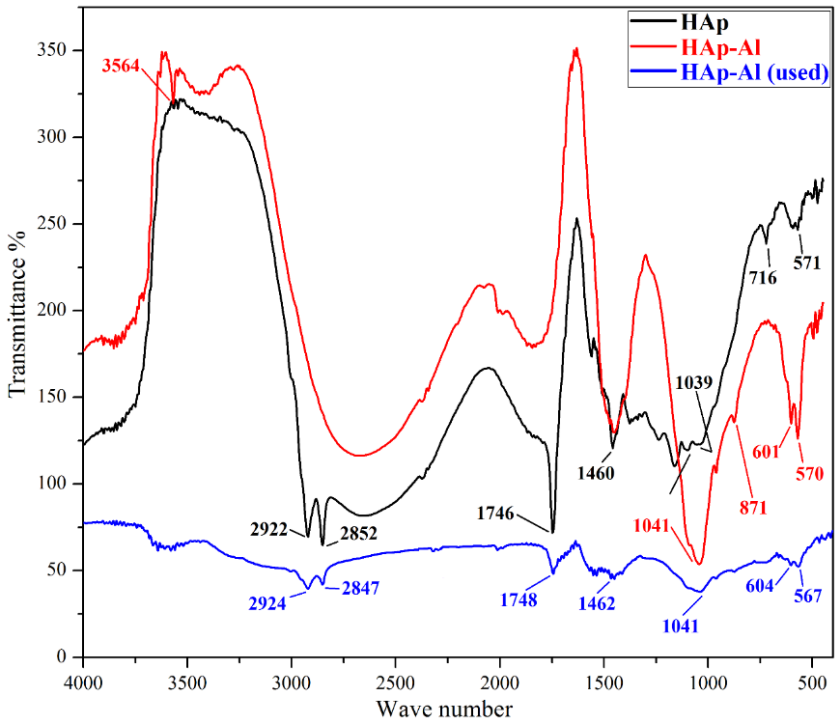

Figure 4-2 FTIR spectrum of HAp, HAp-Al and HAp-Al after use

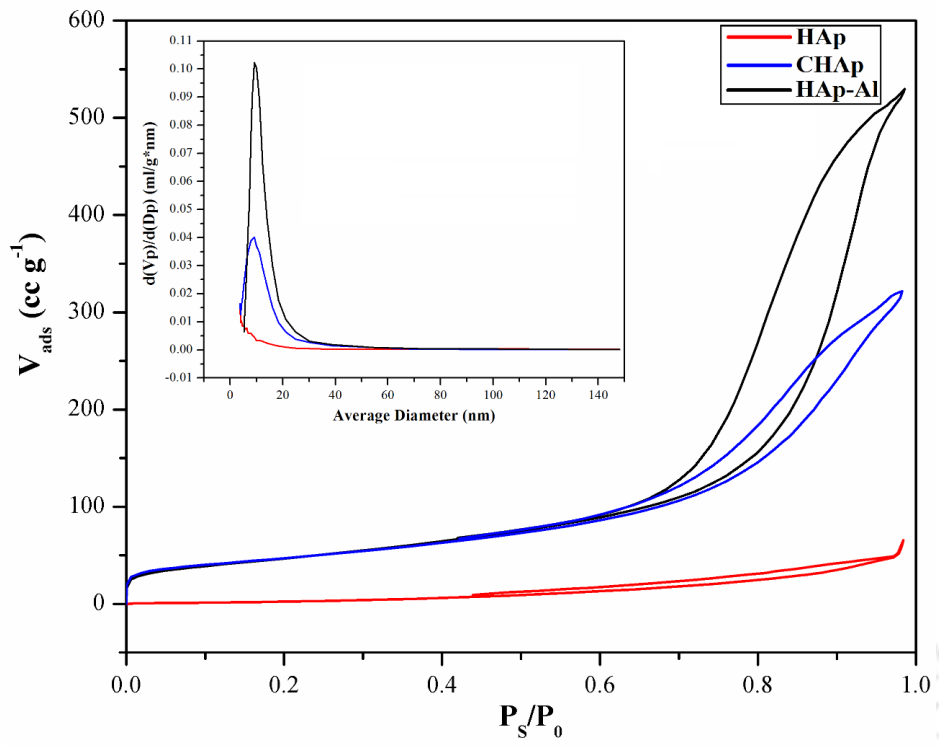

Figure 4-3 Adsorption and desorption isotherms of N_2 for HAp, CHAp and HAp-Al

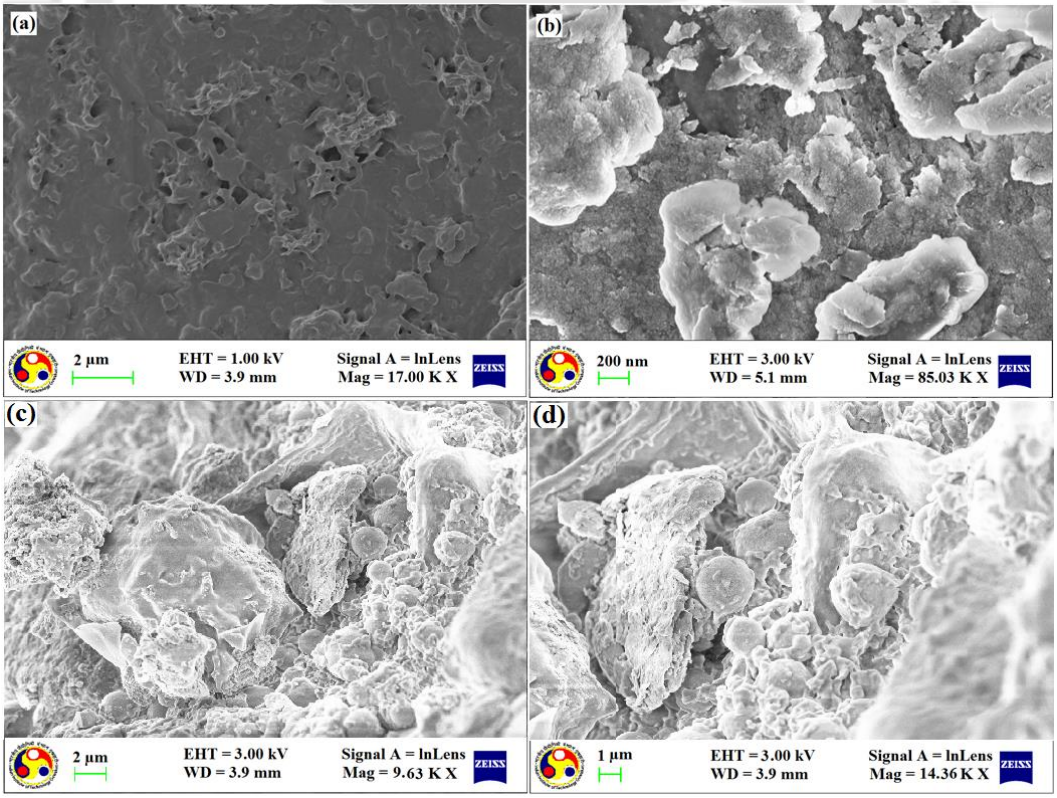

Figure 4-4 FESEM micrographs of HAp (a), (b) and HAp-Al (c), (d)

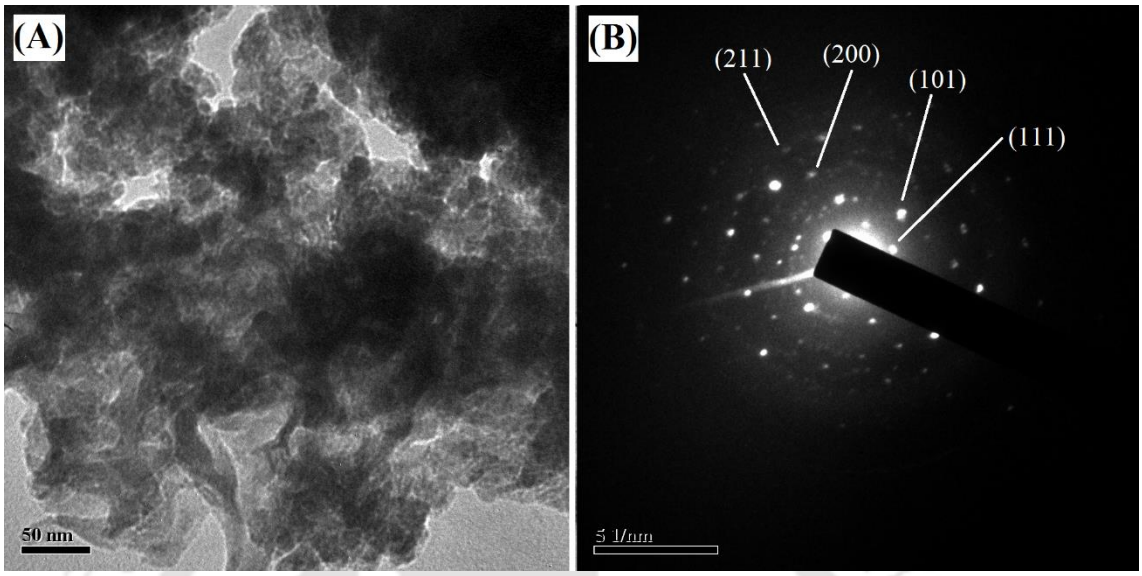

Figure 4-5 (A) Cross-sectional TEM image and (B) the SAED pattern of polycrystalline Al on HAp (1 0 0)

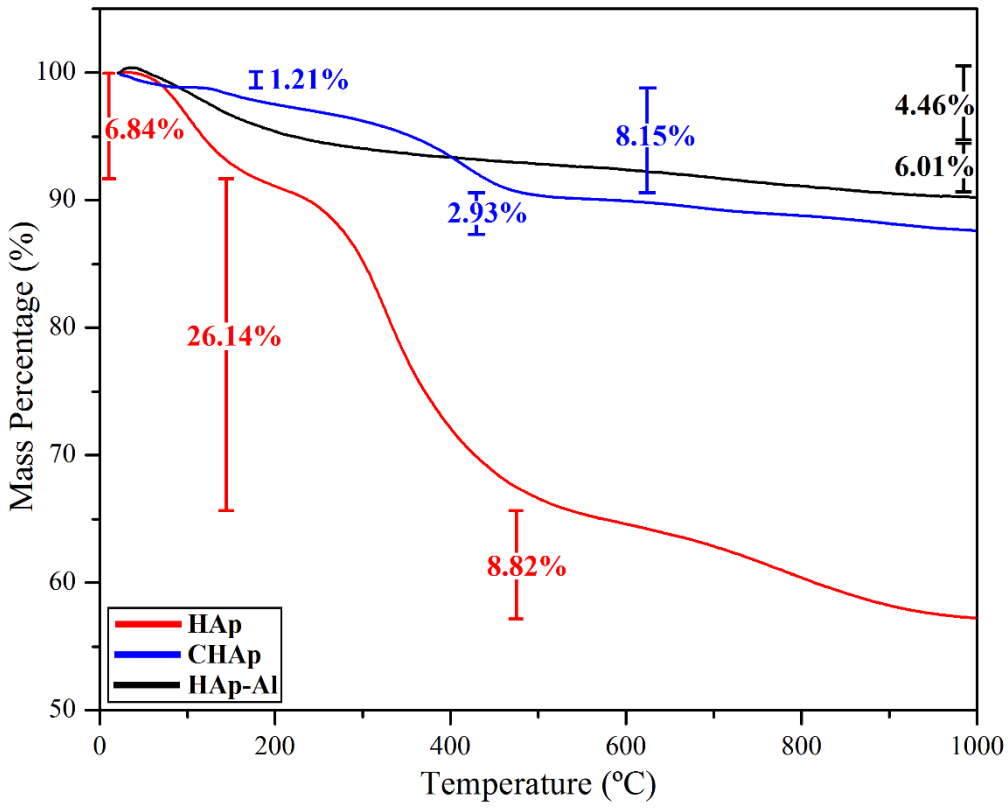

Figure 4-6 Thermal gravimetric analysis of HAp, CHAp and HAp-Al

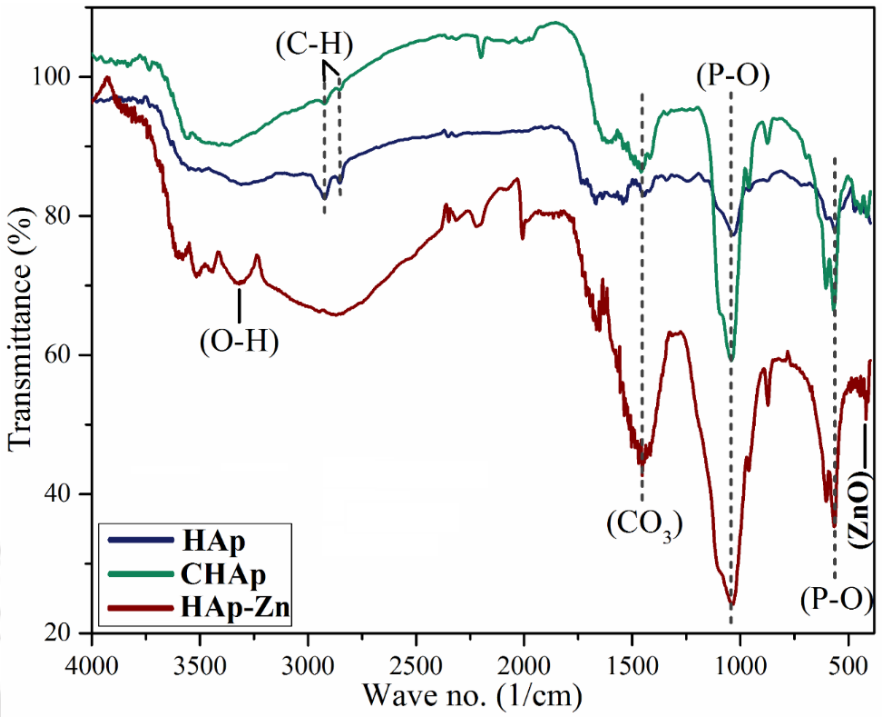

Figure 4-7 FTIR spectra illustrating characteristic phosphate band, carbonate band and ZnO stretching band of HAp, CHAp and HAp-Zn

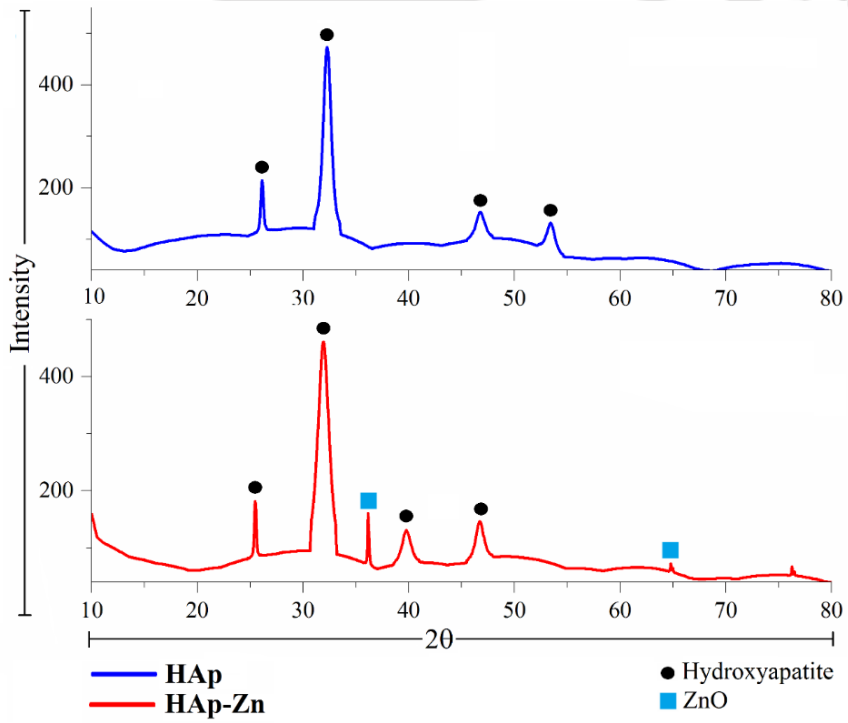

Figure 4-8 XRD patterns of HAp and HAp-Zn illustrating distinctive peaks of ZnO and hydroxyapatite

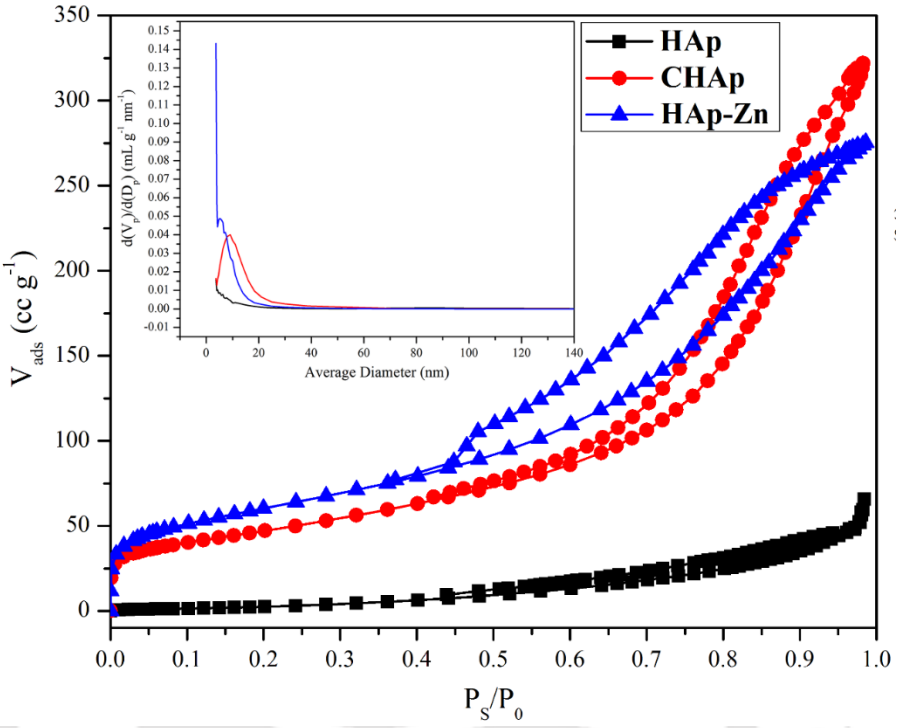

Figure 4-9 N_2 Adsorption and desorption isotherms showing hysteresis loop of HAp, CHAp and HAp-Zn (Pore volume distribution vs. Average pore diameter inside)

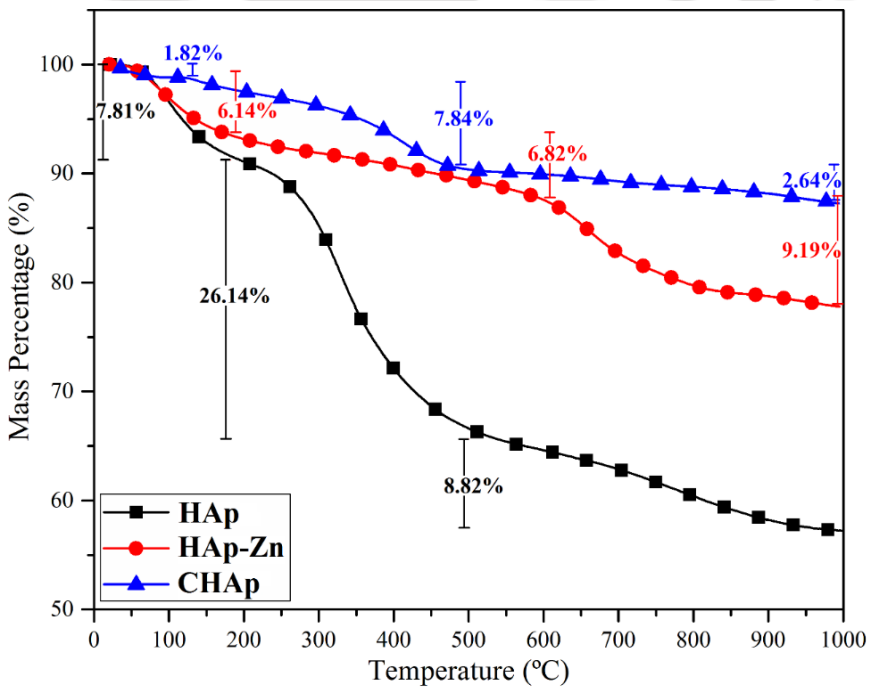

Figure 4-10 Graphical illustration of temperature vs. mass percentage of HAp, CHAp and HAp-Zn providing insight to the stability of developed catalyst

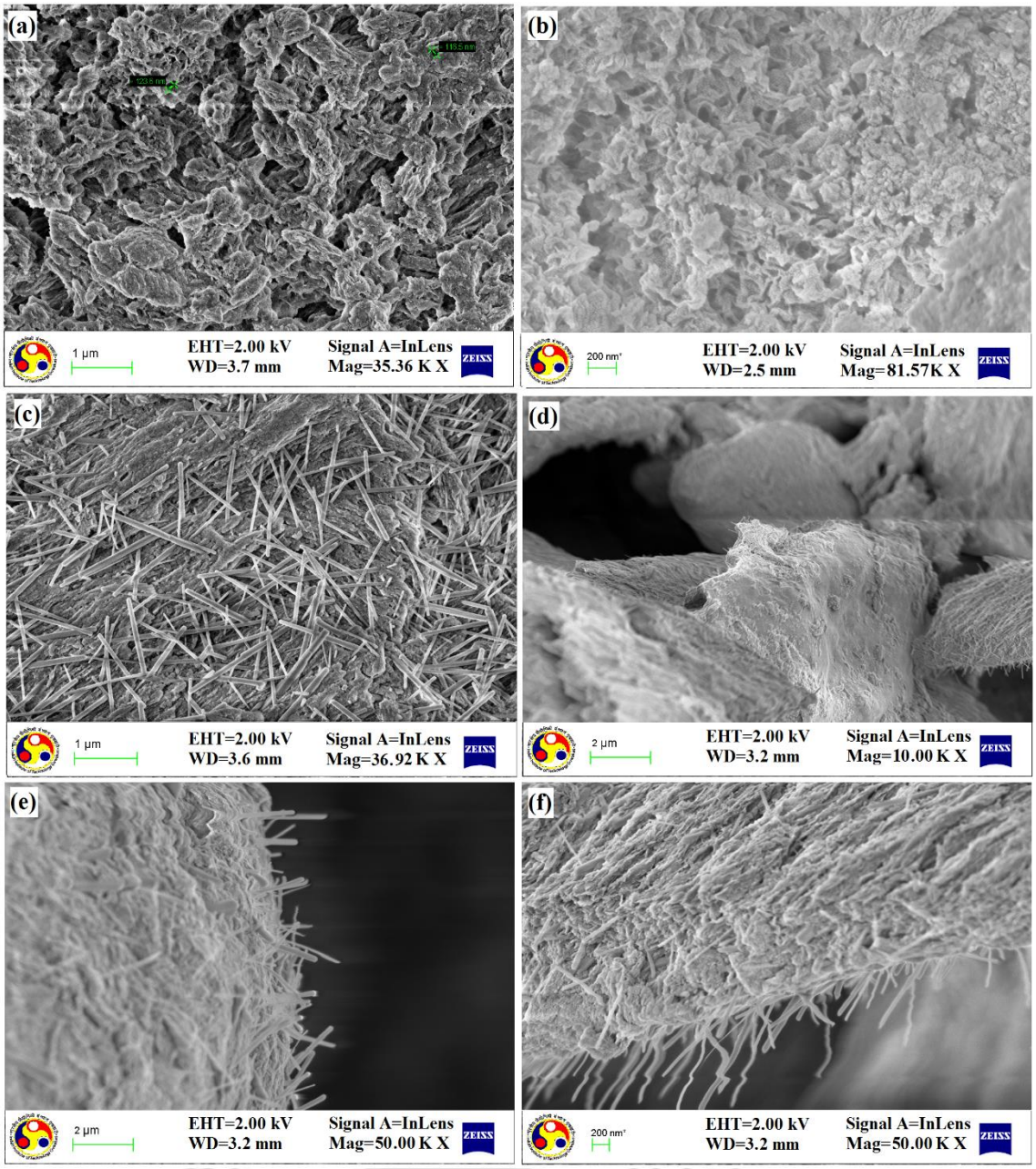

Figure 4-11 FESEM micrographs of CHAp (a, b) and HAp-Zn (c, d, e, f)

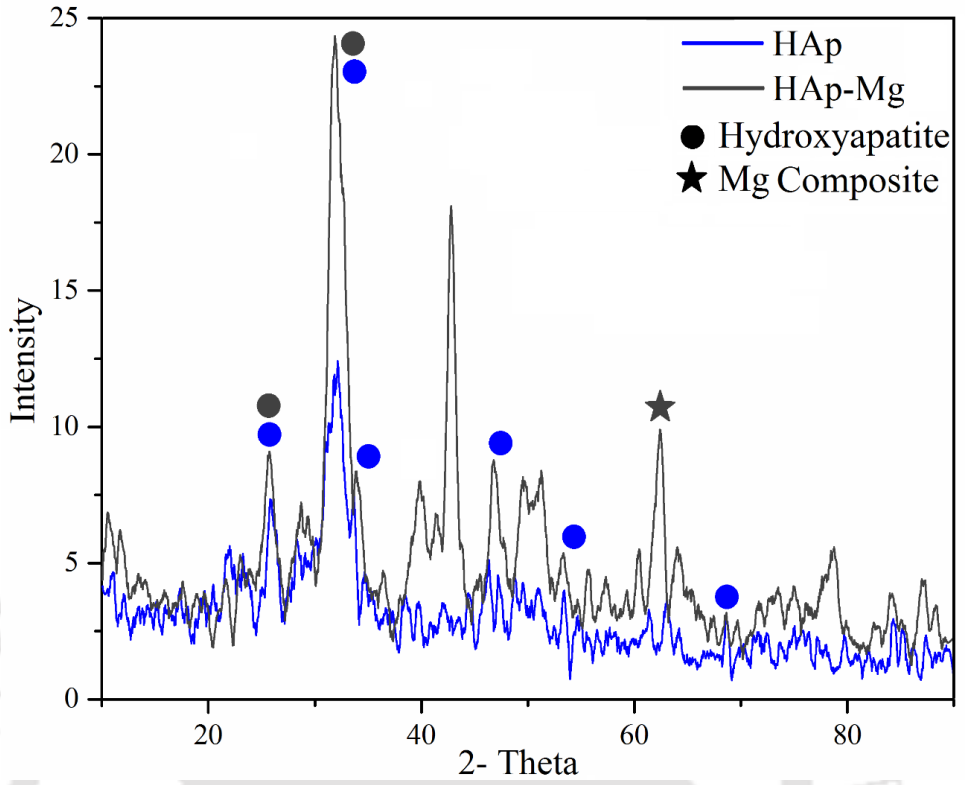

Figure 4-12 X-ray diffraction pattern of HAp and HAp-Mg

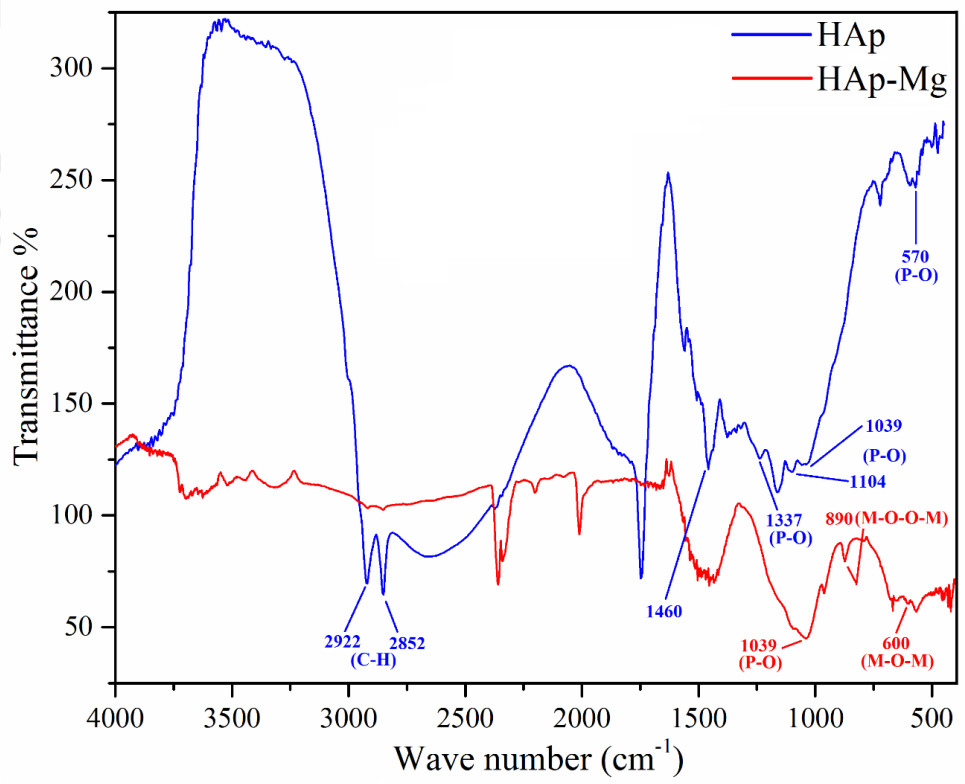

Figure 4-13 FTIR of HAp and HAp-Mg showing relevant functional groups

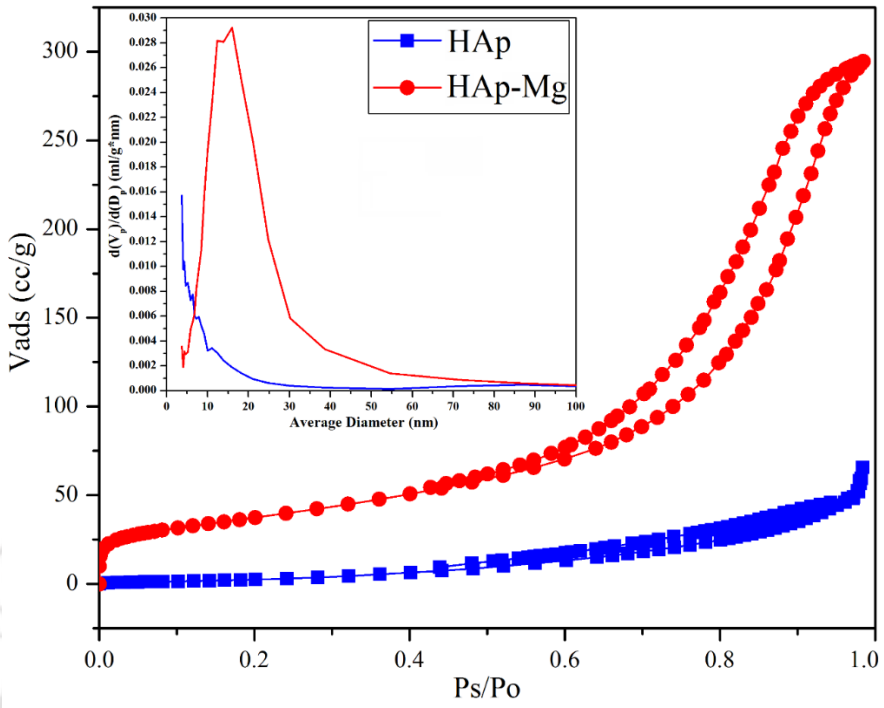

Figure 4-14 N_2 adsorption and desorption of HAp and HAp-Mg, volumetric distribution (in side)

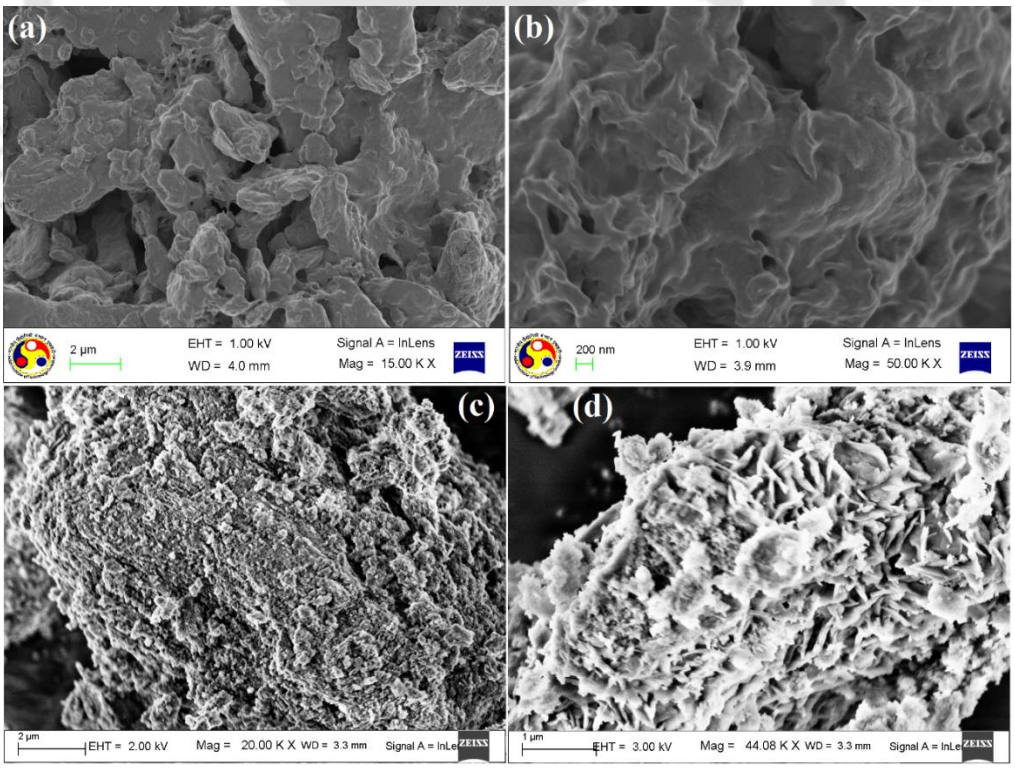

Figure 4-15 SEM images of HAp (a), (b) and HAp-Mg (c), (d) showing surface morphology

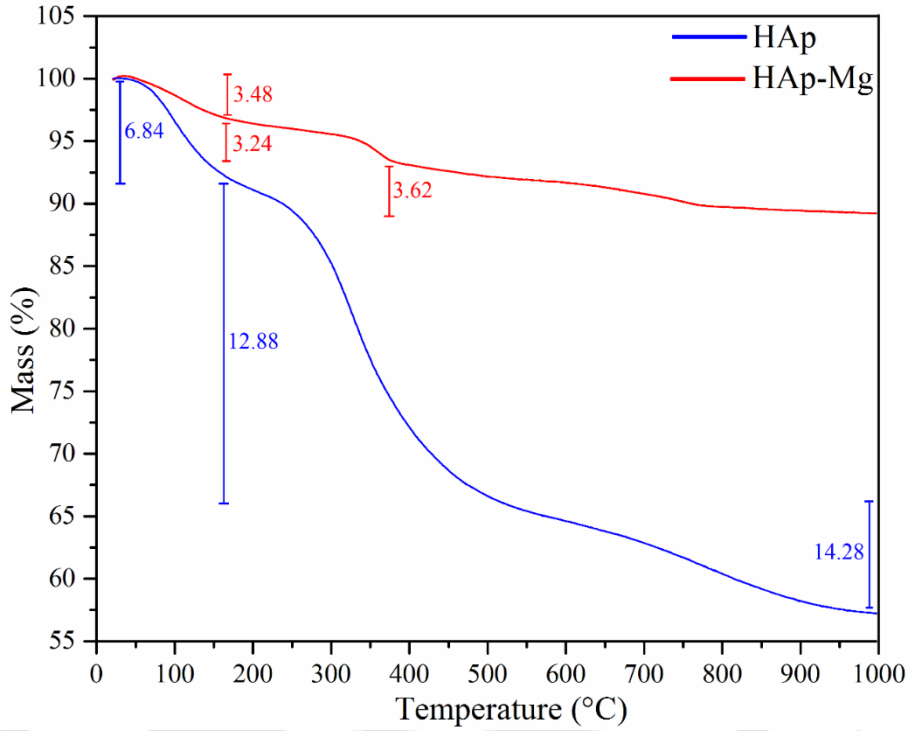

Figure 4-16 Thermogravimetric analysis of HAp and HAp-Mg

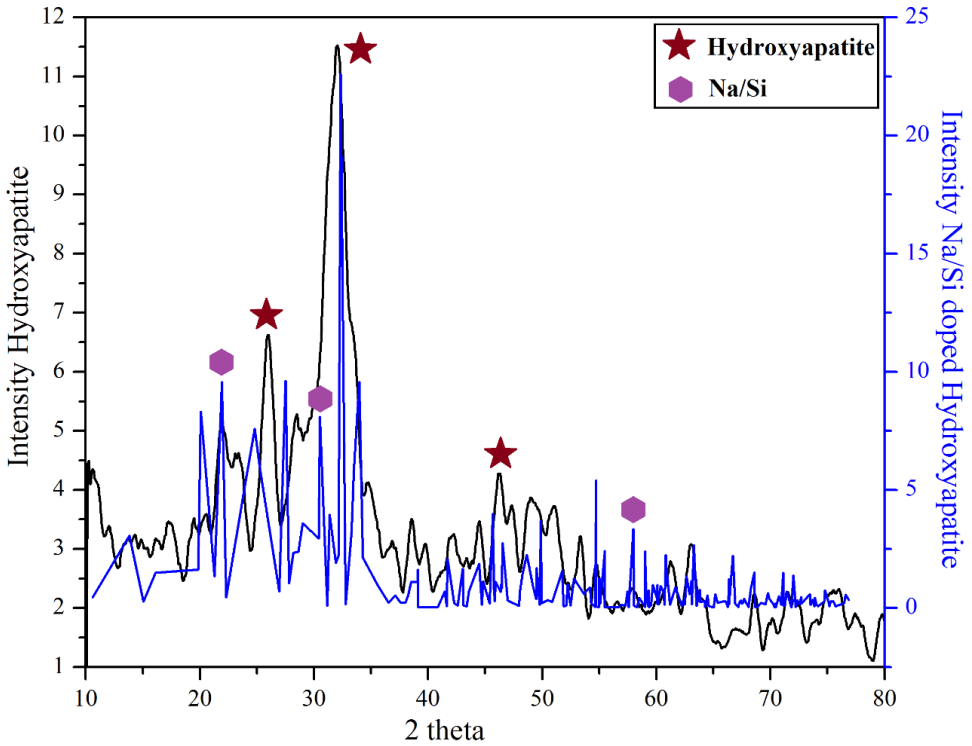

Figure 4-17 X-ray diffraction patterns of raw hydroxyapatite and Na/Si doped hydroxyapatite showing characteristic peaks

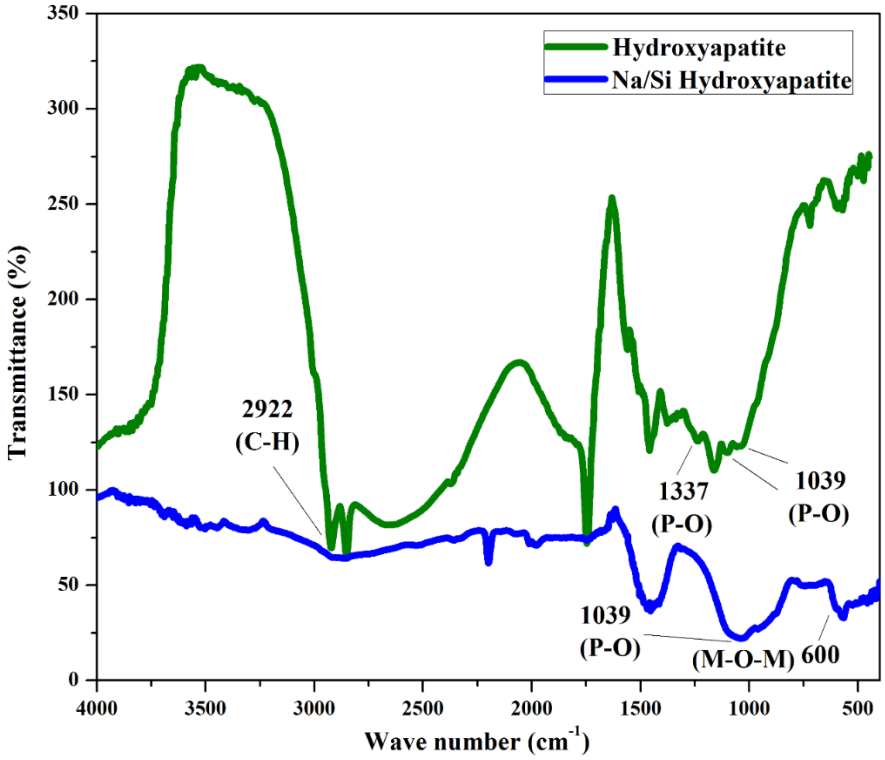

Figure 4-18 FTIR spectrum of raw hydroxyapatite and Na/Si doped hydroxyapatite

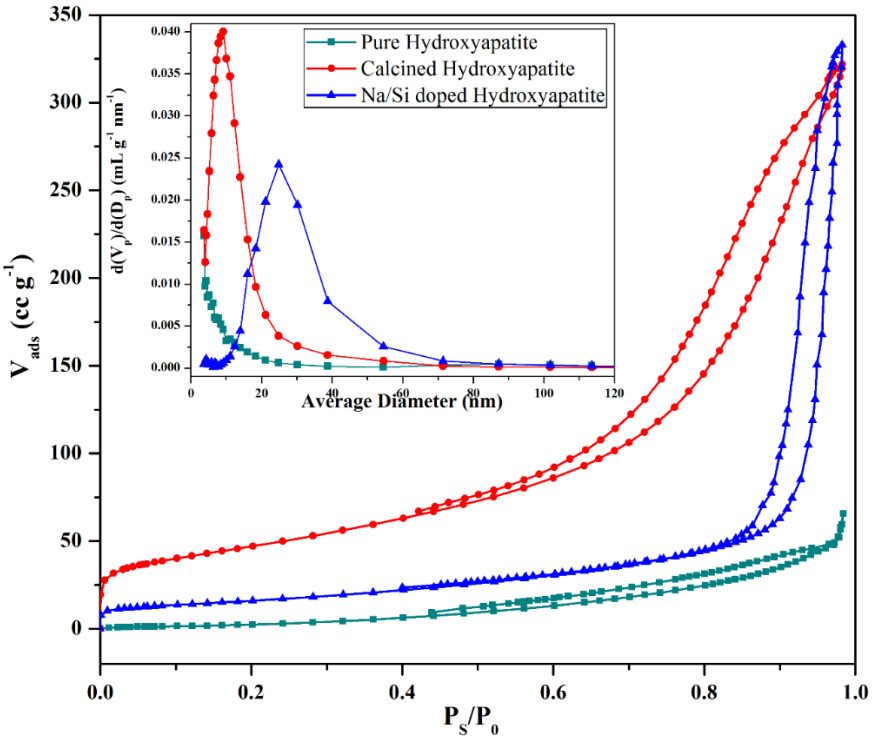

Figure 4-19 Adsorption and desorption isotherms of N_2 for raw hydroxyapatite and Na/Si doped hydroxyapatite

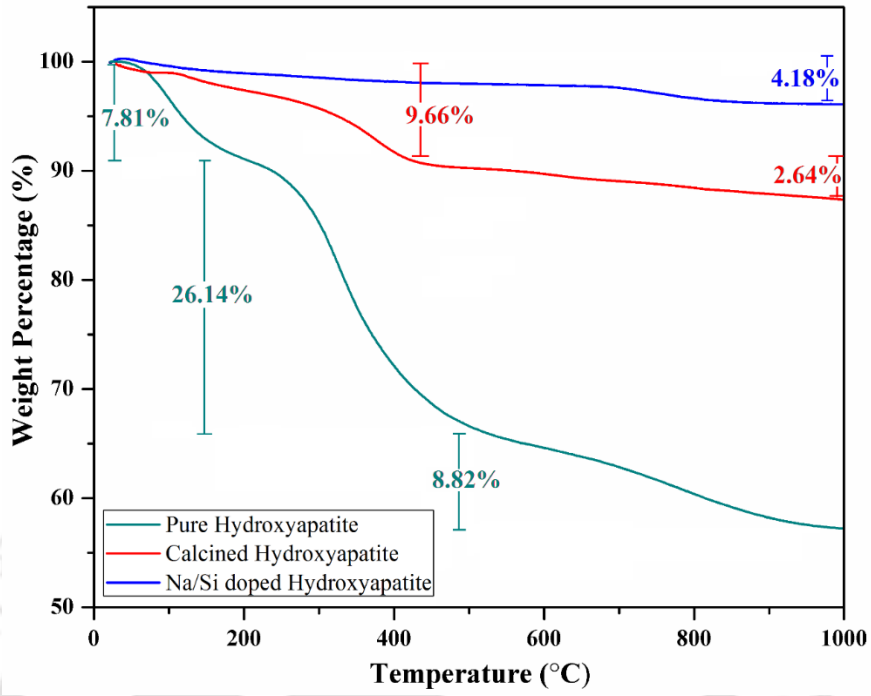

Figure 4-20 Thermal gravimetric analysis of raw, calcined and Na/Si doped hydroxyapatite

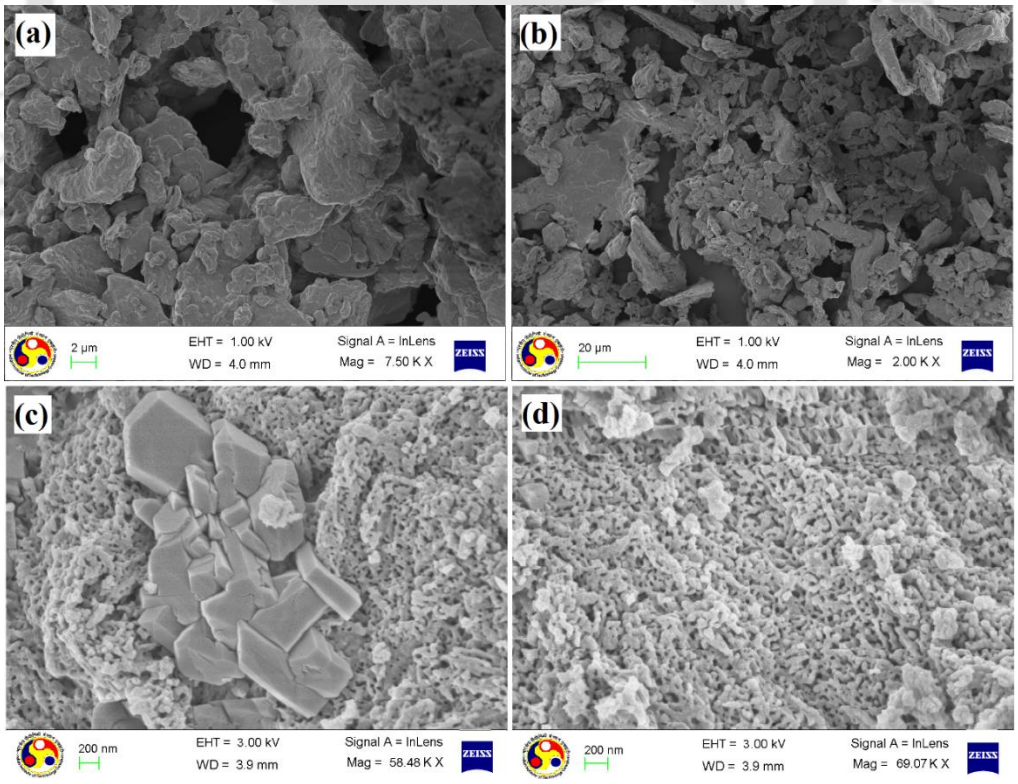

Figure 4-21 FESEM micrograph of raw hydroxyapatite and Na/Si doped hydroxyapatite

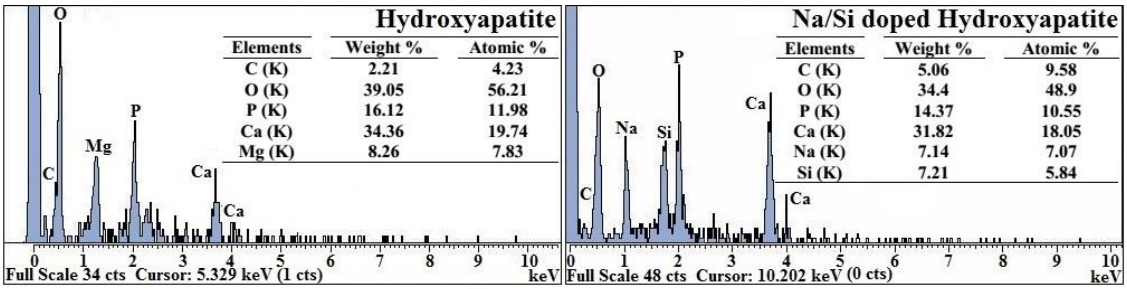

Figure 4-22 EDX analysis of raw hydroxyapatite and Na/Si doped hydroxyapatite

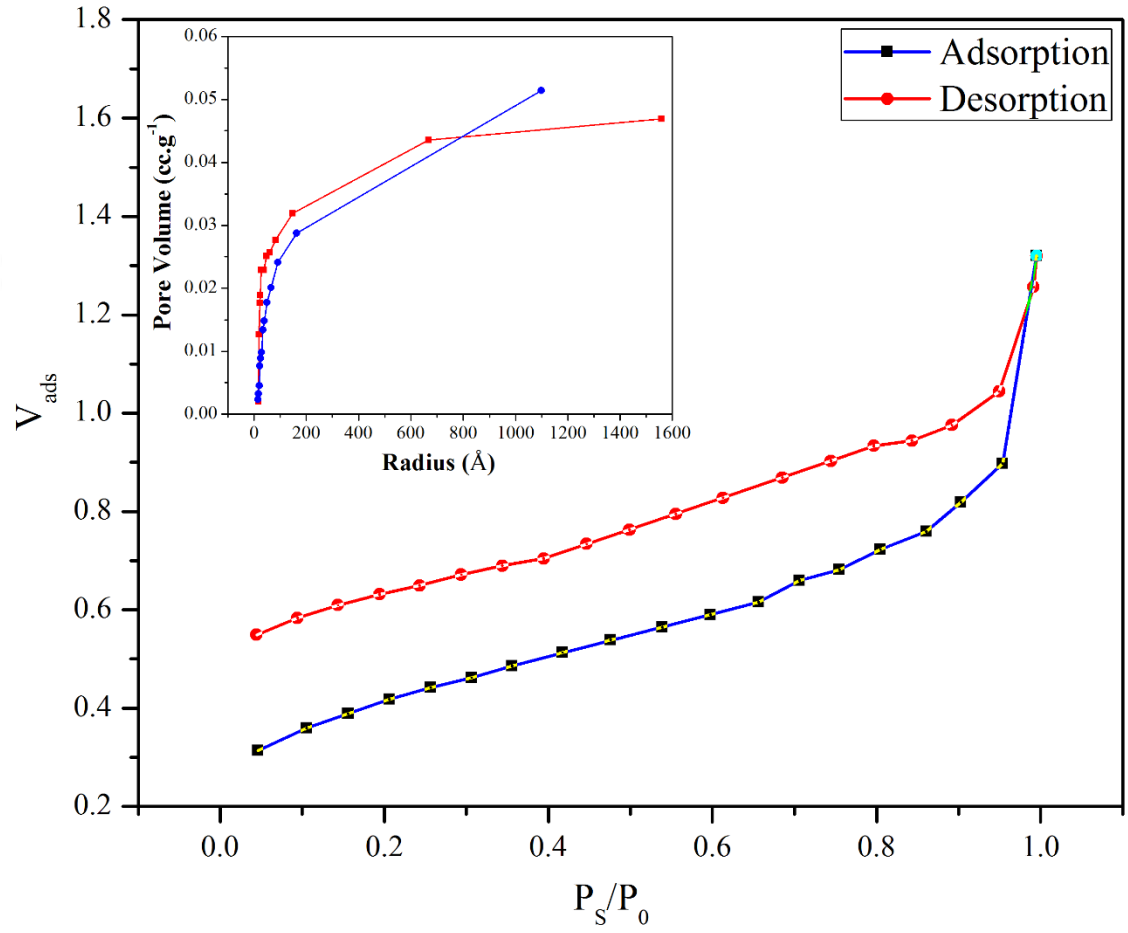

Figure 4-23 N_2 adsorption and desorption of WGS-Mg 11 as well as the pore volume distribution with respect to the pore radius

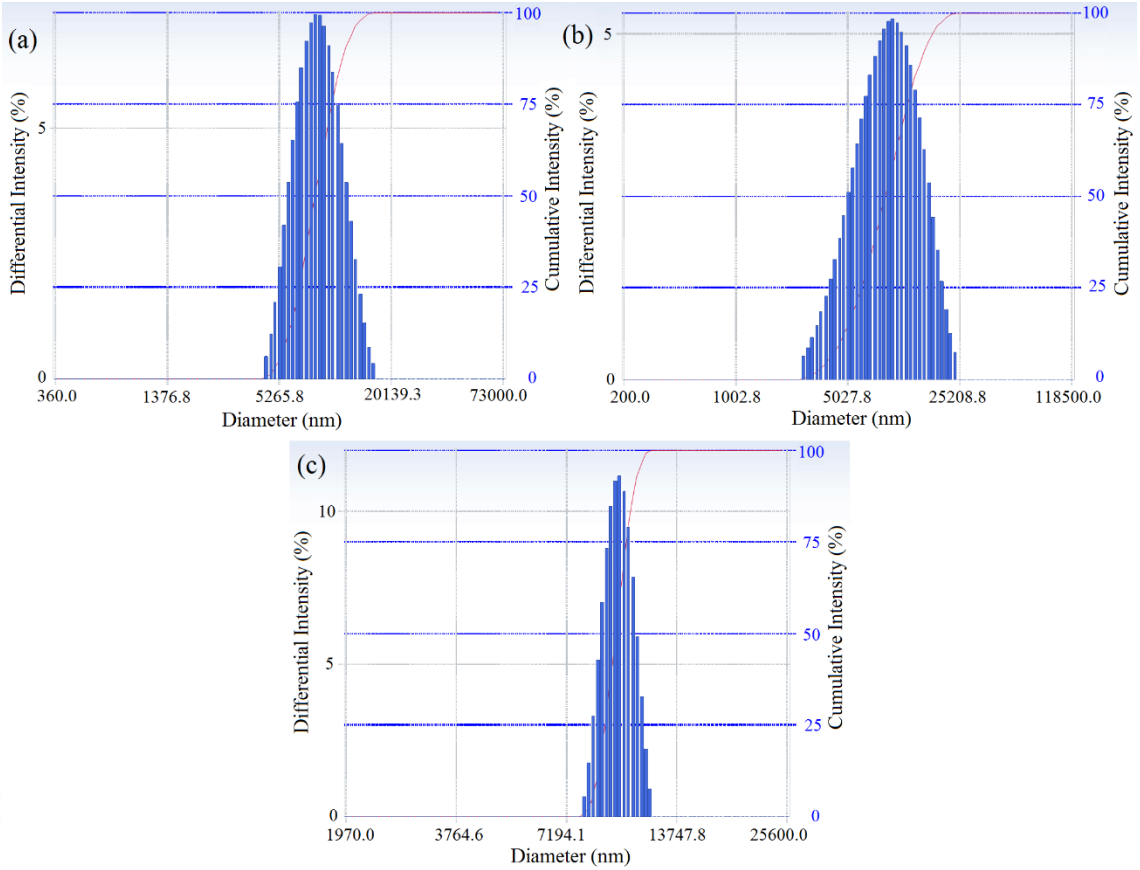

Figure 4-24 Particle size distribution of (a) WGS-Mg 11 (b) WGS-Mg 12 (c) WGS-Mg 21

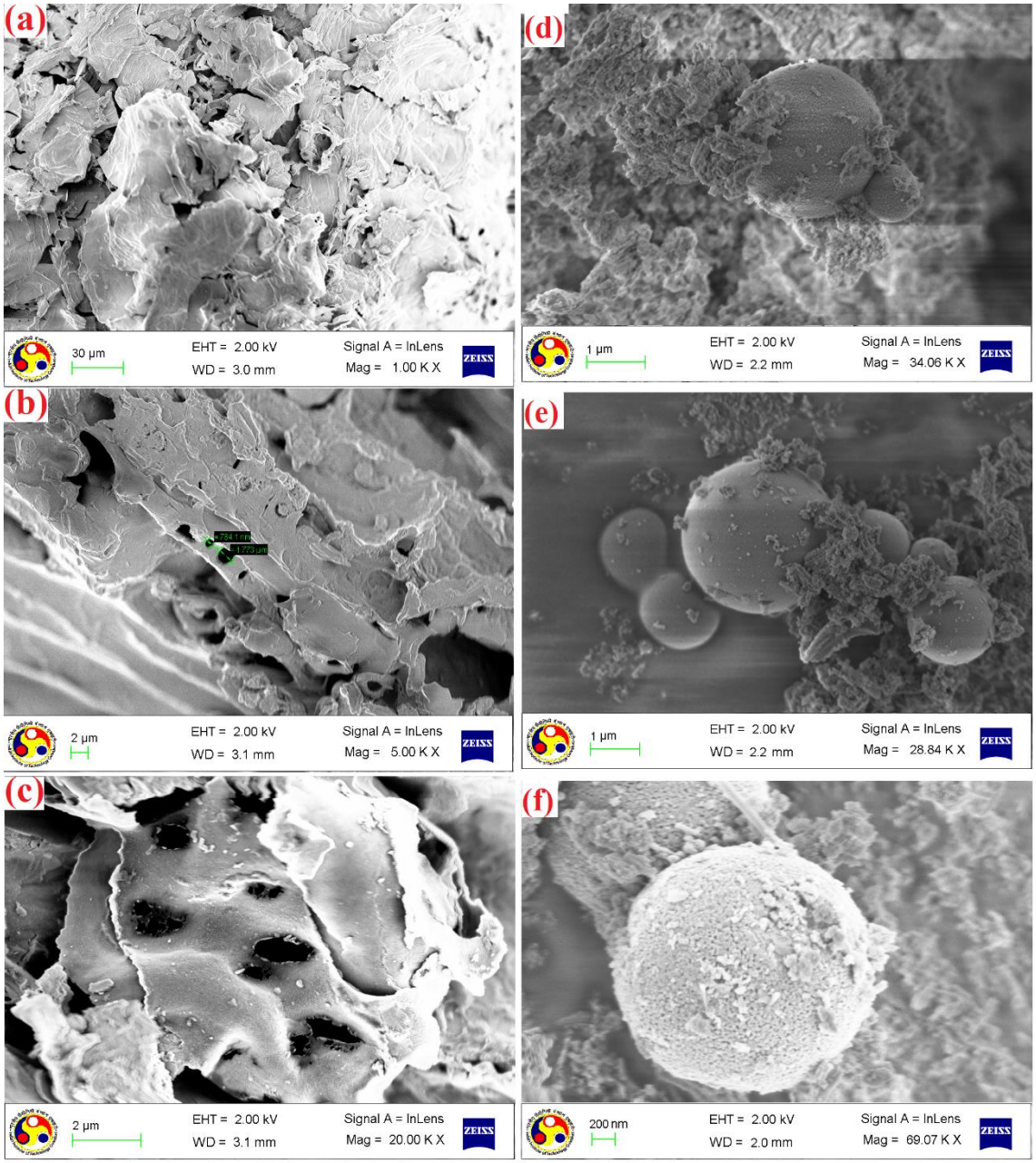

Figure 4-25 Micro-structure analysis of WGS (a), (b), (c) and WGS-Mg 11 (d), (e), (f)

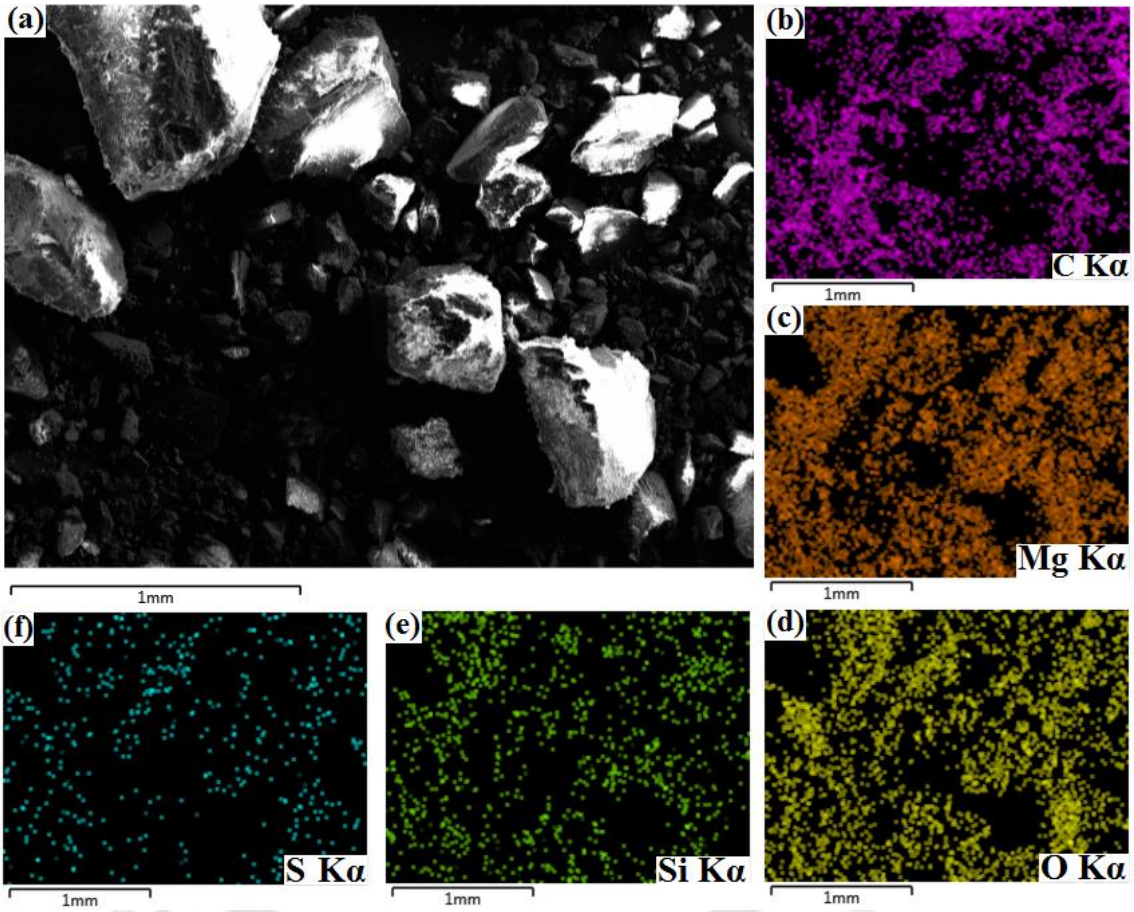

Figure 4-26 SEM-EDX micrograph and mapping of elemental distribution on the surface of WGS-Mg 11

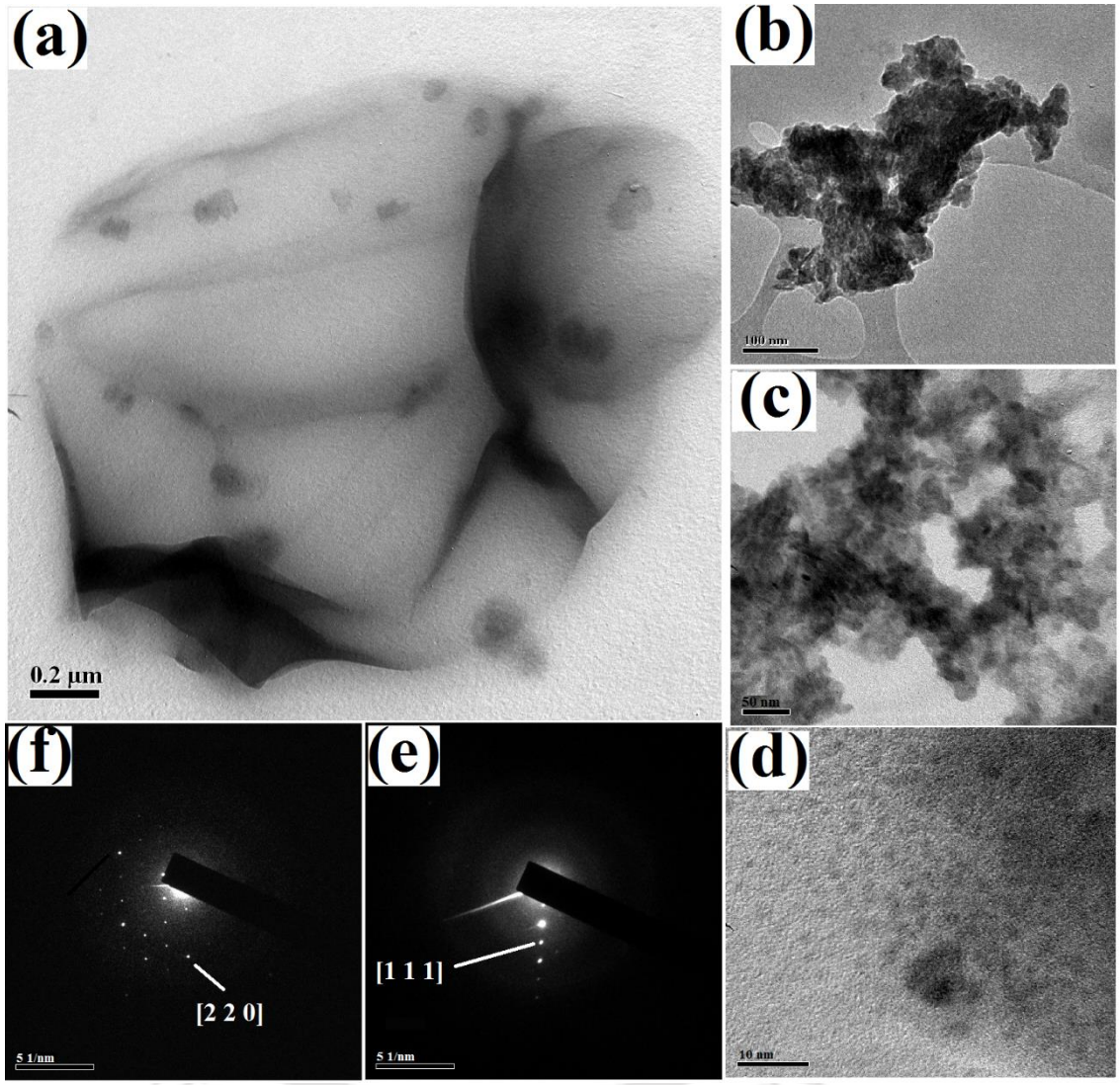

Figure 4-27 TEM images of WGS-Mg at different scale and the SAED pattern

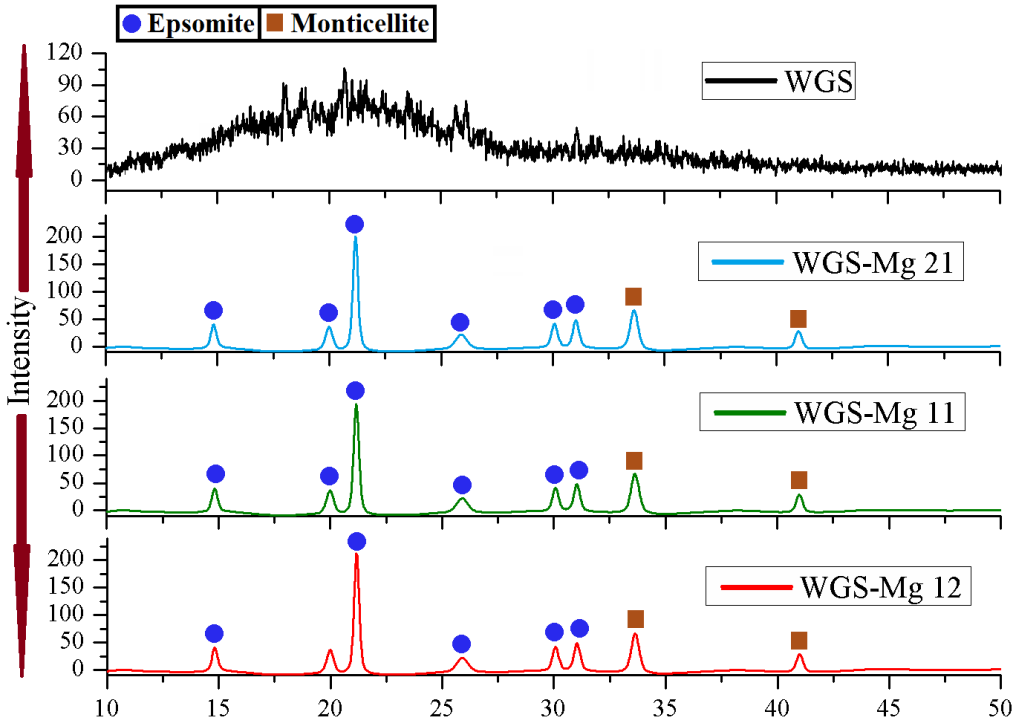

Figure 4-28 XRD pattern of WGS and WGS-Mg identifying Mg based composite

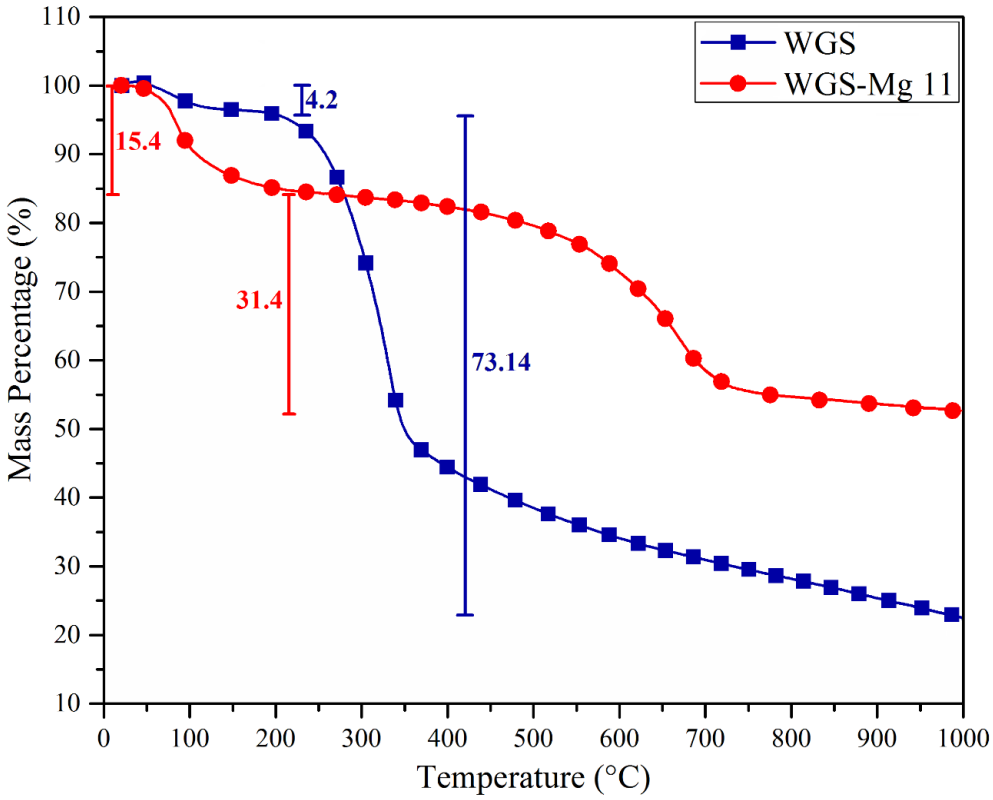

Figure 4-29 Thermal degradation profile of WGS and WGS-Mg 11

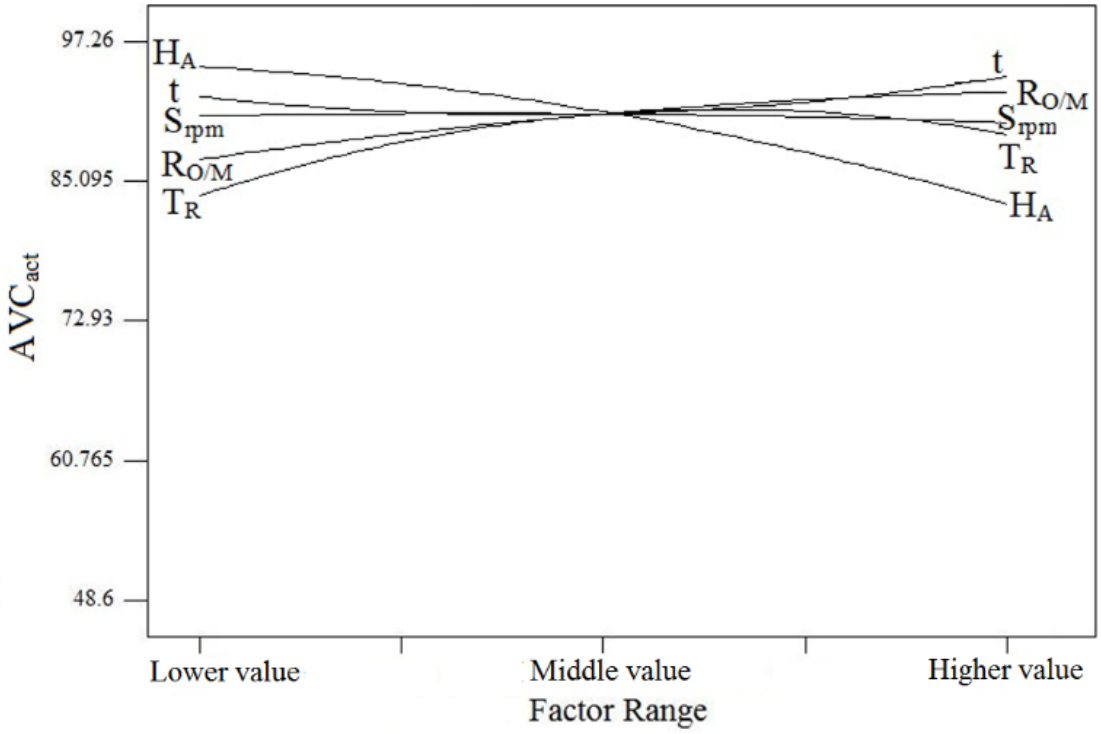

Figure 4-30 Effect of independent variables on actual acid value conversion

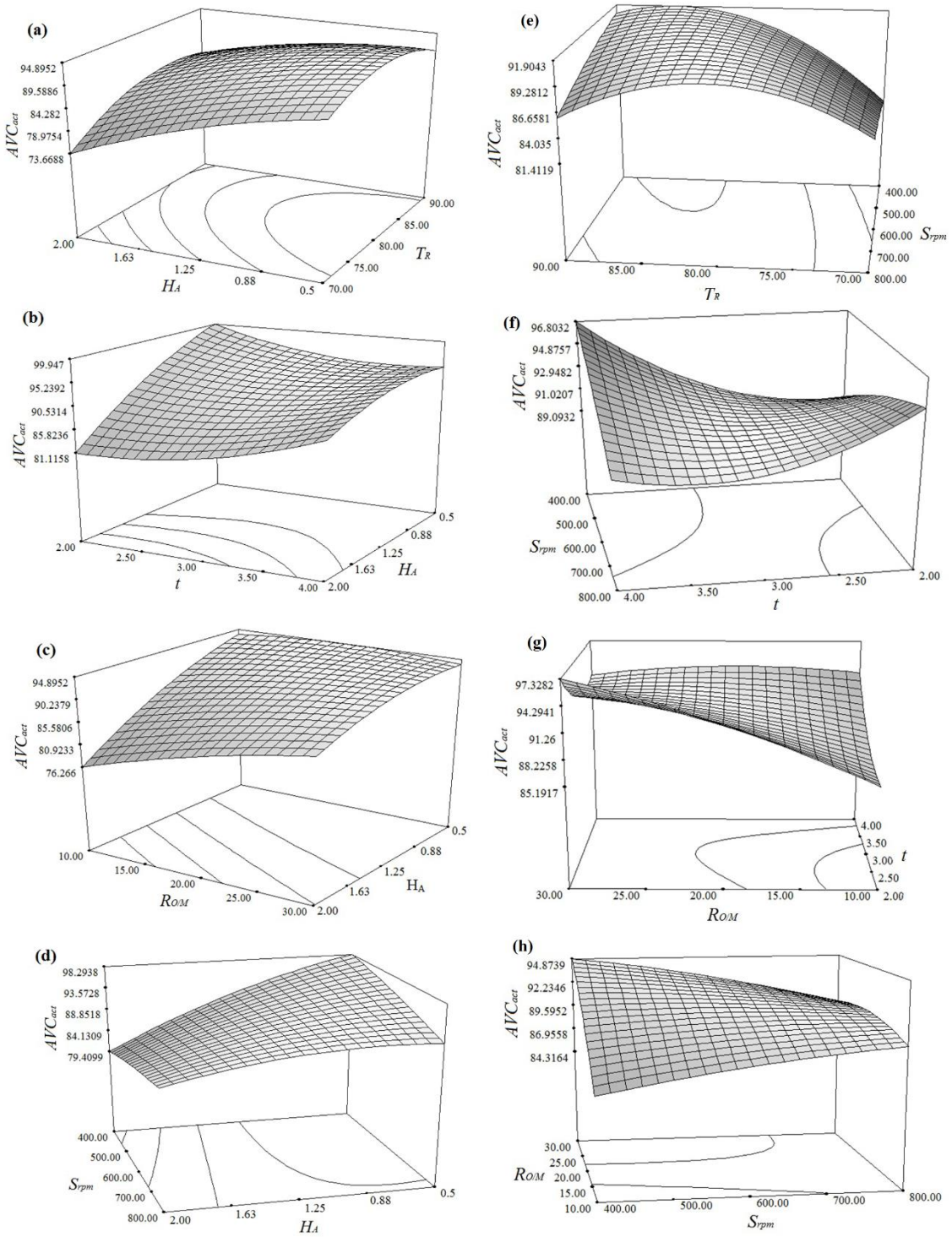

Figure 4-31 (a) Effect of H_A and T_R (b) Effect of H_A and t (c) Effect of $R_{O/M}$ and H_A (d) Effect of H_A and S_{rpm} (e) Effect of T_R and S_{rpm} (f) Effect of S_{rpm} and t (g) Effect of $R_{O/M}$ and t (h) Effect of $R_{O/M}$ and S_{rpm} on AVC_{act}

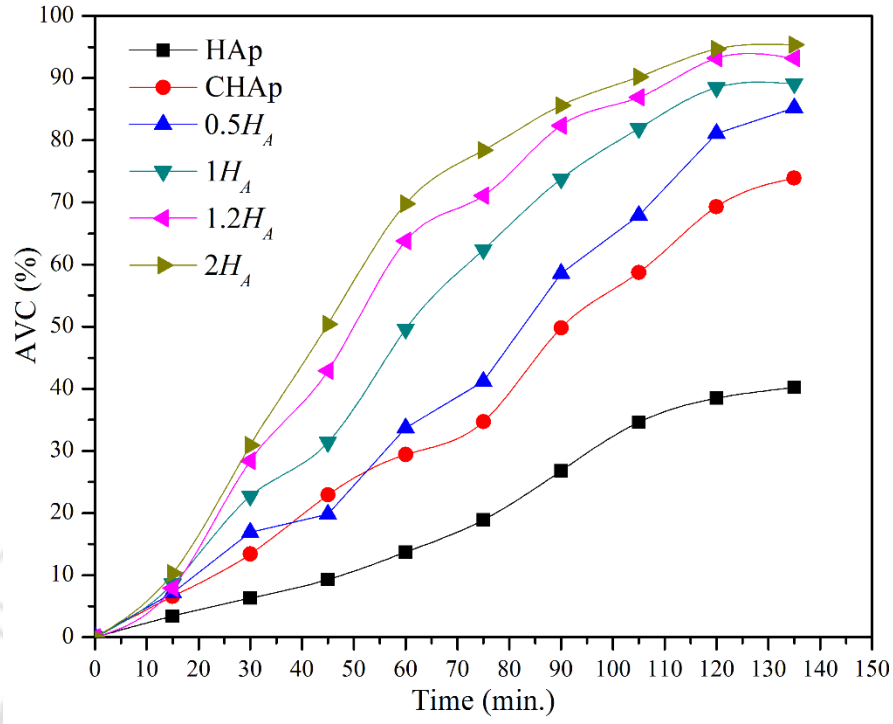

Figure 4-32 Acid value conversion w.r.t reaction time for HAp, CHAp, 0.5H_A, 1H_A, 1.2H_A, 2H_A at optimal condition

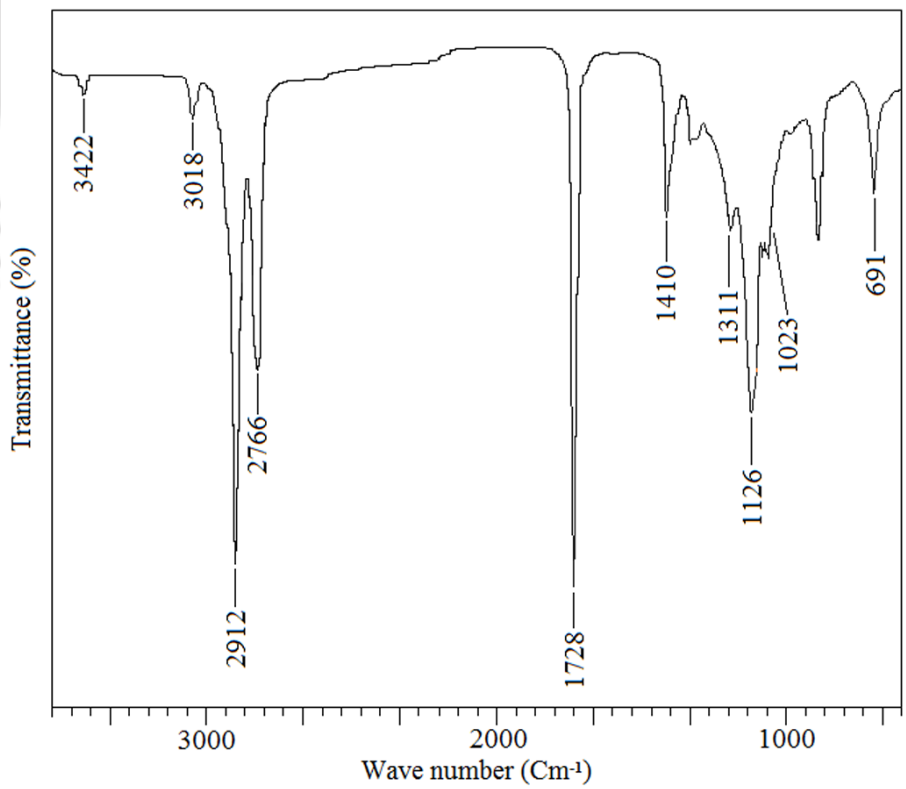

Figure 4-33 FTIR spectrum of trans-esterified Neem oil at optimal parametric condition

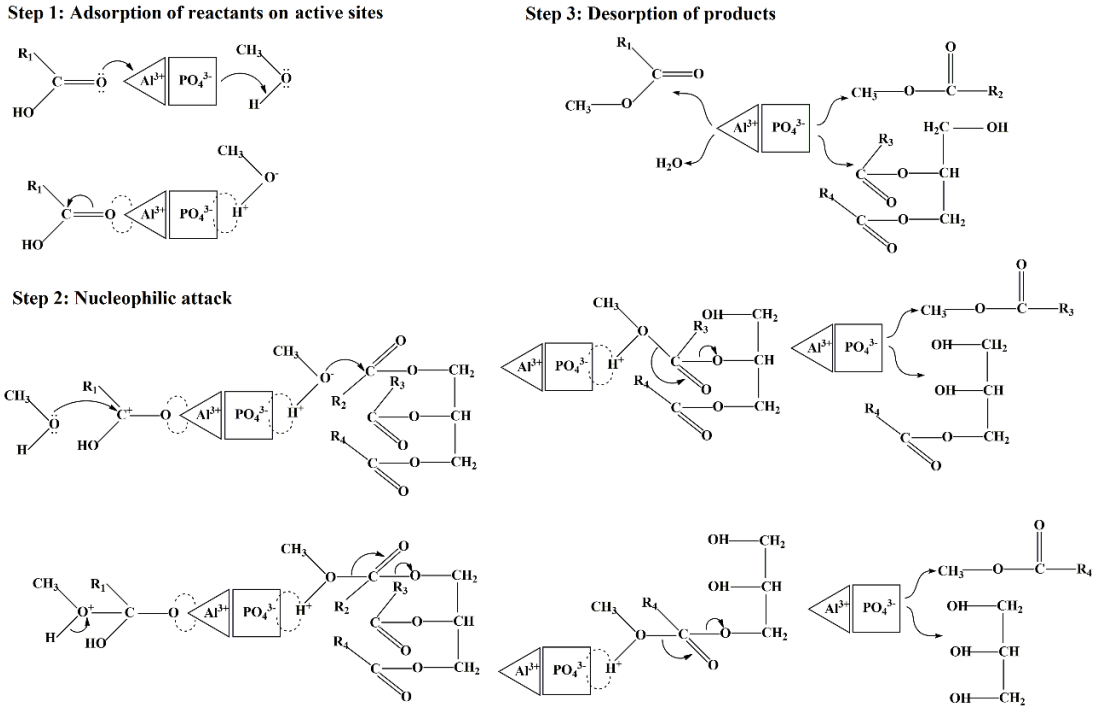

Figure 4-34 Reaction mechanism showing adsorption of reactant (step 1), neucleophilic reaction (step 2) and desorption of product (step 3)

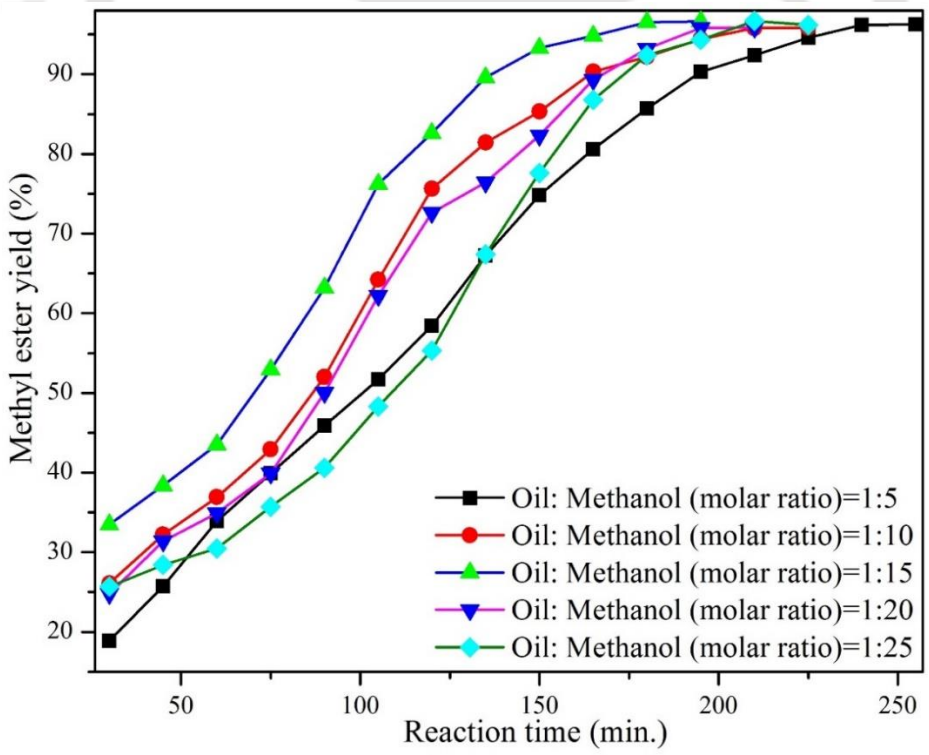

Figure 4-35 Effects on FFA conversion with reference to reaction time at varying oil to methanol ratio

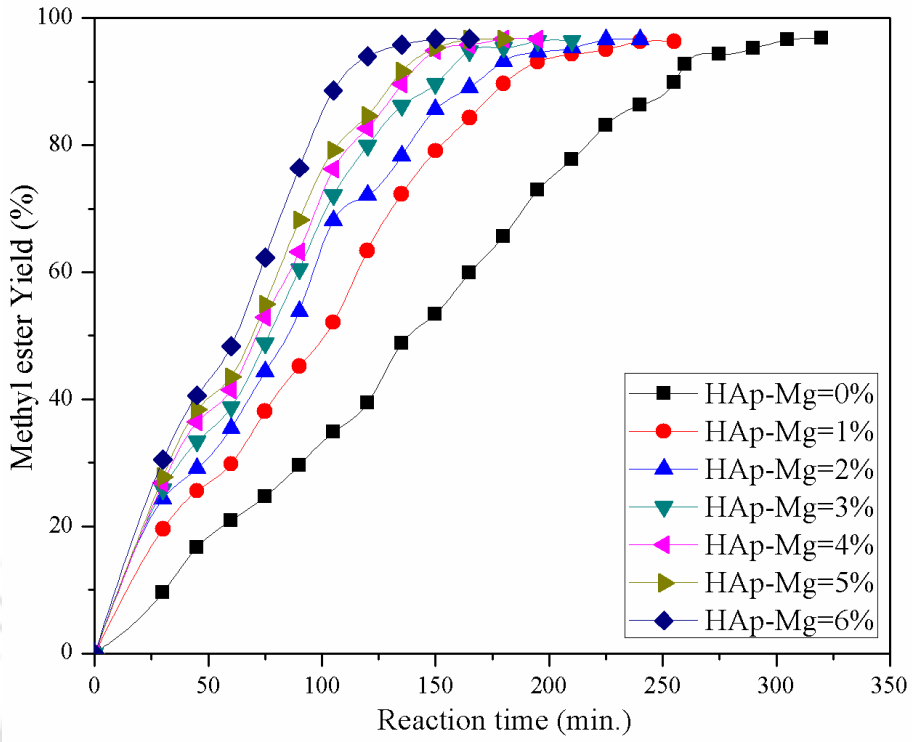

Figure 4-36 Effects on methyl ester yield with reference to reaction time at varying catalyst loading

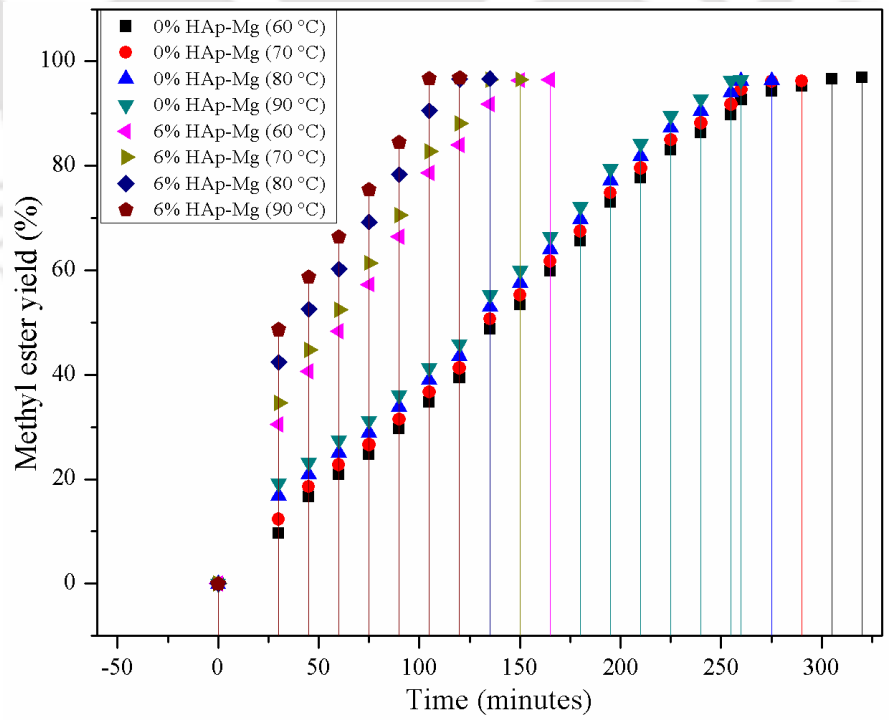

Figure 4-37 Effects of methyl ester yield with reference to reaction time at varying reaction temperature for 0% and 6% catalyst loading

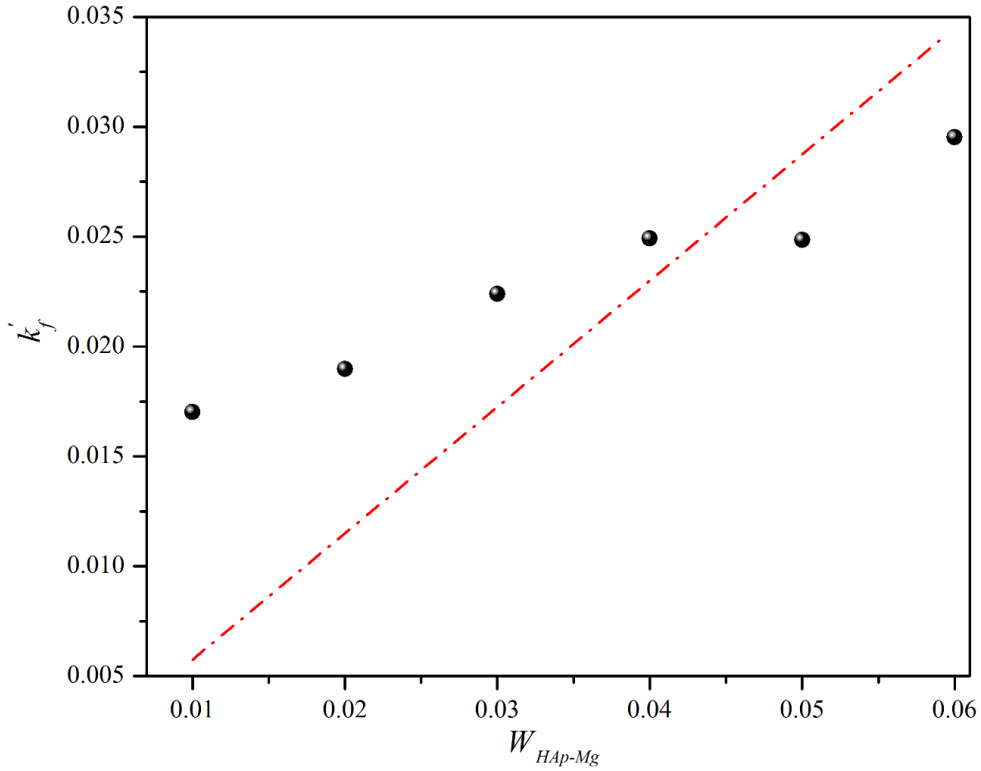

Figure 4-38 Graph of k_f' vs w_{HAp-Mg}

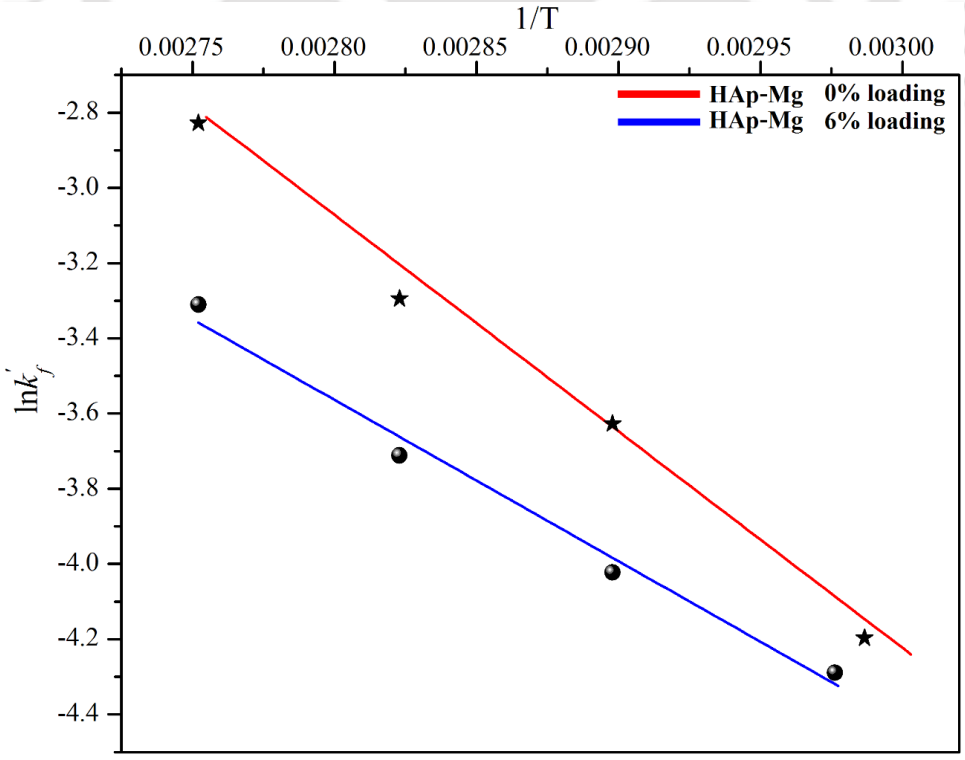

Figure 4-39 Plot showing linear correlation between $\ln k_f'$ and 1/T

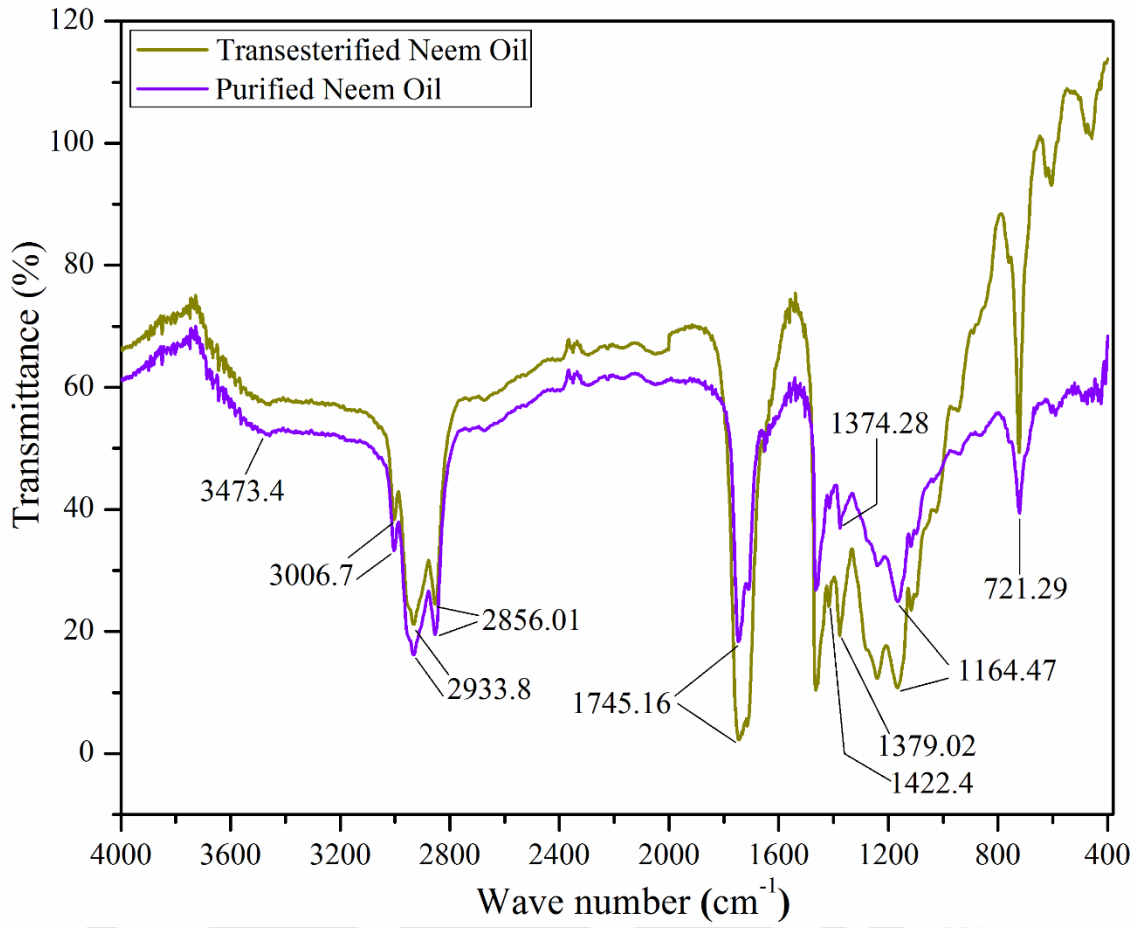

Figure 4-40 FTIR of purified and esterified neem oil

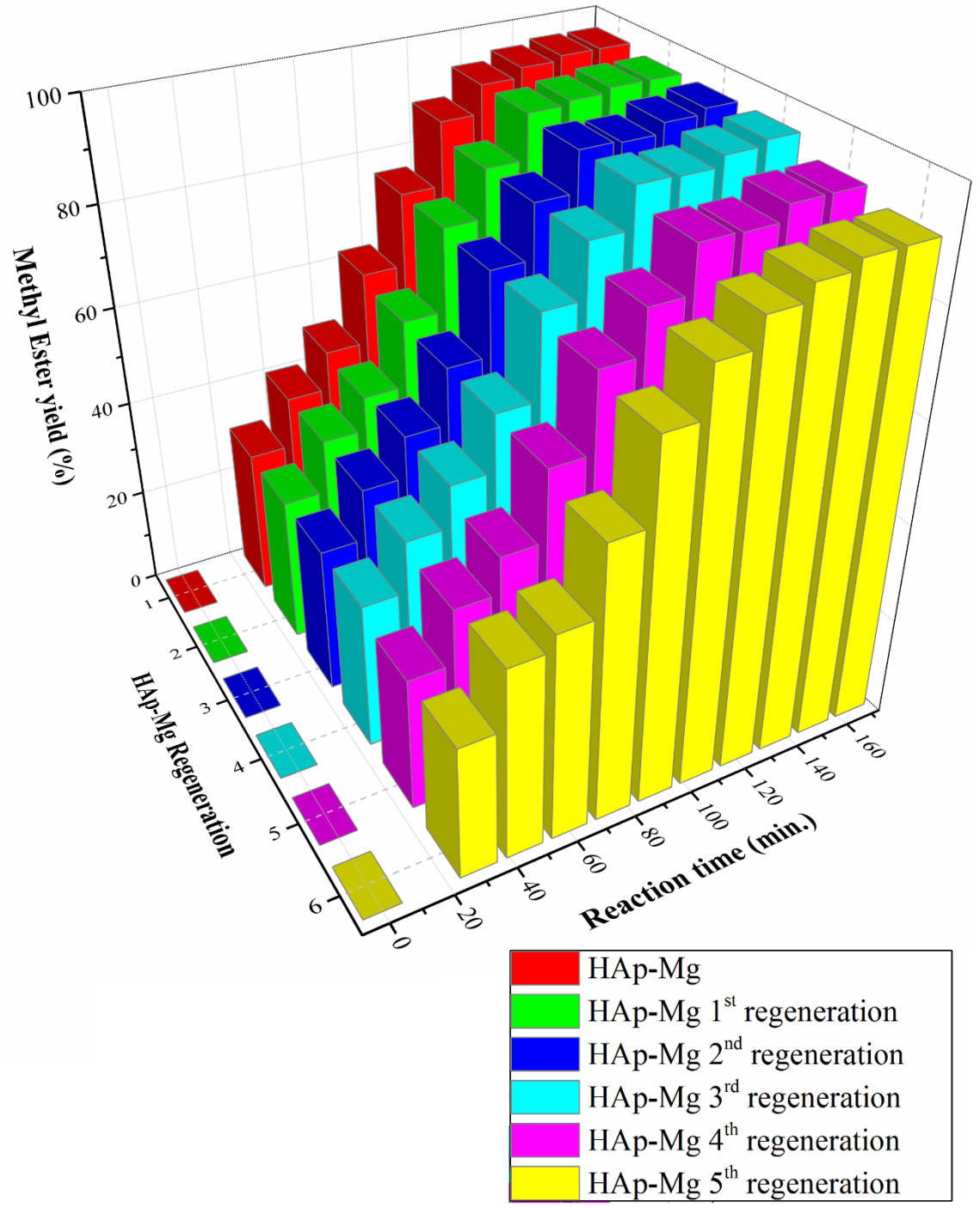

Figure 4-41 Regeneration profile of HAp-Mg

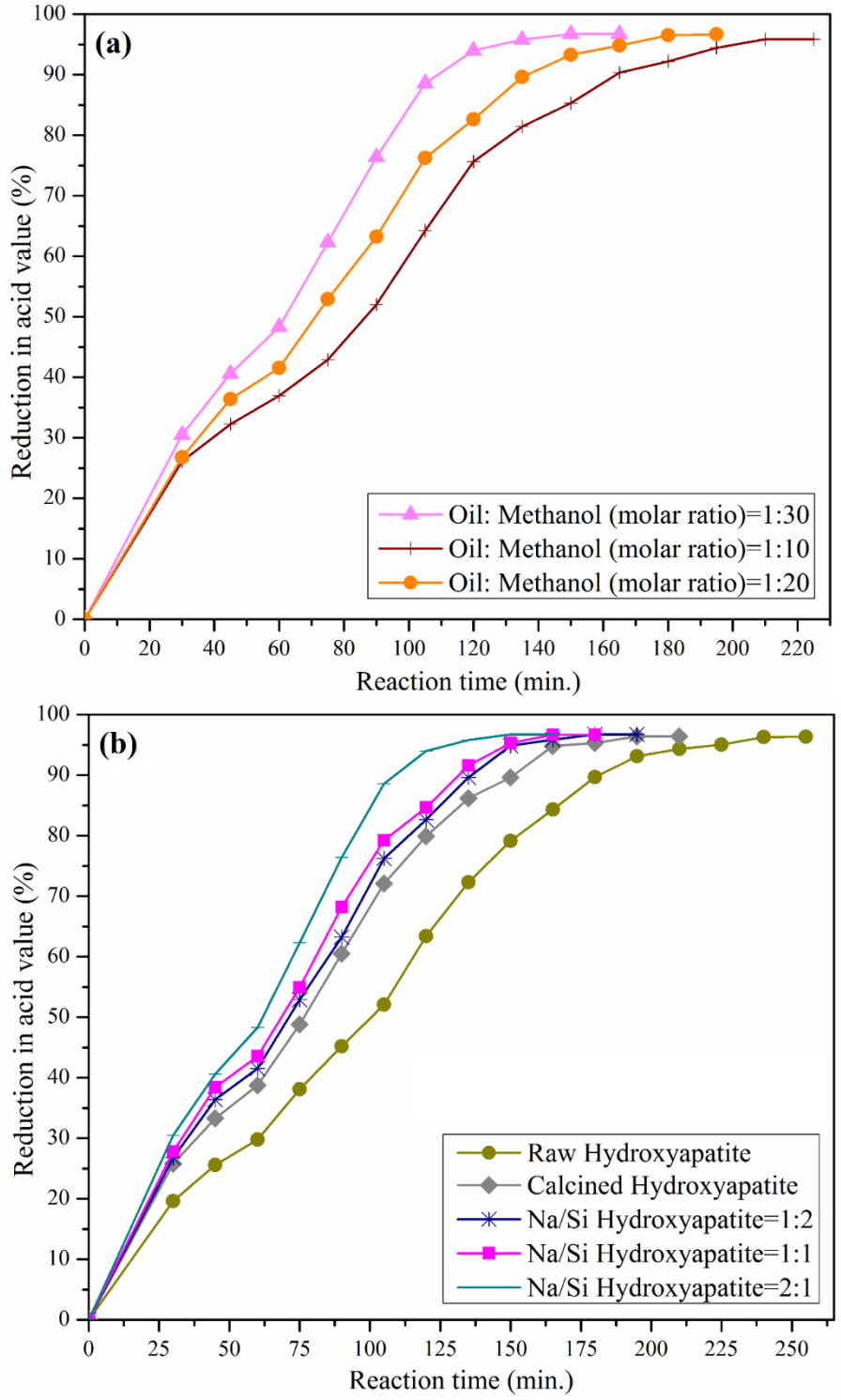

Figure 4-42 Effect on reduction of acid value (%) with respect to reaction time by varying (a) oil:methanol and (b) different catalyst

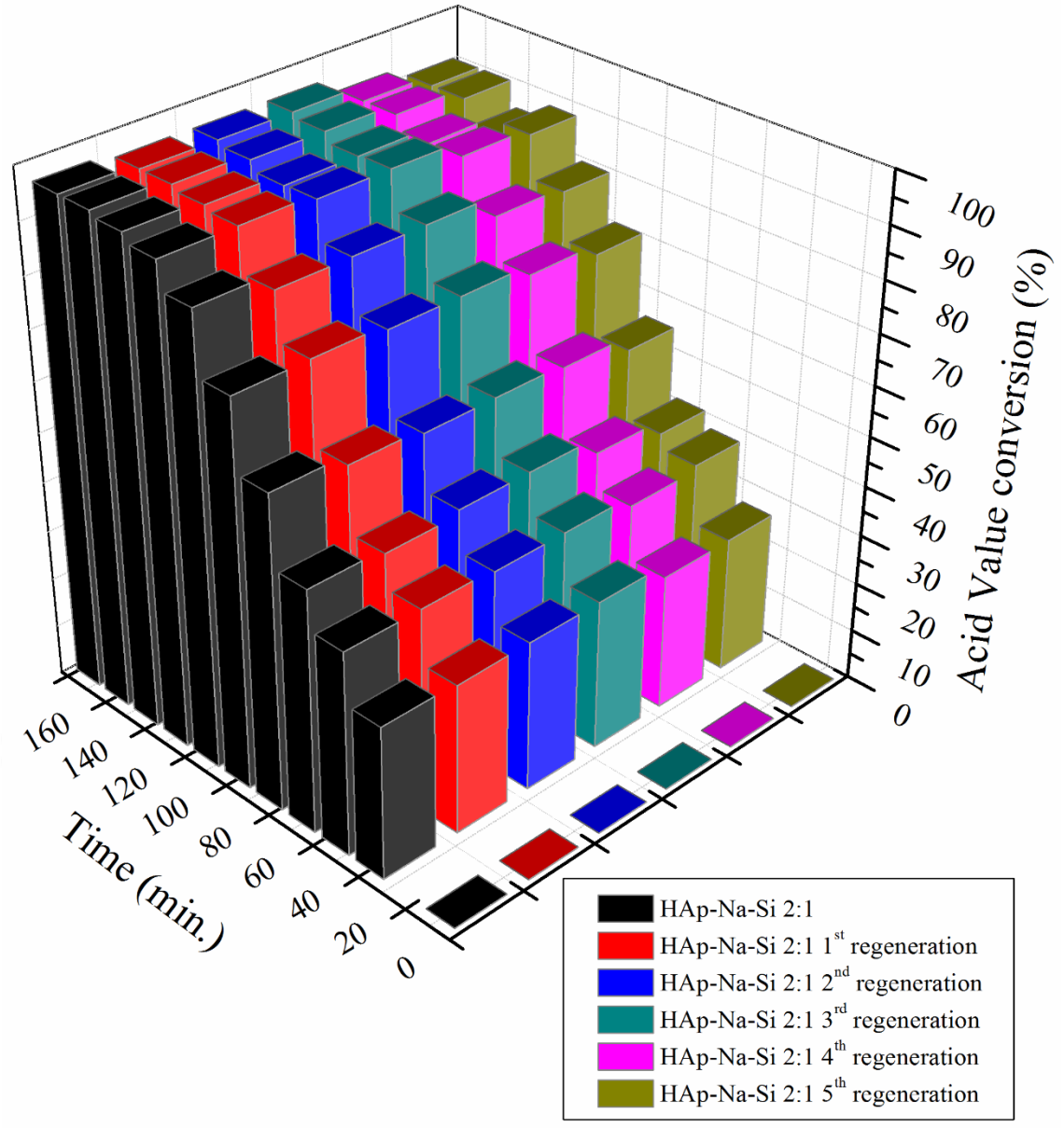

Figure 4-43 Acid Value Conversion of neem oil with respect to time for Na/Si doped hydroxyapatite 2:1 and the regenerated Na/Si doped hydroxyapatite 2:1

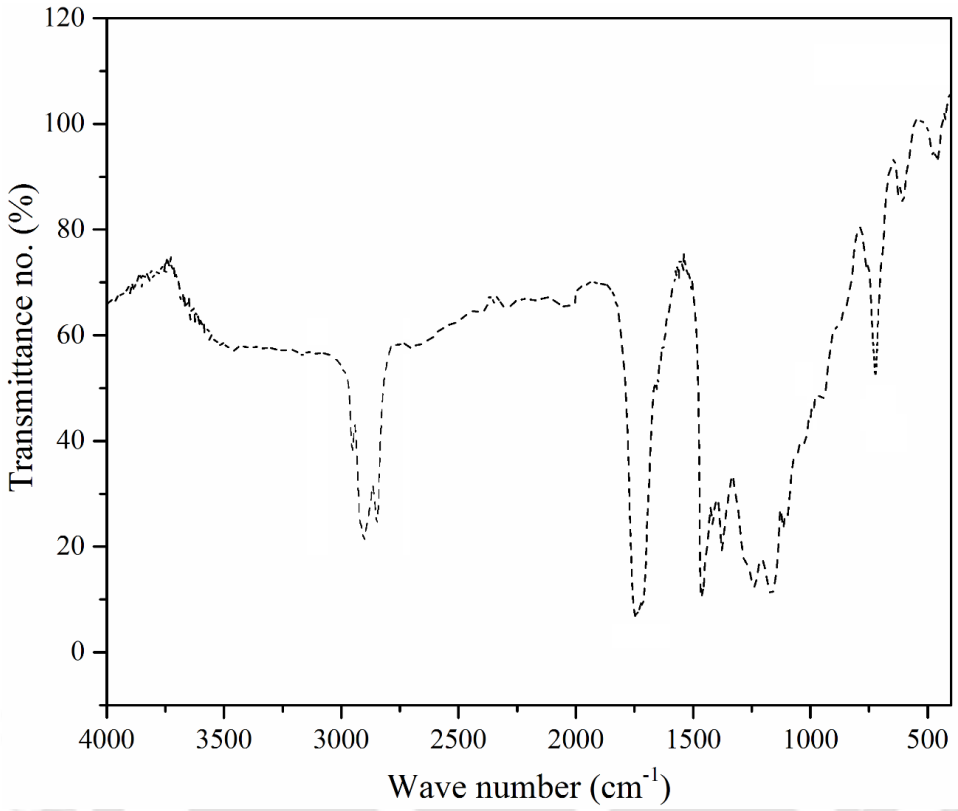

Figure 4-44 FTIR of trans-esterified neem oil

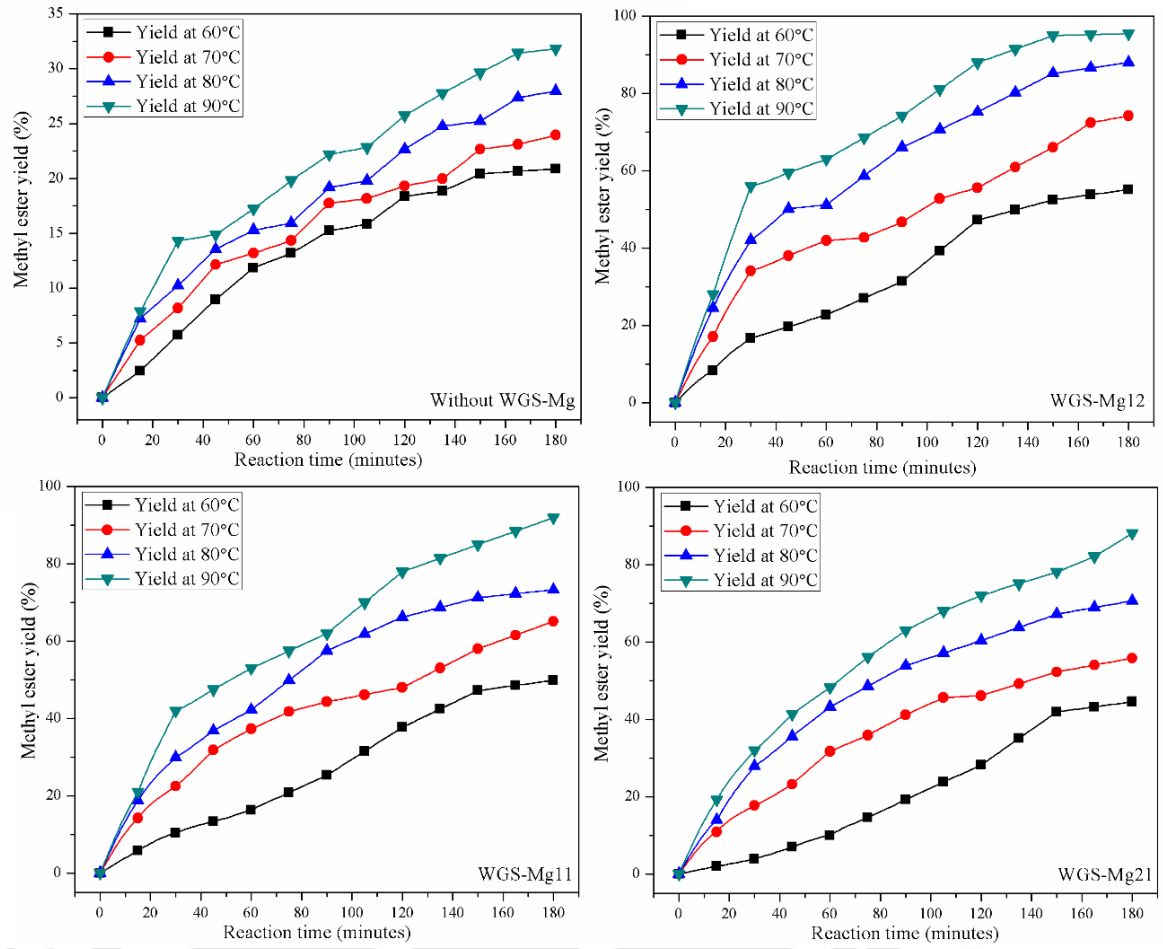

Figure 4-45 Illustration of effectiveness in rising temperature (T °C) with varying reaction time period (h) up on yield of Methyl ester in (a) absence of catalyst, presence of (b) WGS-Mg 11 (c) WGS-Mg 12 (d) WGS-Mg 21

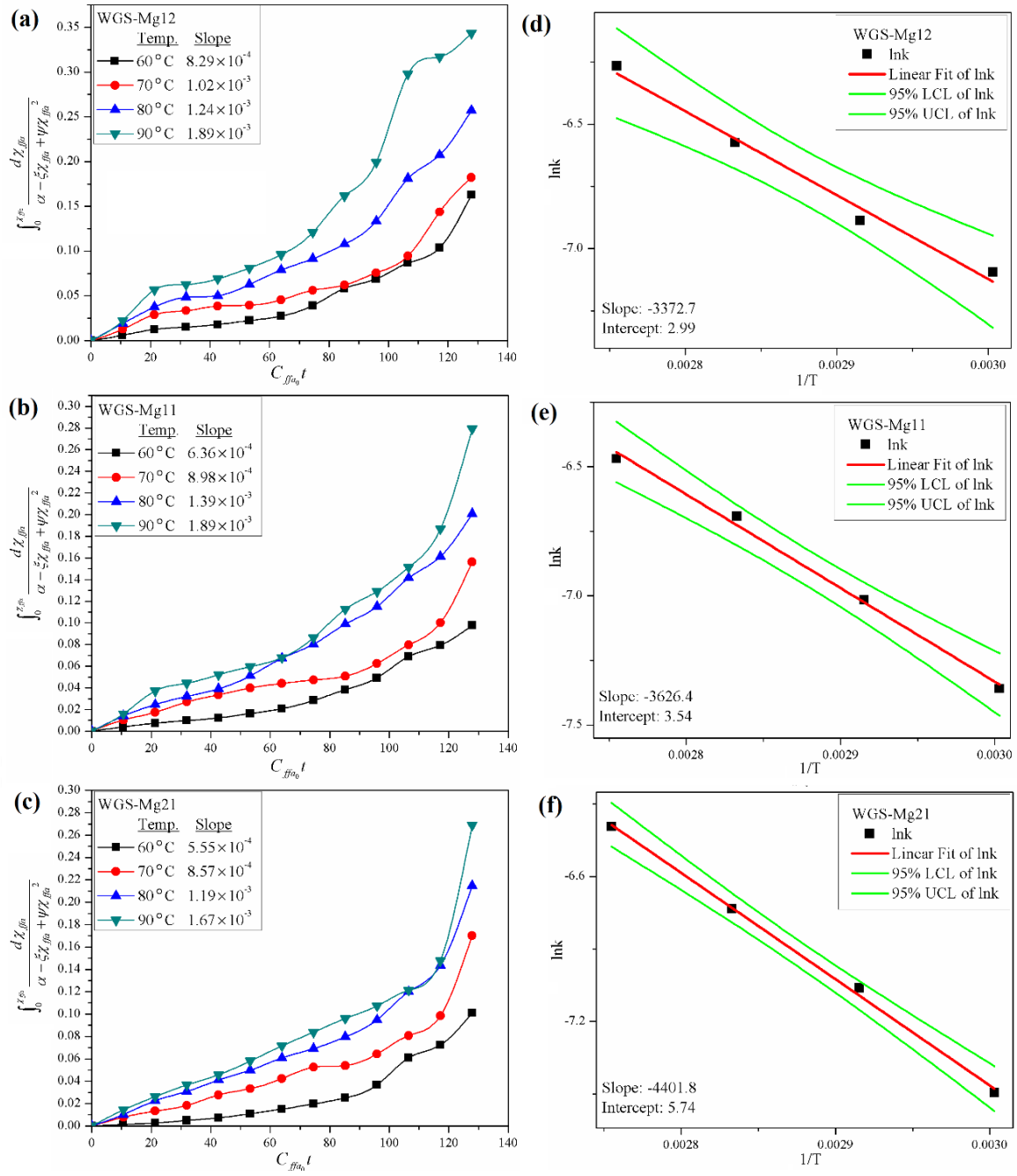

Figure 4-46 Graph of $\int_0^{\chi_{ffa}} \frac{d\chi_{ffa}}{\alpha - \xi\chi_{ffa} + \psi\chi_{ffa}^2}$ vs $C_{ffa_0}t$ for (a) WGS-Mg 12 (b) WGS-Mg 11 (c) WGS-Mg 21, Graph of ln k and 1/T for all (d) WGS-Mg 12 (e) WGS-Mg 11 (f) WGS-Mg 21

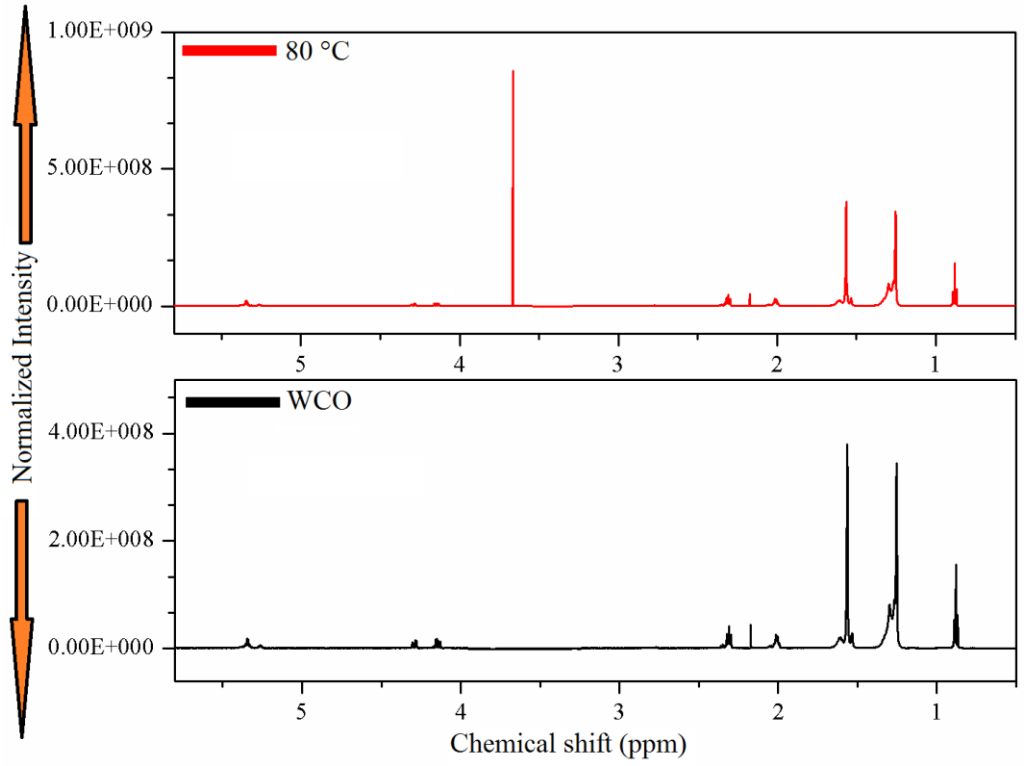

Figure 4-47 [1]HNMR analysis of WCO and esterified WCO at 80 °C reaction temperatures

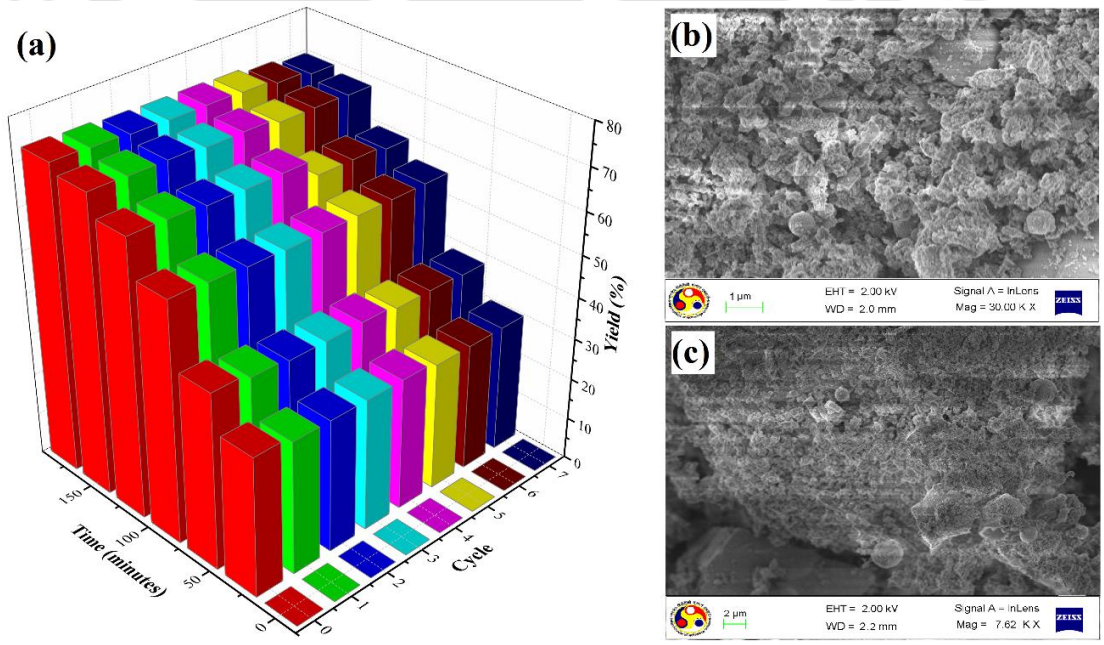

Figure 4-48 (a) Graph between yield and time illustrating the chemical stability of catalyst after every cycle (b), (c) FESEM image of WGS-Mg11 recovered after 7th cycle

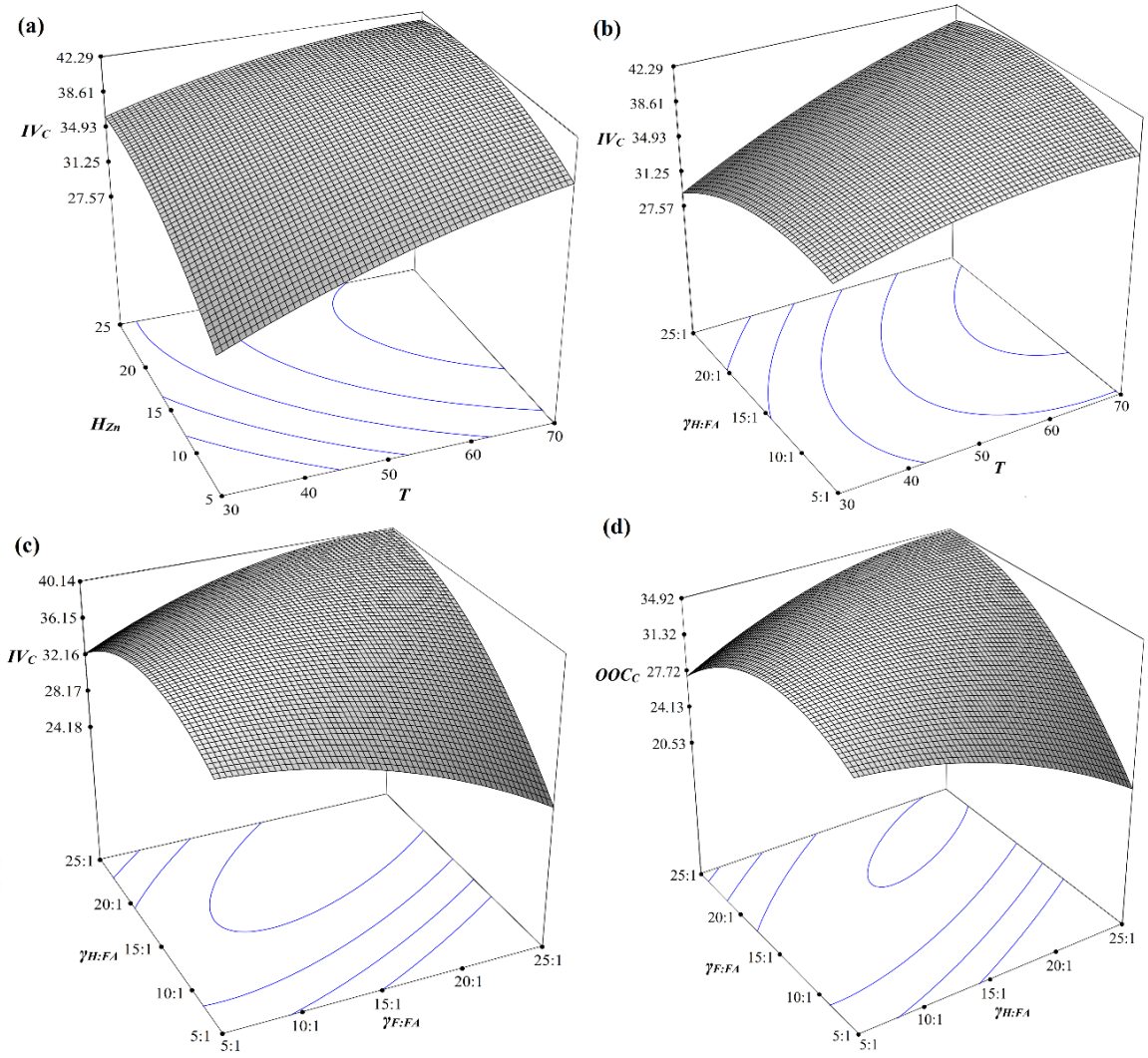

Figure 4-49 Effect of H_{Zn} and T, 5b Effect of $\gamma_{F:FA}$ and T, 5c Effect of $\gamma_{H:FA}$ and $\gamma_{F:FA}$ on IV_C, 5d Effect of $\gamma_{F:FA}$ and $\gamma_{H:FA}$ on OOC_C

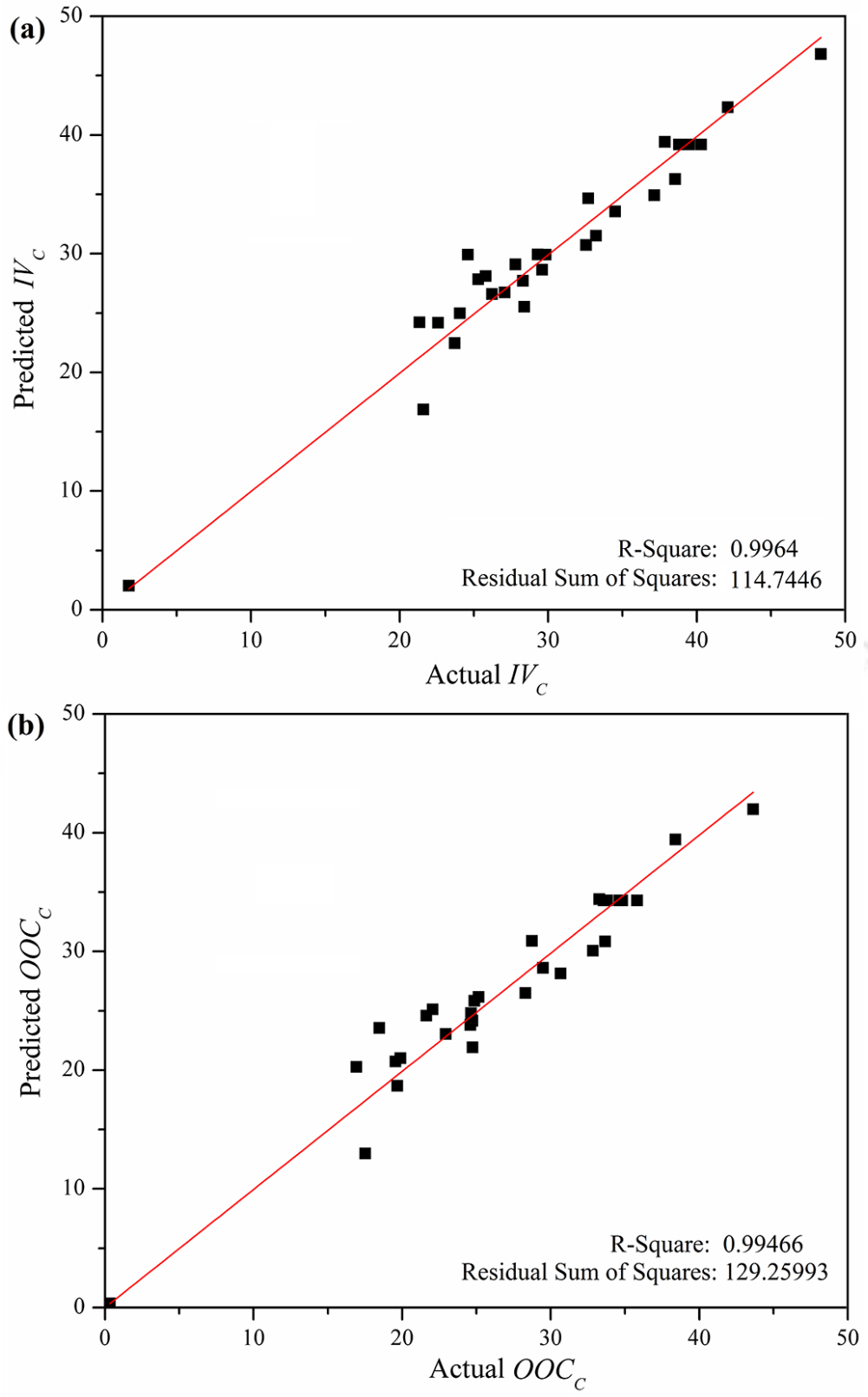

Figure 4-50 Predicted and experimental value of IV_C and OOC_C

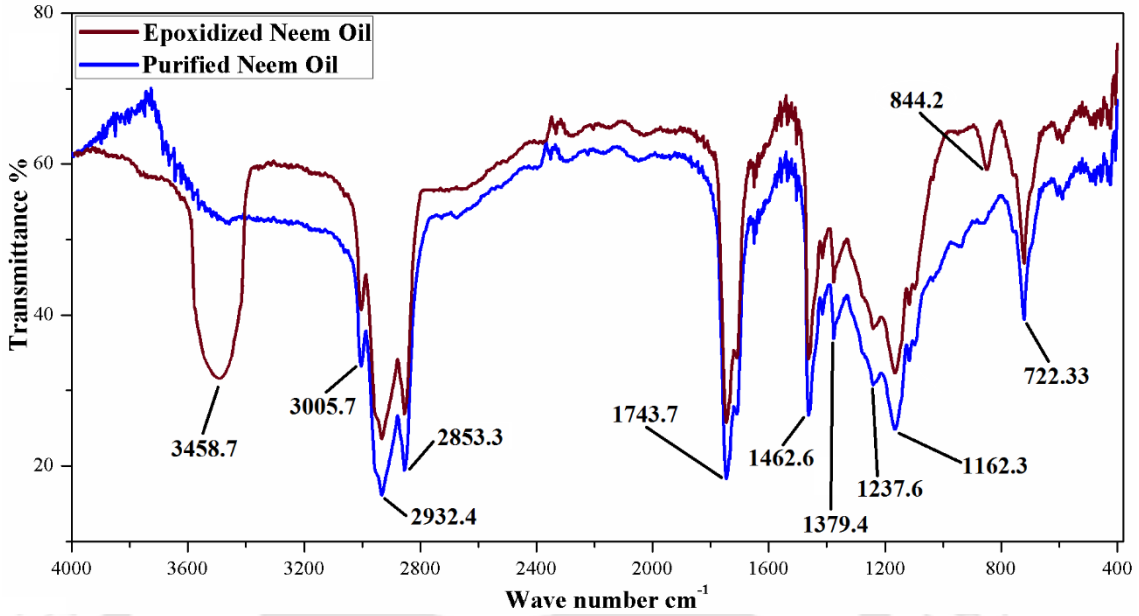

Figure 4-51 FTIR spectrum of PNO and ENO showing characteristic band of epoxide formation

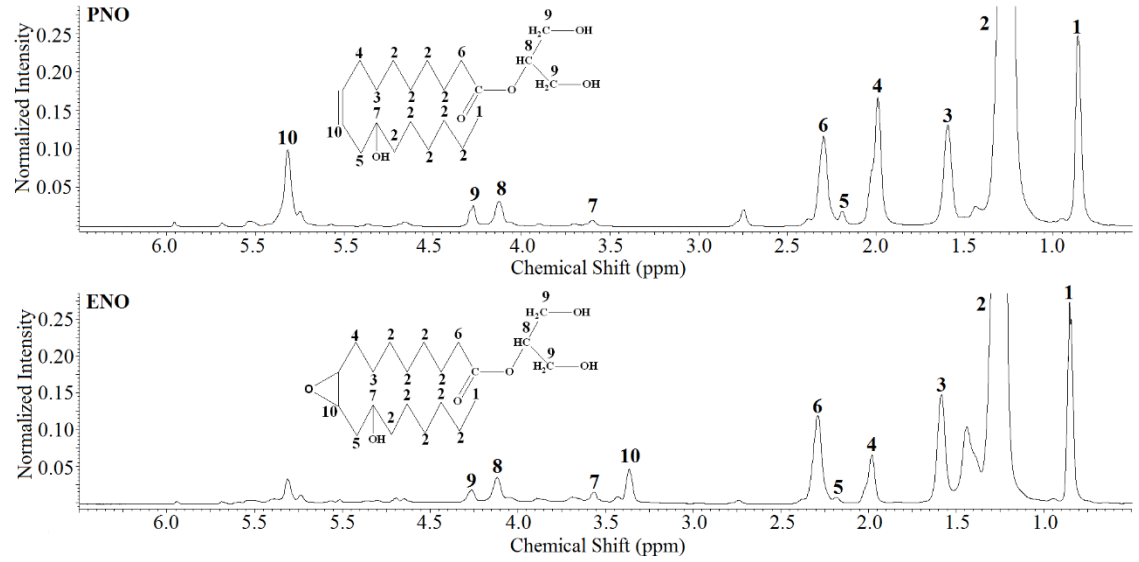

Figure 4-52 ^{1}HNMR spectra of PNO and ENO

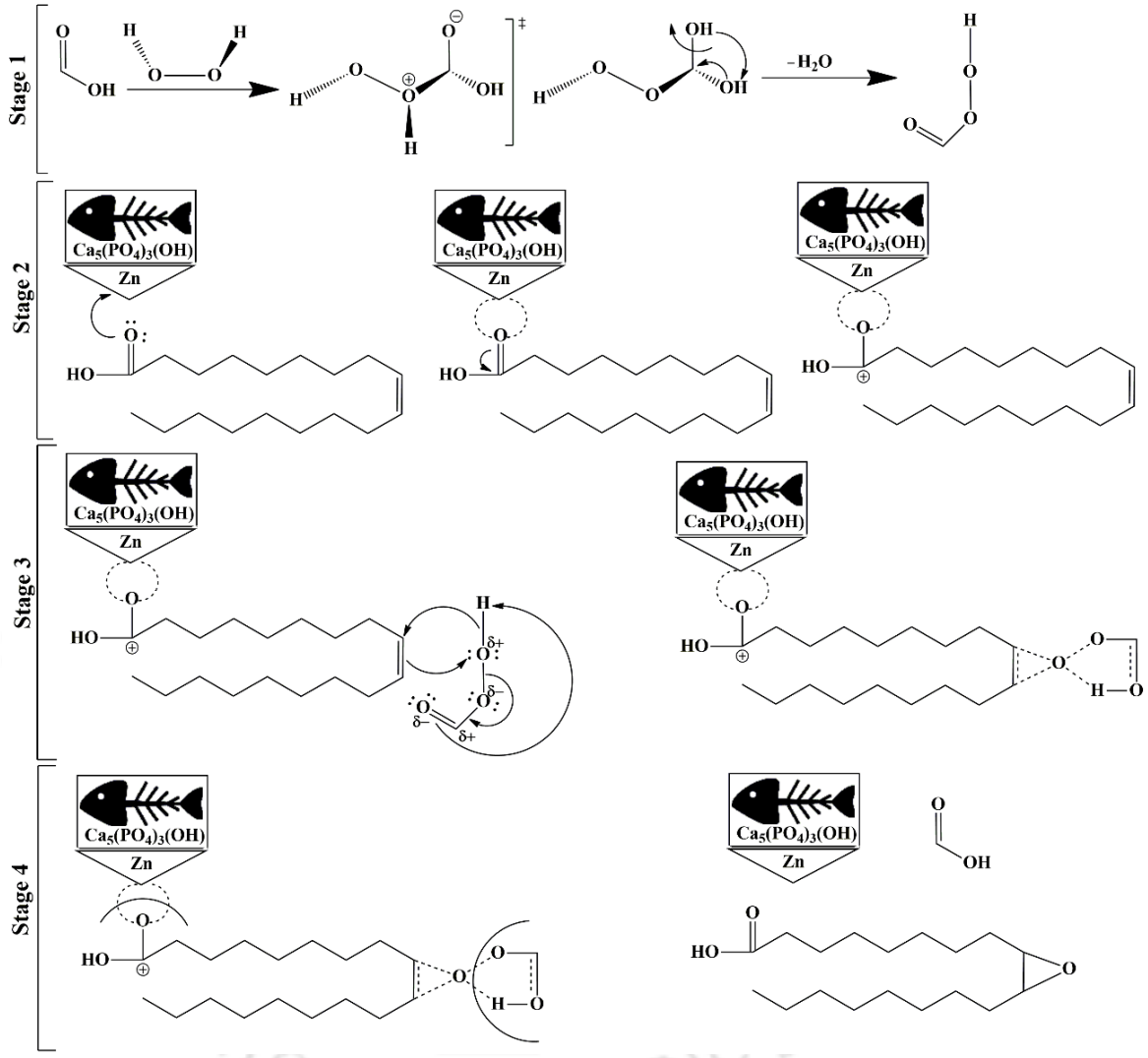

Figure 4-53 Probable mechanism of fatty acid peroxidation in neem oil in presence of HAp-Zn

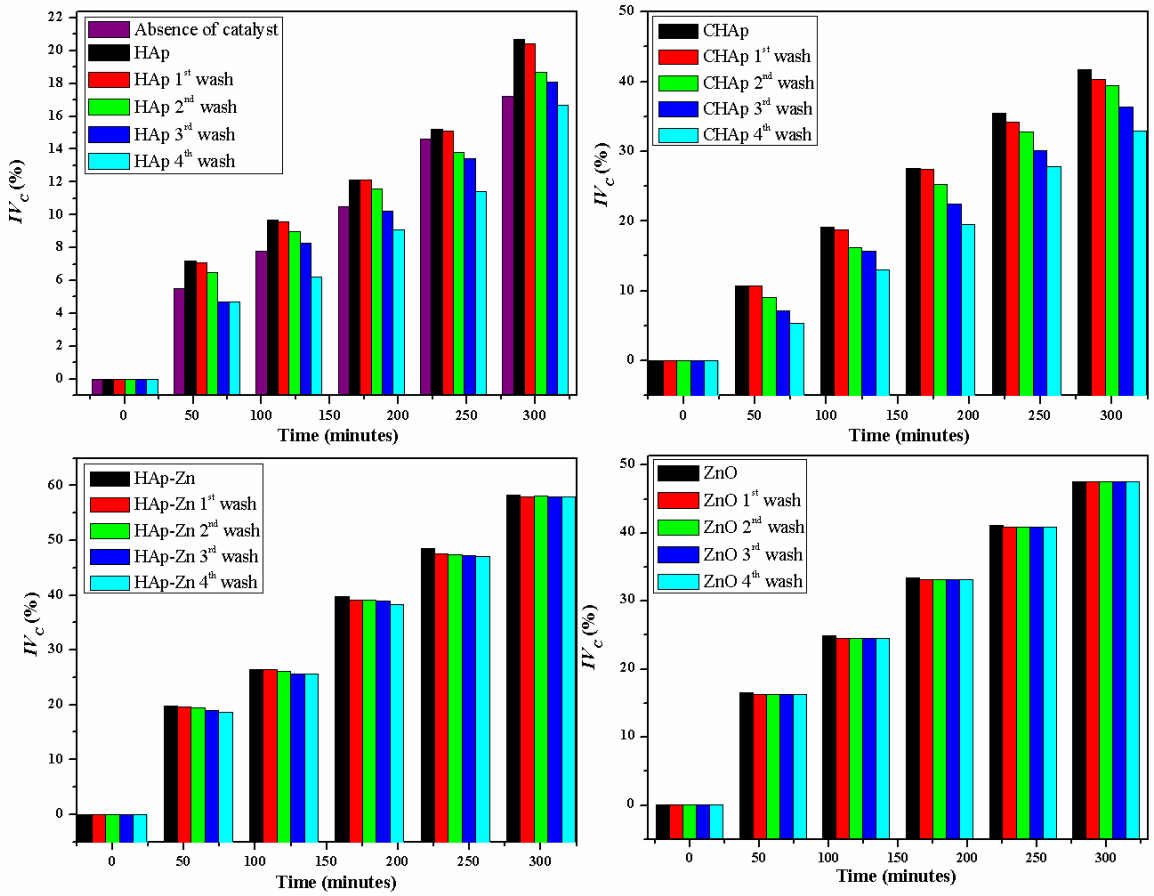

Figure 4-54 Iodine value conversion after each regeneration for HAp, CHAp, HAp-Zn and ZnO showing the stability of catalyst quantitatively

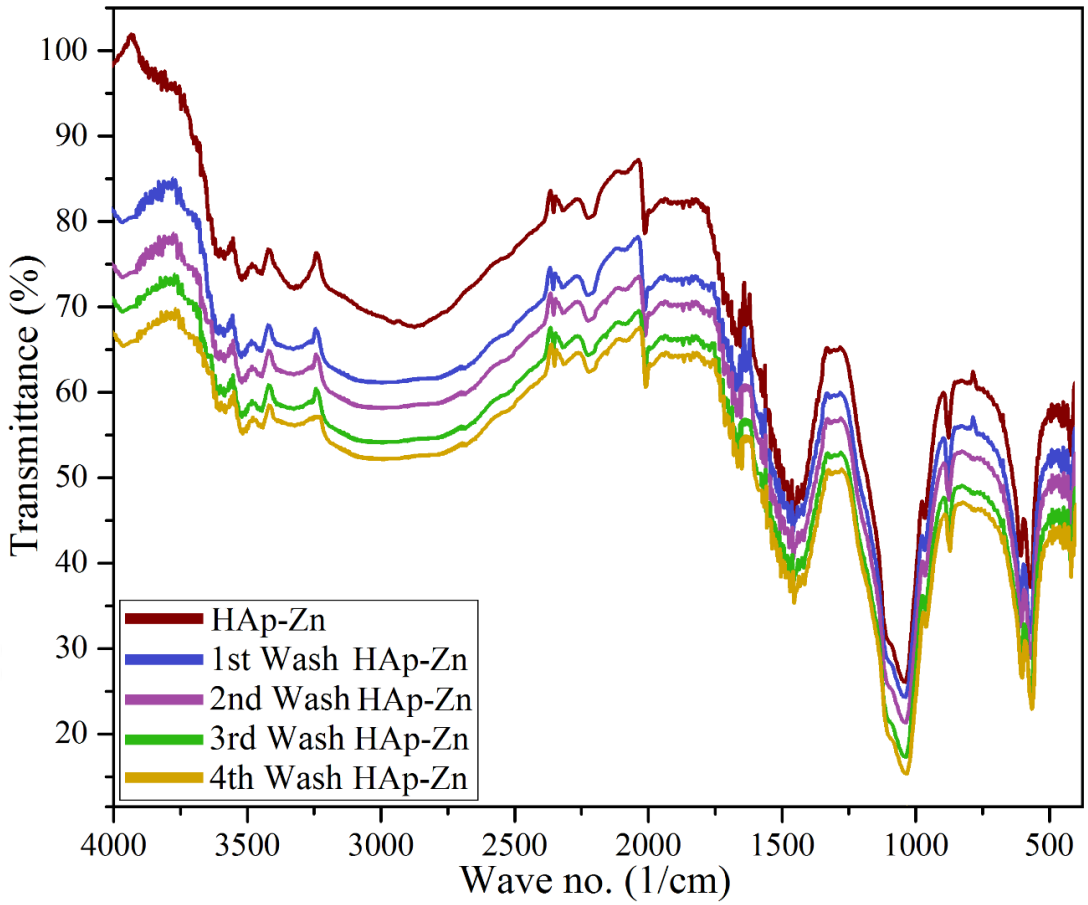

Figure 4-55 FTIR spectrum of original catalyst (HAp-Zn) and regenerated catalyst after every wash up to 4 cycle

5 CONCLUSION AND FUTURE SCOPE

"What is research but a blind date with knowledge?"

Will Harvey

(Silicon Valley entrepreneur)

5.1 Concluding Remarks

Five bio-waste derived metal doped catalysts were developed from waste cooked fishbone and waste groundnut shell by wet impregnation method and was characterized. Few works were reported in the literature using fishbone as hydroxyapatite source with limited success. The catalyst prepared in this work was thermally more stable, had better surface area and pore volume and also showed its efficiency in transesterification and peroxidation of raw Neem oil. During Neem oil methanolysis using HAp-Al, all the parameters showed a positive response individually. A maximum acid value conversion of 97.26 % was obtained at 90 °C (T_R), 1 (H_A), 4 h (t), 400 rpm (S_{rpm}), 30 ($R_{O/M}$). The transesterification rate of reaction was found to be $3.46\times10^{-5}\,mol^{-1}l^{-1}\,\text{min}^{-1}$ at optimal parametric conditions. The reusability study inferred the chemical stability of the newly developed catalyst. The regenerated catalyst could render almost the same conversion as fresh catalyst for 7 successive reaction cycles; which ascertains the stability of the catalyst advocating its suitability for reusability. After doping Mg ion and Na-Si ion by impregnation followed by calcination was also resulted in high surface area and pore volume. The methanolysis of Neem oil using HAp-Mg and HAp-Na-Si showed significant results in methyl ester yield. The major factor of using a catalyst is reusability. The recycled catalyst rendered its performance above 5 cycles.

Similarly, the use of HAp-Zn during peroxidation of Neem oil was studied thoroughly. After deposition of Zn followed by calcination increased the surface area and

pore volume significantly, which provide an active area for catalytic reaction. The optimized parametric values for T, t, H_{Zn}, $\gamma_{H:FA}$, $\gamma_{F:FA}$ were found to be 60 °C, 3.88 h, 20 wt%, 19.05:1, 19.85:1 respectively which showed maximum desirability. After extending the reaction time to 8 h, the maximum conversion of 84.3% was observed. The regeneration and simultaneous reusability of the material were studied both qualitatively and quantitatively for consecutive reaction cycles. These studies ascertain that the catalyst retains its properties even after four reaction cycles. The comparison of earlier and recent study also indicated the advancement in the present work. Although the IV_C conversion was a bit low comparison to the other researchers, the use of heterogeneous catalyst derived from waste sources will give a new horizon to the peroxidation process.

Another biodegradable waste i.e. groundnut shell which is abundant in India was utilized for the preparation of a heterogeneous catalyst. The results of the present investigation showed that the Mg grafted on waste groundnut shell enhanced its catalytic properties. Waste cooking oil which has no commercial value was used as the base material for methanolysis. The catalytic effect of Mg ion percentage on the WGS was studied thoroughly by studying a second order rate kinetic model. Also an extensive reusability study showed the catalyst is stable even after seven successive uses. The present work was compared with earlier reported works and it was confirmed that the WGS-Mg catalyst has superior properties and can be used for similar types of reactions.

The method of reusing bio-wastes to prepare catalyst could help waste recycling, contaminants minimization, cost reduction and making the catalyst environmentally viable. This high efficient and low-cost catalyst could make the process of methanolysis and peroxidation economic also. Thus, it can be anticipated that this low-cost catalyst if utilized in a large-scale industrial process, will make the entire process sustainable as well as low cost. Also this work gives a new horizon towards the use of various bio-wastes for the development of heterogeneous catalysts. So, it can be anticipated that the low-cost catalyst could be utilized in a large-scale industrial process of bio-fuel, will lead to cheap and ecologically viable process.

5.2 Future scope

The developed catalysts can be used for high temperature and high pressure reaction because of their good thermal stability.

Apart from the metal ions used in the present work, other metal ions can be used for doping and can be used for various other applications which are not studied in the present work.

A uniform doping of ions on these type of waste materials can be developed.

6 REFERENCES

1. *India Energy Outlook*. 2015: France. p. 183.
2. Forster, P., et al., *Changes in atmospheric constituents and in radiative forcing. Chapter 2*, in *Climate Change 2007. The Physical Science Basis*. 2007.
3. Thomas, J.M., J.C. Hernandez-Garrido, and R.G. Bell, *A general strategy for the design of new solid catalysts for environmentally benign conversions.* Topics in Catalysis, 2009. **52**(12): p. 1630-1639.
4. Miyagawa, H., et al., *Fracture toughness and impact strength of anhydride‐cured biobased epoxy.* Polymer Engineering & Science, 2005. **45**(4): p. 487-495.
5. Miyagawa, H., et al., *Biobased epoxy/clay nanocomposites as a new matrix for CFRP.* Composites Part A: Applied Science and Manufacturing, 2006. **37**(1): p. 54-62.
6. Sithique, M.A., S. Nagendiran, and M. Alagar, *Synthesis and characterization of bismaleimide-modified, soy-based epoxy matrices for flame-retardant applications.* High Performance Polymers, 2010. **22**(3): p. 328-344.
7. Lin, B., et al., *Kinetic studies on oxirane cleavage of epoxidized soybean oil by methanol and characterization of polyols.* Journal of the American Oil Chemists' Society, 2008. **85**(2): p. 113-117.
8. Meyer, P., et al., *Epoxidation of soybean oil and Jatropha oil.* Thammasat Int J Sci Technol, 2008. **13**: p. 1-5.
9. Lu, J. and R.P. Wool, *Additive toughening effects on new bio-based thermosetting resins from plant oils.* Composites Science and Technology, 2008. **68**(3): p. 1025-1033.
10. Park, S.J., F.L. Jin, and J.R. Lee, *Effect of biodegradable epoxidized castor oil on physicochemical and mechanical properties of epoxy resins.* Macromolecular Chemistry and Physics, 2004. **205**(15): p. 2048-2054.
11. Jin, F.-L. and S.-J. Park, *Thermal and rheological properties of vegetable oil-based epoxy resins cured with thermally latent initiator.* Journal of Industrial and Engineering Chemistry, 2007. **13**(5): p. 808-814.
12. Cheong, M.Y., et al., *Synthesis and characterization of palm‐based resin for UV coating.* Journal of Applied Polymer Science, 2009. **111**(5): p. 2353-2361.
13. Ortiz, R.A., et al., *A kinetic study of the acceleration effect of substituted benzyl alcohols on the cationic photopolymerization rate of epoxidized natural oils.* Polymer, 2005. **46**(5): p. 1535-1541.

14. Dinda, S., et al., *Epoxidation of cottonseed oil by aqueous hydrogen peroxide catalysed by liquid inorganic acids.* Bioresource technology, 2008. **99**(9): p. 3737-3744.

15. Goud, V.V., N.C. Pradhan, and A.V. Patwardhan, *Epoxidation of karanja (Pongamia glabra) oil by H2O2.* Journal of the American Oil Chemists' Society, 2006. **83**(7): p. 635-640.

16. Gerbase, A.E., et al., *Epoxidation of soybean oil by the methyltrioxorhenium-CH2Cl2/H2O2 catalytic biphasic system.* Journal of the American Oil Chemists' Society, 2002. **79**(2): p. 179-181.

17. Meyer, F. and C. Limberg, *Organometallic oxidation catalysis*. Vol. 22. 2007: Springer.

18. Nørskov, J.K., et al., *Towards the computational design of solid catalysts.* Nature chemistry, 2009. **1**(1): p. 37-46.

19. Ma, F. and M.A. Hanna, *Biodiesel production: a review.* Bioresource technology, 1999. **70**(1): p. 1-15.

20. Van Gerpen, J., *Biodiesel processing and production.* Fuel processing technology, 2005. **86**(10): p. 1097-1107.

21. Knothe, G., J. Krahl, and J. Van Gerpen, *The biodiesel handbook*. 2015: Elsevier.

22. Meher, L., D.V. Sagar, and S. Naik, *Technical aspects of biodiesel production by transesterification—a review.* Renewable and sustainable energy reviews, 2006. **10**(3): p. 248-268.

23. Mittelbach, M. and C. Remschmidt, *Biodiesel: the comprehensive handbook.* 2004: Martin Mittelbach.

24. Knothe, G., *Biodiesel: current trends and properties.* Topics in Catalysis, 2010. **53**(11-12): p. 714-720.

25. Kikhtyanin, O.V., et al., *Hydroconversion of sunflower oil on Pd/SAPO-31 catalyst.* Fuel, 2010. **89**(10): p. 3085-3092.

26. Simakova, I., et al., *Decarboxylation of fatty acids over Pd supported on mesoporous carbon.* Catalysis Today, 2010. **150**(1): p. 28-31.

27. Šimáček, P. and D. Kubička, *Hydrocracking of petroleum vacuum distillate containing rapeseed oil: evaluation of diesel fuel.* Fuel, 2010. **89**(7): p. 1508-1513.

28. Guzman, A., et al., *Hydroprocessing of crude palm oil at pilot plant scale.* Catalysis today, 2010. **156**(1): p. 38-43.

29. Rozmysłowicz, B., et al., *Catalytic deoxygenation of tall oil fatty acids over a palladium-mesoporous carbon catalyst: a new source of biofuels.* Topics in Catalysis, 2010. **53**(15-18): p. 1274-1277.

30. Huber, G.W. and A. Corma, *Synergies between Bio‐and Oil Refineries for the Production of Fuels from Biomass.* Angewandte Chemie International Edition, 2007. **46**(38): p. 7184-7201.

31. Huber, G.W., P. O'Connor, and A. Corma, *Processing biomass in conventional oil refineries: Production of high quality diesel by hydrotreating vegetable oils in heavy vacuum oil mixtures.* Applied Catalysis A: General, 2007. **329**: p. 120-129.

32. Snåre, M., et al., *Heterogeneous catalytic deoxygenation of stearic acid for production of biodiesel.* Industrial & engineering chemistry research, 2006. **45**(16): p. 5708-5715.

33. Kubičková, I., et al., *Hydrocarbons for diesel fuel via decarboxylation of vegetable oils.* Catalysis Today, 2005. **106**(1): p. 197-200.

34. Na, J.-G., et al., *Hydrocarbon production from decarboxylation of fatty acid without hydrogen.* Catalysis Today, 2010. **156**(1): p. 44-48.

35. Tamunaidu, P. and S. Bhatia, *Catalytic cracking of palm oil for the production of biofuels: optimization studies.* Bioresource Technology, 2007. **98**(18): p. 3593-3601.

36. Twaiq, F.A., et al., *Catalytic conversion of palm oil over mesoporous aluminosilicate MCM-41 for the production of liquid hydrocarbon fuels.* Fuel Processing Technology, 2003. **84**(1): p. 105-120.

37. Serrano-Ruiz, J.C., D. Wang, and J.A. Dumesic, *Catalytic upgrading of levulinic acid to 5-nonanone.* Green Chemistry, 2010. **12**(4): p. 574-577.

38. Chheda, J.N., G.W. Huber, and J.A. Dumesic, *Liquid‐phase catalytic processing of biomass‐derived oxygenated hydrocarbons to fuels and chemicals.* Angewandte Chemie International Edition, 2007. **46**(38): p. 7164-7183.

39. Huber, G.W., et al., *Production of liquid alkanes by aqueous-phase processing of biomass-derived carbohydrates.* Science, 2005. **308**(5727): p. 1446-1450.

40. Simonetti, D.A. and J.A. Dumesic, *Catalytic Production of Liquid Fuels from Biomass‐Derived Oxygenated Hydrocarbons: Catalytic Coupling at Multiple Length Scales.* Catalysis Reviews, 2009. **51**(3): p. 441-484.

41. Zhang, W., *Automotive fuels from biomass via gasification.* Fuel Processing Technology, 2010. **91**(8): p. 866-876.

42. Abatzoglou, N., et al. *Green diesel from Fischer–Tropsch synthesis: challenges and hurdles*. in *3rd IASME/WSEAS international conference on energy, environment, ecosystems and sustainable development, Greece*. 2007. Citeseer.

43. Rostrup-Nielsen, J.R., *Making fuels from biomass.* Science, 2005. **308**(5727): p. 1421-1422.

44. Rostrup‐Nielsen, J.R., *Fuels and energy for the future: the role of catalysis.* Catalysis reviews, 2004. **46**(3-4): p. 247-270.

45. Donnis, B., et al., *Hydroprocessing of bio-oils and oxygenates to hydrocarbons. Understanding the reaction routes.* Topics in Catalysis, 2009. **52**(3): p. 229-240.

46. Zhang, S., et al., *Upgrading of liquid fuel from the pyrolysis of biomass.* Bioresource technology, 2005. **96**(5): p. 545-550.

47. Laurent, E. and B. Delmon, *Influence of water in the deactivation of a sulfided NiMoγ-Al2O3 catalyst during hydrodeoxygenation.* Journal of Catalysis, 1994. **146**(1): p. 281288-285291.

48. Wildschut, J., et al., *Hydrotreatment of fast pyrolysis oil using heterogeneous noble-metal catalysts.* Industrial & Engineering Chemistry Research, 2009. **48**(23): p. 10324-10334.

49. Carlson, T.R., et al., *Catalytic fast pyrolysis of glucose with HZSM-5: the combined homogeneous and heterogeneous reactions.* Journal of Catalysis, 2010. **270**(1): p. 110-124.

50. Stöcker, M., *Biofuels and biomass‐to‐liquid fuels in the biorefinery: Catalytic conversion of lignocellulosic biomass using porous materials.* Angewandte Chemie International Edition, 2008. **47**(48): p. 9200-9211.

51. Knothe, G., *Analyzing biodiesel: standards and other methods.* Journal of the American Oil Chemists' Society, 2006. **83**(10): p. 823-833.

52. Mikkonen, S., *Second-generation renewable diesel offers advantages.* Hydrocarbon processing, 2008. **87**(2): p. 63-66.

53. Koskinen, M., M. Sourander, and M. Nurminen, *Apply a comprehensive approach to biofuels: Clean fuels.* Hydrocarbon processing, 2006. **85**(2): p. 81-86.

54. Srivastava, A. and R. Prasad, *Triglycerides-based diesel fuels.* Renewable and sustainable energy reviews, 2000. **4**(2): p. 111-133.

55. Huber, G.W., S. Iborra, and A. Corma, *Synthesis of transportation fuels from biomass: chemistry, catalysts, and engineering.* Chemical reviews, 2006. **106**(9): p. 4044-4098.

56. Lotero, E., et al., *Synthesis of biodiesel via acid catalysis.* Industrial & engineering chemistry research, 2005. **44**(14): p. 5353-5363.

57. Jacobson, K., et al., *Solid acid catalyzed biodiesel production from waste cooking oil.* Applied Catalysis B: Environmental, 2008. **85**(1): p. 86-91.

58. Casanave, D., J.-L. Duplan, and E. Freund, *Diesel fuels from biomass.* Pure and Applied Chemistry, 2007. **79**(11): p. 2071-2081.

59. Sivasamy, A., et al., *Catalytic applications in the production of biodiesel from vegetable oils.* ChemSusChem, 2009. **2**(4): p. 278-300.

60. Demirbas, A., *Biodiesel production from vegetable oils via catalytic and non-catalytic supercritical methanol transesterification methods.* Progress in energy and combustion science, 2005. **31**(5): p. 466-487.

61. Verziu, M., et al., *Mesoporous Tin-Triflate Based Catalysts for Transesterification of Sunflower Oil.* Topics in Catalysis, 2010. **53**(11-12): p. 763-772.

62. Mo, X., et al., *A novel sulfonated carbon composite solid acid catalyst for biodiesel synthesis.* Catalysis Letters, 2008. **123**(1-2): p. 1-6.

63. Mungroo, R., et al., *Epoxidation of canola oil with hydrogen peroxide catalyzed by acidic ion exchange resin.* Journal of the American Oil Chemists' Society, 2008. **85**(9): p. 887-896.

64. Goud, V.V., A.V. Patwardhan, and N.C. Pradhan, *Studies on the epoxidation of mahua oil (Madhumica indica) by hydrogen peroxide.* Bioresource technology, 2006. **97**(12): p. 1365-1371.

65. Sinadinović-Fišer, S., M. Janković, and Z.S. Petrović, *Kinetics of in-situ epoxidation of soybean oil in bulk catalyzed by ion exchange resin.* Journal of the American Oil Chemists' Society, 2001. **78**(7): p. 725-731.

66. Campanella, A. and M.A. Baltanás, *Degradation of the oxirane ring of epoxidized vegetable oils in a liquid–liquid–solid heterogeneous reaction system.* Chemical Engineering and Processing: Process Intensification, 2007. **46**(3): p. 210-221.

67. Du, G., et al., *Catalytic epoxidation of methyl linoleate.* Journal of the American Oil Chemists' Society, 2004. **81**(5): p. 477-480.

68. Biedermann-Brem, S., et al., *Plasticizers in PVC toys and childcare products: What succeeds the phthalates? Market survey 2007.* Chromatographia, 2008. **68**(3-4): p. 227-234.

69. Javni, I., et al., *Thermal stability of polyurethanes based on vegetable oils.* Journal of Applied Polymer Science, 2000. **77**(8): p. 1723-1734.

70. Prileschajew, N., *Oxydation ungesättigter Verbindungen mittels organischer Superoxyde.* European Journal of Inorganic Chemistry, 1909. **42**(4): p. 4811-4815.

71. Warwel, S., *Chemo-enzymatic epoxidation of unsaturated carboxylic acids.* Journal of Molecular Catalysis B: Enzymatic, 1995. **1**(1): p. 29-35.

72. Arends, I. and R. Sheldon, *Recent developments in selective catalytic epoxidations with H2O2.* Topics in catalysis, 2002. **19**(1): p. 133-141.

73. Bartók, M. and A. Molnar, *Dehydration of diols*. 1980: Wiley Online Library.

74. Beletskaya, I.P. and A.V. Cheprakov, *The Heck reaction as a sharpening stone of palladium catalysis.* Chemical Reviews, 2000. **100**(8): p. 3009-3066.

75. De Vries, J.G., *The Heck reaction in the production of fine chemicals.* Canadian Journal of Chemistry, 2001. **79**(5-6): p. 1086-1092.

76. Castro, G.R. and T. Knubovets, *Homogeneous biocatalysis in organic solvents and water-organic mixtures.* Critical Reviews in Biotechnology, 2003. **23**(3): p. 195-231.

77. Yamada, H. and M. Kobayashi, *Nitrile hydratase and its application to industrial production of acrylamide.* Bioscience, biotechnology, and biochemistry, 1996. **60**(9): p. 1391-1400.

78. Guidotti, M., et al., *Epoxidation of unsaturated FAMEs obtained from vegetable source over Ti (IV)-grafted silica catalysts: a comparison between ordered and non-ordered mesoporous materials.* Journal of Molecular Catalysis A: Chemical, 2006. **250**(1): p. 218-225.

79. Pontikes, Y., et al., *Effect of firing temperature and atmosphere on sintering of ceramics made from Bayer process bauxite residue.* Ceramics international, 2009. **35**(1): p. 401-407.

80. Wang, S., H. Ang, and M. Tade, *Novel applications of red mud as coagulant, adsorbent and catalyst for environmentally benign processes.* Chemosphere, 2008. **72**(11): p. 1621-1635.

81. Paramguru, R., P. Rath, and V. Misra, *Trends in red mud utilization–a review.* Mineral Processing & Extractive Metall. Rev., 2004. **26**(1): p. 1-29.

82. Sushil, S. and V.S. Batra, *Catalytic applications of red mud, an aluminium industry waste: A review.* Applied Catalysis B: Environmental, 2008. **81**(1): p. 64-77.

83. Pratt, K.C. and V. Christoverson, *Hydrogenation of a model hydrogen-donor system using activated red mud catalyst.* Fuel, 1982. **61**(5): p. 460-462.

84. Yokoyama, S., et al., *Catalytic activity of sulphate for hydroliquefaction of coal by using diphenylether and diphenylmethane.* Fuel, 1989. **68**(4): p. 531-533.

85. Legarreta, J.A., et al., *Comparison of the effect of catalysts in coal liquefaction with tetralin and coal tar distillates.* Fuel, 1997. **76**(13): p. 1309-1313.

86. Ordonez, S., H. Sastre, and F. Dıez, *Catalytic hydrodechlorination of tetrachloroethylene over red mud.* Journal of hazardous materials, 2001. **81**(1): p. 103-114.

87. Paredes, J., et al., *Catalytic combustion of methane over red mud-based catalysts.* Applied Catalysis B: Environmental, 2004. **47**(1): p. 37-45.

88. Sınağ, A., M. Sungur, and M. Canel, *Effect of experimental conditions on the yields during the copyrolysis of Mustafa Kemal Paşa (MKP) lignite (Turkey) with low-density polyethylene.* Energy & fuels, 2006. **20**(4): p. 1609-1613.

89. Shinzato, M. and R. Hypolito, *Solid waste from aluminum recycling process: characterization and reuse of its economically valuable constituents.* Waste management, 2005. **25**(1): p. 37-46.

90. Balakrishnan, M., et al., *Waste materials–catalytic opportunities: an overview of the application of large scale waste materials as resources for catalytic applications.* Green Chemistry, 2011. **13**(1): p. 16-24.

91. Wang, S., *Application of solid ash based catalysts in heterogeneous catalysis.* Environmental science & technology, 2008. **42**(19): p. 7055-7063.

92. Xuan, X., et al., *Selective catalytic reduction of NO by ammonia with fly ash catalyst☆.* Fuel, 2003. **82**(5): p. 575-579.

93. Li, L., et al., *Catalytic decomposition of ammonia over fly ash supported Ru catalysts.* Fuel processing technology, 2008. **89**(11): p. 1106-1112.

94. Dunens, O.M., K.J. MacKenzie, and A.T. Harris, *Synthesis of multiwalled carbon nanotubes on fly ash derived catalysts.* Environmental science & technology, 2009. **43**(20): p. 7889-7894.

95. Wang, S. and G. Lu, *Effect of chemical treatment on Ni/fly-ash catalysts in methane reforming with carbon dioxide.* Studies in surface science and catalysis, 2007. **167**: p. 275-280.

96. Born, J.G., P. Mulder, and R. Louw, *Fly ash mediated reactions of phenol and monochlorophenols: oxychlorination, deep oxidation, and condensation.* Environmental science & technology, 1993. **27**(9): p. 1849-1863.

97. Kastner, J.R., K. Das, and N.D. Melear, *Catalytic oxidation of gaseous reduced sulfur compounds using coal fly ash.* Journal of hazardous materials, 2002. **95**(1): p. 81-90.

98. Kastner, J.R., et al., *Low temperature catalytic oxidation of hydrogen sulfide and methanethiol using wood and coal fly ash.* Environmental science & technology, 2003. **37**(11): p. 2568-2574.

99. Kastner, J.R., et al., *Catalytic ozonation of gaseous reduced sulfur compounds using wood fly ash.* Environmental science & technology, 2005. **39**(6): p. 1835-1842.

100. Leventouri, T., *Synthetic and biological hydroxyapatites: crystal structure questions.* Biomaterials, 2006. **27**(18): p. 3339-3342.

101. Klose, F., et al., *Catalysts from waste materials.* Applied Catalysis B: Environmental, 2000. **28**(3): p. 209-221.

102. Kuwahara, Y., et al., *A novel synthetic route to hydroxyapatite–zeolite composite material from steel slag: investigation of synthesis mechanism and evaluation of physicochemical properties.* Journal of Materials Chemistry, 2009. **19**(39): p. 7263-7272.

103. Kuwahara, Y., et al., *A novel conversion process for waste slag: synthesis of a hydrotalcite-like compound and zeolite from blast furnace slag and evaluation of adsorption capacities.* Journal of Materials Chemistry, 2010. **20**(24): p. 5052-5062.

104. Wei, Z., C. Xu, and B. Li, *Application of waste eggshell as low-cost solid catalyst for biodiesel production.* Bioresource technology, 2009. **100**(11): p. 2883-2885.

105. Helwani, Z., et al., *Solid heterogeneous catalysts for transesterification of triglycerides with methanol: a review.* Applied Catalysis A: General, 2009. **363**(1): p. 1-10.

106. Macquarrie, D.J. and J.J. Hardy, *Applications of functionalized chitosan in catalysis.* Industrial & engineering chemistry research, 2005. **44**(23): p. 8499-8520.

107. Leonhardt, S.E., et al., *Chitosan as a support for heterogeneous Pd catalysts in liquid phase catalysis.* Applied Catalysis A: General, 2010. **379**(1): p. 30-37.

108. Wei, D., et al., *Chitosan as an active support for assembly of metal nanoparticles and application of the resultant bioconjugates in catalysis.* Carbohydrate research, 2010. **345**(1): p. 74-81.

109. Primo, A. and F. Quignard, *Chitosan as efficient porous support for dispersion of highly active gold nanoparticles: design of hybrid catalyst for carbon–carbon bond formation.* Chemical Communications, 2010. **46**(30): p. 5593-5595.

110. Rustad, T., *Utilisation of marine by-products.* Electronic Journal of Environmental, Agricultural and Food Chemistry, 2003. **2**(4): p. 458-463.

111. Obadiah, A., et al., *Biodiesel production from Palm oil using calcined waste animal bone as catalyst.* Bioresource technology, 2012. **116**: p. 512-516.

112. Best, S., et al., *Bioceramics: past, present and for the future.* Journal of the European Ceramic Society, 2008. **28**(7): p. 1319-1327.

113. Hunt, L., et al., *Rice hulls as a raw material for producing silicon.* Journal of the Electrochemical Society, 1984. **131**(7): p. 1683-1686.

114. Ismagilov, Z.R., et al., *Preparation of carbonized rice husk monoliths and modification of the porous structure by SiO 2 leaching.* Catalysis Today, 2009. **147**: p. S58-S65.

115. Oliveira, F., et al., *Copper and lead removal by peanut hulls: Equilibrium and kinetic studies.* Desalination, 2009. **248**(1-3): p. 931-940.

116. Sree, R., et al., *Transesterification of edible and non-edible oils over basic solid Mg/Zr catalysts.* Fuel Processing Technology, 2009. **90**(1): p. 152-157.

117. Kozlowski, J.T., M.T. Aronson, and R.J. Davis, *Transesterification of tributyrin with methanol over basic Mg: Zr mixed oxide catalysts.* Applied Catalysis B: Environmental, 2010. **96**(3): p. 508-515.

118. de Caland, L.B., et al., *Preparation and study of bimetallic compounds efficiency in the synthesis of biodiesel fuel.* Catalysis letters, 2009. **128**(3-4): p. 392-400.

119. Bournay, L., et al., *New heterogeneous process for biodiesel production: A way to improve the quality and the value of the crude glycerin produced by biodiesel plants.* Catalysis Today, 2005. **106**(1): p. 190-192.

120. Pugnet, V., et al., *Stability, activity and selectivity study of a zinc aluminate heterogeneous catalyst for the transesterification of vegetable oil in batch reactor.* Applied Catalysis A: General, 2010. **374**(1): p. 71-78.

121. Russbueldt, B.M. and W.F. Hoelderich, *New rare earth oxide catalysts for the transesterification of triglycerides with methanol resulting in biodiesel and pure glycerol.* Journal of Catalysis, 2010. **271**(2): p. 290-304.

122. Kawashima, A., K. Matsubara, and K. Honda, *Development of heterogeneous base catalysts for biodiesel production.* Bioresource technology, 2008. **99**(9): p. 3439-3443.

123. Shu, Q., et al., *Synthesis of biodiesel from soybean oil and methanol catalyzed by zeolite beta modified with La 3+*. Catalysis Communications, 2007. **8**(12): p. 2159-2165.

124. Macario, A., et al., *Biodiesel production process by homogeneous/heterogeneous catalytic system using an acid–base catalyst.* Applied Catalysis A: General, 2010. **378**(2): p. 160-168.

125. Li, E. and V. Rudolph, *Transesterification of vegetable oil to biodiesel over MgO-functionalized mesoporous catalysts.* Energy & Fuels, 2007. **22**(1): p. 145-149.

126. Georgogianni, K., et al., *Transesterification of soybean frying oil to biodiesel using heterogeneous catalysts.* Fuel Processing Technology, 2009. **90**(5): p. 671-676.

127. Georgogianni, K., et al., *Transesterification of rapeseed oil for the production of biodiesel using homogeneous and heterogeneous catalysis.* Fuel processing technology, 2009. **90**(7): p. 1016-1022.

128. Zeng, H.-y., et al., *Activation of Mg–Al hydrotalcite catalysts for transesterification of rape oil.* Fuel, 2008. **87**(13): p. 3071-3076.

129. Cantrell, D.G., et al., *Structure-reactivity correlations in MgAl hydrotalcite catalysts for biodiesel synthesis.* Applied Catalysis A: General, 2005. **287**(2): p. 183-190.

130. Liu, Y., et al., *Transesterification of poultry fat with methanol using Mg–Al hydrotalcite derived catalysts.* Applied Catalysis A: General, 2007. **331**: p. 138-148.

131. Brito, A., et al., *Biodiesel production from waste oil using Mg− Al layered double hydroxide catalysts.* Energy & Fuels, 2009. **23**(6): p. 2952-2958.

132. Kim, M.J., et al., *Transesterification of triacetin, tributyrin, and soybean oil with methanol over hydrotalcites with different water contents.* Fuel Processing Technology, 2010. **91**(6): p. 618-624.

133. Chuayplod, P. and W. Trakarnpruk, *Transesterification of rice bran oil with methanol catalyzed by Mg (Al) La hydrotalcites and metal/MgAl oxides.* Industrial & Engineering Chemistry Research, 2009. **48**(9): p. 4177-4183.

134. Macala, G.S., et al., *Transesterification catalysts from iron doped hydrotalcite-like precursors: solid bases for biodiesel production.* Catalysis Letters, 2008. **122**(3-4): p. 205-209.

135. Li, E., Z.P. Xu, and V. Rudolph, *MgCoAl–LDH derived heterogeneous catalysts for the ethanol transesterification of canola oil to biodiesel.* Applied Catalysis B: Environmental, 2009. **88**(1): p. 42-49.

136. Guerreiro, L., et al., *PVA embedded hydrotalcite membranes as basic catalysts for biodiesel synthesis by soybean oil methanolysis.* Catalysis Today, 2010. **156**(3): p. 191-197.

137. Schuchardt, U., R.M. Vargas, and G. Gelbard, *Alkylguanidines as catalysts for the transesterification of rapeseed oil.* Journal of Molecular Catalysis A: Chemical, 1995. **99**(2): p. 65-70.

138. Schuchardt, U., R.M. Vargas, and G. Gelbard, *Transesterification of soybean oil catalyzed by alkylguanidines heterogenized on different substituted polystyrenes.* Journal of Molecular Catalysis A: Chemical, 1996. **109**(1): p. 37-44.

139. Villa, A., et al., *Amino-functionalized carbon nanotubes as solid basic catalysts for the transesterification of triglycerides.* Chemical Communications, 2009(29): p. 4405-4407.

140. Cerro-Alarcón, M., et al., *Methanolysis of sunflower oil using gem-diamines as active organocatalysts for biodiesel production.* Applied Catalysis A: General, 2010. **382**(1): p. 36-42.

141. Cerro-Alarcón, M., et al., *Biomass to fuels: A water-free process for biodiesel production with phosphazene catalysts.* Applied Catalysis A: General, 2008. **346**(1): p. 52-57.

142. Kim, M.-Y., et al., *The exceptional activity of a phosphazenium hydroxide catalyst incorporated onto silica in the transesterification of tributyrin with methanol.* Chemical Communications, 2009(21): p. 3110-3112.

143. Saravanamurugan, S., et al., *Transesterification reactions over morphology controlled amino-functionalized SBA-15 catalysts.* Catalysis Communications, 2008. **9**(1): p. 158-163.

144. Savonnet, M., et al., *Solvent free base catalysis and transesterification over basic functionalised Metal-Organic Frameworks.* Green Chemistry, 2009. **11**(11): p. 1729-1732.

145. Liu, Y., et al., *Transesterification of triacetin using solid Brønsted bases.* Journal of Catalysis, 2007. **246**(2): p. 428-433.

146. Sunita, G., et al., *Synthesis of biodiesel over zirconia-supported isopoly and heteropoly tungstate catalysts.* Catalysis Communications, 2008. **9**(5): p. 696-702.

147. Park, Y.-M., et al., *Esterification of used vegetable oils using the heterogeneous WO 3/ZrO 2 catalyst for production of biodiesel.* Bioresource technology, 2010. **101**(1): p. S59-S61.

148. Komintarachat, C. and S. Chuepeng, *Solid acid catalyst for biodiesel production from waste used cooking oils.* Industrial & Engineering Chemistry Research, 2009. **48**(20): p. 9350-9353.

149. Rao, K.N., et al., *Zirconium phosphate supported tungsten oxide solid acid catalysts for the esterification of palmitic acid.* Green Chemistry, 2006. **8**(9): p. 790-797.

150. Ngaosuwan, K., et al., *Effect of solvent on hydrolysis and transesterification reactions on tungstated zirconia.* Applied Catalysis A: General, 2010. **380**(1): p. 81-86.

151. Kulkarni, M.G., et al., *Solid acid catalyzed biodiesel production by simultaneous esterification and transesterification.* Green Chemistry, 2006. **8**(12): p. 1056-1062.

152. Zhang, X., et al., *Heteropolyacid nanoreactor with double acid sites as a highly efficient and reusable catalyst for the transesterification of waste cooking oil.* Energy & Fuels, 2009. **23**(9): p. 4640-4646.

153. Morin, P., et al., *Transesterification of rapeseed oil with ethanol: I. Catalysis with homogeneous Keggin heteropolyacids.* Applied Catalysis A: General, 2007. **330**: p. 69-76.

154. Caetano, C., et al., *Esterification of free fatty acids with methanol using heteropolyacids immobilized on silica.* Catalysis Communications, 2008. **9**(10): p. 1996-1999.

155. Oliveira, C.F., et al., *Esterification of oleic acid with ethanol by 12-tungstophosphoric acid supported on zirconia.* Applied Catalysis A: General, 2010. **372**(2): p. 153-161.

156. Cardoso, A.L., R. Augusti, and M.J. Da Silva, *Investigation on the esterification of fatty acids catalyzed by the H3PW12O40 heteropolyacid.* Journal of the American Oil Chemists' Society, 2008. **85**(6): p. 555-560.

157. de Godói Silva, V.W., L.O. Laier, and M.J. Da Silva, *Novel H3PW12O40: catalysed esterification reactions of fatty acids at room temperature for biodiesel production.* Catalysis letters, 2010. **135**(3-4): p. 207-211.

158. Xu, L., et al., *Preparation of mesoporous polyoxometalate-tantalum pentoxide composite catalyst and its application for biodiesel production by esterification and transesterification.* Green Chemistry, 2008. **10**(7): p. 746-755.

159. Srilatha, K., et al., *Esterification of free fatty acids for biodiesel production over heteropoly tungstate supported on niobia catalysts.* Applied Catalysis A: General, 2009. **365**(1): p. 28-33.

160. Xu, L., et al., *Simultaneous esterification and transesterification of soybean oil with methanol catalyzed by mesoporous Ta 2 O 5/SiO 2–[H 3 PW 12 O 40/R](R= Me or Ph) hybrid catalysts.* Green Chemistry, 2009. **11**(3): p. 314-317.

161. Alsalme, A., E.F. Kozhevnikova, and I.V. Kozhevnikov, *Heteropoly acids as catalysts for liquid-phase esterification and transesterification.* Applied Catalysis A: General, 2008. **349**(1): p. 170-176.

162. Lam, M.K., K.T. Lee, and A.R. Mohamed, *Sulfated tin oxide as solid superacid catalyst for transesterification of waste cooking oil: an optimization study.* Applied Catalysis B: Environmental, 2009. **93**(1): p. 134-139.

163. Suwannakarn, K., et al., *Stability of sulfated zirconia and the nature of the catalytically active species in the transesterification of triglycerides.* Journal of Catalysis, 2008. **255**(2): p. 279-286.

164. Hu, X., et al., *Esterification of fatty acid by zirconic catalysts.* Catalysis letters, 2009. **133**(1-2): p. 90.

165. Du, Y., et al., *Synthesis of sulfated silica-doped tin oxides and their high activities in transesterification.* Catalysis Letters, 2008. **124**(1-2): p. 133-138.

166. Lopez, D.E., et al., *Esterification and transesterification using modified-zirconia catalysts.* Applied Catalysis A: General, 2008. **339**(1): p. 76-83.

167. Rattanaphra, D., A. Harvey, and P. Srinophakun, *Simultaneous conversion of triglyceride/free fatty acid mixtures into biodiesel using sulfated zirconia.* Topics in Catalysis, 2010. **53**(11-12): p. 773-782.

168. Yu, G., et al., *Esterification over rare earth oxide and alumina promoted SO 4 2−/ZrO 2.* Catalysis today, 2009. **148**(1): p. 169-173.

169. de Almeida, R.M., et al., *Transesterification reaction of vegetable oils, using superacid sulfated TiO 2–base catalysts.* Applied Catalysis A: General, 2008. **347**(1): p. 100-105.

170. Juan, J.C., J. Zhang, and M.A. Yarmo, *Structure and reactivity of silica-supported zirconium sulfate for esterification of fatty acid under solvent-free condition.* Applied Catalysis A: General, 2007. **332**(2): p. 209-215.

171. Shi, W., et al., *Preparation and characterization of the organic–inorganic hybrid membrane for biodiesel production.* Bioresource technology, 2010. **101**(5): p. 1501-1505.

172. Chung, K.-H., D.-R. Chang, and B.-G. Park, *Removal of free fatty acid in waste frying oil by esterification with methanol on zeolite catalysts.* Bioresource Technology, 2008. **99**(16): p. 7438-7443.

173. Carmo, A.C., et al., *Production of biodiesel by esterification of palmitic acid over mesoporous aluminosilicate Al-MCM-41.* Fuel, 2009. **88**(3): p. 461-468.

174. Jiménez-Morales, I., et al., *Zirconium doped MCM-41 supported WO 3 solid acid catalysts for the esterification of oleic acid with methanol.* Applied Catalysis A: General, 2010. **379**(1): p. 61-68.

175. Dhainaut, J., et al., *Hierarchical macroporous–mesoporous SBA-15 sulfonic acid catalysts for biodiesel synthesis.* Green chemistry, 2010. **12**(2): p. 296-303.

176. Shibasaki-Kitakawa, N., et al., *Simple continuous production process of biodiesel fuel from oil with high content of free fatty acid using ion-exchange resin catalysts.* Energy & Fuels, 2010. **24**(6): p. 3634-3638.

177. Bianchi, C., et al., *Low temperature de-acidification process of animal fat as a pre-step to biodiesel production.* Catalysis letters, 2010. **134**(1-2): p. 179-183.

178. Özbay, N., N. Oktar, and N.A. Tapan, *Esterification of free fatty acids in waste cooking oils (WCO): Role of ion-exchange resins.* Fuel, 2008. **87**(10): p. 1789-1798.

179. Park, J.-Y., D.-K. Kim, and J.-S. Lee, *Esterification of free fatty acids using water-tolerable Amberlyst as a heterogeneous catalyst.* Bioresource technology, 2010. **101**(1): p. S62-S65.

180. Feng, Y., et al., *Biodiesel production using cation-exchange resin as heterogeneous catalyst.* Bioresource Technology, 2010. **101**(5): p. 1518-1521.

181. Caetano, C., et al., *Esterification of fatty acids to biodiesel over polymers with sulfonic acid groups.* Applied Catalysis A: General, 2009. **359**(1): p. 41-46.

182. Grossi, C.V., et al., *Sulfonated polystyrene: a catalyst with acid and superabsorbent properties for the esterification of fatty acids.* Fuel, 2010. **89**(1): p. 257-259.

183. Soldi, R.A., et al., *Soybean oil and beef tallow alcoholysis by acid heterogeneous catalysis.* Applied Catalysis A: General, 2009. **361**(1): p. 42-48.

184. Okayasu, T., et al., *Preparation of a novel poly (vinylsulfonic acid)-grafted solid phase acid catalyst and its use in esterification reactions.* Chemical Communications, 2009(31): p. 4708-4710.

185. Melero, J.A., et al., *Biodiesel production over arenesulfonic acid-modified mesostructured catalysts: optimization of reaction parameters using response surface methodology.* Topics in Catalysis, 2010. **53**(11-12): p. 795-804.

186. Zięba, A., et al., *Activity and stability of polyaniline-sulfate-based solid acid catalysts for the transesterification of triglycerides and esterification of fatty acids with methanol.* Applied Catalysis A: General, 2010. **383**(1): p. 169-181.

187. Toda, M., et al., *Green chemistry: biodiesel made with sugar catalyst.* Nature, 2005. **438**(7065): p. 178-178.

188. Suganuma, S., et al., *Hydrolysis of cellulose by amorphous carbon bearing SO3H, COOH, and OH groups.* Journal of the American Chemical Society, 2008. **130**(38): p. 12787-12793.

189. Hara, M., *Biodiesel production by amorphous carbon bearing SO3H, COOH and phenolic OH groups, a solid Brønsted acid catalyst.* Topics in Catalysis, 2010. **53**(11-12): p. 805-810.

190. Dehkhoda, A.M., A.H. West, and N. Ellis, *Biochar based solid acid catalyst for biodiesel production.* Applied Catalysis A: General, 2010. **382**(2): p. 197-204.

191. Takagaki, A., et al., *Esterification of higher fatty acids by a novel strong solid acid.* Catalysis Today, 2006. **116**(2): p. 157-161.

192. Lien, Y.-S., L.-S. Hsieh, and J.C. Wu, *Biodiesel synthesis by simultaneous esterification and transesterification using oleophilic acid catalyst.* Industrial & Engineering Chemistry Research, 2010. **49**(5): p. 2118-2121.

193. Nakajima, K., et al., *Amorphous carbon bearing sulfonic acid groups in mesoporous silica as a selective catalyst.* Chemistry of Materials, 2008. **21**(1): p. 186-193.

194. Peng, L., et al., *Preparation of sulfonated ordered mesoporous carbon and its use for the esterification of fatty acids.* Catalysis Today, 2010. **150**(1): p. 140-146.

195. Salimon, J. and N. Salih, *Improved low temperature properties of 2-ethylhexyl 9 (10)-hydroxy-10 (9)-acyloxystearate derivatives.* European Journal of Scientific Research, 2009. **31**(4): p. 583-591.

196. Campanella, A., C. Fontanini, and M.A. Baltanas, *High yield epoxidation of fatty acid methyl esters with performic acid generated in situ.* Chemical Engineering Journal, 2008. **144**(3): p. 466-475.

197. La Scala, J. and R.P. Wool, *Effect of FA composition on epoxidation kinetics of TAG.* Journal of the American Oil Chemists' Society, 2002. **79**(4): p. 373-378.

198. Okieimen, F., O. Bakare, and C. Okieimen, *Studies on the epoxidation of rubber seed oil.* Industrial Crops and Products, 2002. **15**(2): p. 139-144.

199. Orellana-Coca, C., et al., *Lipase mediated simultaneous esterification and epoxidation of oleic acid for the production of alkylepoxystearates.* Journal of Molecular Catalysis B: Enzymatic, 2007. **44**(3): p. 133-137.

200. Orellana‐Coca, C., et al., *Chemo‐enzymatic epoxidation of linoleic acid: Parameters influencing the reaction.* European Journal of Lipid Science and Technology, 2005. **107**(12): p. 864-870.

201. Törnvall, U., et al., *Stability of immobilized Candida antarctica lipase B during chemo-enzymatic epoxidation of fatty acids.* Enzyme and microbial technology, 2007. **40**(3): p. 447-451.

202. Poli, E., et al., *Solvent-free selective epoxidation of fatty esters over a tungsten-based catalyst.* Catalysis Today, 2009. **140**(1): p. 19-22.

203. Benaniba, M.T., N. Belhaneche‐Bensemra, and G. Gelbard, *Kinetics of tungsten‐catalyzed sunflower oil epoxidation studied by 1H NMR.* European journal of lipid science and technology, 2007. **109**(12): p. 1186-1193.

204. Herrmann, W.A., et al., *Methyltrioxorhenium/pyrazole—A highly efficient catalyst for the epoxidation of olefins.* Journal of organometallic chemistry, 1998. **555**(2): p. 293-295.

205. Meshram, P.D., R.G. Puri, and H.V. Patil, *Epoxidation of wild safflower (Carthamus oxyacantha) Oil with peroxy acid in presence of strongly acidic cation exchange resin IR-122 asCatalyst".* Int J Chem Tech Res, 2011. **3**(3): p. 1152-1163.

206. Herrmann, W.A., et al., *Methyltrioxorhenium (VII) as catalyst for epoxidations: structure of the active species and mechanism of catalysis.* Angewandte Chemie International Edition in English, 1993. **32**(8): p. 1157-1160.

207. Campanella, A., et al., *Soybean oil epoxidation with hydrogen peroxide using an amorphous Ti/SiO 2 catalyst.* Green Chemistry, 2004. **6**(7): p. 330-334.

208. Rinaldi, R., et al., *Tuning the acidic properties of aluminas via sol-gel synthesis: New findings on the active site of alumina-catalyzed epoxidation with hydrogen peroxide.* Journal of Catalysis, 2006. **244**(1): p. 92-101.

209. Gurbanov, M.S., et al., *Epoxidation of soybean oil in the course of cooxidation with hydrogen peroxide in the presence of propanoic acid and chlorinated ku-2×8 cation exchanger.* Russian journal of applied chemistry, 2005. **78**(10): p. 1678-1682.

210. Boey, P.-L., G.P. Maniam, and S.A. Hamid, *Biodiesel production via transesterification of palm olein using waste mud crab (Scylla serrata) shell as a heterogeneous catalyst.* Bioresource Technology, 2009. **100**(24): p. 6362-6368.

211. Boey, P.-L., G.P. Maniam, and S.A. Hamid, *Utilization of waste crab shell (Scylla serrata) as a catalyst in palm olein transesterification.* Journal of oleo science, 2008. **58**(10): p. 499-502.

212. Boey, P.-L., et al., *Utilization of waste cockle shell (Anadara granosa) in biodiesel production from palm olein: optimization using response surface methodology.* Fuel, 2011. **90**(7): p. 2353-2358.

213. Yang, L., A. Zhang, and X. Zheng, *Shrimp shell catalyst for biodiesel production.* Energy & Fuels, 2009. **23**(8): p. 3859-3865.

214. Nakatani, N., et al., *Transesterification of soybean oil using combusted oyster shell waste as a catalyst.* Bioresource Technology, 2009. **100**(3): p. 1510-1513.

215. Boro, J., A.J. Thakur, and D. Deka, *Solid oxide derived from waste shells of Turbonilla striatula as a renewable catalyst for biodiesel production.* Fuel Processing Technology, 2011. **92**(10): p. 2061-2067.

216. Hu, S., Y. Wang, and H. Han, *Utilization of waste freshwater mussel shell as an economic catalyst for biodiesel production.* biomass and bioenergy, 2011. **35**(8): p. 3627-3635.

217. Viriya-empikul, N., et al., *Waste shells of mollusk and egg as biodiesel production catalysts.* Bioresource technology, 2010. **101**(10): p. 3765-3767.

218. Chojnacka, K., *Biosorption of Cr (III) ions by eggshells.* Journal of Hazardous Materials, 2005. **121**(1): p. 167-173.

219. Semwal, S., et al., *Preparation of novel catalyst composition from natural waste for biodiesel production.* 2011.

220. Konsomboon, S., et al., *Effect of kaolin addition on ash characteristics of palm empty fruit bunch (EFB) upon combustion.* Applied Energy, 2011. **88**(1): p. 298-305.

221. Boey, P.-L., et al., *Utilization of BA (boiler ash) as catalyst for transesterification of palm olein.* Energy, 2011. **36**(10): p. 5791-5796.

222. Imaduddin, M., Y. Yoeswono, and I. Tahir, *Ekstraksi kalium dari abu tandan kosong sawit sebagai katalis pada reaksi transesterifikasi minyak sawit.* Bulletin of Chemical Reaction Engineering & Catalysis, 2008. **3**(1-3): p. 14-20.

223. Yaakob, Z., et al., *Utilization of palm empty fruit bunch for the production of biodiesel from Jatropha curcas oil.* Bioresource technology, 2012. **104**: p. 695-700.

224. Ojha, K., N.C. Pradhan, and A.N. Samanta, *Kinetics of batch alkylation of phenol with tert-butyl alcohol over a catalyst synthesized from coal fly ash.* Chemical Engineering Journal, 2005. **112**(1): p. 109-115.

225. Jain, D., C. Khatri, and A. Rani, *Fly ash supported calcium oxide as recyclable solid base catalyst for Knoevenagel condensation reaction.* Fuel Processing Technology, 2010. **91**(9): p. 1015-1021.

226. Chakraborty, R., S. Bepari, and A. Banerjee, *Transesterification of soybean oil catalyzed by fly ash and egg shell derived solid catalysts.* Chemical Engineering Journal, 2010. **165**(3): p. 798-805.

227. Kotwal, M., et al., *Transesterification of sunflower oil catalyzed by flyash-based solid catalysts.* Fuel, 2009. **88**(9): p. 1773-1778.

228. Babajide, O., et al., *Use of coal fly ash as a catalyst in the production of biodiesel.* 2010.

229. Aderemi, B.O. and B. Hameed, *Alum as a heterogeneous catalyst for the transesterification of palm oil.* Applied Catalysis A: General, 2009. **370**(1): p. 54-58.

230. Ilgen, O., *Dolomite as a heterogeneous catalyst for transesterification of canola oil.* Fuel Processing Technology, 2011. **92**(3): p. 452-455.

231. Ngamcharussrivichai, C., et al., *Biodiesel production through transesterification over natural calciums.* Fuel Processing Technology, 2010. **91**(11): p. 1409-1415.

232. Chakraborty, R., S. Bepari, and A. Banerjee, *Application of calcined waste fish (Labeo rohita) scale as low-cost heterogeneous catalyst for biodiesel synthesis.* Bioresource technology, 2011. **102**(3): p. 3610-3618.

233. Gerpen, J.v., D. Clements, and G. Knothe, *Biodiesel Production Technology August 2002-January 2004, National Renewable Energy Laboratory*. 2004, NREL/SR-510-36244.

234. Shagal, M.H., et al., *Epoxidation of Ximenia americana seed oil.* Journal of Petroleum Technology and Alternative Fuels 2013. **4**(4): p. 72-77.

235. Paquot, C., *Standard methods for the analysis of oils, fats and derivatives*. 7 ed. 2013.

236. Rocha, J., et al., *Hydroxyapatite scaffolds hydrothermally grown from aragonitic cuttlefish bones.* Journal of Materials Chemistry, 2005. **15**(47): p. 5007-5011.

237. Varma, H. and S.S. Babu, *Synthesis of calcium phosphate bioceramics by citrate gel pyrolysis method.* Ceramics International, 2005. **31**(1): p. 109-114.

238. Kloprogge, J. and R. Frost, *Raman and infrared spectroscopic investigation of the neutralisation of aluminium in the presence of monomeric orthosilicic acid.* Spectrochimica Acta Part A: Molecular and Biomolecular Spectroscopy, 1999. **55**(7): p. 1359-1369.

239. Pacewska, B. and M. Keshr, *Thermal transformations of aluminium nitrate hydrate.* Thermochimica Acta, 2002. **385**(1): p. 73-80.

240. Chakraborty, R. and D. RoyChowdhury, *Fish bone derived natural hydroxyapatite-supported copper acid catalyst: Taguchi optimization of semibatch oleic acid esterification.* Chemical engineering journal, 2013. **215**: p. 491-499.

241. Wang, Z., et al., *Low-temperature synthesis of ZnO nanoparticles by solid-state pyrolytic reaction.* Nanotechnology, 2002. **14**(1): p. 11.

242. Chandramohan, R., J. Thirumalai, and T.A. Vijayan, *Nanocrystalline Mn and Fe doped ZnO thin films prepared using SILAR method for dilute magnetic semiconductor application.* Mater. Sci. Adv. Top. ISBN, 2013: p. 978-953.

243. Maensiri, S., P. Laokul, and V. Promarak, *Synthesis and optical properties of nanocrystalline ZnO powders by a simple method using zinc acetate dihydrate and poly (vinyl pyrrolidone).* Journal of crystal growth, 2006. **289**(1): p. 102-106.

244. Maddila, S. and S.B. Jonnalagadda, *One-pot three-component synthesis of 4-aryl-3, 4-dihydro-pyrimidin-2 (1 H)-thiones catalyzed by Ni loaded SiO 2.* Bulletin of the Chemical Society of Ethiopia, 2012. **26**(1).

245. Musić, S., N. Filipović-Vinceković, and L. Sekovanić, *Precipitation of amorphous SiO2 particles and their properties.* Brazilian journal of chemical engineering, 2011. **28**(1): p. 89-94.

246. Gleysteen, L.F. and V. Deitz, *Hysteresis in the physical adsorption of nitrogen on Bone Char and other adsorbents.* J. Res. of the National Bureau Standards, 1945. **35**.

247. Lowell, S., et al., *Characterization of porous solids and powders: surface area, pore size and density*. Vol. 16. 2012: Springer Science & Business Media.

248. Zeng, D., et al., *Synthesis, characterization and acid catalysis of solid acid from peanut shell.* Applied Catalysis A: General, 2014. **469**: p. 284-289.

249. Dai, Y.-M., et al., *Application of Peanut Husk Ash as a Low-Cost Solid Catalyst for Biodiesel Production.* International Journal of Chemical Engineering and Applications, 2014. **5**(3): p. 276.

250. Zhao, W., et al., *Etherification of glycerol with isobutylene to produce oxygenate additive using sulfonated peanut shell catalyst.* Industrial & Engineering Chemistry Research, 2010. **49**(24): p. 12399-12404.

251. Malik, R., D. Ramteke, and S. Wate, *Physico-chemical and surface characterization of adsorbent prepared from groundnut shell by ZnCl 2 activation and its ability to adsorb colour*. 2006.

252. Xie, S., et al., *Intense and wavelength-tunable photoluminescence from surface functionalized MgO nanocrystal clusters.* Journal of Materials Chemistry, 2011. **21**(20): p. 7263-7268.

253. Cheng, G., et al., *Transition of cellulose crystalline structure and surface morphology of biomass as a function of ionic liquid pretreatment and its relation to enzymatic hydrolysis.* Biomacromolecules, 2011. **12**(4): p. 933-941.

254. Pornsawan, A., P. Jintanavasan, and P. Kitchaiya, *Adsorption of FFA, Soap and Glycerine in Biodiesel Using Magnesium Silicate.* Chemical Engineering Transactions, 2015. **43**: p. 1135-40.

255. Bynes, A.N., I. Eide, and K.B. Jørgensen, *Optimization of acid catalyzed transesterification of jatropha and rapeseed oil with 1-butanol.* Fuel, 2014. **137**: p. 94-99.

256. Encinar, J.M., J.F. Gonzalez, and A. Rodríguez-Reinares, *Biodiesel from used frying oil. Variables affecting the yields and characteristics of the biodiesel.* Industrial & Engineering Chemistry Research, 2005. **44**(15): p. 5491-5499.

257. Radha, K. and G. Manikandan. *Novel production of biofuels from neem oil*. in *World Renewable Energy Congress-Sweden; 8-13 May; 2011; Linköping; Sweden*. 2011. Linköping University Electronic Press.

258. Yan, S., S.O. Salley, and K.S. Ng, *Simultaneous transesterification and esterification of unrefined or waste oils over ZnO-La 2 O 3 catalysts.* Applied Catalysis A: General, 2009. **353**(2): p. 203-212.

259. Furuta, S., H. Matsuhashi, and K. Arata, *Biodiesel fuel production with solid superacid catalysis in fixed bed reactor under atmospheric pressure.* Catalysis communications, 2004. **5**(12): p. 721-723.

260. Xie, W., H. Peng, and L. Chen, *Calcined Mg–Al hydrotalcites as solid base catalysts for methanolysis of soybean oil.* Journal of Molecular Catalysis A: Chemical, 2006. **246**(1): p. 24-32.

261. Wang, Y., et al., *Preparation of macrospherical magnesia-rich magnesium aluminate spinel catalysts for methanolysis of soybean oil.* Chemical Engineering Science, 2008. **63**(17): p. 4306-4312.

262. Arzamendi, G., et al., *Synthesis of biodiesel with heterogeneous NaOH/alumina catalysts: comparison with homogeneous NaOH.* Chemical Engineering Journal, 2007. **134**(1): p. 123-130.

263. Antunes, W.M., C. de Oliveira Veloso, and C.A. Henriques, *Transesterification of soybean oil with methanol catalyzed by basic solids.* Catalysis Today, 2008. **133**: p. 548-554.

264. Shumaker, J.L., et al., *Biodiesel synthesis using calcined layered double hydroxide catalysts.* Applied Catalysis B: Environmental, 2008. **82**(1): p. 120-130.

265. Di Serio, M., et al., *Transesterification of soybean oil to biodiesel by using heterogeneous basic catalysts.* Industrial & Engineering Chemistry Research, 2006. **45**(9): p. 3009-3014.

266. Vyas, A.P., N. Subrahmanyam, and P.A. Patel, *Production of biodiesel through transesterification of Jatropha oil using KNO 3/Al 2 O 3 solid catalyst.* Fuel, 2009. **88**(4): p. 625-628.

267. Liu, X., et al., *Transesterification of soybean oil to biodiesel using CaO as a solid base catalyst.* Fuel, 2008. **87**(2): p. 216-221.

268. Il Choi, J., W.H. Hong, and H.N. Chang, *Reaction kinetics of lactic acid with methanol catalyzed by acid resins.* International journal of chemical kinetics, 1996. **28**(1): p. 37-41.

269. Jazie, A.A., H. Pramanik, and A. Sinha, *Transesterification of peanut and rapeseed oils using waste of animal bone as cost effective catalyst.* Materials for Renewable and Sustainable Energy, 2013. **2**(2): p. 11.

270. Xie, J., et al., *Biont shell catalyst for biodiesel production.* Green chemistry, 2009. **11**(3): p. 355-364.

271. Araujo, L.R.R.d., et al., *H3PO4/Al2O3 catalysts: characterization and catalytic evaluation of oleic acid conversion to biofuels and biolubricant.* Materials Research, 2006. **9**(2): p. 181-184.

272. Xie, J., et al., *Biont shell catalyst for biodiesel production.* Green Chem., 2009. **11**(3): p. 355-364.

273. Shang, Y., Y. Jiang, and J. Gao, *One-step Synthesis of Peanut Shell-derived Solid Acid for Biodiesel Production.* Energy Sources, Part A: Recovery, Utilization, and Environmental Effects, 2015. **37**(10): p. 1039-1045.

274. Meshram, P.D., R.G. Puri, and H.V. Patil, *Epoxidation of wild safflower (Carthamus oxyacantha) oil with peroxy acid in presence of strongly acidic cation exchange resin IR-122 as catalyst.* International Journal of ChemTech Research, 2011. **3**(3): p. 1152-1163.

275. Rothenberg, G., *Catalysis: concepts and green applications*. 2015: WILEY-VCH Verlag GmbH & Co. KGaA, Weinheim. 279.

276. Guidotti, M., et al., *Epoxidation of unsaturated FAMEs obtained from vegetable source over Ti(IV)-grafted silica catalysts: A comparison between ordered and non-ordered mesoporous materials.* Journal of Molecular Catalysis A: Chemical, 2006. **250**(1-2): p. 218-225.

277. Goud, V.V., A.V. Patwardhan, and N.C. Pradhan, *Studies on the epoxidation of mahua oil (Madhumica indica) by hydrogen peroxide.* Bioresour Technol, 2006. **97**(12): p. 1365-71.

278. Sepulveda, J., S. Teixeira, and U. Schuchardt, *Alumina-catalyzed epoxidation of unsaturated fatty esters with hydrogen peroxide.* Applied Catalysis A: General, 2007. **318**: p. 213-217.

279. Rios, L., et al., *Mesoporous and amorphous Ti–silicas on the epoxidation of vegetable oils.* Journal of Catalysis, 2005. **232**(1): p. 19-26.

280. Åkerman, C.O., et al., *Clean synthesis of biolubricants for low temperature applications using heterogeneous catalysts.* Journal of Molecular Catalysis B: Enzymatic, 2011. **72**(3-4): p. 263-269.

281. Cai, S. and L. Wang, *Epoxidation of Unsaturated Fatty Acid Methyl Esters in the Presence of SO3H-functional Bronsted Acidic Ionic Liquid as Catalyst.* Chinese Journal of Chemical Engineering, 2011. **19**(1): p. 57-63.

282. Sharma, R.V. and A.K. Dalai, *Synthesis of bio-lubricant from epoxy canola oil using sulfated Ti-SBA-15 catalyst.* Applied Catalysis B: Environmental, 2013. **142-143**: p. 604-614.

283. Campanella, A., et al., *Soybean oil epoxidation with hydrogen peroxide using an amorphous Ti/SiO2catalyst.* Green Chem., 2004. **6**(7): p. 330-334.

284. Sinadinović-Fišer, S., M. Janković, and Z.S. Petrović, *Kinetics of in situ epoxidation of soybean oil in bulk catalyzed by ion exchange resin.* Journal of the American Oil Chemists' Society, 2001. **78**(7): p. 725-731.

285. Farias, M., M. Martinelli, and D.P. Bottega, *Epoxidation of soybean oil using a homogeneous catalytic system based on a molybdenum (VI) complex.* Applied Catalysis A: General, 2010. **384**(1-2): p. 213-219.

286. Benaniba, M.T., N. Belhaneche-Bensemra, and G. Gelbard, *Kinetics of tungsten-catalyzed sunflower oil epoxidation studied by1H NMR.* European Journal of Lipid Science and Technology, 2007. **109**(12): p. 1186-1193.

287. Yao, M.-Y., et al., *Highly Efficient Silica-Supported Peroxycarboxylic Acid for the Epoxidation of Unsaturated Fatty Acid Methyl Esters and Vegetable Oils.* ACS Sustainable Chemistry & Engineering, 2016. **4**(7): p. 3840-3849.